TRACING THE TRANSPORT, GEOCHEMICAL CYCLING AND FATE OF IODINE-129 IN EARTH SURFACE RESERVOIRS

Matthew Noel Herod

Thesis submitted to the
Faculty of Graduate & Postdoctoral Studies
in partial fulfillment of the requirements
for the Doctorate in Philosophy degree in Earth Sciences

Ottawa-Carleton Geoscience Centre
and
University of Ottawa
Ottawa, Canada

Thèse soumise à
Faculté des etudes supérieures et postdoctorales
Université d'Ottawa
en vue d'obtention du doctorate en
Sciences de la Terre

Centre Géoscientifique d'Ottawa-Carleton
et
Université d'Ottawa
Ottawa, Canada

Table of Contents

LIST OF ABBREVIATIONS

NFRP – Nuclear Fuel Reprocessing Plant

FDNA – Fukushima-Daiichi Nuclear Accident

DIW – Deionized Water

ICP-MS – Inductively Coupled Plasma Mass Spectrometer

AMS – Accelerator Mass Spectrometer

NWT – Northwest Territories

YT – Yukon Territory

NOAA – National Oceanic and Atmospheric Administration

HYSPLIT - Hybrid Single-Particle Lagrangian Integrated Trajectory

WCRB – Wolf Creek Research Basin

HDPE – High Density Polyethylene

PCA – Principal Component Analysis

AHC – Agglomerative Hierarchical Clustering

DIC – Dissolved Inorganic Carbon

DOC – Dissolved Organic Carbon

pMC – Percent Modern Carbon

TU – Tritium Units

SOM – Soil Organic Matter

VS2DTI – Variably Saturated Flow and Solute Transport Computer Program

NADP – National Atmospheric Deposition Program

ASA – Abbotsford Sumas Aquifer

ABSTRACT

Iodine-129 is a naturally and anthropogenically produced radioisotope (half-life: 15.7 million years) the majority of which is produced by nuclear fuel reprocessing. These releases have dispersed ^{129}I throughout the environment making it possible to use ^{129}I as a tracer. It is also of concern for the disposal of radioactive waste. This research develops a new laboratory method for ^{129}I extraction and analysis, and explores the geochemical cycling and environmental fate of ^{129}I in remote catchments following the Fukushima-Daiichi Nuclear Accident (FDNA).

A new technique was developed to investigate ^{129}I partitioning and quantitatively extract it from solid samples. Samples are combusted and volatilized iodine is trapped in solution. The efficiency is traced using the iodine isotope, ^{125}I. This technique was proven using standard reference materials and is used in other chapters of this thesis.

A baseline study of ^{129}I in Yukon watersheds was undertaken to determine the impact of anthropogenic ^{129}I emissions and identify possible sources. Using atmospheric back-trajectory modeling, sources of ^{129}I from Fukushima, nuclear fuel reprocessing and marine volatilization were identified in remote watersheds. Peat moss samples showed significant retention of ^{129}I in modern samples.

Following the reconnaissance study, a catchment scale investigation of anthropogenic ^{129}I cycling was undertaken through precipitation and runoff monitoring. ^{129}I was found to be an excellent indicator of initial snowmelt contributions to discharge due to enrichment by dry deposition. Furthermore, water source transitions in discharge were recorded by ^{129}I, ^{127}I and the ^{129}I/^{127}I ratio showing iodine can be used as a tracer of

hydrologic processes. A mass balance found that 77% of the ^{129}I mass input accumulates annually, primarily in organic soils.

Sampling of Vancouver, B.C. precipitation and groundwater was done following the FDNA to determine the fate of ^{129}I and evaluate it as a tracer of groundwater recharge. Immediately following the FDNA the ^{129}I concentration in precipitation increased 6 times above background. Groundwater samples also showed ^{129}I increases consistent with expected recharge times indicating FDNA derived ^{129}I was transported into groundwater with minimal retardation, likely via preferential flowpaths.

RÉSUMÉ

L'iode-129 est un isotope radioactif (demi-vie de 15,7 millions d'années) produit de façons naturelle et anthropogénique, majoritairement par le traitement de combustibles nucléaires. Sa dispersion dans l'environnement le rend utilisable comme marqueur anthropogénique; il est donc un isotope d'intérêt pour les dépôts de déchets radioactifs. Cette thèse décrit une nouvelle technique de laboratoire visant à extraire le ^{129}I. Les différentes sources d'iode-129 dans les régions éloignées y sont énumérées, et le cycle géochimique de l'iode-129 dans un bassin versant avant et après l'accident nucléaire de Fukushima-Daiichi y est expliqué.

Une nouvelle technique a été développée pour extraire quantitativement l'iode-129 d'échantillons solides. Les échantillons sont volatilisés par combustion et l'iode est récupéré en solution. L'efficacité est mesurée par la détection d'un autre isotope, le ^{125}I. Cette technique a été effectuée avec succès sur des standards, et est utilisée dans plusieurs chapitres de cette thèse.

Une étude des niveaux de base d'iode-129 a été effectuée au Yukon, afin de d'identifier les sources possibles d'iode-129 et de déterminer l'impact des émissions anthropogéniques dans les bassins versants du territoire. La modélisation des trajectoires atmosphériques de Fukushima vers le Yukon a permis d'identifier le traitement de combustibles nucléaires et la volatilisation marine comme sources majeures de ^{129}I. La mousse de tourbe a montré une rétention d'iode-129 particulièrement élevée dans les échantillons récents.

Suite à cette première phase, une étude plus approfondie sur le cycle du ^{129}I a été entreprise. L'eau des précipitations a été récoltée puis analysée; l'iode-129 y a été détecté. Il se trouve que l'isotope est un excellent indicateur de la contribution de la fonte initiale des neiges aux débits d'eau, dû à l'enrichissement par déposition sèche. De plus, le ^{129}I, ^{127}I, et le ratio $^{129}I/^{127}I$ ont été analysés dans les sources d'eau et à différents endroits des cours d'eau. Les résultats montrent que ces isotopes

peuvent être utilisés comme marqueur dans les processus hydrologiques. Le bilan massique montre que 88% de l'iode-129 qui entre dans le système s'y accumule annuellement, principalement dans les sols organiques.

L'eau des précipitations ainsi que les eaux souterraines de Vancouver ont également été échantillonnées suite à l'accident nucléaire Fukushima-Daiichi, afin d'évaluer l'iode-129 comme un marqueur potentiel pour la recharge des eaux souterraines. Immédiatement après l'accident nucléaire, les concentrations de ^{129}I dans les précipitations ont été multipliées par 7 comparativement aux niveaux de base. Les échantillons d'eaux souterraines ont montré une augmentation des concentrations d'iode-129 à une vitesse correspondant aux temps de recharge attendus. Ceci indique que l'iode-129 libéré par l'accident nucléaire a pu être transporté dans les eaux souterraines avec très peu de retard, probablement par les chemins d'écoulement préférentiels.

ACKNOWLEDGMENTS

My Ph.D. has been a fantastic six years and I really mean that.

I am truly thrilled to be finished, proud of what I have accomplished and the personal growth of the last 6 years. On the other, I am sad to move on from uOttawa and the great department I have been privileged to be a part of and the great people I have worked with, complained with and shared a few beers with. I'm a different person now than when I started.

Ian, your patience, guidance, and infectious enthusiasm for our work has kept me motivated and inspired. I have enjoyed working with you tremendously and your mentorship and readiness to explore new avenues and questions has taught me so much about how to be a scientist and how to keep an open mind while still questioning what I see. The experience of going to the Yukon three times, using an AMS, and building a lab is something that I'll never forget.

Jack, thank you for your unceasing encouragement, open door policy, and willingness help me when the going got tough. Your help has been truly invaluable to the completion of this thesis and I have really enjoyed working together. Every time we speak I learn something from you. You have been a wonderful mentor.

Liam and Xiao-lei, thank you for making this thesis possible. Your expertise and guidance making ^{129}I measurements was incredible and more importantly your patience in explaining the in's and out's of AMS to a geologist was saint-like.

To the Jan Veizer Stable Isotope Lab: Paul, Patricia, and Wendy for putting up with me taking your space and stuff as well as always being ready with a helpful suggestion or a kind word. Paul your sense of humour is fantastic. Also, keep channeling the spirit of Paul Coffey when you play and thanks for bringing me into Gang de Gars! I loved every minute of it. I swear I'll get that bottle of wine to you soon….

Nimal, Ping and Smita: thank you for your help, all of the analyses and patience explaining the workings of ICP-MS to me. Monika, thank you for help with many, many samples over the years and for keeping me organized.

To Martin, thanks for making Chapter 5 possible. It was great working with you!

Mom, Dad and Meg thank you for encouraging and inspiring me. Your support when I decided that I wanted to be a geologist by taking me to KRFC club meetings and on field trips, putting up with a house full of rocks is the reason why I am a geologist today and why I love science. I could never have done this PhD without your support.

Kim, Clyde and Bob thank you so much for your encouragement and support over the past 5 years. You have really made me feel like part of your family throughout my time in Ottawa and on Garden Island, which became my sanctuary and where I always am able to refresh and relax my mind. Some of my best work happened in the Sail Loft.

To my former housemate Chris "Brensy" Brens, you're a fantastic guy and friend. Thank you for always brightening my day by just being you and for introducing me to the delightful, although murderous world of Midsomer. Barnaby is the best!

Nathan S, John J, Nick U, Mike P, Mel, Laurianne, Natalia, Anthony, Grinter, Shamus, Colt and other office mates and friends throughout the years you all made my time here so much more enjoyable by always being up for a hike or a talk and more importantly a beer.

To Helene, Caroline and Lisa thank you for helping me navigate the intricate and confusing world of uOttawa bureaucracy. I wouldn't have known how to do anything from register for a course, switch from MSc to PhD or even submit my thesis without your patience and help.

Gilles, thank you for applying your insatiable curiosity to helping me solve my analytical problems. Your ability to understand literally everything is astounding and I really appreciated your willingness to help and always excellent suggestions.

To my examiners, thank you for your careful and considered evaluation of my thesis. You have truly improved it. I can't believe you actually all read this thing.

Finally, Laura, you deserve a huge part of the credit for this thesis. You kept me sane, happy and supported every second. You put up with my nonsense after a bad day, and kept me focused and motivated through the good and the bad. I could never have succeeded without you.

CHAPTER 1 – INTRODUCTION, SCOPE AND OBJECTIVES

1.1 Isotopes of Iodine

There are two isotopes of iodine that occur ubiquitously throughout the environment. ^{127}I is the only stable isotope and ^{129}I is the only long lived radioactive isotope [*Hou et al.*, 2009]. There are numerous additional iodine isotopes that can be produced through anthropogenic nuclear activities, spontaneous fission reactions or which existed as primordial isotopes (Table 1.1). ^{131}I is a short lived isotope that poses a high radiological risk should releases occur due to its short half-life (8.04 days) and relatively high energy gamma emissions, and its biophilic nature.

Isotope	Mass	Half Life	Decay Modes, Radiations, Major Energies (MeV), Absolute Intensities
^{124}I	123.9	4.18 d	EC; β+ 2.1, 1.5; γ 0.60272 (61.1% A), 0.72278 (10.1% A), 1.50949 (3.02% A), 1.69102 (10.5%A)
^{125}I	124.9	60.14 d	EC; γ 0.03546 (6.67%A)
^{126}I	125.9	13.02 d	EC; β+ 1.1; β- 0.86, 1.2; γ 0.3885 (32%A), 0.4920 (1.9% A), 0.6662 (29.1% A), 0.7537 (3.7%A)
^{127}I	**126.9**	**STABLE**	**----------**
^{129}I	**128.9**	**1.57 x10^{7} y**	**β- 0.15; γ 0.03958 (7.50% A)**
^{131}I	130.9	8.04 d	β- 0.61, 0.33; γ 0.080183 (2.62% A), 0.284298 (6.06% A), 0.364480 (81.2% A), 0.636973 (7.27% A), 0.722893 (1.80% A)

Table 1.1: Table of Iodine Isotopes (with half lives over 1 day)

1.1.1 Iodine-127

Iodine-127 is a necessary micronutrient for humans. As such iodine deficiency is considered a serious public health issue throughout the world [*de Benoist et al.*, 2004]. Iodine is essential for hormone production in the thyroid gland, which when iodine deficient, can lead to impaired thyroid function. In adults and children this can result in goiter, impaired mental

function, increased susceptibility to nuclear radiation via ^{131}I absorption and developmental delays [*de Benoist et al.*, 2004].

1.1.2 Iodine-129

^{129}I is the longest lived isotope of iodine and has a half life of 1.57×10^7 years and decays through β^- decay into ^{129}Xe, which is stable [*Hou et al.*, 2009]. The natural abundance of ^{129}I is negligible with respect to ^{127}I, which makes up 100% of the global iodine inventory. However, despite representing a miniscule fraction of the global iodine inventory, ^{129}I is studied due to the extensive environmental contamination that has taken place, its potential as a tracer of earth processes and its importance as a long lived fission product in radioactive waste.

1.2 Sources and Levels of ^{129}I in the Environment

1.2.1 ^{129}I in Pre-Nuclear Age Materials

Few measurements of ^{129}I in pre-nuclear age materials have been successfully performed. Pre-nuclear concentrations of ^{129}I in the environment have been estimated based on natural cosmogenic and geogenic production. The estimated $^{129}I/^{127}I$ ratio in the oceans from natural sources was 1.5×10^{-12} based on analysis of shallow marine sediment and seaweed [*Snyder et al.*, 2010]. An estimate based on cosmogenic and geogenic inputs yielded a $^{129}I/^{127}I$ range from $0.3 - 3 \times 10^{-12}$ [*Fabryka-Martin et al.*, 1985]. An estimated marine concentration of ^{129}I was 0.44×10^6 atoms/L [*Snyder et al.*, 2010], which results in total mass of ~130 kg of ^{129}I in the pre-nuclear ocean. The ^{129}I concentration in freshwater is estimated to be 0.037×10^6 atoms/L. Thus, the total mass of iodine in global freshwater reservoirs was estimated to be 11 kg [*Snyder et al.*, 2010]**.** The few pre-nuclear age soil

samples that have been measured yield $^{129}I/^{127}I$ ratios ranging from 0.57-16.8 x 10^{-11} [*Szidat et al.*, 2000]. *Wallner et al.*, 2007 measured the $^{129}I/^{127}I$ ratio in a Tertiary lignite sample to range from 6 - 22 x 10^{-12}. A recent measurement of bulk coral found a $^{129}I/^{127}I$ ratio of 48 x 10^{-12} [*Hou et al.*, 2010] and previous coral samples of pre-bomb age were around 0.5 x 10^{-12} . Many of these measurements are greater than the pre-nuclear age estimate for the $^{129}I/^{127}I$ ratio suggesting that a truly accurate analysis of pre-nuclear $^{129}I/^{127}I$ has yet to be performed due to difficulties obtaining reagents without ^{129}I contamination or contamination during sampling.

1.2.2 Geogenic Production of ^{129}I

^{129}I is produced in the subsurface primarily through the spontaneous fission of ^{238}U. Thus, the rate of in situ ^{129}I production varies based on the ^{238}U concentration of the host rocks or fluids. The spontaneous fission yield of ^{129}I from ^{238}U is 0.0003% [*Sabu*, 1971]. Neutron induced fission of ^{235}U, and neutron activation or spallation of ^{128}Te and ^{130}Te can also produce ^{129}I [*Fabryka-Martin*, 1988; *Andrews et al.*, 1989; *Fabryka-Martin et al.*, 1989]. In fractured basalt that has a concentration of 1 mg/kg U the ^{129}I porewater concentration at secular equilibrium, which is reached in 78 million years, is 3.8 x 10^{8} atoms/L [*Bottomley et al.*, 2002]. However, each bedrock system will vary based on factors such as porosity, the ^{238}U concentration and the calculated emanation efficiency of ^{129}I from the rock to pore fluids [*Fabryka-Martin et al.*, 1989; *Bottomley et al.*, 2002].

1.2.3 Cosmogenic Production of ^{129}I

^{129}I is naturally produced through the spallation of stable Xe isotopes by bombardment of high energy cosmic ray nucleons in the upper atmosphere (Fabryka-

Martin et al., 1987). The effective environmental cross section for the production of ^{129}I is 10 mbarn, which yields a steady state surface density of 10^6 atoms/cm^2 [*Edwards*, 1962]. Very little has been published on the production of ^{129}I by spallation reactions and therefore the rate of production and the corresponding rate of fallout/rainout solely from cosmogenic production have never been measured accurately.

1.2.4 Anthropogenic Production of ^{129}I

Since 1950, when nuclear weapons testing and the use of nuclear energy increased, anthropogenic emissions of ^{129}I have been the dominant source in the environment [*Englund et al.*, 2008]. This has caused the ratio of $^{129}I/^{127}I$ to increase dramatically from calculated and measured pre-nuclear ratios of 10^{-15} to 10^{-12} up to 10^{-10} to 10^{-4} in many types of environmental samples [*Hou et al.*, 2009; *Snyder et al.*, 2010]. Correspondingly, the ^{129}I concentrations in most environmental samples have also increased considerably, particularly in Europe, which has several ^{129}I point sources (Table 1.2) [*Reithmeier et al.*, 2006]. The largest modern releases have come from La Hague, France and Sellafield, UK, which emit ^{129}I to the atmosphere and release it into the ocean (Table 1.2). The total mass of ^{129}I added to the hydrosphere by reprocessing has been estimated to be approximately 5,400 kg, far surpassing the estimated natural inventory of ~250 kg or less [*Rao and Fehn*, 1999; *Snyder et al.*, 2010]. Most of the fuel reprocessing plants currently in operation are located in the northern hemisphere resulting in significantly elevated ^{129}I concentrations in the northern hemisphere compared to the southern [*Negri et al.*, 2013]. Nuclear weapons testing and nuclear accidents have also contributed some ^{129}I to the environment since the start of the atomic age. Nuclear weapons testing has contributed about 50 kg of ^{129}I to the

atmosphere [*Oktay et al.*, 2000]. In addition to fuel reprocessing and weapons testing ^{129}I has been released by nuclear accidents such as Chernobyl and Fukushima [*Paul et al.*, 1987; *Xu et al.*, 2013]. It is estimated that Chernobyl released ~1.3 kg and Fukushima ~1.2 kg of ^{129}I to the atmosphere.

Country	Site	Operation		Processing Capacity (t U/yr)		^{129}I Emitted (kg)		Reference
		Start	End	Present	Future	Liquid	Atmosphere	
Belgium	MOL	1966	1975			ND	ND	
China	Jiuquan	?			25	ND	ND	
	Lanzhou	2020			800	ND	ND	
France	Marcoule	1958	1997			46	184	[*Reithmeier et al.*, 2006, 2010]
	La Hague	1967			1600	3169	67	[*Reithmeier et al.*, 2006]
Germany	Karlsruhe	1971	1990			ND	ND	
India	Trombay	1964		60	60	2.5	ND	
	Tarapur	1974		100	100	ND	ND	
	Kalpakkan	1988		100	100	ND	ND	
Japan	Tokai-mura	1977		90	90		~1	[*Toyama et al.*, 2012]
	Rokkasho-mura	2005			800	ND	ND	
Russia	Chelyabinsk	1971	1986	400	400		161	[*Reithmeier et al.*, 2010]
	Krasnoyarsk	2020			1500		21	[*Reithmeier et al.*, 2010]
	Seversk	1956	1995				35	[*Reithmeier et al.*, 2010]
UK	Sellafield	1967		900	2700	1378	153	[*Rao and Fehn*, 1999]
	Dounreay	1980	2001			ND	ND	
US	West Valley	1966	1972				11	[*Rao and Fehn*, 1999]
	Hanford	1956	1989		2300		81	[*Reithmeier et al.*, 2010]
	Savannah River	1954	1989		2700		41	[*Reithmeier et al.*, 2010]
	Idaho Falls	1959	1992			ND	ND	
Accidents	Chernobyl						1.3	[*Paul et al.*, 1987]
					Total	**4593**	**757**	

Table 1.2: Locations, operation window, reprocessing capacity and estimates of ^{129}I released by the major nuclear fuel reprocessing facilities around the world. ND represents facilities for which ^{129}I estimates were not available. Table is modified from [*IAEA*, 2005].

1.3 Environmental Reservoirs and Cycling of ^{129}I

1.3.1 Iodine Cycling

Iodine moves throughout the environment readily and both ^{127}I and ^{129}I are found in all environmental reservoirs (Figure 1.1). Iodine is a redox sensitive element and may be found as a variety of species depending on local pH and redox conditions many of which are soluble or volatile (Figure 1.2). The most common inorganic species of iodine are I^- (iodide), IO_3^- (iodate) and I_2 (elemental iodine). However, due to its biophilic nature, numerous organic forms, such as humic and fulvic acid complexes or volatile hydrocarbon species such as CH_3I are also very common. Because of the variety of iodine species and their occurrence in all parts of the geosphere a detailed understanding of its geochemical behavior is essential in order to predict the transport and fate of ^{129}I as an environmental contaminant and tracer.

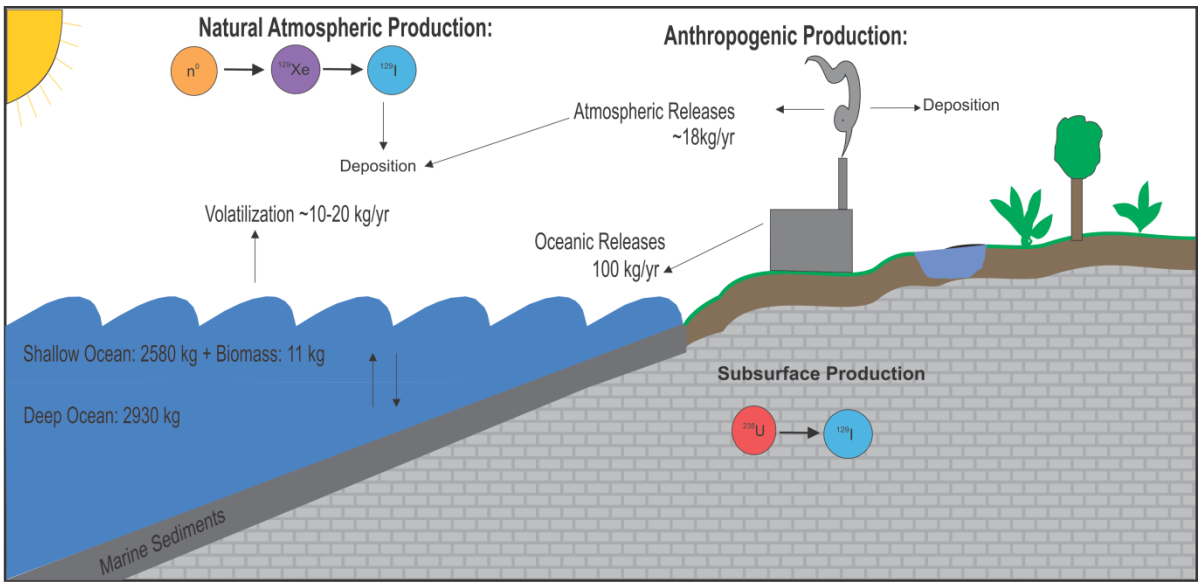

Figure 1.1: Conceptual model showing the cycle and approximate mass fluxes of ^{129}I between environmental reservoirs as well as the mechanisms of natural and anthropogenic production.

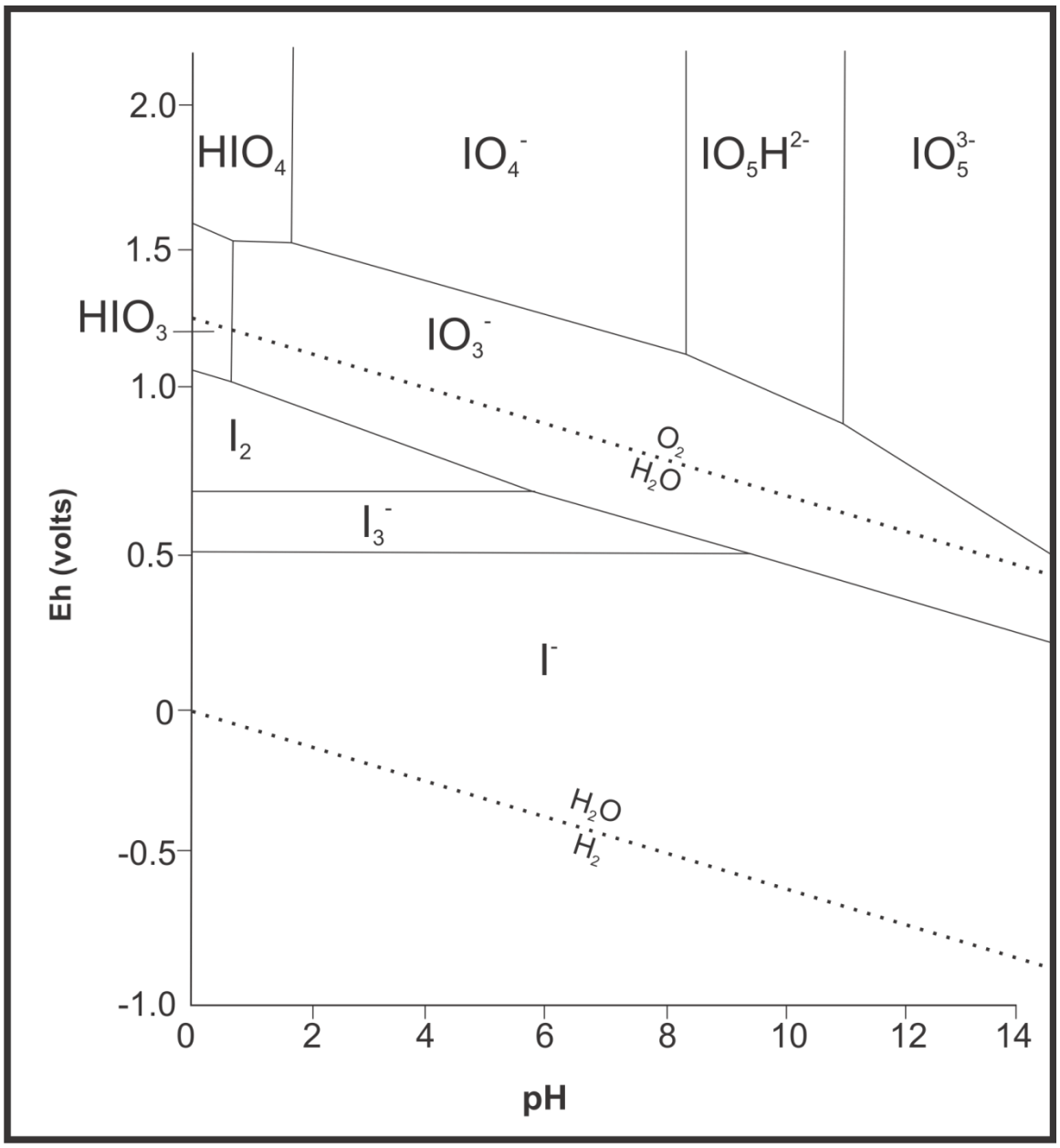

Figure 1.2: eH-pH diagram showing the inorganic speciation of iodine in the environment.

1.3.2 ^{129}I in the Oceans

The largest reservoir of ^{129}I and ^{127}I on Earth is the oceans which store approximately 70% of the global inventory [*Hou et al.*, 2009]. The residence time of iodine in the oceans is approximately 300,000 years [*Fehn et al.*, 1990] and given that the general ocean mixing time is approximately 1,600 years this has resulted in extensive mixing of ^{127}I

and pre-nuclear ^{129}I [*He et al.*, 2013]. Indeed, depth profiles of ^{127}I in the ocean have shown that concentrations are relatively uniform [*Tsunogai*, 1971]. However, as large quantities of ^{129}I have been added to the ocean over the past 60 years by weapons testing and fuel reprocessing, there has been a substantial increase in ^{129}I concentrations and the ^{129}I/^{127}I ratio, particularly at the ocean surface (Figure 1.3, Figure 1.4) [*Raisbeck and Yiou*, 1999; *He et al.*, 2013]. Indeed, ^{129}I concentrations in the North Atlantic have reached up to 10^{12} atoms/L [*He et al.*, 2013]. These increases have been particularly noticeable around Northern Europe due to nearby reprocessing facilities, Sellafield and La Hague, which both discharge into the Atlantic Ocean where currents distribute these ^{129}I inputs allowing its use as a tracer of ocean currents [*Raisbeck et al.*, 1995; *Smith et al.*, 1999, 2011].

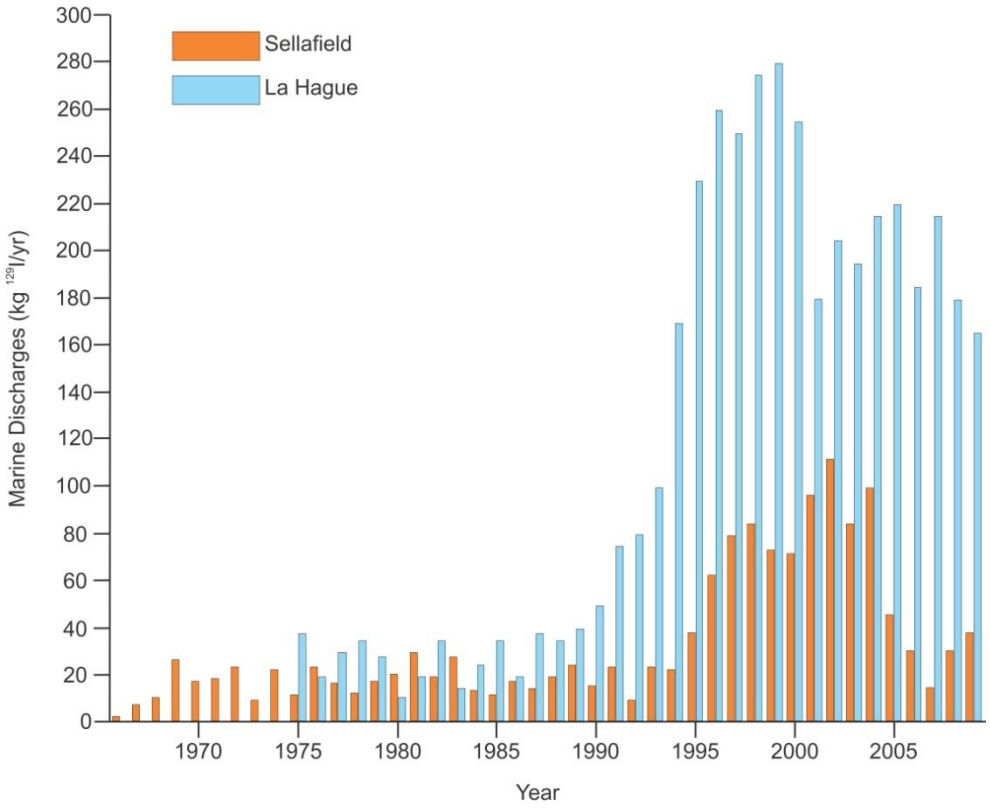

Figure 1.3: Liquid discharges from the Sellafield and La Hague nuclear fuel reprocessing sites which are the two largest contributors of ^{129}I to the environment. Modified from [*He et al.*, 2013]

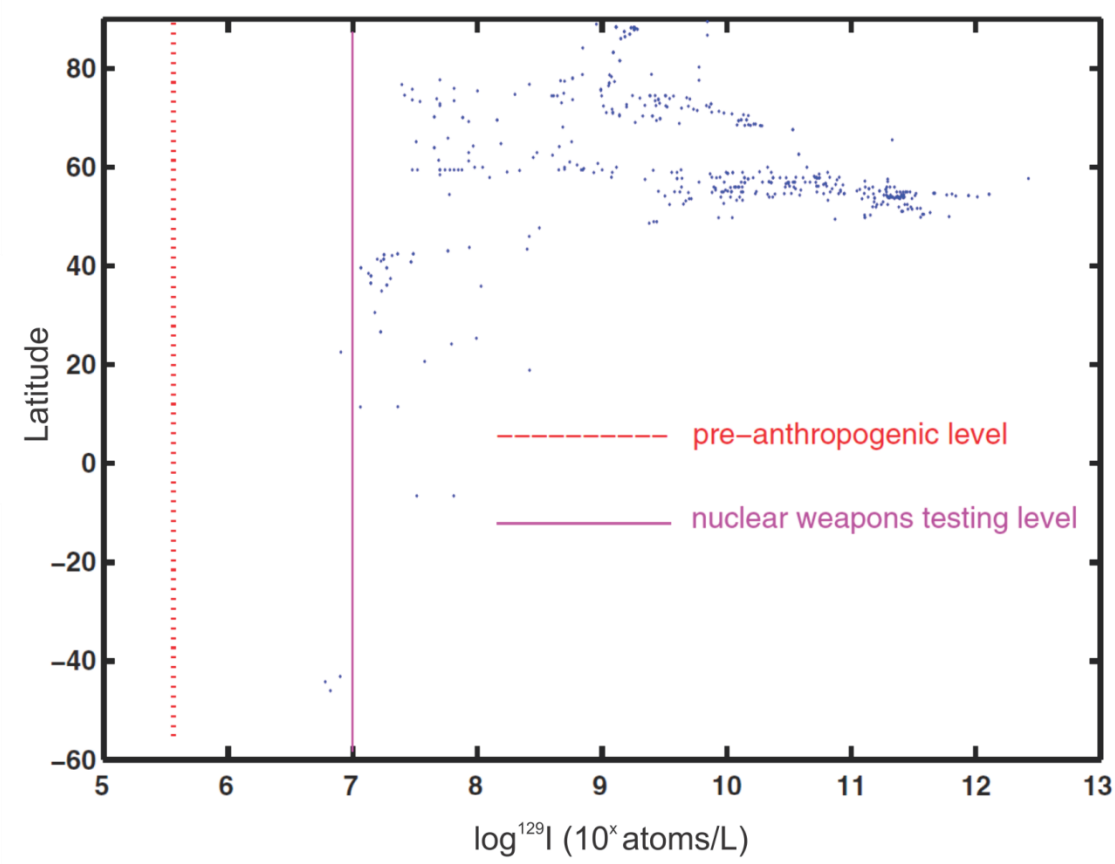

Figure 1.4: Distribution of ^{129}I in marine water as a function of latitude. Modified from [*He et al.*, 2013]

1.3.3 ^{129}I in Surface Water and Groundwater

In surface freshwater, such as lakes and rivers, iodine usually exists as iodate, iodide or organic iodine based on the local pH and redox conditions. Numerous studies have shown that natural sources provide a negligible input of ^{129}I and that most ^{129}I is contamination from anthropogenic sources that has been transported atmospherically and deposited in precipitation and dry fallout [*Aldahan et al.*, 2007; *Snyder et al.*, 2010; *Chen et al.*, 2015]. Many of the ^{129}I measurements in freshwater have been done near point sources and show significant increases in ^{129}I concentration and a concomitant increase in the ^{129}I/^{127}I ratio [*Snyder and Fehn*, 2004; *Keogh et al.*, 2010]. Indeed, in Europe ^{129}I

concentrations in freshwater are typically around 10^{7} to 10^{11} atoms/L and ratios up to 10^{-6} [*Atarashi-Andoh et al.*, 2007; *Chen et al.*, 2015] and references therein. Measurements made far from point sources nevertheless show an enrichment of at least 1-2 orders of magnitude in their ^{129}I concentration and ratio due to long distance transport of NFRP emissions, ocean volatilization and atomic weapons testing [*Snyder and Fehn*, 2004; *Aldahan et al.*, 2006] (Figure 1.5). In North America concentrations and ratios are lower and usually range from 10^{6} to 10^{8} and 10^{-11} to 10^{-8} respectively, although levels can be substantially higher near point sources such as West Valley, New York; Hanford, Washington, Idaho Falls National Labs, Idaho and Savannah River National Labs, Georgia [*Rao and Fehn*, 1999; *Moran et al.*, 2002]. Concentrations in the Southern Hemisphere are even lower and have been measured at 10^{5} to 10^{6} atoms/L with ratios of 10^{-12} to 10^{-11}, which are likely mostly due to weapons test fallout and less from ^{129}I dispersed by nuclear fuel reprocessing [*Negri et al.*, 2013]. Once deposited, ^{129}I in freshwater systems is then subject to physical hydrological and geochemical cycles that determine the hydrology and hydrochemistry of waters. Evapotranspiration in arid regions can enrich ^{129}I and ^{127}I concentrations in groundwater, rivers and lakes over precipitation by a factor of 2 to 10 [*Oktay et al.*, 2001; *Moran et al.*, 2002]. However, in less arid environments freshwater is typically depleted in ^{129}I relative to precipitation due to interactions of ^{129}I with soil, which can efficiently adsorb iodine [*Buraglio et al.*, 2001; *Reithmeier et al.*, 2007]. The cycle of ^{129}I in context with other hydrochemical tracers has not been investigated rigorously. However, a few studies have shown that ^{129}I is often associated with Cl, due to a shared input from ocean volatilization [*Moran et al.*, 2002; *Aldahan et al.*, 2006], DOC and K, due to a

contribution of ^{129}I from soil leaching as well as P and NO_3, from applications of fertilizer in rivers affected by agricultural activities [*Kekli et al.*, 2003]. Significant work remains in order to understand the geochemical cycle of ^{129}I in context with other hydrochemical tracers.

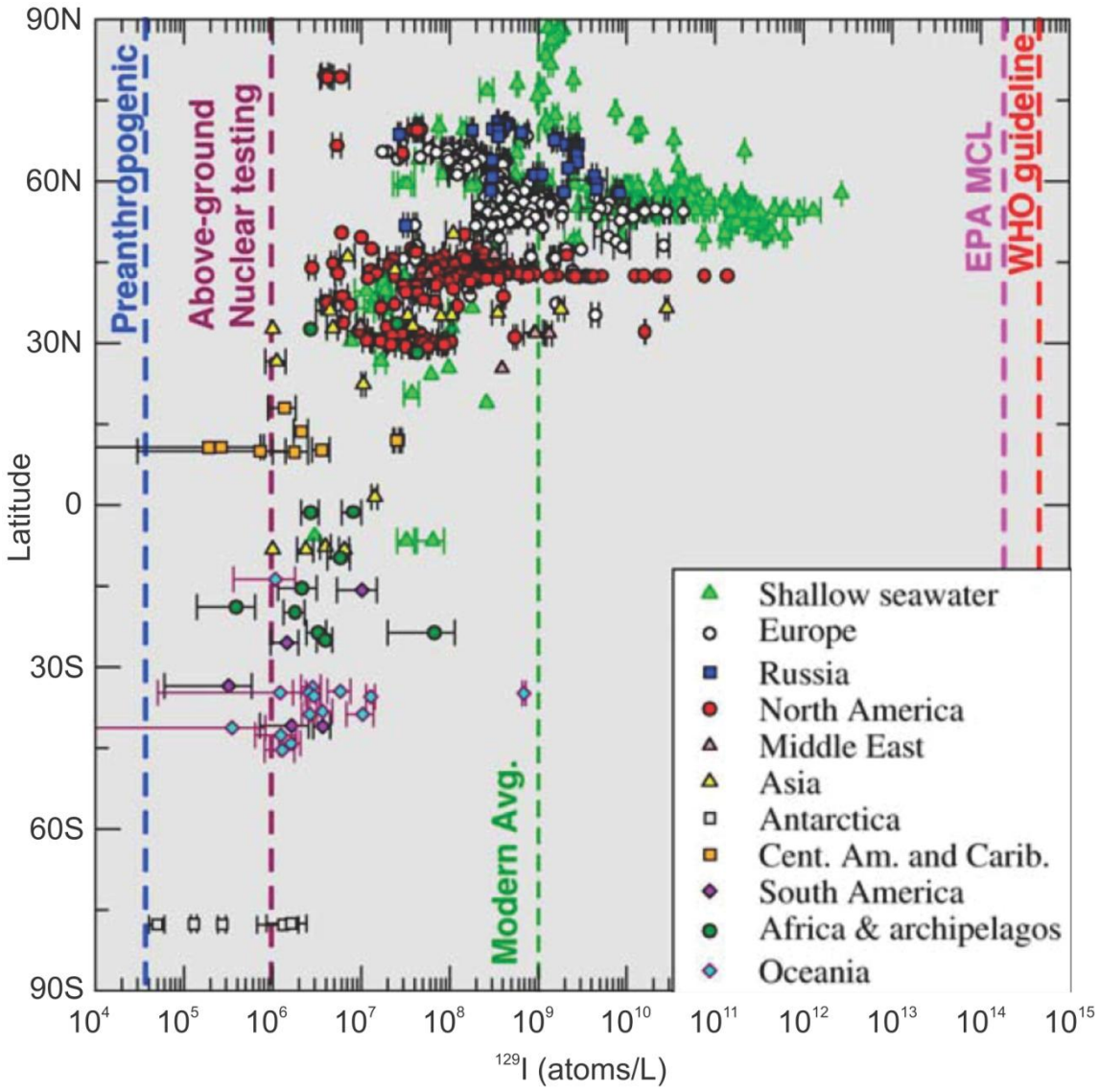

Figure 1.5: Distribution of ^{129}I in fresh water and shallow marine water as a function of latitude and delineated by continent. The gross beta activity limit for the EPA (4 mrem/yr = 1.8 x 10^{14} atoms ^{129}I/L) and the WHO guideline (10 mrem/yr = 4.5 x 10^{14} atoms ^{129}I/L) in drinking water are pictured although levels in fresh water are significantly lower. Modified from [*Snyder et al.*, 2010].

In shallow groundwater ^{129}I in recharge is primarily derived from atmospheric fallout [*Renaud et al.*, 2005]. However, ^{129}I concentrations are frequently reduced during infiltration through the vadose zone by adsorption to soils. Therefore, in order to trace ^{129}I into groundwater, soil interactions must be considered, particularly the interaction between ^{129}I and soil organic matter, which adsorbs ^{129}I much more efficiently than inorganic soils [*Alvarado-Quiroz et al.*, 2002; *Schwehr et al.*, 2009]. Studies investigating ^{129}I in shallow groundwater have found that groundwater recharged post-1950's is enriched in ^{129}I due to inputs from NFRP's and atomic weapons testing with concentrations ranging from 10^6 to 10^7 atoms/L and $^{129}I/^{127}I$ ratios of 10^{-9} to 10^{-11} in California and Southern Ontario wells [*Renaud et al.*, 2005; *Schwehr et al.*, 2005]. Furthermore, a common finding between several studies is that the ^{127}I concentration in recharge and groundwater is not significantly different while the ^{129}I concentration is much greater in recharge [*Renaud et al.*, 2005; *Schwehr et al.*, 2005]. This disequilibrium is attributed to the different sources of ^{129}I and ^{127}I which likely means these isotopes are not in the same chemical form and thus their behavior is not analogous during transport. Evapotranspiration can also play a role in concentrating ^{129}I and ^{127}I in recharge similar to other contaminants [*Schwehr et al.*, 2005].

Deep aquifers, porewater and basin brines often contain ^{129}I from non-anthropogenic sources and thus often have low ^{129}I concentrations and low $^{129}I/^{127}I$ ratios compared to modern surface water reflecting their pre-nuclear ages [*Fehn*, 2012]. However, in certain cases in-situ production of ^{129}I or mixing with other geogenically enriched water may raise ^{129}I concentrations and the $^{129}I/I$ ratio in such waters and allow their use as tracers and dating tools [*Fehn*, 2012]. In systems with trapped seawater it is

possible to use the decay of ^{129}I, which correspondingly leads to an exponential decrease in the $^{129}I/^{127}I$ ratio as a dating tool if the initial ratio is assumed to be fixed over geologic time, there are no inputs of geogenic ^{129}I and there is enough sample to measure the $^{129}I/^{127}I$ ratio without the addition of iodine carrier [*Fehn et al.*, 1990; *Fehn*, 2012]. This method has successfully been applied to oil field brines. An alternative method uses the ^{129}I ingrowth and can be used to date fluids less than 80 million years old. A minimum residence time constraint can be placed on fluids that have been in situ for greater than 80 million years. This method had been used to constrain the age of ancient pore fluids and brines [*Fabryka-Martin et al.*, 1989; *Bottomley et al.*, 2002; *Snyder and Fabryka-Martin*, 2007] and relies on modeling the in situ concentration of ^{129}I from the spontaneous fission of ^{238}U. The calculated ^{129}I concentration may then be compared to the measured value to see if secular equilibrium has been reached. If the measured ^{129}I concentration is lower than the calculated value an exact residence time may be calculated, if the two concentrations are equal the fluid is at secular equilibrium and the rate of ^{129}I production and decay are equivalent thus the fluid has been in situ for a minimum of 80 million years. If the measured concentration is higher than calculated, the fluid either mixed with a second fluid containing excess ^{129}I or has been transported from rocks enriched with ^{238}U within the last 80 million years.

1.3.4 ^{129}I in Soils

Iodine behavior in soils is complex due to the large number of factors that affect its transport and sorption. The dominant source of ^{129}I in northern hemisphere soils is atmospheric fallout but there are also contributions from the decomposition of organic

matter and potentially from soil fertilization in agricultural regions [*Moran et al.*, 2002; *Kekli et al.*, 2003; *Shetaya et al.*, 2012]. Adsorption of iodine is likely not a fractionating process and therefore, the behavior of both ^{129}I and ^{127}I in soils can generally be considered identical. The dominant factor affecting sorption and in determining the equilibrium sorption coefficient (K_d) of iodine on soils is the presence of organic matter and biological activity [*Bostock et al.*, 2003]. Indeed, numerous field and lab studies have found that iodine partitions primarily on organic matter, particularly on humic substances as part of phenol groups or as covalent C-I bonds [*Zhang et al.*, 2011]. Furthermore, adsorption on sterilized soils is significantly reduced implying that living biological activity plays a key role in retaining iodine [*Steinberg et al.*, 2008; *Söderlund et al.*, 2011; *Lusa et al.*, 2015]. Adsorption of iodine on organic matter can also occur as anion exchange following a linear isotherm [*Sheppard et al.*, 1996]. There are numerous other factors that also influence the sorption behavior of iodine particularly speciation, pH, redox, moisture content and soil mineralogy. Typically, IO_3^- is sorbed preferentially to I^- in most soils and hence factors such as pH and redox can greatly influence sorption as they affect iodine speciation [*Fukui et al.*, 1996; *Söderlund et al.*, 2011]. Due to the difference in sorption behavior of I^- and IO_3^- they have different residence times in soils [Hu et al., 2005]. In addition, soils with low moisture content, which are typically oxic, tend to adsorb iodine more efficiently than more saturated soils in which anoxic conditions prevail resulting in lower bioavailability and a greater proportion of I^-, which is adsorbed less readily [*Sheppard and Hawkins*, 1995; *Ashworth and Shaw*, 2006]. pH conditions in soils also greatly affect sorption. As pH increases iodine sorption tends to decrease for both I^- and IO_3^-, although the decrease is

more pronounced for I^- [*Fukui et al.*, 1996]. The influence of pH is explained by the higher positive surface charge on particles at low pH resulting in more efficient adsorption [*Fukui et al.*, 1996]. Soil mineralogy can also affect iodine sorption. Aluminum and iron oxides are the most important inorganic adsorbents of iodine and act most strongly below pH 6 [*Whitehead*, 1974].

Anthropogenic releases of ^{129}I have contaminated soils around the globe, particularly in the vicinity of ^{129}I point sources. Within soils both ^{127}I and ^{129}I are typically partitioned preferentially into the organic fraction such as humic and fulvic acids or organic residues compared to inorganic solids, oxides and the surface adsorbed fraction (Figure 1.6) [*Englund et al.*, 2010b; *Hansen et al.*, 2011; *Luo et al.*, 2013]. Soils in Europe, near Chernobyl, which are most heavily contaminated, have ^{129}I concentrations up to 10^9 atoms/g and $^{129}I/^{127}I$ ratios as high as 10^{-7} particularly in near surface soils, which is 5 orders of magnitude higher than the estimated pre-nuclear ratio of 1.5×10^{-12} [*Strachnov et al.*, 1996; *Englund et al.*, 2010b; *Hansen et al.*, 2011]. More remote soils, such as those in Asia and North America, have ^{129}I concentrations around 10^6 to 10^8 atoms/g and $^{129}I/^{127}I$ ratios around 10^{-11} to 10^{-8} depending on their composition, proximity to a current ^{129}I point source and the degree of contamination from nuclear weapons fallout [*Oktay et al.*, 2000; *Muramatsu et al.*, 2008; *Luo et al.*, 2013].

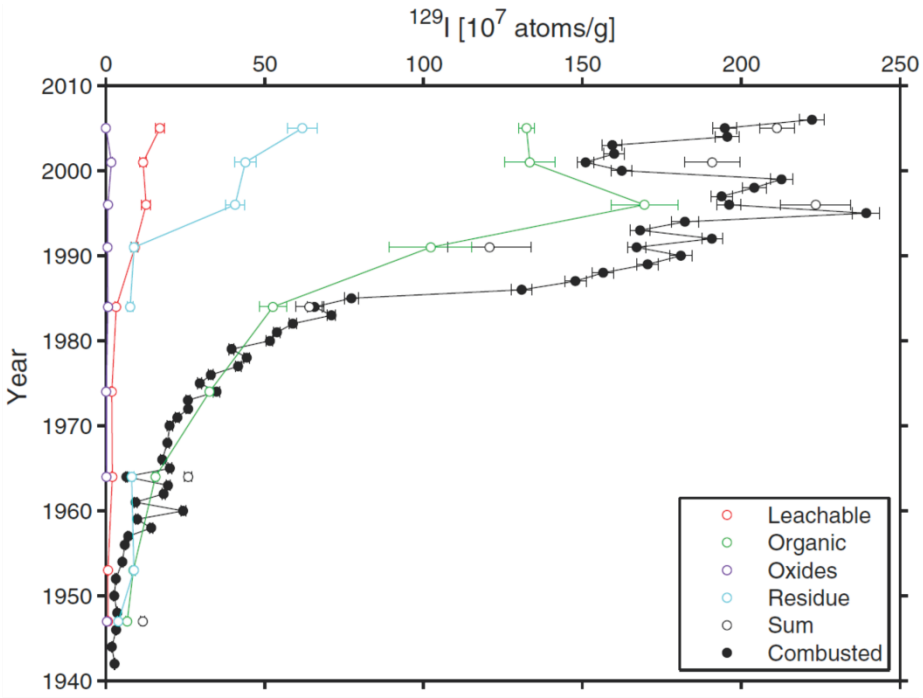

Figure 1.6: Depth profile of ^{129}I concentrations in sediment fractions and their sum as well as the result of combustion of the total sample. The majority of ^{129}I was found in the organic fraction and the combustion results agreed well with the sum of each sediment component. Modified from [*Englund et al.*, 2010b]

1.3.5 ^{129}I in the Atmosphere and Precipitation

Atmospheric transport is one of the principal dispersal mechanisms of iodine in the environment and can spread emissions of ^{129}I great distances from point sources in short periods of time. An example of such rapid transport is Fukushima in which ^{131}I was detected 1000's of kilometers away within only a few weeks [*Wetherbee et al.*, 2012; *Health Canada*, 2014].

The principal source of iodine to the atmosphere is the volatilization of iodine from the ocean surface by inorganic photochemical reactions and more importantly microalgal transformation of iodine to volatile species such as I_2, CH_3I, CH_2IX, etc. [*Carpenter*, 2003; *Saiz-Lopez et al.*, 2012] with ~50% as organic species, most commonly CH_3I [*Jabbar et al.*,

2013] (Figure 1.7). It is believed that the majority of atmospheric iodine is from this source (~550 Gg/yr) as opposed to anthropogenic releases from fossil fuel combustion and terrestrial sources (80-110 Gg/yr) [*Carpenter*, 2003; *Saiz-Lopez et al.*, 2012]. This means that ^{129}I releases to the ocean from nuclear fuel reprocessing that are volatilized can be equally or more important for depositing ^{129}I terrestrially [*Englund et al.*, 2010a].

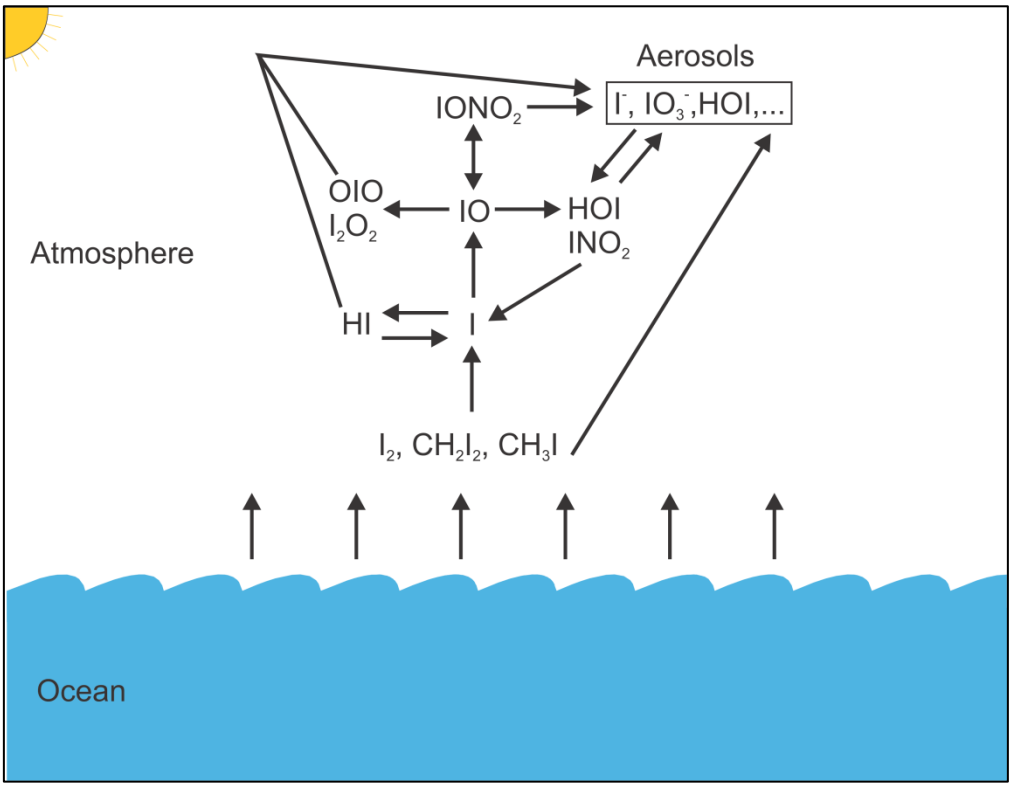

Figure 1.7: Simplified reaction pathways for the volatilization and speciation of iodine from the ocean surface via photolysis or as an aerosol. Modified from [*Carpenter*, 2003]

The residence time of total iodine in the atmosphere is approximately 2-3 weeks [*Moran et al.*, 1999; *Jabbar et al.*, 2013] allowing global dispersal and mixing of ^{129}I releases. This has resulted in a standing crop of ~0.7 kg of ^{129}I in the northern hemisphere at any given time which is likely renewed annually [*Moran et al.*, 1999; *Buraglio et al.*, 2001].

Atmospheric gaseous iodine is subject to sorption by aerosols and removal by rainfall and gravitational settling as dry fallout. The fallout of iodine represents a critical transport mechanism of iodine to the ground surface and its subsequent partitioning into freshwater, soil, plants, etc. [*Moran et al.*, 2002]. The dominant fallout mechanism is as rainout, also referred to as washout, which constitutes ~60-80% of ^{129}I mass deposition with the remainder as dry fallout [*Englund et al.*, 2010a]. The global mass deposition of ^{129}I has been measured and modeled and is highest near ^{129}I point sources with precipitation corrected annual fallouts of 10^{11} to 10^{14} atoms/m^2 throughout Europe (Figure 1.8) [*Reithmeier et al.*, 2010]. In regions far from point sources such as most of North America and the southern hemisphere ^{129}I fallout rates are expected to be lower with model predictions around 10^{11} atoms/m^2 or less [*Reithmeier et al.*, 2010]. ^{129}I concentrations in precipitation in Europe, close to nuclear fuel reprocessing plants have been found as high as 10^{10} atoms/L and average 10^9 [*Persson et al.*, 2007; *Keogh et al.*, 2010]. In more remote regions, such as North America and the southern hemisphere, ^{129}I concentrations are 10^6 to 10^7 atoms/L [*Moran et al.*, 1999]. Time series of precipitation have shown that concentrations of ^{129}I are highly variable from event to event depending on the point of origin of the air mass [*Persson et al.*, 2007].

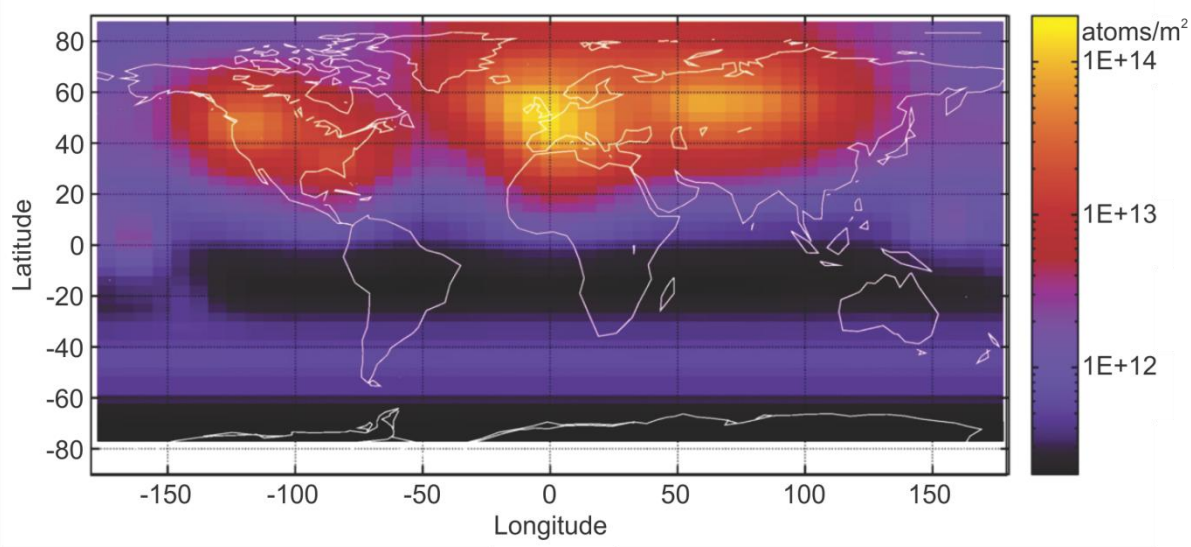

Figure 1.8: Calculated mass deposition of ^{129}I from global atmospheric emissions from atomic weapons testing, nuclear fuel reprocessing plants in Europe, Russia and the USA as well as re-emission from the ocean surface. These are mean values that have not been corrected for local precipitation rates before direct comparison to measured ^{129}I mass deposition. Modified from [*Reithmeier et al.*, 2010].

1.4 Objectives

As an anthropogenically and naturally produced radionuclide with a long half life ^{129}I has been identified as both a contaminant and potential tracer [*Edwards*, 1962; *Fabryka-Martin et al.*, 1985]. However, ^{129}I behavior in natural systems is complex and much of the ^{129}I system remains to be explored with respect to other geochemical cycles, particularly for its storage and mass transfer. Such additional knowledge will foster our understanding of outcomes from future anthropogenic releases and to safely contain ^{129}I produced by radioactive waste in long term storage facilities over geologic time scales. This will also allow ^{129}I to realize its full potential as a tracer [*Nimz*, 1998].

The primary objective of this thesis is to understand the sources and cycling of ^{129}I in a variety of watersheds. A further objective is to quantify mass fluxes, transport and

storage of ^{129}I to elucidate its sources and fate at sites remote from point sources after it has integrated within ongoing elemental cycles. These objectives will be addressed by:

1. Quantifying the background and mass fluxes of ^{129}I in a variety of rivers and soils in the Yukon Territory, which is distal from any anthropogenic sources of ^{129}I. The impact of the Fukushima-Daiichi Nuclear Accident on these remote catchments is also discussed.
2. Investigating the ^{129}I fallout in precipitation from the Fukushima-Daiichi Nuclear Accident and using this time-constrained input into groundwater to understand ^{129}I interactions with soils during recharge.
3. Measuring a time series of ^{129}I in discharge from a single, well studied, watershed in the Yukon as well as a large suite of other isotopic and geochemical parameters and performing a ^{129}I mass balance. This information can be used to place ^{129}I variations into context with the hydrogeochemistry and water sources of discharge and evaluate the flowpaths of ^{129}I and its potential as a tracer.
4. Factors affecting the cycle and storage of ^{129}I will also be quantified in surface reservoirs allowing the long term fate of ^{129}I to be determined.

Collectively this work will allow predictions to be made about the sources, transport and accumulation of ^{129}I in remote regions and its participation in other geochemical cycles such as the water and carbon cycles which will enhance our understanding of its environmental partitioning and the usefulness as a tracer.

1.5 Scope of Work

This thesis is composed of five chapters each representing a distinct project linked by the previously discussed objectives.

Chapter 2 consists of a new methodological development for the extraction of ^{129}I from organic and inorganic solids. The purpose was to improve upon the methods of other researchers who use similar extraction techniques by identifying key factors that affect iodine recovery and evaluate the ability of using ^{125}I as a quantitative yield tracer. The method consists of combusting the sample under an oxygen gas flow and trapping it in a hydroxide solution, which can then be subjected to redox extraction for the production of an AgI AMS target. Several parameters were tested using ^{125}I as a yield tracer including O_2 flow rate, volatilization temperature and physical characteristics of the extraction line. Several sample types were also tested and the methodology was verified using radiolabeled humic acid and standard reference materials for ^{127}I and ^{129}I. The results of this work have been published in the peer reviewed proceedings from the radiochemistry session of the Canadian Society of Chemistry 2013 conference as: Herod, M. N., R. J. Cornett, I. D. Clark, W. E. Kieser, and G. St. Jean (2014), Extraction of ^{129}I and ^{127}I via combustion from organic rich samples using ^{125}I as a quantitative tracer., *J. Environ. Radioact.*, *138*, 323–330, doi:10.1016/j.jenvrad.2014.02.005.

Chapter 3 represents a preliminary investigation into the baseline concentrations of ^{129}I in several rivers throughout the Yukon and Northwest Territories as well as a depth profile of ^{129}I in a peat core. This work establishes a background ^{129}I concentration in a remote region, investigates possible sources for ^{129}I to the region, and compares how several watershed

characteristics affect ^{129}I transport. The results of this work have been published in the peer reviewed proceedings of the 12th International Conference on Accelerator Mass Spectrometry as: Herod, M. N., I. D. Clark, W. E. Kieser, S. Agosta, and X.-L. Zhao (2013), ^{129}I dispersion and sources in Northwest Canada, *Nucl. Instruments Methods Phys. Res. Sect. B Beam Interact. with Mater. Atoms*, *294*, 552–558, doi:10.1016/j.nimb.2012.06.018. Additionally, samples from 2011 and 2012 are discussed as an appendix in context with the effect of ^{129}I fallout from the Fukushima-Daiichi Nuclear Accident on remote Yukon catchments.

In Chapter 4 ^{129}I concentrations and the $^{129}I/^{127}I$ ratio in samples of precipitation and groundwater from the Vancouver, B.C. area are presented that were collected prior to and following the Fukushima-Daichii Nuclear Accident (FDNA). The goal of this project was to determine if ^{129}I released by the FDNA could be detected in Vancouver precipitation and when ^{129}I concentrations returned to pre-FDNA levels. The mass deposition of ^{129}I was also quantified. ^{129}I in groundwater samples from two wells in a nearby unconfined aquifer that had been previously dated using $^{3}H/^{3}He$ were also measured in order to determine if ^{129}I from FDNA could be detected in groundwater [*Wassenaar et al.*, 2006]. Vadose zone modeling using the mass deposition of ^{129}I and hydrogeologic characteristics was performed to assess the feasibility of ^{129}I from FDNA recharging local groundwater. The results of this study provide a holistic look into the long term transport and fate of ^{129}I in the environment and can be used to evaluate ^{129}I as a tracer of groundwater recharge. This work has been accepted by Water Resources Research for publication.

Chapter 5 presents a multivariate approach to understanding the cycle and storage of ^{129}I in a discontinuous permafrost watershed in the Yukon. A time series of water samples from thaw to freeze up were collected as were precipitation and soil samples from throughout the watershed. Samples were then analyzed for a large suite of isotopes and elements including ^{129}I and ^{14}C. The multivariate statistical techniques principal components analysis and agglomerative hierarchical clustering were then used to reveal underlying relationships between analytes and samples. These data were used to interpret the hydrochemical evolution of discharge over the year and identify the water sources contributing to discharge. The ^{129}I results could then be interpreted in light of the hydrologic interpretation to reveal the geochemical behavior and sources of ^{129}I in an extremely rigorous manner. A mass balance of ^{129}I for the watershed was also performed using the precipitation and soil data. Gaining a detailed understanding the geochemical behavior of ^{129}I in the catchment over the course of a year allowed us to evaluate its potential as a hydrologic tracer. Furthermore, from the perspective of radioactive waste disposal understanding the cycle and fate of ^{129}I is of great importance. It is the intention of the author to submit this work to a relevant peer-reviewed journal in the coming months.

1.6 Contributions by Manuscript Collaborators

The majority of the laboratory work, data collection and interpretation were done by the author (MH). However, work presented in these chapters was conducted in collaboration with several other researchers. Their contributions to each chapter are outlined below.

Chapter 2: The implementation of the gamma spectrometry technique based on the work of [*Horrocks and Klein*, 1974] was done by Jack Cornett. The design of the combustion line and subsequent adjustments were done collaboratively by MH, Jack Cornett and Gilles St. Jean.

Chapter 3: Samples were collected by MH and IDC. Solid sample extractions via caustic fusion were done by Monika Wilk and Sarah Agosta.

Chapter 4: Samples of precipitation and groundwater were collected by Martin Suchy. Martin Suchy also participated in data interpretation and wrote the section on sample collection. Jack Cornett assisted with the statistical analysis and interpretation of data.

Chapter 5: Water samples were collected by volunteers from Whitehorse, Yukon. Some of the sample analysis and the initial interpretation of Wolf Creek hydrology was done by Tianjiao Li and incorporated into her master's thesis [*Li*, 2013]. Andre Pellerin assisted with data interpretation and manuscript organization.

Editorial reviews on all chapters were done by Ian Clark with contributions from Jack Cornett, Liam Kieser, Martin Suchy, Andre Pellerin and Gwynn Graham.

References

Aldahan, A., A. Kekli, and G. Possnert (2006), Distribution and sources of 129I in rivers of the Baltic region., *J. Environ. Radioact.*, *88*(1), 49–73, doi:10.1016/j.jenvrad.2006.01.003.

Aldahan, A., V. Alfimov, and G. Possnert (2007), 129I anthropogenic budget: Major sources and sinks, *Appl. Geochemistry*, *22*(3), 606–618, doi:10.1016/j.apgeochem.2006.12.006.

Alvarado-Quiroz, N. G., T. G. Kotzer, G. M. Milton, I. D. Clark, and D. Bottomley (2002), Partitioning of 127I and 129I in an unconfined glaciofluvial aquifer on the Canadian shield, *Radiochim. Acta*, *90*(8), 469–478.

Andrews, J. N., S. N. Davis, J. Fontes, B. E. Lehmann, and H. H. Loosli (1989), The in situ production of radioisotopes in rock matrices with particular reference to the Stripa granite, *Geochim. Cosmochim. Acta*, *53*, 1803–1815.

Ashworth, D. J., and G. Shaw (2006), Effects of moisture content and redox potential on in situ Kd values for radioiodine in soil., *Sci. Total Environ.*, *359*(1-3), 244–54, doi:10.1016/j.scitotenv.2005.04.018.

Atarashi-Andoh, M. et al. (2007), 129I/127I ratios in surface waters of the English Lake District, *Appl. Geochemistry*, *22*(3), 628–636, doi:10.1016/j.apgeochem.2006.12.008.

De Benoist, B., M. Andersson, I. Egli, B. Takkouche, and H. Allen (2004), *Iodine status worldwide: WHO Golbal Database on Iodine Deficiency*.

Bostock, A. C., G. Shaw, and J. N. B. Bell (2003), The volatilisation and sorption of 129I in coniferous forest, grassland and frozen soils., *J. Environ. Radioact.*, *70*(1-2), 29–42, doi:10.1016/S0265-931X(03)00120-6.

Bottomley, D. J., R. Renaud, T. G. Kotzer, and I. D. Clark (2002), Iodine-129 constraints on residence times of deep marine brines in the Canadian Shield, *Geology*, *30*(7), 587–590.

Buraglio, N., A. Aldahan, Gö. Possnert, and I. Vintersved (2001), 129I from the Nuclear Reprocessing Facilities Traced in Precipitation and Runoff in Northern Europe, *Environ. Sci. Technol.*, *35*(8), 1579–1586, doi:10.1021/es001375n.

Carpenter, L. J. (2003), Iodine in the marine boundary layer., *Chem. Rev.*, *103*(12), 4953–62, doi:10.1021/cr0206465.

Chen, X., M. Gong, P. Yi, A. Aldahan, Z. Yu, G. Possnert, and L. Chen (2015), Distribution of 129I in terrestrial surface water environments, *Nucl. Instruments Methods Phys. Res. Sect. B Beam Interact. with Mater. Atoms*, doi:10.1016/j.nimb.2015.04.073.

Edwards, R. R. (1962), Iodine-129: its occurrence in nature and its utility as a tracer., *Science (80-.).*, *137*(3533), 851–3.

Englund, E., A. Aldahan, G. Possnert, E. Haltia-Hovi, X. Hou, I. Renberg, and T. Saarinen (2008), Modeling fallout of anthropogenic 129I., *Environ. Sci. Technol.*, *42*(24), 9225–30.

Englund, E., A. Aldahan, X. L. Hou, G. Possnert, and C. Söderström (2010a), Iodine (129I and 127I) in aerosols from northern Europe, *Nucl. Instruments Methods Phys. Res. Sect. B Beam Interact. with Mater. Atoms*, *268*(7-8), 1139–1141, doi:10.1016/j.nimb.2009.10.118.

Englund, E., A. Aldahan, X. L. Hou, R. Petersen, and G. Possnert (2010b), Speciation of iodine (127I and 129I) in lake sediments, *Nucl. Instruments Methods Phys. Res. Sect. B Beam Interact. with Mater. Atoms*, *268*(7-8), 1102–1105, doi:10.1016/j.nimb.2009.10.109.

Fabryka-Martin, J., H. Bentley, D. Elmore, and P. Airey (1985), Natural iodine-129 as an environmental tracer, *Geochim. Cosmochim. Acta*, *49*(2), 337–347, doi:10.1016/0016-7037(85)90027-4.

Fabryka-Martin, J., S. N. Davis, D. Elmore, and P. Kubik (1989), In situ production and migration of 129I in the Stripa granite, Sweden, *Geochim. Cosmochim. Acta*, *53*, 1817–1823.

Fabryka-Martin, J. T. (1988), Production of Radionuclides in the Earth and their Hydrogeologic Significance, with Emphasis on Chlorine-36 and Iodine-129.

Fehn, U. (2012), Tracing Crustal Fluids: Applications of Natural 129I and 36Cl, *Annu. Rev. Earth Planet. Sci.*, *40*(1), 45–67, doi:10.1146/annurev-earth-042711-105528.

Fehn, U., S. Tullaifitzpatrick, R. Teng, H. Gove, P. Kubik, P. Sharma, and D. Elmore (1990), Dating of oil field brines using 129I, *Nucl. Instruments Methods Phys. Res. Sect. B Beam Interact. with Mater. Atoms*, *52*(3-4), 446–450, doi:10.1016/0168-583X(90)90455-4.

Fukui, M., Y. Fujikawa, and N. Satta (1996), Factors affecting interaction of radioiodide and iodate species with soil, *J. Environ. Radioact.*, *31*(2), 199–216, doi:10.1016/0265-931X(95)00039-D.

Hansen, V., P. Roos, A. Aldahan, X. Hou, and G. Possnert (2011), Partition of iodine (129I and 127I) isotopes in soils and marine sediments., *J. Environ. Radioact.*, *102*(12), 1096–104, doi:10.1016/j.jenvrad.2011.07.005.

He, P., a. Aldahan, G. Possnert, and X. L. Hou (2013), A summary of global 129I in marine waters, *Nucl. Instruments Methods Phys. Res. Sect. B Beam Interact. with Mater. Atoms*, *294*, 537–541, doi:10.1016/j.nimb.2012.08.036.

Health Canada (2014), Radiation Monitoring Data and the Nuclear Emergency in Japan, Available from: http://www.hc-sc.gc.ca/hc-ps/ed-ud/respond/nuclea/data-donnees-eng.php

Horrocks, D. L., and P. R. Klein (1974), Theoretical Considerations for Standardization of 125I by the Coincidence Method, *Nucl. Instruments Methods Phys. Res.*, *124*(3), 585–589.

Hou, X., V. Hansen, A. Aldahan, G. Possnert, O. C. Lind, and G. Lujaniene (2009), A review on speciation of iodine-129 in the environmental and biological samples., *Anal. Chim. Acta*, *632*(2), 181–96, doi:10.1016/j.aca.2008.11.013.

Hou, X., W. Zhou, N. Chen, L. Zhang, Q. Liu, M. Luo, Y. Fan, W. Liang, and Y. Fu (2010), Determination of ultralow level 129I/127I in natural samples by separation of microgram carrier free iodine and accelerator mass spectrometry detection., *Anal. Chem.*, *82*(18), 1–6, doi:10.1021/ac101558k.

Hu, Q., P. Zhao, J. E. Moran, and J. C. Seaman (2005), Sorption and transport of iodine species in sediments from the Savannah River and Hanford Sites., *J. Contam. Hydrol.*, *78*(3), 185–205, doi:10.1016/j.jconhyd.2005.05.007.

IAEA (2005), *Status and trends in spent fuel reprocessing IAEA-TECDOC-1467*.

Jabbar, T., G. Wallner, and P. Steier (2013), A review on (129)I analysis in air., *J. Environ. Radioact.*, *126C*, 45–54, doi:10.1016/j.jenvrad.2013.07.013.

Kekli, A., A. Aldahan, M. Meili, G. Possnert, N. Buraglio, and R. Stepanauskas (2003), 129I in Swedish rivers: distribution and sources., *Sci. Total Environ.*, *309*(1-3), 161–72, doi:10.1016/S0048-9697(03)00010-X.

Keogh, S. M., A. Aldahan, G. Possnert, L. L. Vintró, P. I. Mitchell, K. J. Smith, and P. McGinnity (2010), Anthropogenic 129I in precipitation and surface waters in Ireland, *Nucl. Instruments Methods Phys. Res. Sect. B Beam Interact. with Mater. Atoms*, *268*(7-8), 1232–1235, doi:10.1016/j.nimb.2009.10.141.

Li, T. (2013), The Geochemistry and Runoff Process in Wolf Creek Research Basin, Whitehorse, Yukon Territory.

Luo, M., X. Hou, W. Zhou, C. He, N. Chen, Q. Liu, and L. Zhang (2013), Speciation and migration of 129I in soil profiles., *J. Environ. Radioact.*, *118*, 30–39, doi:10.1016/j.jenvrad.2012.11.011.

Lusa, M., M. Bomberg, H. Aromaa, J. Knuutinen, and J. Lehto (2015), Sorption of radioiodide in an acidic, nutrient-poor boreal bog: insights into the microbial impact, *J. Environ. Radioact.*, *143*, 110–122, doi:10.1016/j.jenvrad.2015.02.022.

Moran, J. E., S. D. Oktay, P. H. Santschi, and D. R. Schink (1999), Atmospheric Dispersal of 129 Iodine from Nuclear Fuel Reprocessing Facilities, *Environ. Sci. Technol.*, *33*(15), 2536–2542.

Moran, J. E., S. D. Oktay, and P. H. Santschi (2002), Sources of iodine and iodine 129 in rivers, *Water Resour. Res.*, *38*(8), 1–10.

Muramatsu, Y., Y. Takada, H. Matsuzaki, and S. Yoshida (2008), AMS analysis of 129I in Japanese soil samples collected from background areas far from nuclear facilities, *Quat. Geochronol.*, *3*(3), 291–297, doi:10.1016/j.quageo.2007.08.002.

Negri, A. E., J. O. Fernández Niello, A. Wallner, A. Arazi, L. K. Fifield, and S. G. Tims (2013), 129I dispersion in Argentina: concentrations in fresh and marine water and deposition fluences in Patagonia, *Environ. Sci. Technol.*, *47*(17), 9693–8, doi:10.1021/es400610h.

Nimz, G. J. (1998), *Isotope Tracers in Catchment Hydrology - Chapter 8 - Lithogenic and Cosmogenic Tracers in Catchment Hydrology*, edited by C. Kendall and J. J. Macdonell, Elsevier.

Oktay, S. D., P. H. Santschi, J. E. Moran, and P. Sharma (2000), Iodine bomb pulse recorded in Mississippi River Delta sediments : Results from isotopes of I, Pu, Cs, Pb, and C, *Geochim. Cosmochim. Acta*, *64*(6), 989–996.

Oktay, S. D., P. H. Santschi, J. E. Moran, and P. Sharma (2001), 129I and 127I Transport in the Mississippi River, *Environ. Sci. Technol.*, *35*(22), 4470–6.

Paul, M., D. Fink, G. Hollos, A. Kaufman, W. Kutschera, and M. Magaritz (1987), Measurement of 129I concentrations in the environment after the Chernobyl reactor accident, *Nucl. Instruments Methods Phys. Res.*, *29*(1-2), 341–345, doi:10.1016/0168-583X(87)90262-X.

Persson, S., A. Aldahan, G. Possnert, V. Alfimov, and X. Hou (2007), 129I Variability in precipitation over Europe, *Nucl. Instruments Methods Phys. Res. Sect. B Beam Interact. with Mater. Atoms*, *259*(1), 508–512, doi:10.1016/j.nimb.2007.01.193.

Raisbeck, G. M., and F. Yiou (1999), 129I in the oceans: origins and applications., *Sci. Total Environ.*, *237-238*, 31–41.

Raisbeck, G. M., F. Yiou, Z. Q. Zhou, and L. R. Kilius (1995), 129I from nuclear fuel reprocessing facilities at Sellafield (U.K.) and La Hague (France); potential as an oceanographic tracer, *Jounal Mar. Syst.*, *6*, 561–570.

Rao, U., and U. Fehn (1999), Sources and reservoirs of anthropogenic iodine-129 in western New York, *Geochim. Cosmochim. Acta*, *63*(13-14), 1927–1938, doi:10.1016/S0016-7037(99)00133-7.

Reithmeier, H., V. Lazarev, W. Rühm, T. M. Schwikowski, H. W. Gäggeler, and E. Nolte (2006), Estimate of European 129I releases supported by 129I analysis in an Alpine ice core., *Environ. Sci. Technol.*, *40*(19), 5891–6.

Reithmeier, H., V. Lazarev, W. Rühm, and E. Nolte (2007), 129I measurements in lake water for an estimate of regional 129I depositions., *Sci. Total Environ.*, *376*(1-3), 285–93, doi:10.1016/j.scitotenv.2006.11.027.

Reithmeier, H., V. Lazarev, W. Rühm, and E. Nolte (2010), Anthropogenic 129I in the atmosphere: overview over major sources, transport processes and deposition pattern., *Sci. Total Environ.*, *408*(21), 5052–64, doi:10.1016/j.scitotenv.2010.07.015.

Renaud, R., I. D. Clark, T. G. Kotzer, G. M. Milton, and D. J. Bottomley (2005), The mobility of anthropogenic 129 I in a shallow sand aquifer at Sturgeon Falls, Ontario, Canada, *Radiochim. Acta*, *93*(6-2005), 363–371, doi:10.1524/ract.93.6.363.65641.

Sabu, D. D. (1971), On mass-yield of xenon and krypton isotopes in the spontaneous fission of uranium, *J. Inorg. Nucl. Chem.*, *33*(5), 1509–1513, doi:10.1016/0022-1902(71)80448-7.

Saiz-Lopez, A., J. M. C. Plane, A. R. Baker, L. J. Carpenter, R. von Glasow, J. C. G. Martín, G. McFiggans, and R. W. Saunders (2012), Atmospheric chemistry of iodine., *Chem. Rev.*, *112*(3), 1773–804, doi:10.1021/cr200029u.

Schwehr, K. A., P. H. Santschi, J. E. Moran, and D. Elmore (2005), Near-conservative behavior of 129I in the Orange County aquifer system, California, *Appl. Geochemistry*, *20*(8), 1461–1472, doi:10.1016/j.apgeochem.2005.02.003.

Schwehr, K. A., P. H. Santschi, D. J. Kaplan, C. M. Yeager, and R. Brinkmeyer (2009), Organo-iodine formation in soils and aquifer sediments at ambient concentrations., *Environ. Sci. Technol.*, *43*(19), 7258–64.

Sheppard, M. I., and J. L. Hawkins (1995), Iodine and microbial interactions in an organic soil, *J. Environ. Radioact.*, *29*(2), 91–109, doi:10.1016/0265-931X(95)00022-3.

Sheppard, M. I., J. L. Hawkins, and P. A. Smith (1996), Soil Processes and Chemical Transport: Linearity of Iodine Sorption and Sorption Capacities for Seven Soils, *J. Environ. Qual.*, *25*, 1261–1267.

Shetaya, W. H., S. D. Young, M. J. Watts, E. L. Ander, and E. H. Bailey (2012), Iodine dynamics in soils, *Geochim. Cosmochim. Acta*, *77*, 457–473, doi:10.1016/j.gca.2011.10.034.

Smith, J. N., K. M. Ellis, and T. Boyd (1999), Circulation features in the central Arctic Ocean revealed by nuclear fuel reprocessing tracers from Scientific Ice Expeditions 1995 and 1996, *J. Geophys. Res.*, *104*(C12), 29663–29.

Smith, J. N., F. a. McLaughlin, W. M. Smethie, S. B. Moran, and K. Lepore (2011), Iodine-129, 137 Cs, and CFC-11 tracer transit time distributions in the Arctic Ocean, *J. Geophys. Res.*, *116*(C4), 1–19, doi:10.1029/2010JC006471.

Snyder, G., and U. Fehn (2004), Global distribution of 129I in rivers and lakes: implications for iodine cycling in surface reservoirs, *Nucl. Instruments Methods Phys. Res. Sect. B Beam Interact. with Mater. Atoms*, *223-224*, 579–586, doi:10.1016/j.nimb.2004.04.107.

Snyder, G., A. Aldahan, and G. Possnert (2010), Global distribution and long-term fate of anthropogenic 129I in marine and surface water reservoirs, *Geochemistry Geophys. Geosystems*, *11*(4), doi:10.1029/2009GC002910.

Snyder, G. T., and J. T. Fabryka-Martin (2007), 129I and 36Cl in dilute hydrocarbon waters: Marine-cosmogenic, in situ, and anthropogenic sources, *Appl. Geochemistry*, *22*(3), 692–714, doi:10.1016/j.apgeochem.2006.12.011.

Söderlund, M., M. Lusa, J. Lehto, and M. Hakanen (2011), *POSIVA Working Report 2001-04: Sorption of Iodine, Chlorine, Technetium and Cesium in Soil*.

Steinberg, S. M., G. M. Kimble, G. T. Schmett, D. W. Emerson, M. F. Turner, and M. Rudin (2008), Abiotic reaction of iodate with sphagnum peat and other natural organic matter, *J. Radioanal. Nucl. Chem.*, *277*(1), 185–191, doi:10.1007/s10967-008-0728-1.

Strachnov, V., J. Larosa, R. Dekner, R. Zeisler, and A. Fajeglj (1996), *Report on the Intercomparison Run IAEA-375: Determination of Radionuclides in Soil Samples IAEA-375*.

Szidat, S., A. Schmidt, J. Handl, D. Jakob, W. Botsch, R. Michel, H. –. Synal, C. Schnabel, M. Suter, and J. . López-Gutiérrez (2000), Iodine-129: Sample preparation, quality control and analyses of pre-nuclear materials and of natural waters from Lower Saxony, Germany, *Nucl. Instruments Methods Phys. Res. Sect. B Beam Interact. with Mater. Atoms*, *172*(1-4), 699–710, doi:10.1016/S0168-583X(00)00377-3.

Toyama, C., Y. Muramatsu, Y. Uchida, Y. Igarashi, M. Aoyama, and H. Matsuzaki (2012), Variations of (129)I in the atmospheric fallout of Tokyo, Japan: 1963-2003., *J. Environ. Radioact.*, *113*, 116–122, doi:10.1016/j.jenvrad.2012.04.014.

Tsunogai, S. (1971), Iodine in the deep water of the ocean, *Deep Sea Res.*, *18*, 913–919.

Wallner, G., P. Steier, T. Brandl, M. E. Friesacher, P. Hille, W. Kutschera, M. Tatzber, and S. Ayromlou (2007), Developments toward the measurement of I-129 in lignite, *Nucl. Instruments Methods Phys. Res. Sect. B Beam Interact. with Mater. Atoms*, *259*(1), 714–720, doi:10.1016/j.nimb.2007.01.217.

Wassenaar, L. I., M. J. Hendry, and N. Harrington (2006), Decadal geochemical and isotopic trends for nitrate in a transboundary aquifer and implications for agricultural beneficial management practices., *Environ. Sci. Technol.*, *40*(15), 4626–32.

Wetherbee, G. A., D. A. Gay, T. M. Debey, C. M. B. Lehmann, and M. A. Nilles (2012), Wet Deposition of Fission-Product Isotopes to North America from the Fukushima Dai-ichi Incident, March 2011, *Environ. Sci. Technol.*, *46*(5), 2574–2582.

Whitehead, D. C. (1974), The sorption of iodide by soil components, *J. Sci. Food Agric.*, *25*(1), 73–79, doi:10.1002/jsfa.2740250109.

Xu, S., S. P. H. T. Freeman, X. Hou, A. Watanabe, K. Yamaguchi, and L. Zhang (2013), Iodine isotopes in precipitation: temporal responses to 129I emissions from the Fukushima nuclear accident, *Environ. Sci. Technol.*, doi:10.1021/es401527q.

Zhang, S. et al. (2011), Concentration-dependent mobility, retardation, and speciation of iodine in surface sediment from the Savannah River Site., *Environ. Sci. Technol.*, *45*(13), 5543–9, doi:10.1021/es1040442.

CHAPTER 2 – EXTRACTION OF ^{129}I AND ^{127}I VIA COMBUSTION FROM ORGANIC RICH SAMPLES USING ^{125}I AS A QUANTITATIVE TRACER

ABSTRACT

Iodine-129 (^{129}I) is a biophilic, naturally occurring radioisotope (half-life: 1.57 x 10^7 years) that has been released in large quantities by nuclear fuel reprocessing. This iodine has cycled throughout the globe and chiefly the northern hemisphere and can be found in a wide variety of environmental materials, particularly organic rich soil and organic matter. Extracting iodine reliably from solid samples has been done by a variety of methods; however, pyrohydrolysis has been the most widely used. There is a wide variation between existing pyrohydrolysis techniques and this raises questions about the quantitative recovery of iodine from method to method. In order to quantify iodine recovery from pyrohydrolysis we have spiked samples with an iodine-125 radiotracer prior to combustion and trapping in an alkaline solution. Inorganic ^{125}I tracer was used as well as humic acid labeled with ^{125}I to simulate the behavior of ^{129}I and ^{127}I in complex organic substances and extract iodine regardless of how it is partitioned. Using these tracers we explored the effect on recovery of ^{125}I under a variety of combustion parameters. These include carrier gas flow rate and iodine volatilization temperature. We observed that the best recoveries of ^{125}I were at flow rates between 400-800 mL/min and most ^{125}I recoveries were above 85%. The experiment to determine the temperature at which iodine volatilizes from the sample showed two distinct trends for the release of iodine. One trend showed that most iodine is released at approximately 525°C, while the other trend showed that the samples needed to reach 800°C and remain there for at least an hour. These findings illustrate the usefulness and importance of using a quantitative recovery tracer for every iodine extraction. We then

combusted and precipitated several Atlantic Ocean seaweed and standard reference materials for AMS analysis as AgI. The ^{129}I concentration of the seaweed ranged between 4.4 - 5.5 x 10^{9} atoms/g and the $^{129}I/^{127}I$ ratio was 2.3 – 2.9 x 10^{-9}, both of which compare well to published values for Atlantic seaweed. The results for the standard reference materials also agree with specified values indicating that this technique is reliable. By optimizing pyrohydrolysis conditions and testing the recovery of iodine with a ^{125}I tracer it is possible to quantify and maximize recovery from organic samples. This will allow for the investigation of variations in the ^{129}I concentration and $^{129}I/^{127}I$ ratio with a high degree of precision in complex, organic rich samples.

1.0 INTRODUCTION

The environmental cycling of stable iodine-127 and radioactive isotopes iodine-129 (half –life: 15.7 million years) and iodine-131 (half-life: 8.02 days) is a subject that has received a large degree of scrutiny in recent years (Muramatsu et al., 2008). As a product of nuclear fuel reprocessing and a principal nuclide of concern for radioactive waste disposal, the behavior of ^{129}I has been studied extensively in a variety of materials such as groundwater, surface water, numerous soil types and organic materials [*Moran et al.*, 2002; *Snyder and Fehn*, 2004; *Toyama et al.*, 2013][*Fabryka-Martin et al.*, 1985]. Iodine is a very mobile element and can be transferred in aqueous or aerosol form, which allows it to cycle readily through many facets of the environment. Iodine can then be deposited on soils in rain or as dry deposition [*Moran et al.*, 1999]. It is also very biophilic and therefore is often concentrated in plants or soils with a high organic content, such as peats (Sheppard and Hawkins, 1995; Sheppard et al., 1993; Keppler et al., 2003). Accurately determining the

concentration of ^{127}I and ^{129}I in soils and organic materials is therefore of great importance to understanding the environmental cycling of iodine isotopes.

Several techniques for extracting iodine from soils have been developed which include caustic fusion followed by acid leaching and pyrohydrolysis (M-Y. Luo et al., 2011; Marchetti et al., 1994; Y. Muramatsu et al., 2008; Schnetger and Y. Muramatsu, 1996). This body of work has shown that it is possible to extract iodine efficiently from natural inorganic and organic samples; however, there is a large degree of variation within these methods. Indeed, the success of caustic fusion can vary tremendously depending on the sample type and the subsequent extraction of iodine can often fail if the optimal conditions are not found. There is also greater potential for contamination of ^{127}I and ^{129}I with this technique. The existing methods for pyrohydrolysis mostly extracted I from soil, rock and sediment and used trap solutions which varied from method to method. For example, Muramatsu et al., (2008) use a trap solution of TMAH and K_2SO_3, while Cornett et al., (1996) use double distilled water and Hou et al., (2010) uses NaOH and $NaHSO_3$. Furthermore, the number of furnace zones, heating protocols and carrier gas flow rate and gas composition differed from method to method likely due to individual equipment available in each lab. However, this lack of standardization raises questions about the iodine recovery in the different pyrohydrolysis methods particularly since iodine speciation and partitioning varies in soil, organic matter and other matrices. The variation of iodine species in natural samples could affect the recovery of iodine, which could lead to an underestimation of total iodine or ^{129}I in the sample. Furthermore, most iodine in soil and biological matrices occurs in organic molecules so it is important to demonstrate that all

iodine can be extracted from a sample regardless of the type of iodine present [*Hansen et al.*, 2011]. In a study of the partitioning of iodine isotopes in ocean sediments, Danish soil and IAEA-375 Hansen et al., (2011) showed that the majority of ^{127}I and ^{129}I was found primarily in humic and fulvic acids but a significant fraction was also observed in Fe-Mn oxides as well. The findings of this study underscore the importance of efficient iodine extraction from both organic and inorganic compounds in samples and the need to trace the recovery of iodine from samples.

This paper tests the efficacy of the pyrohydrolysis technique for soil and organic samples using iodine-125 as a tracer of recovery. The use of a radio-iodine tracer allows the effectiveness of the extraction to be quantified for a wide variety of sample types and provides a measure of the efficiency (yield) of the extraction prior to analysis by AMS or ICP-MS. Furthermore, humic acid was labeled with ^{125}I to determine the extraction efficiency from organic substances, which provides certainty that all iodine in the sample can be extracted regardless of how it is partitioned. We also analyzed a standard reference material and several natural samples via AMS and ICP-MS to show that this technique is reproducible and yields results in agreement with published literature values for reference materials and similar samples.

2.0 METHODS

2.1 Apparatus and Chemicals

The equipment used in the combustion of samples were two 40 cm Lindberg horizontal tube furnaces that had been retrofitted with digital temperature controllers (Figure 2.1). The combustion line and sample tubes were custom blown quartz. The quartz glass sample

tubes were 15-20 cm long with an inner diameter of 0.8-1.2 cm and the combustion line had an inner diameter of 2.1 cm. The bubbler and condenser were Pyrex, which was attached to the combustion tube using a ¾ inch stainless steel ultra-torr vacuum fitting with viton o-rings (Swagelok SS-12-UT-6 (fitting), VT-7-OR-116 (o-ring)). The bubbler and condenser are separate pieces that are connected using an RF19 Rotulex spherical joint and clip.

The glass trap for the main trap and condenser is connected to the main line using an RF35 Rotulex spherical joint. 10-15 g of quartz wool and ~10 g copper windings was loosely packed into the combustion tube. Iodine-125 tracer was ordered from Perkin Elmer (NEZ033A001MC) and diluted for use as a recovery tracer. The ^{125}I trap solution was gamma counted on a PerkinElmer Wizard 2 Automatic Gamma Counter (2470-0020). All chemicals used in the combustion, sample precipitation or sample digestion were analytical grade reagents including: $NaHSO_3$, NaOH, $AgNO_3$, HNO_3, NaI, Hexane, $NaNO_2$, TMAH (Tetra-Methyl Ammonium Hydroxide). All solutions were prepared using 18MΩ de-ionized water. The humic acid used in the radioiodinating procedure was Sigma Aldrich Humic Acid (68131-04-4). Chernobyl soil (IAEA-375) was used as a standard reference material for ^{127}I, ^{129}I and the $^{129}I/^{127}I$ ratio since all values are known to verify the robustness of this technique on a natural soil.

2.2 Sample Preparation

Samples of whole wheat flour, seaweed and peat moss were all extracted by this procedure. Both the seaweed and flour were commercial products intended for human consumption and were finely ground and dried when purchased. The seaweed, *Fucus*

vesiculosus, is sold commercially as a dietary iodine supplement (Mountain Rose Herbs Bladderwrack) and the entire plant was washed, dried and ground very finely. The seaweed is from the east coast of Canada. The peat was collected in the Northwest Territories, Canada at the site of a retrogressive thaw slump near Fort McPherson in August, 2010 (67.43° N, 134.88° W). The peat was dried at 60 °C and ground. All large roots and rocks were removed in an effort to obtain the most homogenous sample possible. The specific peat samples used in this study have already been extracted for ^{129}I by caustic fusion and the results published in Herod et al., (2012).

2.3 Radio-iodination of Humic Acid

Humic acid was labeled with iodine-125 to test the behaviour of covalently bound iodine isotopes during the combustion. This approach also tested the recovery of iodine using ^{125}I labeled organic material as a tracer rather than inorganic $Na^{125}I$. The reaction used to radiolabel humic acid was derived from Warwick et al., (1993) and Warwick et al., (1993b). Sodium salt and humic acid (Sigma-Aldrich 68131-04-4) were dissolved in 10^{-4} NaOH. 5 mL of the humic acid solution was then taken and mixed with Chloramine-T (1.4 mg/mL), and ^{125}I and allowed to sit for 30 minutes. Sodium metabisulphite (84 mg/mL), a reducing agent, was then added to terminate the iodination reaction and stabilize the iodinated humic acid [*Carlsena et al.*, 1993][*Warwick et al.*, 1993a]. Dialysis was used to separate the iodinated humic acid from any free ^{125}I in solution. The sample was placed in a dialysis bag with a molecular weight cut off of 3,500 Daltons. This means that molecules larger than 3,500 Daltons are retained within the bag, whereas smaller molecules readily diffuse through. The molecular mass of the humic acid used ranges from 2000-500,000 Daltons,

meaning the majority is retained. The bag was soaked in de-ionized water for 20 minutes prior to sample addition and then placed in a large beaker filled with 1.5 L of de-ionized water and left to equilibrate for 4 hours. After this time had elapsed a sample of the water was taken to measure the ^{125}I and the water was changed. This step was repeated three times or until the withdrawn water sample showed no ^{125}I activity. The radio-iodinated humic acid was then placed in a sealed beaker, ready for use.

2.4 Separation of Iodine by Pyrohydrolysis

2-4 grams of sample material was weighed precisely and placed in a quartz boat with 0.05mL of inorganic or organic ^{125}I tracer, 100,000 Bq/mL and 3500 Bq/mL, respectively. Samples were then placed in Zone 1 of the furnace tube and burnt, under pure O_2 flow, until all organic matter was fully combusted (Figure 2.1). The furnace tube also contained quartz wool and CuO catalyst, which was located in Zone 2, in order to ensure complete combustion and oxidation of any organic matter and iodine that was released before the sample was fully combusted. Zone 2 and Zone 1 were on separate heating protocols, outlined in Table 2.1**.** Zone 1 was heated gradually over a long period of time to lessen the likelihood of the sample catching on fire, which poses a possible safety hazard to the user. However, the heating of Zone 1 often released partially combusted organic matter at low temperatures and therefore Zone 2 was rapidly heated to 800°C in 30 minutes to ensure no uncombusted material could reach the bubbler or condense on the line, which were shown to greatly inhibit the recovery of ^{125}I and hence ^{127}I and ^{129}I as well.

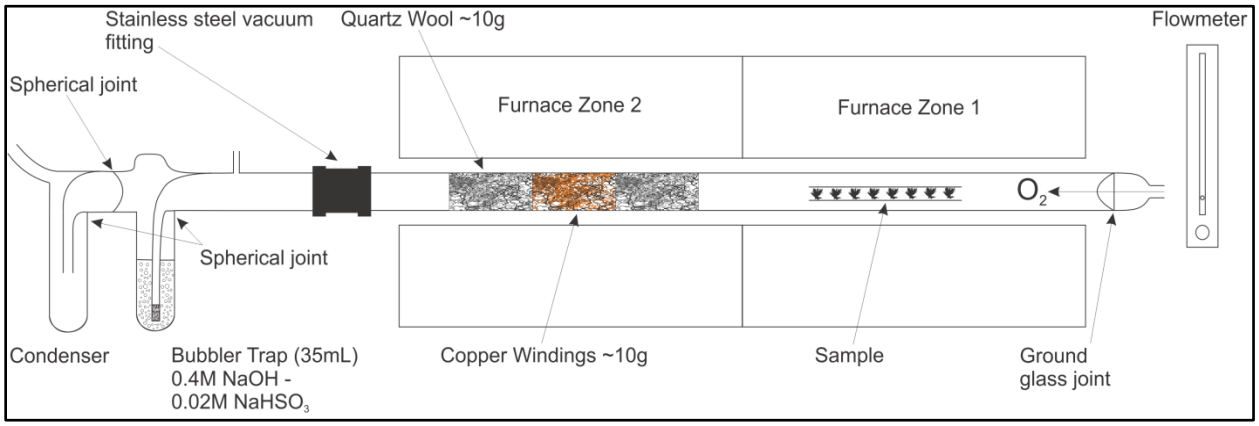

Figure 2.1: Schematic of the combustion apparatus used for extracting iodine from organic rich solid samples.

Furthermore, it was impossible to use the trap solution for analysis of ^{127}I or extraction of ^{129}I if uncombusted organic matter reached the bubbler. Testing of the system revealed that this two zone system is essential for efficient recoveries when combusting organic samples. Heat tape was also wrapped around the furnace tube between the exit of Zone 2 and the bubbler to make sure the O_2 carrier gas remained at a temperature above 120 °C as it entered the bubbler and to prevent the condensation iodine on the line or steel connector at this point. The O_2 gas carried the iodine through the combustion tube into the bubbler, which was fitted with a glass frit. The trap was filled with 35 mL of 0.4 M NaOH – 0.02 M $NaHSO_3$ solution [*Hou et al.*, 2010]. It is possible that the size of the bubbles plays a role in iodine recovery as finer bubbles could lead to increased transfer of iodine from the carrier gas to the trap solution, presumably due to the increased surface area. However, the risk of using too fine a frit is that this can lead to a buildup of backpressure within the line that can result in leaks and loss of the carrier gas. Several frits were tried and the finest one possible that did not create excessive back pressure was used. After the combustion, the trap solution and any solution in the condenser were transferred to separate 50 mL

centrifuge tubes and 1 mL of each was taken for ^{125}I counting via gamma spectrometry to calculate iodine recovery using the coincidence sum gamma counting method to determine absolute sample activity [*Horrocks and Klein*, 1974][*Horrocks*, 1974]. The remaining trap solution was then saved for ICP-MS and for the preparation of an AMS target. Following every extraction the glassware, with the exception of the main furnace tube, was soaked overnight in 0.05M NaOH, rinsed in DIW and dried to ensure no iodine contamination could occur from sample to sample.

Time elapsed (mins)	**Temperature (°C)**	
	Sample Zone	Combustion Zone
30	20-100	0-800
240	100-800	800
300	800	800

Table 2.1: The furnace program used for the pyrohydrolysis technique.

2.5 Precipitation and Preparation of an AMS Target

AMS targets were prepared from the trap solution using a modification of the method outlined in Hou et. al. (2010) and Sheppard and Herod, (2012). The trap solution was first acidified to ~pH 1 using concentrated HNO_3 and then ~2 mg of NaI carrier ($^{129}I/^{127}I$: 1.56 ± 0.06 x 10^{-13}) was added and its precise weight recorded. 1 M $NaHSO_3$ was then added as a reducing agent and the sample was left to sit for 30 minutes. 15 mL of hexane and 0.1 mL of 6 M $NaNO_2$ were added to the solution. The trap solution was then shaken, causing the iodine to oxidize rapidly and become trapped in the hexane, which caused it to turn purple. The whole solution was then transferred to a separatory funnel and the water and hexane fractions collected separately. Fresh hexane was then added, but no new $NaNO_2$. The

separation was then repeated until the hexane remained clear. All of the hexane collected was then placed in the separatory funnel and 10 mL de-ionized water and 1M $NaHSO_3$ were added to back extract the iodine from the hexane into the water. The water was then acidified with 100µL of concentrated HNO_3 and heated to 90°C. 1mL of 0.1M $AgNO_3$ was then added to precipitate AgI. The precipitate was then centrifuged and dried for preparation of an AMS target. The precipitate can also be counted for ^{125}I in order to determine the efficiency of the precipitation protocol at recovering iodine from the trap solution as opposed to only that added by the NaI carrier. This test showed that an average of 76% (n=4) of the ^{125}I added is present in the precipitate, which was made from the NWT peat samples. Targets for the AMS were made by mixing 1-2mg of AgI precipitate with high purity niobium powder and pressing the powder into a stainless steel cathode and analyzed at uOttawa's IsoTrace laboratory.

2.6 Blanks

Several process blanks were performed by combusting an empty tube with O_2 gas bubbling into 35mL of trap solution, which was then gamma counted to look for any ^{125}I that had condensed on the line during previous extractions, which could lead to a memory effect. Only one of the blanks was found to contain 5.4Bq of ^{125}I activity, which constitutes less than 0.1% of the ^{125}I added for each extraction, while the other blanks contained no measureable ^{125}I. This indicates that memory effects from the combustion line are negligible with respect to ^{125}I, and we can assume that this holds for ^{127}I and ^{129}I as well meaning contamination from sample to sample is not an issue as long as proper cleaning protocols are observed.

3.0 RESULTS AND DISCUSSION

3.1 Optimization of Experimental Conditions

3.1.1 Effect of Flow Rate on ^{125}I Recovery

One of the key parameters that affects the recovery of ^{125}I and ultimately ^{127}I and ^{129}I is the flow rate of O_2 gas through the furnace tube and into the bubbler. Flow was measured at the exit point of the condenser using a digital flow meter and a variety of different flow rates ranging from 100-1000mL/min and their effect on ^{125}I recovery were compared. This comparison was performed using whole wheat flour and dried and ground seaweed as organic sample types. A further test was performed to determine if the type of ^{125}I tracer had any effect on recovery at varying flow rates (Figure 2.2). As can be seen from the figure the best recoveries of inorganic ^{125}I from seaweed ranged from 400-800 mL/min whereas with flour optimal recovery was seen at 700-900 mL/min. The mean recovery for flour samples was 85% and within the optimal flow window it was 96%, which is excellent. For seaweed the average recovery was 80% and within the optimal window it was 88%. One possible reason for the slight loss of recovery using seaweed is the fineness of the seaweed powder, which results in a more densely packed sample and less efficient combustion. Samples of peat were also extracted, all of which were combusted at 800 mL/min and recoveries ranged from 75-99% with a mean of 91.5% recovery (n=4). Based on these results the optimal flow rate of iodine extraction from an organic sample or a soil with a high organic content is 600-800 mL/min. The flow experiment was repeated using humic acid labeled with ^{125}I added to whole wheat flour in order to more accurately simulate the conditions required to volatilize iodine efficiently from organic samples. The results of this experiment can be seen in Figure 2.2 and Table 2.2. Using the radio-labeled humic acid,

excellent recoveries with an average of 87% were obtained at flow rates ranging from 300-800 mL/min. At flow rates above 800 mL/min the recovery of ^{125}I dropped and this is likely due to incomplete trapping of ^{125}I which likely also applies to ^{127}I and ^{129}I at the high flow rate.

The results from both types of tracer, inorganic ^{125}I and radio-labeled humic acid confirm that high flow rates are optimal for achieving the highest possible iodine recoveries from organic samples. The reason that high flow rates are essential for ensuring high iodine recoveries is that within the optimal flow rate range iodine doesn't condense on the line as there is limited reaction time for this to occur. This finding is consistent with the observations of [*Cornett et al.*, 1997], who found that high flow rates (2.0L/min) were essential to efficiently recover iodine from teeth and bones. Given the more readily combustible nature of organic soils compared to teeth and bones it is not surprising that a lower flow rate is adequate in this case.

At higher flow rates of 900-1000 mL/min there is the possibility that iodine recovery can decrease. One possible reason for this drop is that it is difficult to prevent substantial loss of the trap solution into the condenser which increases the likelihood of blowing iodine straight through the system. Additionally, the transfer of iodine from the gaseous state in the carrier gas to the aqueous could also be inhibited at high flow rates due to the speed at which the bubbles pass through the trap solution. It is also possible that extremely high flow rates over such long periods of time could begin to strip iodine from the trap solution, although we believe this is less likely. We also observed that at low flow rates iodine

recovery was also inhibited. This is likely due to the condensation of iodine on parts of the line such as the steel connector, quartz wool or tubing at the furnace exit, where the temperature decreases. In order, to limit loss in this way the furnace tube was well wrapped in heating tape; however, at low flow rates the loss still occurs. It is also possible that at low flow rates back pressure can build in the line due to the packing of quartz wool. In some instances, usually at low flow rates, condensation of organic matter was observed at the entrance to the quartz tube after combustion. This indicates that high back pressure within the line was preventing the transfer of carrier gas through the tube and to the trap solution and some backflow occurred. The use of higher flow rates can help to overcome this buildup.

Sample ID	Flow (mL/min)	Sample Type	^{125}I Tracer	Recovery (%)
CF62	100	Seaweed	Na^{125}I - Inorganic	36
CF34	100	Seaweed	Na^{125}I - Inorganic	41
CF39	200	Seaweed	Na^{125}I - Inorganic	71
CF38	300	Seaweed	Na^{125}I - Inorganic	77
CF40	400	Seaweed	Na^{125}I - Inorganic	89
CF33	500	Seaweed	Na^{125}I - Inorganic	85
CF 41	600	Seaweed	Na^{125}I - Inorganic	88
CF55	700	Seaweed	Na^{125}I - Inorganic	94
CF29	700	Seaweed	Na^{125}I - Inorganic	78
CF43	800	Seaweed	Na^{125}I - Inorganic	93
CF53	800	Seaweed	Na^{125}I - Inorganic	89
CF42	900	Seaweed	Na^{125}I - Inorganic	72
CF57	900	Seaweed	Na^{125}I - Inorganic	92
CF61	1000	Seaweed	Na^{125}I - Inorganic	90.5
CF15	100	Flour	Na^{125}I - Inorganic	75
CF46	200	Flour	Na^{125}I - Inorganic	89
CF21	300	Flour	Na^{125}I - Inorganic	75.5
CF60	300	Flour	Na^{125}I - Inorganic	102
CF44	400	Flour	Na^{125}I - Inorganic	104
CF16	500	Flour	Na^{125}I - Inorganic	77
CF18	500	Flour	Na^{125}I - Inorganic	76
CF63	500	Flour	Na^{125}I - Inorganic	87
CF56	600	Flour	Na^{125}I - Inorganic	103
CF45	700	Flour	Na^{125}I - Inorganic	97
CF47	800	Flour	Na^{125}I - Inorganic	99
CF54	900	Flour	Na^{125}I - Inorganic	92
CF20	1000	Flour	Na^{125}I - Inorganic	85
CF28	800	Blank	None	5.4 Bq
CF35	800	Blank	None	0 Bq
CF74	100	Blank	None	0 Bq
CF77	100	Flour	^{125}I Humic Acid	83
CF73	300	Flour	^{125}I Humic Acid	89
CF76	400	Flour	^{125}I Humic Acid	99
CF72	500	Flour	^{125}I Humic Acid	95
CF71	600	Flour	^{125}I Humic Acid	85
CF75	700	Flour	^{125}I Humic Acid	101
CF69	800	Flour	^{125}I Humic Acid	84
CF74	900	Flour	^{125}I Humic Acid	77

Table 2.2: Analytical results of ^{125}I yield for all pyrohydrolysis extractions. Sample type, flow rate and the type of ^{125}I tracer used are all shown. Note the unit change to Bq for the process blank samples

.

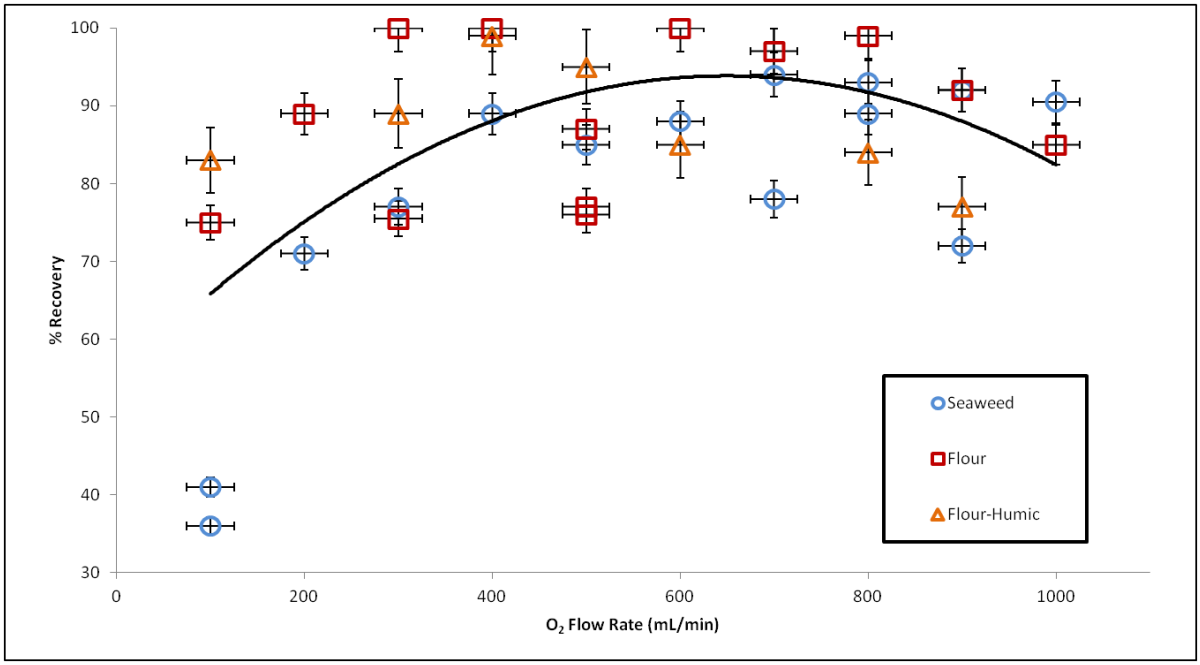

Figure 2.2: The effect of O_2 flow rate on recovery. Recovery is low at low flow rates and is highest between ~400-800mL/min. The trendline shown is a second order polynomial with an r^2=0.38.

3.1.2 Volatilization Temperature

The volatilization temperature of iodine-125 from different organic sample types was investigated in order to optimize iodine recovery and ensure that combustion was complete. All four extractions in this experiment were run at a flow rate of 800 mL/min. The heating protocols for the two seaweed samples were identical with 800°C being reached after 170 minutes and for both flour samples 800°C was reached after 230 minutes. During a single combustion process, samples of trap solution were removed by briefly detaching the trap solution reservoir from the bubbler and quickly withdrawing 1mL of trap solution and pipetting it into a gamma counting vial. This was repeated at roughly 100°C intervals throughout the process for all sample types and the 1mL samples were then gamma counted. Figure 2.3 shows there are two distinct patterns for the recovery of ^{125}I

from the sample. The first pattern, which agrees well with that observed by Muramatsu et al., (2008) shows a trend that volatilization of iodine began to occur between 300-400°C and then peaked by 500-600°C. Both samples that showed this pattern used inorganic ^{125}I and one was flour and the other seaweed, which is referred to as seaweed-A in the figure. The total recovery of ^{125}I for the flour sample was 77% and 85% for the seaweed. In the case of the seaweed sample, the maximum activity was not reached until 525°C. The second pattern observed showed a very different trend. In this instance a sample of seaweed, referred to as seaweed-B and identical in composition to seaweed-A was labeled with inorganic ^{125}I and a sample of flour spiked with ^{125}I labeled humic acid were used. The results of these two extractions show similar trends to one another, although they differ significantly from that observed in seaweed-A and the inorganically labeled flour. In these two extractions, significant volatilization of ^{125}I did not occur until the sample had reached 800°C and was held there for at least one hour. The recovery of ^{125}I from seaweed-B was 89% and from the flour was 96% effective, which shows that despite the recovery of ^{125}I taking place late in the extraction its efficiency is still comparable to that of the previous samples. One possibility for these different trends is that sample density or packing varied which affects the flow of the carrier gas around the samples within the combustion tube and hence influences the speed at which the sample combusts and the iodine volatilizes. A greater sample density results in less gas flow through the sample and delays the combustion of the sample and the volatilization of iodine until the entire system reaches 800°C. On the other hand a less dense or lightly packed sample would allow the O_2 to flow freely through it and interact with a greater proportion of the sample resulting in a more

rapid combustion and volatilization. However, the exact reason is still a matter for further study, given the sensitivity of the system, and we believe the two different trends observed illustrate the need for the use of a recovery tracer with every sample even if they are the same sample type and treatment is identical. These different trends also emphasize the unpredictable nature of iodine behavior in natural samples and show that the volatilization of iodine is complex even if by all appearances the samples should behave identically. Based on these observations it is crucial for organic samples to reach a minimum temperature of 800°C and be held there for at least one hour in order to obtain a full recovery of iodine from the sample and to ensure that any condensed organic matter on the furnace tube or line is fully combusted. This finding agrees well with previous work on inorganic soils that found the temperature had to reach 700-1000°C to obtain maximum recovery [*Muramatsu et al.*, 2008][*Cornett et al.*, 1996][*Hansen et al.*, 2011].

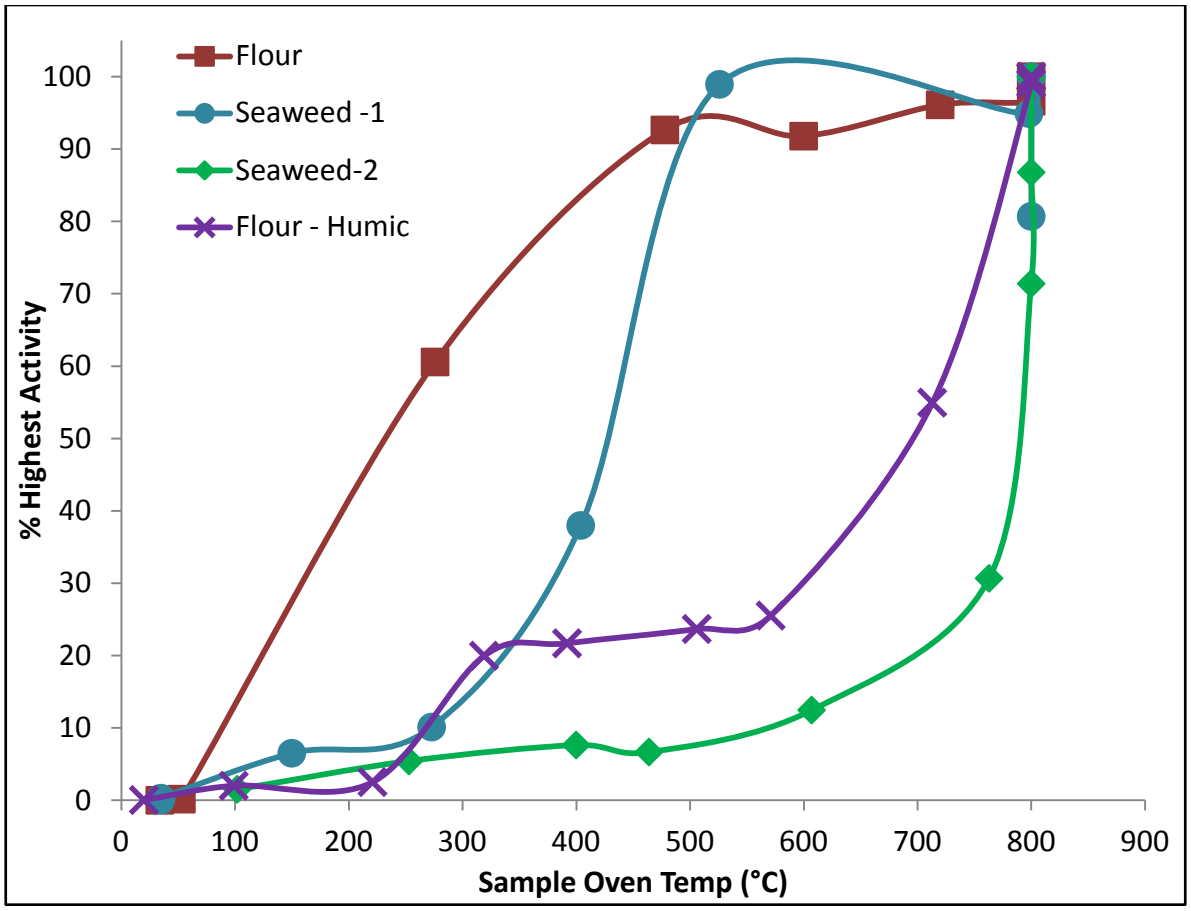

Figure 2.3: The volatilization of ^{125}I as temperature rises from flour and seaweed labeled with inorganic ^{125}I and flour with ^{125}I labeled humic acid. The y-axis is given as % highest activity, which is the activity of each aliquot normalized to the aliquot with the highest activity sampled. This allows all sample types to be compared.

3.1.3 ^{125}I Loss from Trap Solution

The loss of iodine-125 from the trap solution was tested in order to ensure it is effective at trapping iodine when high volumes of air or O_2 are passed through the solution and to ensure stripping of iodine does not occur when high volumes of air are bubbled through. The results of this test can be seen in Figure 2.4, which shows that bubbling at 600mL/min for up to 75 minutes caused no loss of iodine from the trap solution and confirms that

stripping of iodine from the trap solution during the combustion of the sample is not a concern.

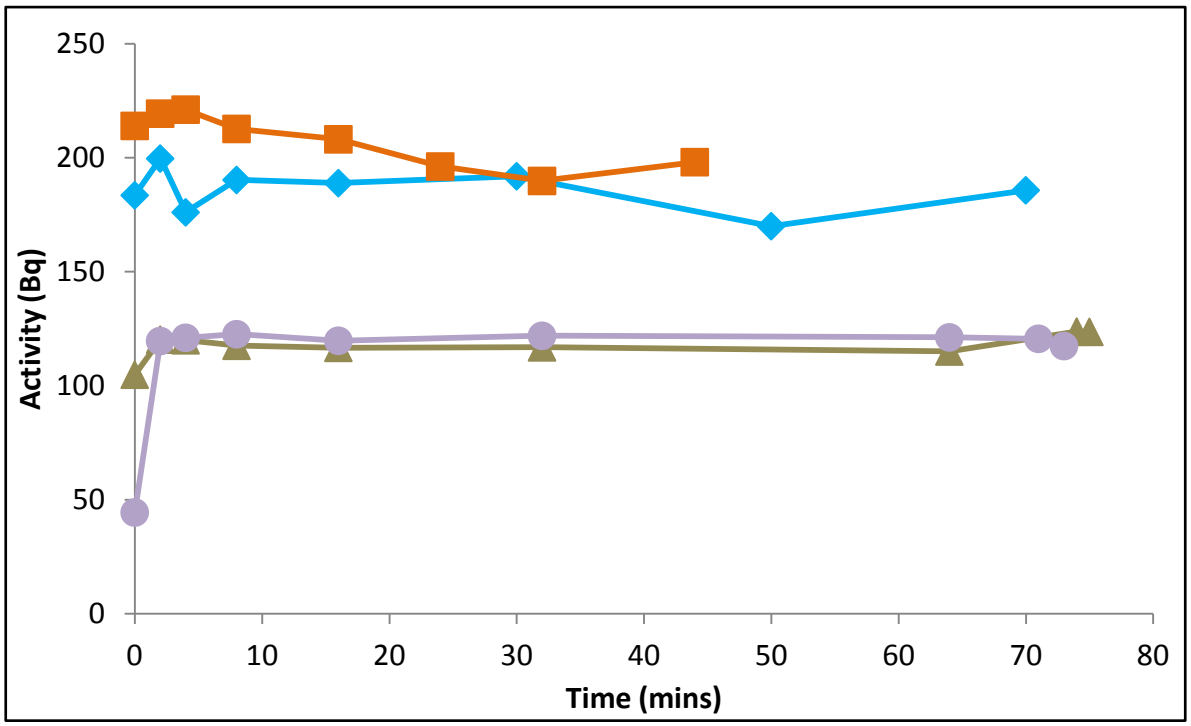

Figure 2.4: The loss of ^{125}I from the trap solution over time as air bubbled thorough it. Loss of activity over time is negligible in all four identical tests suggesting that stripping of iodine from the trap solution is not a concern. Error bars for this data are hidden by the data points.

3.2 Standard Reference Materials

In order to determine the reliability of our method we combusted three samples ranging from 0.5-0.6g of the ^{129}I standard reference material IAEA-375 (Chernobyl soil) and the results are shown in Table 2.3. We used a slightly modified technique from the one outlined herein in which we added vanadium pentoxide as an accelerator to aid volatilization from soil components with a high melting point. The vanadium pentoxide was added in a 5:1 ratio of V_2O_5 to sample and the temperature of combustion was raised to 1000°C [*Cornett et al.*, 1997]. The reason for these changes is that the high inorganic content of IAEA-375

would not be combusted efficiently at lower temperatures and iodine recovery would likely have been reduced. The ^{127}I was analyzed in the trap solution directly by ICP-MS and the $^{129}I/^{127}I$ ratio was calculated using the average ^{127}I value obtained. The concentration of ^{129}I in IAEA375 is given as Bq/kg, which can be converted to atoms/kg using a conversion factor of 7.148×10^{14}. The results we obtained were then corrected for ^{125}I recovery and all three samples fell within the 95% confidence interval recommended by the IAEA [*Strachnov et al.*, 1996] for both ^{129}I and ^{127}I. This shows that this technique is reliable and reproducible for small sample masses and a wide variety of materials with high and low organic contents.

Extraction	Recovery (%)	^{127}I Value (ppm)	^{129}I Value (10^8 atoms/g)	$^{129}I/^{127}I$ (x 10^{-7})
1 (CF64)	73.5	2.73	9.55 ± 0.22	1.09
2 (CF65)	71.7	1.28	9.85 ± 0.23	1.12
3 (CF66)	77.8	1.55	9.98 ± 0.21	1.14
Average	74.3	1.85	9.79 ± 0.22	1.12
IAEA-375 Reference Value		1.91	12.2	1.34
IAEA-375 95% Interval		0.69-3.13	9.29-15	1.03 - 1.66

Table 2.3: AMS results for ^{129}I, and $^{129}I/^{127}I$ of the standard reference material IAEA-375, which is composed of Chernobyl soil. The $^{129}I/^{127}I$ values were calculated using the ^{127}I concentration provided for IAEA-375.

3.3 ^{127}I and ^{129}I in Blanks and Seaweed

Numerous seaweed samples were combusted at a variety of flow rates. Of these three were selected for AMS analysis along with a process blank in which no sample was combusted. The results for the process blank, which trapped O_2 gas flowing at 800mL/min through an empty tube for the entire combustion showed no detectable ^{125}I, which suggests that the system was clean and had no ^{125}I contamination. In order to test that there was no ^{129}I contamination in the line, the trap solution for the process blank was precipitated for ^{129}I via AMS. The ^{129}I concentration in the blank was 6.04 x 10^6 atoms/g (assuming that the sample mass was 3.5 grams; the standard sample size used) and had an AMS $^{129}I/^{127}I$ ratio of 2.45 x 10^{-12}, which is the raw measurement from the AMS system for

Sample ID	Sample Type	Location	Date	^{127}I (ppm)	^{129}I (x10^9 atoms/g)	$^{129}I/^{127}I$ (x 10^{-9})	Recovery (%)	Corrected ^{129}I (x 10^9)	Corrected $^{129}I/^{127}I$
CF29	*F. vesiculosus*	Nova Scotia, Canada	May-12	409.7	3.47 ± 0.13	1.78 ± 0.19	78	4.45 ± 0.18	2.29E-09 ± 0.24
CF38	*F. vesiculosus*	Nova Scotia, Canada	May-12	409.7	4.26 ± 0.16	2.19 ± 0.23	77	5.53 ± 0.22	2.85E-09 ± 0.3
CF40	*F. vesiculosus*	Nova Scotia, Canada	May-12	409.7	4.14 ± 0.15	2.13 ± 0.22	89	4.65 ± 0.18	2.39E-09 ± 0.25
CF35	Process Blank	NA	NA	0.002	0.006 ± 0.0004	3.11 x 10^{-12} ± 0.37	NA	NA	NA

Table 2.4: Analytical results for ^{129}I and the $^{129}I/^{127}I$ ratio in Atlantic seaweed (Fucus vesiculosus) as well as the corrected results when the ^{125}I recovery is considered.

^{129}I and ^{127}I in the AgI precipitate (Table 2.4). This blank value is less than 1% of the iodine ratio measured in the samples.

Seaweed samples were digested in TMAH according to the procedure outlined in Fecher et al., (1998). In brief, 0.2 grams of seaweed were placed in a 50mL centrifuge tube with 1mL TMAH and 5ml de-ionized water. The samples were digested at 90°C for five days. The sample was then diluted and measured using ICP-MS. The ^{127}I results ranged from 396.5-428.5ppm with an average of 410 ppm (n=5). ^{129}I results in the seaweed samples ranged from 4.4 – 5.5 x 10^{9} atoms/g after correction for combustion recovery, which was calculated using the yield of the ^{125}I tracer as a quantitative proxy. The corrected $^{129}I/^{127}I$ ratio ranged from 2.3 - 2.9 x 10^{-9} (Table 2.5) These values for ^{129}I concentration and the $^{129}I/^{127}I$ ratio compare well to previously analyzed samples of seaweed from elsewhere in the Atlantic Ocean (Table 2.5)[*Kilius et al.*, 1992][*Hou et al.*, 2000][*Gómez-Guzmán et al.*, 2013] . This agreement with similar sample types from similar locations indicates that the combustion system is capable of producing repeatable results for ^{129}I concentration and the $^{129}I/^{127}I$ ratio.

In this instance the ^{129}I concentrations were corrected for the efficiency of the combustion system by using the percentage of ^{125}I recovered to correct the AMS concentration yielding the most accurate concentration of ^{129}I possible. The reason this is necessary is that the calculation for the concentration of ^{129}I is calculated from the ratio generated by the AMS from the AgI target produced from the trap solution whereas the concentration of ^{127}I in the TMAH digestate is measured by ICP-MS and is assumed to measure 100% of the iodine

in the sample. Therefore, the calculated concentration of ^{129}I using this ratio is an underestimate of total concentration as the recovery of ^{129}I in the sample is assumed to equal the percentage of ^{125}I recovered. Therefore, when calculating the ^{129}I concentration and the $^{129}I/^{127}I$ ratio using the ICP-MS data it is necessary to apply the correction factor determined by the ^{125}I recovery. However, if the ^{127}I concentration is measured directly in the trap solution this correction can be made for both isotopes.

Sample Type	Location	Date	^{127}I (ppm)	^{129}I (x 10^{9} atoms/g)	$^{129}I/^{127}I$ (x 10^{-9})	Reference
F. vesiculosus	Nova Scotia, Canada	May-12	410	4.45 ± 0.18	2.29 ± 0.24	This work
F. vesiculosus	Nova Scotia, Canada	May-12	410	5.53 ± 0.22	2.85 ± 0.3	This work
F. vesiculosus	Nova Scotia, Canada	May-12	410	4.65 ± 0.18	2.39 ± 0.25	This work
Algae	Matamek River, Quebec	1981	NA	NA	0.19	Kilius et. al. 1992
F. vesiculosus	Baltic - Swedish Coast	1982	54-178 (n=18)	0.82-5.89	2.27 - 8.8	Gómez-Guzmán et. al., 2013
F. vesiculosus	Baltic - Swedish Coast	1986	35-372 (n=31)	1.33 - 38.8	3.8 - 30.5	Gómez-Guzmán et. al., 2013
F. vesiculosus	Greenland A	1997	241	1.7	1.51	Hou et. al., 2000
F. distichus	Greenland B	1997	212	1.34	1.36	Hou et. al., 2000
F. distichus	Greenland C	1997	203	1.09	1.16	Hou et. al., 2000
F. distichus	Greenland D	1997	292	1.65	1.21	Hou et. al., 2000
F. distichus	Greenland E	1997	368	1.9	1.11	Hou et. al., 2000
F. distichus	Greenland F	1997	305	1.24	0.82	Hou et. al., 2000
F. distichus	Greenland G	1997	300	0.976	0.7	Hou et. al., 2000

Table 2.5: Comparison of ^{129}I concentrations and $^{129}I/^{127}I$ ratios in seaweed (Fucus vesiculosus) measured in this work to those measured in other seaweed samples from the Atlantic Ocean. The ^{127}I concentration given for the three seaweed samples measured via combustion is the average ^{127}I concentration measured after TMAH digestion of five seaweed replicates.

4.0 CONCLUSIONS

We successfully extracted iodine from soil and organic materials by using pyrohydrolysis and trapping iodine in an alkaline solution using inorganic ^{125}I and ^{125}I bound to humic acids, which simulates organically bound iodine, as quantitative recovery tracers. These results outline the optimal conditions needed to efficiently recover iodine that is bound within the samples using pyrohydrolysis. It was found that at an O_2 flow rate 400-800 mL/min is the optimal range for ^{125}I recovery regardless of the type of spike used. Two volatilization patterns were observed suggesting that samples must be heated to 800 °C and held there for at least an hour in order to recover all iodine in the sample. Furthermore, the different trends observed serve to highlight the complexity of iodine's behavior and show that a ^{125}I tracer is needed for every sample extraction. We examined the accuracy and reproducibility of the combustion system using two standard reference materials. IAEA-375 was used as a reference for ^{129}I. The ^{127}I concentration is also known so the $^{129}I/^{127}I$ ratio can be calculated. The results from these extractions show that this technique produces reliable and reproducible results in agreement with international standard reference materials. AMS targets of AgI were prepared for analysis following combustion and solvent extraction of seaweed samples to determine if this system is capable of producing repeatable results for ^{127}I and ^{129}I that agree with ^{129}I concentrations and $^{129}I/^{127}I$ ratios for seaweed generated by other methods and other labs. The ^{129}I concentration for seaweed was found to range between 4.4 - 5.5 x 10^9 atoms/g and the $^{129}I/^{127}I$ ratio was 2.3 – 2.9 x 10^{-9}, both of which compare well to published values. This indicates that ^{125}I can be used as a

quantitative recovery tracer for the extraction of ^{129}I and ^{127}I from solid organic materials. Throughout the experimental process we discovered that certain physical characteristics of the laboratory equipment are essential for efficient recovery of iodine. The most important feature is to have two furnace zones, with the sample zone gradually heating, while the second zone is heated rapidly to combust any partially combusted organic compounds that are released from the sample. Ultimately, this combustion technique has demonstrated the importance of using a ^{125}I tracer and helped unify some of the existing differences between previously published combustion methods for the extraction of ^{129}I and ^{127}I from organic rich materials.

Acknowledgements

We are very grateful for the continual advice and assistance from Paul Middlestead and other staff of the G.G. Hatch Stable Isotope Lab as well as the laboratory assistance from François Lagacé and David Chiumera. Thanks are also extended to Xiao-lei Zhao at the IsoTrace AMS Laboratory, Nimal Da Silva for the ICP-MS analysis and Sheila Kramer for providing us with a sample of IAEA-375.

References

Carlsena, L., Lassena, P.I.A., Warwickb, P., Randallb, A., 1993. Radio Labelled Humic Materials in Migration Studies. Mater. Res. Soc. Symp. Proc. 294, 811–816.

Cornett, R.J., Andrews, H.R., Chant, L., Chaput, T., Imahori, Y., Jirovec, J., Kramer, S., Koslowsky, V.T., Milton, G.M., Milton, J.C.D., 1996. High temperature pyrolysis to extract 36Cl for Accelerator Mass Spectrometry measurements. Nucl. Instruments Methods Phys. Res. B 117, 436–440.

Cornett, R.J., Chant, L., Andrews, H.R., Davies, W.G., Greiner, B.F., Imahori, Y., Koslowsky, V.T., Kotzer, T., Milton, J.C.D., Milton, G.M., 1997. 36Cl and 129I in teeth and bones. Nucl. Instruments Methods Phys. Res. B 123, 249–253.

Fabryka-Martin, J., Bentley, H., Elmore, D., Airey, P., 1985. Natural iodine-129 as an environmental tracer. Geochim. Cosmochim. Acta 49, 337–347.

Fecher, P.A., Goldmann, I., Nagengast, A., 1998. Determination of iodine in food samples by inductively coupled plasma mass spectrometry after alkaline extraction. J. Anal. At. Spectrom. 13, 977–982.

Gómez-Guzmán, J.M., Villa, M., Le Moigne, F., López-Gutiérrez, J.M., García-León, M., 2013. AMS measurements of 129I in seawater around Iceland and the Irminger Sea. Nucl. Instruments Methods Phys. Res. Sect. B Beam Interact. with Mater. Atoms 294, 547–551.

Hansen, V., Roos, P., Aldahan, A., Hou, X., Possnert, G., 2011. Partition of iodine (129I and 127I) isotopes in soils and marine sediments. J. Environ. Radioact. 102, 1096–104.

Herod, M.N., Clark, I.D., Kieser, W.E., Agosta, S., Zhao, X.-L., 2012. 129I dispersion and sources in Northwest Canada. Nucl. Instruments Methods Phys. Res. Sect. B Beam Interact. with Mater. Atoms 1–7.

Horrocks, D.L., 1974. Measurements of Disintegration Rates of ^{125}I Sources with a Single Well-Type NaI(Tl) Detector. Nucl. Instruments Methods Phys. Res. 125, 1–7.

Horrocks, D.L., Klein, P.R., 1974. Theoretical Considerations for Standardization of 125I by the Coincidence Method. Nucl. Instruments Methods Phys. Res. 124, 585–589.

Hou, X., Zhou, W., Chen, N., Zhang, L., Liu, Q., Luo, M., Fan, Y., Liang, W., Fu, Y., 2010. Determination of ultralow level 129I/127I in natural samples by separation of microgram carrier free iodine and accelerator mass spectrometry detection. Anal. Chem. 82, 1–6.

Hou, X.L., Dahlgaard, H., Nielsen, S.P., 2000. Iodine-129 Time Series in Danish, Norwegian and Northwest Greenland Coast and the Baltic Sea by Seaweed. Estuar. Coast. Shelf Sci. 51, 571–584.

Keppler, F., Biester, H., Putschew, A., Silk, P.J., Scholer, H.F., Mller, G., 2003. Organoiodine formation during humification in peatlands. Environ. Chem. Lett. 1, 219–223.

Kilius, L.R., Litherland, a. E., Rucklidge, J.C., Baba, N., 1992. Accelerator mass-spectrometric measurements of heavy long-lived isotopes. Int. J. Radiat. Appl. Instrumentation. Part A. Appl. Radiat. Isot. 43, 279–287.

Luo, M.-Y., Zhou, W.-J., Hou, X.-L., Chen, N., Zhang, L.-Y., Liu, Q., He, C.-H., Fan, Y.-K., Liang, W.-G., Wang, Z.-W., Fu, Y.-C., 2011. Determination of Low Level 129I in Soil Samples Using Coprecipitation Separation of Carrier Free Iodine and Accelerator Mass Spectrometry Measurement. Chinese J. Anal. Chem. 39, 193–197.

Marchetti, A.A., Rose, L., Straume, T., 1994. A simple and reliable method to extract and measure iodine in soils. Anal. Chim. Acta 296, 243–247.

Moran, J.E., Oktay, S.D., Santschi, P.H., 2002. Sources of iodine and iodine 129 in rivers. Water Resour. Res. 38, 1–10.

Moran, J.E., Oktay, S.D., Santschi, P.H., Schink, D.R., 1999. Atmospheric Dispersal of 129 Iodine from Nuclear Fuel Reprocessing Facilities. Environ. Sci. Technol. 33, 2536–2542.

Muramatsu, Y., Takada, Y., Matsuzaki, H., Yoshida, S., 2008. AMS analysis of 129I in Japanese soil samples collected from background areas far from nuclear facilities. Quat. Geochronol. 3, 291–297.

Schnetger, B., Muramatsu, Y., 1996. Determination of halogens, with special reference to iodine, in geological and biological samples using pyrohydrolysis for preparation and inductively coupled plasma mass spectrometry and ion chromatography for measurement. Analyst 121, 1627–31.

Sheppard, M.I., Hawkins, J.L., 1995. Iodine and microbial interactions in an organic soil. J. Environ. Radioact. 29, 91–109.

Sheppard, S.C., Evenden, W.G., Amiro, B.D., 1993. Investigation of the Soil-to-Plant Pathway for I, Br, Ci and F. J. Environ. Radioact. 21, 9–32.

Sheppard, S.C., Herod, M., 2012. Variation in background concentrations and specific activities of 36Cl, 129I and U/Th-series radionuclides in surface waters. J. Environ. Radioact. 106, 27–34.

Snyder, G., Fehn, U., 2004. Global distribution of ^{129}I in rivers and lakes: implications for iodine cycling in surface reservoirs. Nucl. Instruments Methods Phys. Res. Sect. B Beam Interact. with Mater. Atoms 223-224, 579–586.

Strachnov, V., Larosa, J., Dekner, R., Zeisler, R., Fajeglj, A., 1996. Report on the Intercomparison Run IAEA-375: Determination of Radionuclides in Soil Samples IAEA-375.

Toyama, C., Muramatsu, Y., Igarashi, Y., Aoyama, M., 2013. Atmospheric fallout of (129)I in Japan before the Fukushima accident: Regional and global contributions (1963-2005). Environ. Sci. Technol.

Warwick, P., Carlsen, L., Randall, A., Zhao, R., Lassen, P., 1993a. 14C and 125I Labelling of Humic Material for Use in Environmental Studies. Chem. Ecol. 8, 65–80.

Warwick, P., Zhao, R., Higgo, J.J., Smith, B., Williams, G.M., 1993b. The mobility and stability of iodine-humic and iodine-fulvic complexes through sand. Sci. Total Environ. 130-131, 459–465.

CHAPTER 3 – ^{129}I DISPERSION AND SOURCES IN NORTHWEST CANADA

ABSTRACT

Radioiodine, ^{129}I is a biophilic and mobile radionuclide, and a major contaminant of concern for long term radioactive waste disposal. Nuclear fuel reprocessing has released large amounts of anthropogenic ^{129}I in a number of locations globally; this has led to an increase in the concentration of ^{129}I and the ^{129}I/^{127}I ratio in the environment. Therefore, a detailed understanding of its movement and concentration in the environment is essential. While ^{129}I dispersion has been examined in the vicinity of nuclear activities, little is known about its accumulation in remote regions. Accordingly, we have undertaken reconnaissance sampling in the Arctic as a location that may be affected by ^{129}I fallout. Samples from large watersheds were collected in northern Canada on a trajectory starting in Whitehorse, Yukon Territory (60°43'00"N) and moving north to Tsiigehtchic, Northwest Territory (67°26'26"N). Results show concentrations of ^{129}I up to 27 x 10^{6} atoms/L are present in northwest Canada and ^{129}I/^{127}I ratios up to 1.68 x 10^{-10} . Annual ^{129}I fallout ranges from 2.8 to 5.0 x 10^{9} atoms/m^2/yr, calculated by normalizing the measured values to watershed area and discharge. These quantities substantially exceed literature values for waters containing only geogenic or cosmogenic production and are similar for all watersheds regardless of watershed area or discharge. Anthropogenic releases of ^{129}I into the atmosphere or oceans are the major potential sources of ^{129}I in the Arctic.

1.0 INTRODUCTION

It has been well established that Iodine-129 (^{129}I) is a long-lived U fission product of concern, generated by nuclear power production and released during nuclear fuel reprocessing and nuclear bomb tests [*Rao and Fehn*, 1999]. ^{129}I has a half-life of 15.7 million years and is naturally produced by spontaneous fission of ^{238}U in geologic materials and by cosmic-ray induced n-p reaction on ^{129}Xe in the atmosphere [*Edwards*, 1962; *Fabryka-Martin et al.*, 1989]. The natural inventory of ^{129}I is estimated to be ~230kg, most of which is found in the deep oceans [*Rao and Fehn*, 1999; *Snyder et al.*, 2010]. The natural terrestrial inventory is estimated to be approximately 80kg [*Moran et al.*, 1998]. The pre-anthropogenic ocean is estimated to have had a ^{129}I concentration of 0.44 x 10^6 atoms/L or a total of ~130 kg while non marine water had a concentration of 0.037 x 10^6 atoms/L or ~11kg [*Snyder et al.*, 2010]. Industrial releases from reprocessing plants, such as La Hague (France), which has released 3,119 kg of ^{129}I into the English Channel, and an additional 68kg into the atmosphere, and Sellafield which released 1371kg of liquid discharge and 182 kg of atmospheric releases, are the primary source of ^{129}I today [*Keogh et al.*, 2010]. There have also been releases by atmospheric bomb tests which released 50 kg of ^{129}I and nuclear accidents such as Chernobyl (1.3 kg of ^{129}I) and others such as Tomsk, Windscale and Fukushima [*Moran et al.*, 2002]. These anthropogenic contributions to the global ^{129}I inventory have overwhelmed that produced by natural processes and raised the natural ^{129}I/^{127}I ratio by several orders of magnitude [*Rao and Fehn*, 1999]. Previous work has been conducted on the dispersion of ^{129}I to determine baseline levels and the effect of reprocessing plants on ^{129}I concentrations and ratios in the vicinity of ^{129}I point sources

[*Persson et al.*, 2007; *Englund et al.*, 2010a; *Keogh et al.*, 2010; *Reithmeier et al.*, 2010]. It has been shown that significant amounts of ^{129}I have been deposited around nuclear fuel reprocessing plants [*Rao and Fehn*, 1999; *Hu et al.*, 2005; *Engelmann et al.*, 2009]. However, very few studies have investigated the extent to which anthropogenic ^{129}I can be detected on a regional scale or ^{129}I transport dynamics far from ^{129}I sources. [*Beasley et al.*, 1997] and [*Moran et al.*, 2002] have presented data on levels of ^{129}I in the Canadian Arctic from water samples, however no comprehensive study has been performed in this remote region. Data on the Mackenzie River has been presented previously with four samples taken between 1994 and 1996. The results show that ^{129}I concentrations range from 3-4.7 x 10^7 atoms/L during this time and the only ^{129}I/I ratio measured was 2153 x 10^{-12} [*Beasley et al.*, 1997; *Moran et al.*, 2002]. Samples from Axel Heiberg Island in the high Arctic have also been measured and show ^{129}I concentrations that range from 3.9-13 x 10^6 atoms/L and ^{129}I/I ratios from 352.79-1604.64 x 10^{-12} [*Rao and Fehn*, 1999; *Moran et al.*, 2002]. Additionally, ^{129}I fallout in the Arctic was detected by air quality monitoring in 1981-1983 by Environment Canada and the Canadian Radiological Health Monitoring Network [*Kieser et al.*, 2005]. Results of this work showed elevated concentrations of ^{129}I, which ranged from ~0.1 – 15 x 10^6 atoms/m^3 of air, depositing across Canada and the Arctic. Back trajectory analysis of air parcels showed transport from Europe and Russia.

Given recent accidental releases and on-going industrial emissions, it is crucial to establish baseline data in remote regions, such as the Canadian Arctic in order to assess the impact of the nuclear industry worldwide and determine the spatial limits to which anthropogenic ^{129}I can be detected. As an anion, iodine is very mobile in the environment

[*Whitehead*, 1984; *Hou et al.*, 2009]. This allows it to travel great distances from a source before deposition. The cycle of iodine in nature depends upon the redox conditions in host materials. Under reducing conditions, such as marshes, swamps, and anoxic groundwaters, the dominant species of inorganic iodine is iodide, I^- [*Whitehead*, 1984]. Under oxidizing conditions in surface waters and oceans the dominant inorganic species is iodate, IO_3^-. Iodine is also a biophilic element and can exist in many organic forms but dominantly as the volatile species methyl iodide, CH_3I, [*Amachi*, 2008]. The volatile species are mobile by atmospheric transport, followed by wet and/or dry deposition of iodine [*Reithmeier et al.*, 2010]. Investigating rivers and creeks that drain large regions is an effective way of determining if anthropogenic fallout is occurring over a large area [*Rao and Fehn*, 1999; *Kekli et al.*, 2003; *Reithmeier et al.*, 2007, 2010; *Keogh et al.*, 2010]. Also, the biophilic nature of iodine makes it possible to use peat as an environmental archive to estimate the changes in ^{129}I fallout over time in a given region.

2.0 METHODS

2.1 Study Sites

As a first phase in a continental scale investigation, water sampling was conducted at 15 variable-sized watersheds in the Yukon and Northwest Territories, Canada in June 2010 (Figure 3.1). Sample sites were chosen to reflect a wide latitudinal distribution and watersheds of varying size; most drained a minimum of several hundred to thousands of square kilometers. The water samples were collected in 500mL acid washed amber glass or high density polyethylene bottles that were rinsed with site water. The unfiltered water samples were stored in a dark cooler until analysis.

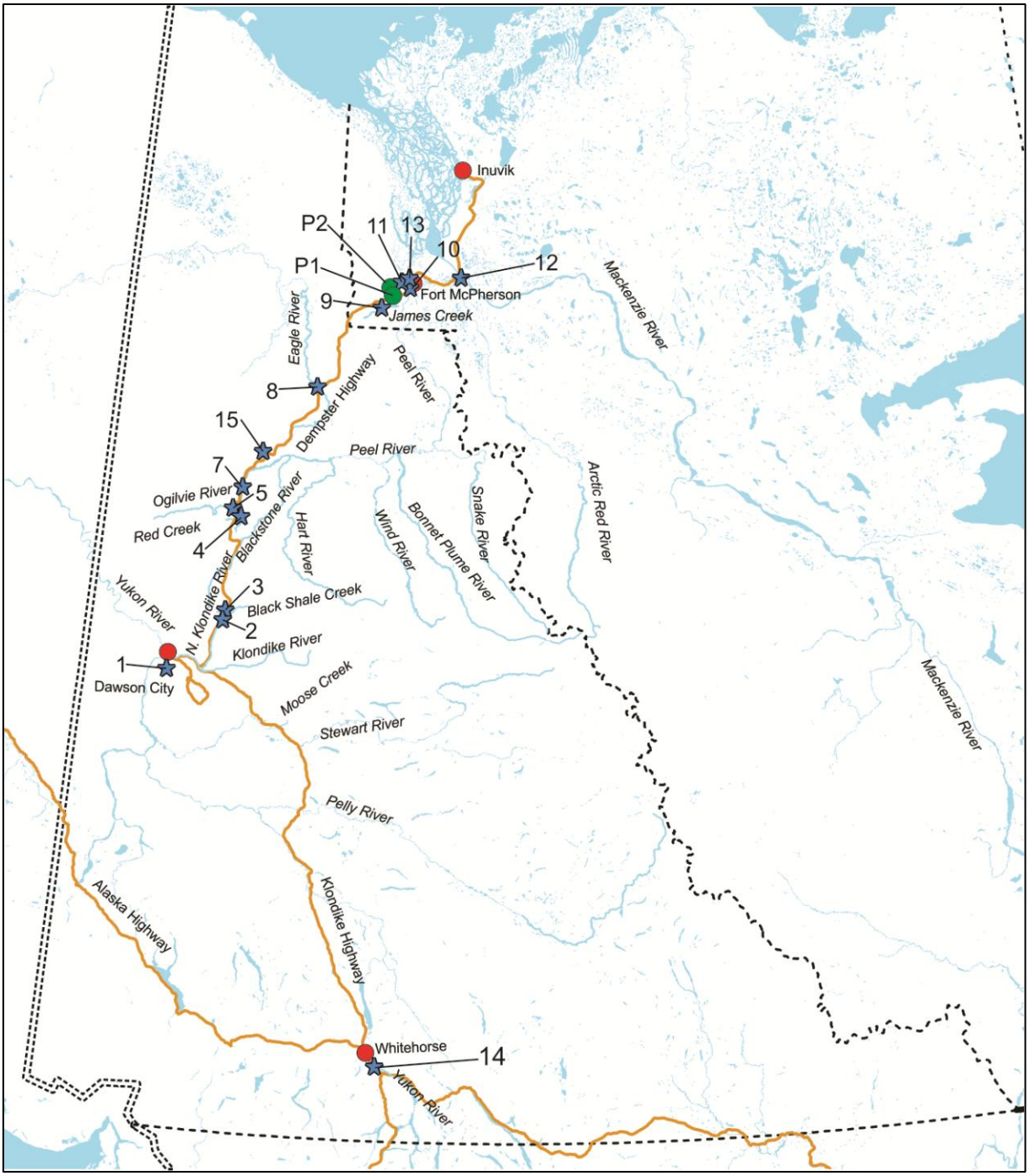

Figure 3.1: Locations of ^{129}I sampling sites. Blue stars are water sample sites and green circles are peat sample sites.

Peat samples were also collected at Fort McPherson, Yukon in peat sections exposed in thaw slumps during June 2010. Living peat was also collected above a permafrost layer. Peat samples were collected by cutting out a section of the peat at approximately 30-50cm intervals from within the section, being careful to take no exposed peat and placing it in a Ziploc bag made of low density polyethylene. They were stored at 4°C until analysis.

2.2 Laboratory and Analytical Methods

2.2.1 Redox Extraction of ^{129}I in Aqueous Samples

A carrier-addition method was used to extract iodine during a series of redox transformations. Aliquots of 200 mL were used. Samples were pre-treated with 0.5 mL of 30% H_2O_2 in order to oxidize any humic and/or fulvic acids that may limit the recovery of iodine. The water was then acidified to pH 2 using 6-N HNO_3 and shaken. The iodine is then reduced to I^- (iodide) using 1-M $NaHSO_3$, followed by the addition of 2 mg of NaI carrier which has a ^{129}I /^{127}I ratio of < 1.56×10^{-13}**.** Iodine was extracted into hexane, which gained a purple tint, by oxidizing it from I^- to I_2 using 6-M $NaNO_2$. The hexane was then removed in a separatory funnel. This step was repeated several times until the added hexane remained clear. The iodine was then back extracted from the hexane into 18 MΩ deionized water to enhance recovery and remove any contamination that may also be present. Finally, the iodine was precipitated using 0.1-M $AgNO_3$ and 6M-HNO_3 and slowly dried. Total iodine was measured in filtered water samples using an Agilent 7700 ICP-MS.

2.2.2 Caustic Fusion Extraction of ^{129}I in Solid Samples

A caustic (alkali) fusion technique was used to extract ^{129}I from solid organic and inorganic materials. Approximately 5 g of sample was placed in a 50°C oven and dried. The

sample was then transferred into a washed 100-mL iron crucible, and 15 g of solid NaOH and 10 g of solid $NaNO_2$ were added to the crucible along with a few mL of mid-Holocene (pre-anthropogenic age with very low levels of ^{129}I) glacial water. 5-20µL of IsoTrace NaI carrier[1] was added, the specific amount depending on the iodine concentration of the sample. The mixture was then stirred gently and covered for a 24h period.

The crucible was then placed in a furnace and heated in steps up to a maximum temperature of 600°C. The stepwise heating allows for the gradual oxidation of organic matter, preventing rapid combustion and possible eruption of the sample. 18 MΩ DIW was added to the crucible and stirred to loosen and dissolve the crust. The mixture was then removed from the crucible. The soluble and insoluble fractions were separated by centrifugation. The insoluble fraction was saved for later treatment and the soluble fraction was put through aqueous redox extraction.

The insoluble fraction was washed with glacial water and 5 mL 6-N HCl was added to the beaker to dissolve the precipitate, and the supernatant was decanted into a separate beaker. This step was repeated to dissolve the remaining precipitate. The sample was then put through an abbreviated aqueous redox extraction.

Targets were prepared for AMS analysis by mixing 1-2mg of AgI precipitate with high purity niobium powder and pressed into a stainless steel cathode for accelerator mass spectrometry analysis at the IsoTrace 3MV Tandem AMS operated by the University of Ottawa.

[1] $^{129}I/^{127}I$ ratio of $(1.56 \pm 0.06) \times 10^{-13}$

3.0 CONCENTRATION OF ^{129}I IN SURFACE WATER

The concentrations of ^{129}I in Arctic water samples do not vary considerably and are summarized in Table 3.1. The mean concentration of the Yukon data is 10.8 x 10^6 ± 4.9 atoms/L, and ranges from 2.5 – 20.7 x 10^6 atoms/L. These values are similar to values previously reported for the Canadian Arctic [*Beasley et al.*, 1997; *Moran et al.*, 2002]. This apparent lack of change over the last 15 years suggests that the fallout of ^{129}I in the Arctic has remained relatively constant. The ^{129}I concentrations observed are two orders of magnitude higher than expected for natural concentrations in surface water, which is estimated to be around 10^4 atoms/L, and is primarily from natural cosmogenic fallout [*Rao and Fehn*, 1999]. Geogenic contributions can be discounted given the rapid circulation of groundwaters in these regions and the extremely low ^{129}I/I ratio in sedimentary bedrock which is calculated to be 3 x 10^{-14} for limestone and 63 x 10^{-14} for shale, which are the dominant bedrock types in this region [*Fabryka-Martin et al.*, 1985; *Utting*, 2011]. The low geogenic ratios for these rocks make the influence of this source negligible on surface water. This suggests that the primary source of ^{129}I in the Arctic is not from natural sources. However, identifying a single source of ^{129}I for this region of the Canadian Arctic is complicated by the great distance from any major emitter of anthropogenic ^{129}I. Furthermore, the small variation of ^{129}I concentrations over time implies that no single ^{129}I release can be identified as the primary source of the enriched background observed. However, this elevated background makes it clear that anthropogenic ^{129}I has moved by atmospheric transport and subsequent wet and dry deposition. Sources of ^{129}I that could have contributed to the concentrations seen in these Arctic watersheds are numerous and

Site #	Site Name	Iodine (µg/L)	^{129}I Concentration (10^6 atoms/kg)	Error (1σ)	^{129}I/I (x 10^{-10})	Error (1σ) (x 10^{-10})	Longitude (°W)	Latitude (°N)	Sampling Date
1	Eldorado Creek (aufeis)	8.35	16.1	1.45	4.06	0.38	139° 14'44.99"	63°51'41.74"	29-May-2010
2	N. Klondike River (aufeis)	3.54	10.96	1.5	6.53	0.90	138° 14'59.84"	64° 30'53.48"	30-May-2010
3	N. Klondike River (downstream)	3.03	7.55	1.59	5.25	1.1	138° 13'30.56"	64° 30'20.83"	30-May-2010
4	Red Creek	2.95	8.16	1.45	5.84	1.0	138°22'12.42"	65° 9'34.05"	31-May-2010
7	Ogilvie River	3.72	8.92	1.13	5.05	0.65	138°18'0.56"	65°21'45.13"	31-May-2010
8	Eagle River	3.69	7.55	1.31	4.32	0.75	136°42'49.30"	66°26'35.80"	1-Jun-2010
9	James Creek	2.72	2.52	0.99	1.95	0.79	136°00'19.30"	67°08'12.7"	1-Jun-2010
10	Peel River	1.88	7.5	1.59	8.41	0.18	134°52'25.92"	67°20'19.04"	3-Jun-2010
11	Unnamed Creek	1.63	17.04	1.55	22	2.0	135°14'30.00"	67°15'18.00"	4-Jun-2010
12	Mackenzie River	5.46	20.74	1.55	8.01	0.60	133°45'46.42"	67°27'24.27"	6-Jun-2010
12	Mackenzie River	5.46	14.76	1.45	5.70	0.56	133°45'46.42"	67°27'24.27"	6-Jun-2010
13	Stony Creek	1.71	11.77	1.41	14.5	1.7	134°55'16.69"	67°23'18.25"	8-Jun-2010
14	Yukon River	3.04	5.98	1.31	4.14	0.91	135°02'08.36"	60°40'56.24"	18-Jun-2010
14	Yukon River	3.04	11.1	1.31	7.69	0.92	135°02'08.36"	60°40'56.24"	18-Jun-2010
15	Blackwater Spring	NA	4.32	1.36	NA	NA	138°13'40.83"	65°16'31.84"	31-May-2010

Table 3.1: Total iodine, raw AMS measurements, ^{129}I/I, coordinates and date for each sample analyzed and organized according to site

span a time range of approximately 60 years. Both atmospheric and direct wastewater releases to the oceans from fuel reprocessing, which are then volatilized, must be considered [*Rao and Fehn*, 1999; *Kekli et al.*, 2003; *Snyder et al.*, 2010]. Volatilization from the upper layers of the oceans contributes as much ^{129}I to the troposphere as atmospheric releases [*Reithmeier et al.*, 2010]. Other possible contributors of ^{129}I are nuclear bomb testing in the 1950s and 1960s as well as nuclear accidents such as Chernobyl, Chelyabinsk and Tomsk, which all released substantial quantities of ^{129}I, albeit far less than the cumulative industrial releases. However, as these are singular events and for the most part remote in time, a continued source of atmospheric ^{129}I from volatilization at the ocean surface and atmospheric releases from nuclear fuel waste reprocessing should be considered as the dominant sources of ^{129}I in the Arctic.

3.1 ^{127}I and ^{129}I/^{127}I in Surface Water

The total concentration of iodine in the samples ranged from 1.6 – 8.3 ppb. These results are comparable to previous values for total iodine in Arctic rivers [*Beasley et al.*, 1997; *Rao and Fehn*, 1999]. There is no observed relationship between the concentration of ^{129}I and the total concentration of iodine in the watersheds sampled. Presumably, both isotopes of iodine behave the same chemically and therefore the variance observed between watersheds suggests that ^{127}I and ^{129}I are from different sources (Figure 3.2). In the rivers sampled most ^{127}I likely comes either from atmospheric fallout or soil and bedrock weathering while ^{129}I comes from wet and dry deposition from the atmosphere**.** It is also unlikely that much iodine is contributed to the watershed from groundwater or watershed soils as much of the region is underlain by continuous or discontinuous permafrost, with

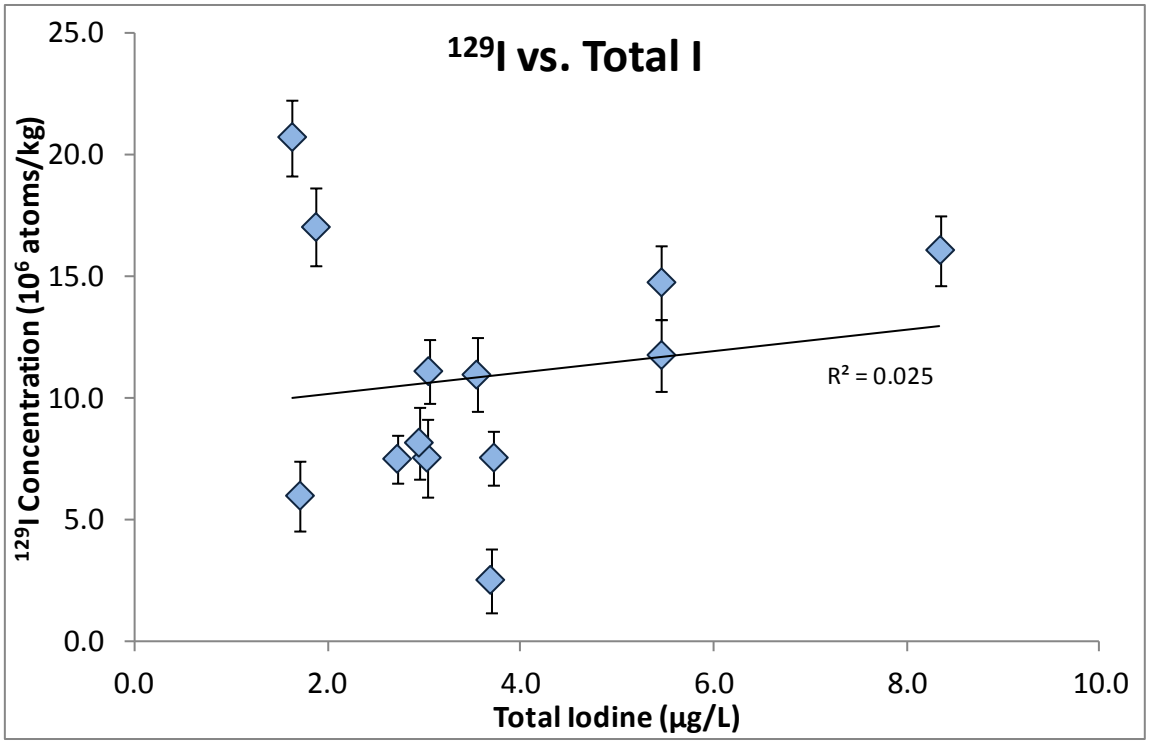

Figure 3.2: Graph showing the relationship between ^{129}I and ^{127}I in surface water.

limited bedrock circulation. ^{129}I /I ratios were calculated using total iodine measurements made by ICP-MS. The $^{129}I/I$ ratio ranges from 1.95×10^{-10} to 22×10^{-10} with an average value of 7.4×10^{-10}. These results agree well with previous samples taken in the Arctic [*Beasley et al.*, 1997; *Rao and Fehn*, 1999; *Moran et al.*, 2002; *Snyder and Fehn*, 2004] demonstrating that little has changed with regards to ^{129}I fallout over the past decade, and showing that ^{129}I cycling is a continuing process in the Arctic. The $^{129}I/I$ ratios are elevated 1-2 orders of magnitude higher than the pre-anthropogenic ratio of 1.5×10^{-12} [*Moran et al.*, 2002]. There are no trends observed with latitude or elevation that could suggest these two factors have an influence on iodine transport within the Arctic for total I or the $^{129}I/I$ ratio.

3.2 Watershed Flux

In order to further understand the sources and cycling of ^{129}I in the Arctic environment the measured concentrations have been normalized to watershed size, discharge, and evapotranspiration (Table 3.2). This makes the data for each watershed comparable, as these factors may affect the quantities of ^{129}I that discharge from the watershed. Another factor that greatly influences the amount of ^{129}I that reaches a river is its interaction with soils and biological materials as they act as traps for iodine in the environment. The equation used to normalize the measured ^{129}I concentrations for each watershed is as follows:

$$\psi = \frac{Q \times {}^{129}I}{WA}$$

Where ψ, is the ^{129}I flux in atoms/m^2 yr which is the number of atoms per square metre depositing in the entire watershed, Q is river discharge (m^3/yr) – assumed to have a 5% uncertainty, ^{129}I is the measured concentration of ^{129}I atoms in the sample in atoms/m^3 and WA is the area of the watershed in m^2 – assumed to have a 5% uncertainty. In order to account for evapotranspiration effects the following calculation must be performed to correct discharge. There is an assumption that change in water stored in the watershed is zero, meaning any precipitation that infiltrates into the soil and is part of groundwater recharge is lost by groundwater discharging into the river.

$$Q = (\mathrm{P} - \mathrm{ET}) \times \mathrm{WA}$$

Where Q, discharge in m^3/yr is equal to P, annual precipitation in m^3/m^2/yr minus ET, annual evapotranspiration in m^3/m^2/yr all times WA, the watershed area in m^2. The

normalized results for ψ range from 1.74 x 10^9 – 7.95 x10^9 atoms/m^2/yr. This shows that within the Arctic environment variability is relatively low and fallout of ^{129}I, which has been determined to be dominantly from anthropogenic sources, is constant across the Yukon. Furthermore, a comparison of the normalized data points with latitude, watershed area and discharge shows no correlation (Figure 3.3). This shows that while the raw concentration measured by AMS is dependent on watershed size and discharge that fallout is constant regionally. Furthermore, it also shows that over the limited range sampled, latitude and/or proximity to the coast do not have an observed influence on ^{129}I deposition in the Canadian Arctic. The results presented in this paper compare very well with samples of the Mackenzie River taken previously by Beasley showing that the change in ^{129}I flux over the last decade has been minimal. The measurements of P and ET are based on measurements made regionally by the nearest available sampling station. Therefore, they do not necessarily represent the specific watersheds individually and similar values are used for several of the watersheds in question. Sensitivity analysis of calculated Q versus Q in watersheds of similar size and latitudes with discharge gauging yields similar results suggesting that while this calculation does contain some uncertainty its results are also reasonable.

Site Name	^{129}I Concentration (10^6 atoms/kg)	Latitude (°N)	Watershed Area (m^2)	Annual Precipitation (L/m^2)	Washout (atoms/m^2)	Specific Discharge (L/yr)	Evapotranspiration (L/m^2)	Yearly ^{129}I Flux (atoms/m^2/yr)	±
Yukon River (1)	5.98	60	3.24E+11	267.4	2.97E+9	7.25E+13	43.4	2.48E+9	3.42E+8
Yukon River (2)	11.1	60	3.24E+11	267.4	1.60E+9	7.25E+13	43.4	1.34E+9	3.09E+8
North Klondike River (1)	10.96	64	1.10E+09	320	3.51E+9	4.10E+11	~60	4.09E+9	6.29E+8
North Klondike River (2)	7.55	64	1.10E+09	320	2.41E+9	4.10E+11	~60	2.81E+9	6.26E+8
Ogilvie River	8.92	65	7.13E+09	300	2.68E+9	1.71E+12	~60	2.14E+9	3.10E+8
Eagle River	7.55	66	1.03E+10	417	3.15E+9	3.68E+12	~60	2.70E+9	5.06E+8
Peel River	7.5	67	7.36E+10	292	2.19E+9	1.71E+13	~60	1.74E+9	3.90E+8
Mackenzie River (1)	20.74	67	1.81E+12	241	5.0E+9	3.06E+14	71.55	3.51E+9	3.60E+8
Mackenzie River (2)	14.76	67	1.81E+12	241	3.56E+9	3.06E+14	71.55	2.50E+9	3.02E+8
Mackenzie River (Beasley)	43	69	1.81E+12	241	1.04E+10	3.06E+14	71.55	7.27E+09	4.13E+8
Mackenzie River (Beasley)	38	69	1.81E+12	241	9.16E+09	3.06E+14	71.55	6.42E+09	3.27E+8
Mackenzie River (Beasley)	47	69	1.81E+12	241	1.13E+10	3.06E+14	71.55	7.95E+09	4.02E+8

Table 3.2: Sites which have requisite watershed data available were normalized to watershed size, and discharge in order to produce, ψ, a yearly ^{129}I fallout per metre squared per year. Also included are samples taken by Beasley et al., 1997 for the Mackenzie River. A 5% error in annual discharge was assumed to calculate the uncertainty in yearly flux.

An estimated global flux of ^{129}I has been presented previously by [*Moran et al.*, 2002]of 1 x 10^{10} atoms/m^2/yr which is an order of magnitude higher than the fluxes presented here. This is likely due to remoteness of the region and the lack of any nearby ^{129}I point source. However, despite this, the data presented here do serve to strengthen the argument that anthropogenic ^{129}I has spread ubiquitously throughout the northern hemisphere and is contaminating remote locations. Cycling of ^{129}I in the Arctic is relatively rapid as there is little interaction with subsurface organic matter. Much of the subsurface is frozen year-round, therefore, most of the ^{129}I that is deposited is either taken up by surface organic matter or is contained in runoff, which contributes ^{129}I to rivers. Furthermore, groundwater inputs in most rivers are limited due to permafrost.

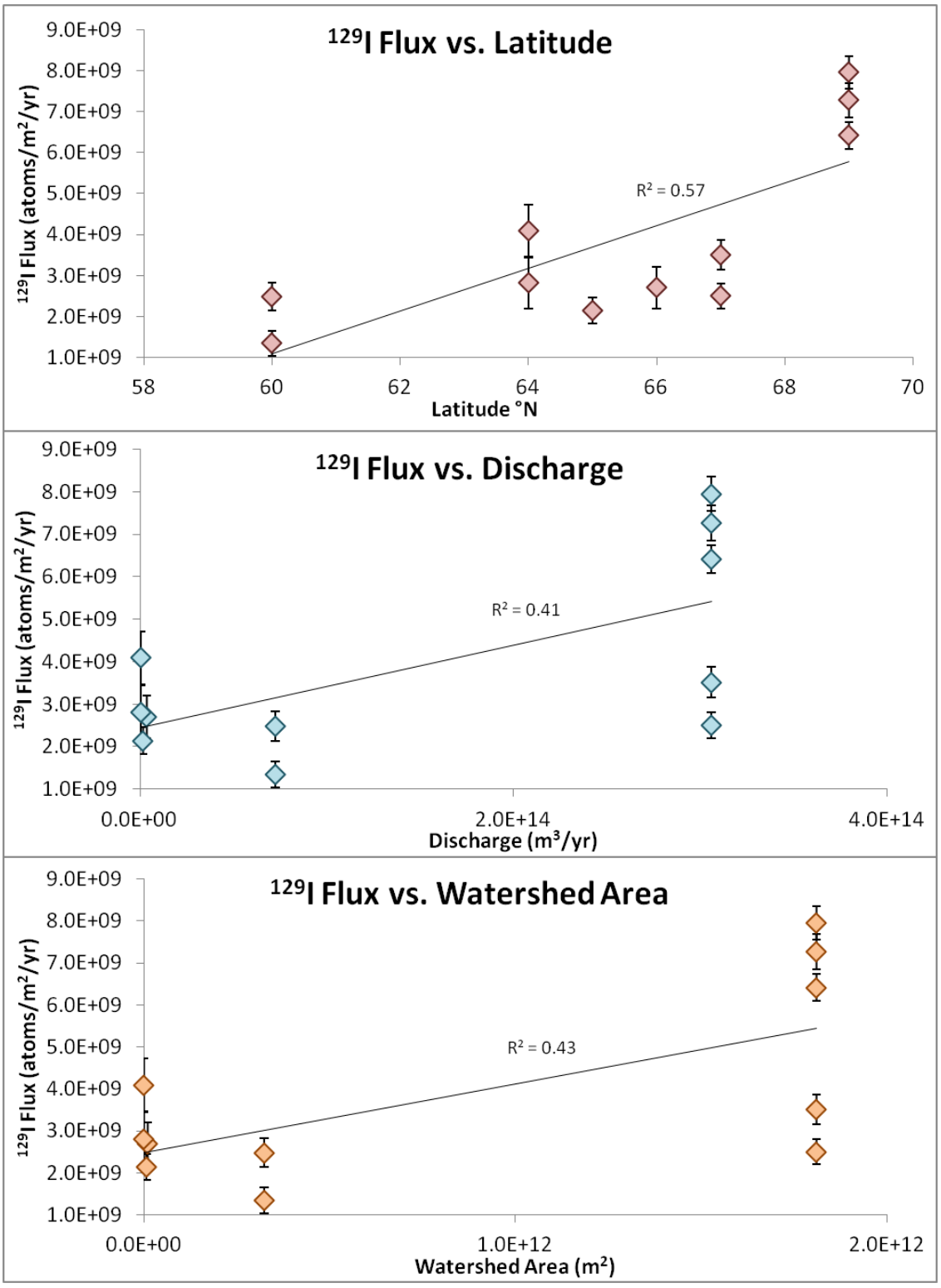

Figure 3.3: Graphs showing ^{129}I deposition flux, ψ, in Yukon watersheds compared to watershed area, latitude and discharge. Watershed area, discharge and latitude all show poor correlations. All error is contained within the data points.

3.3 ^{129}I and ^{129}I/^{127}I in Peat

To provide a contrast between modern and pre-nuclear age fallout of ^{129}I, sampling was conducted from surface to 1.5 m depth for two sections of peat moss near Fort McPherson, NWT. Iodine is concentrated in organic material, making present and ancient peat a potential archive of variations in ^{129}I fallout over time. These samples had a large range of values from 1.2 - 409 x 10^6 atoms/g**.** The highest value was found in the modern peat at surface, while ancient peat moss had very low concentrations of ^{129}I (Table 3.3). The ^{129}I/I ratio was also calculated for all peat samples using total iodine measurements from ICP-MS. The results show enriched ratios near ground surface and just below which suggests ^{129}I fallout is being readily absorbed and fixed by the peat (Figure 3.4). The ratio decreases rapidly with depth to levels comparable to what would be expected for pre-nuclear fallout. Furthermore, the ^{129}I/I ratio is dependent on the concentration of ^{129}I and is not related to the total concentration of iodine (Figure 3.5). The source of the high concentration and ratios for ^{129}I in the modern peat moss is considered to be anthropogenic, while the deeper peat moss pre-dates human nuclear activities. A comparison of the two peat sections sampled, which come from different sites within 3 km of one another, shows that the trend of high surface values and declining values in older, deeper samples is consistent within the region and is not a site specific phenomenon. This also indicates that ^{129}I does not migrate through the peat section. Once it is fixed by the peat it does not remobilize at a later date making peat is an ideal environmental archive to investigate changes in ^{129}I fallout over time.

Sample	Slump Site	Concentration (10^6 atoms/g)	Error (1σ)	$^{129}I/I$	Error (1σ)	Depth bgs (m)	Sampling Date	Longitude °W	Latitude °N
S20	Charras	409	7.2	7.79E-11	1.47E-12	0.1	6-Jun-2010	135°14'03.79"	67°15'15.61"
S01	Charras	224	4.7	8.25E-11	1.73E-12	0.2	6-Jun-2010	135°14'03.79"	67°15'15.61"
S03	Charras	4.6	0.5	2.45E-13	2.67E-14	0.6	6-Jun-2010	135°14'03.79"	67°15'15.61"
S04	Charras	6.4	0.6	1.86E-12	1.60E-13	0.8	6-Jun-2010	135°14'03.79"	67°15'15.61"
S05	Charras	5.8	0.6	1.30E-12	1.36E-13	1	6-Jun-2010	135°14'03.79"	67°15'15.61"
S07	Charras	15	0.9	2.31E-12	1.37E-13	1.5	6-Jun-2010	135°14'03.79"	67°15'15.61"
S16	Melanie	60	1.6	1.47E-11	4.15E-13	0.3	7-Jun-2010	135°16'13.94"	67°15'10.52"
S13	Melanie	1.6	0.5	2.42E-13	7.67E-14	1.5	7-Jun-2010	135°16'13.94"	67°15'10.52"
S11	Melanie	1.2	0.4	3.09E-13	1.03E-13	2.1	7-Jun-2010	135°16'13.94"	67°15'10.52"

Table 3.3: ^{129}I concentration $^{129}I/I$ ratios, date and coordinates for peat samples taken and both the Charras and Melanie retrogressive thaw slump sites.

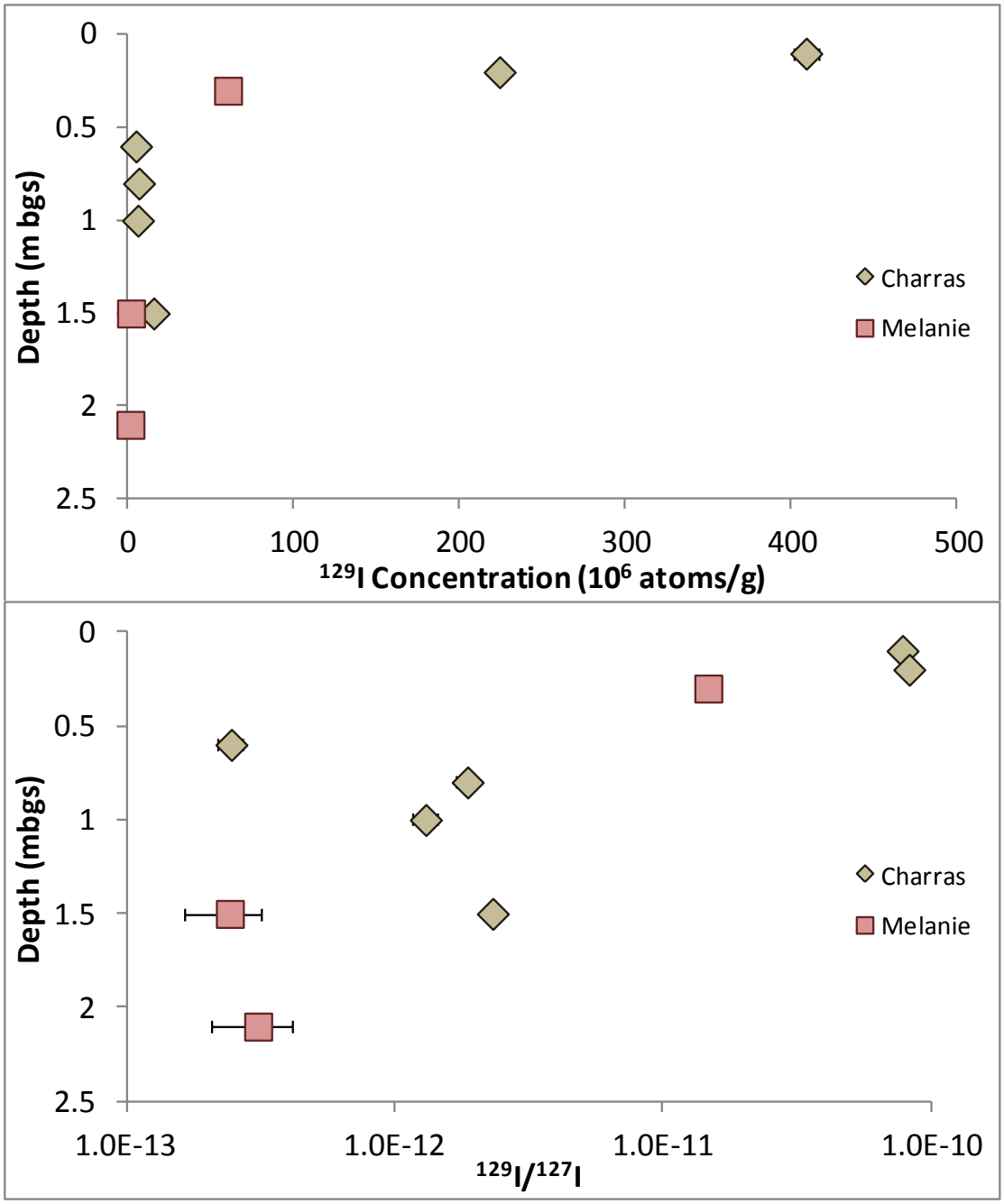

Figure 3.4: Depth profile showing ^{129}I concentrations and ^{129}I/I in peat profiles exposed in retrogressive thaw slumps. Both sites, Chara and Melanie, are with 3km of one another and 20km of Fort McPherson, NWT, Canada. Error bars that are not visible are contained within the data point. mbgs is metres below ground surface.

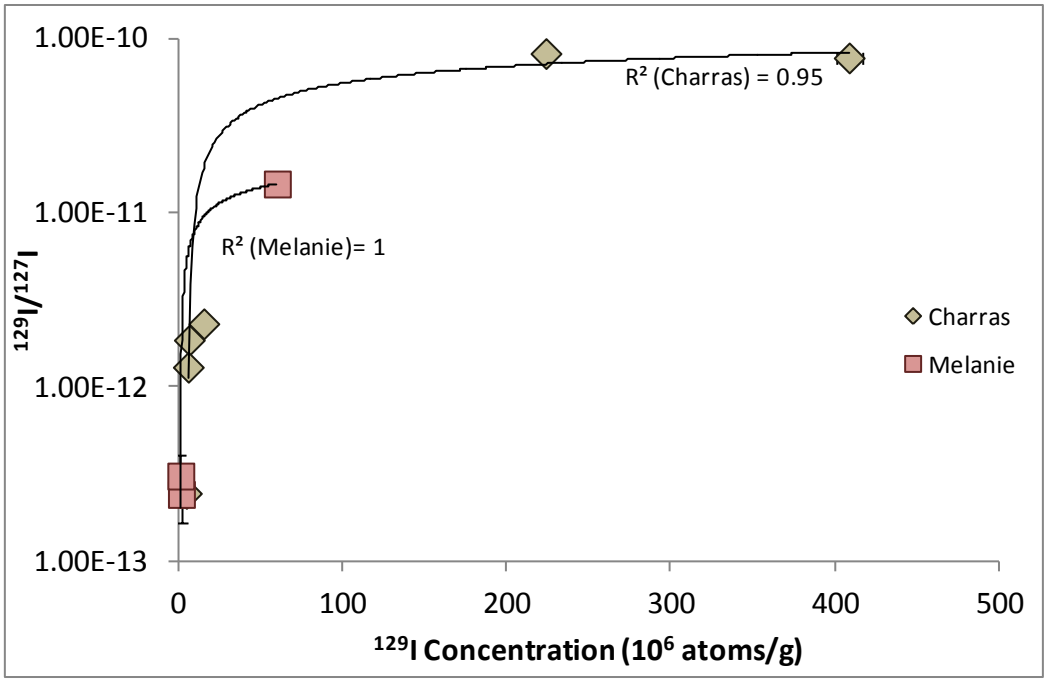

Figure 3.5: There is a strong correlation between the concentration of the ^{129}I and the $^{129}I/^{127}I$ ratio for both sample sites. This indicates that in peat the $^{129}I/^{127}I$ ratio is dependent on the concentration of ^{129}I. Any error that is not visible is contained with the data points.

3.4 Sources and Transport

Much of the ^{129}I released by nuclear fuel reprocessing is in the form of liquid discharges into the oceans, particularly the Irish Sea, which receives ^{129}I discharge from Sellafield (UK) and the English Channel from La Hague (France). Research by Smith et. al. has shown that the dominant mode of transport for fuel reprocessing releases is advective in ocean waters above 1000m depth allowing for the calculation of ^{129}I release times and the use of ^{129}I as a tracer of ocean currents [*Smith et al.*, 2011]. Since the liquid releases from fuel reprocessing plants are in the north Atlantic, which is near the region of ocean bottom water formation, a proportion of the ^{129}I released is incorporated into this. Furthermore, much of the Arctic Ocean is ice covered making ^{129}I volatilization impossible once currents have carried ^{129}I there. However, the volatilization of ^{129}I from shallow ocean waters is still a potential source for the ^{129}I found in the northern Canadian land masses.

Indeed, it is estimated that ~3.52 x 10^{25} atoms of ^{129}I are volatilized from global oceans every year [*Snyder et al.*, 2010]. A fraction of this ^{129}I is then carried to the Arctic via atmospheric transport and subsequent fallout in precipitation or dry deposition as aerosols. To demonstrate that ^{129}I from nuclear fuel reprocessing releases is reaching the Arctic an air parcel backward trajectory analysis was performed using Fort McPherson, NWT as an ending point. It has been shown that iodine has an approximately two week residence time in the atmosphere [*Whitehead*, 1984]. During this time span iodine can travel great distances. The model used was the National Oceanic and Atmospheric Administration (NOAA) Hybrid-Single Particle Lagrangian Integrated Trajectory (HYSPLIT) model for atmospheric transport and dispersion [*Draxler and Rolph*, 2013]. The output of the HYSPLIT model shows pathways and elevations of a variety of air parcels over certain locations for a specified time period. The back trajectories show the paths of those trajectories before they arrive in that location. Modeling of the air parcels that reached the Fort McPherson area indicate an origin in places with known emissions of atmospheric ^{129}I either in the past or present. The variety of wind directions seen in the trajectories suggests that the ^{129}I concentrations found in both surface water and peat result from periodic contributions from multiple distant sources and that no single ^{129}I point source is responsible. The trajectories modeled in this paper are in a good agreement with those presented by [*Kieser et al.*, 2005], which also show air parcels containing elevated concentrations of ^{129}I reaching Canada from sources in Europe and Russia on February 23, 1982.

4.0 CONCLUSIONS

These new data for a remote Arctic landscape show that ^{129}I concentrations are substantially enriched ($10.8 \times 10^6 \pm 4.9$ atoms/L) relative to calculated and measured pre-anthropogenic values (0.037×10^6 atoms/L) for surface water [*Snyder et al.*, 2010]. An earlier dataset, also from the Canadian Arctic, has been compared to verify this conclusion and confirms that ^{129}I concentrations have remained relatively constant over the past 15 years [*Beasley et al.*, 1997]. The surface water dataset shows that anthropogenic ^{129}I is being transported likely via the atmosphere and deposited by aerosols and precipitation in watersheds in the Arctic. $^{129}I/I$ ratios were also calculated for each sample point and showed that the ratio has remained relatively constant over the past decade which suggests ^{129}I fallout has remained constant over time. The measured ^{129}I concentrations were normalized to discharge and watershed size making it possible to compare them and calculate a yearly ^{129}I depositional flux for each watershed. These data have been compared to latitude, watershed size and discharge and show no dependence on any of these variables, suggesting an external airborne source of ^{129}I originating from numerous possible locations. Given the residence time of iodine in the atmosphere and the distances observed by air-trajectory modeling it is reasonable to conclude that ^{129}I from many of the reprocessing plants or volatilization from the oceans in the northern hemisphere are the principle sources in the Arctic. The peat moss data from the Arctic corroborates the conclusion that anthropogenic ^{129}I is reaching the Arctic as both ^{129}I concentrations and $^{129}I/I$ ratios are enriched by 1-2 orders of magnitude at the surface of the peat profile.

Acknowledgements

We thank Carmen Soto for her invaluable advice in setting up the uOttawa ^{129}I extraction lab. We also thank the Northern Scientific Training Program (NSTP) for funding the field component of this research and the NSERC MRS program for assistance with the operation of the preparation lab and the AMS system.

References

Amachi, S., 2008. Microbial Contribution to Global Iodine Cycling: Volatilization, Accumulation, Reduction, Oxidation, and Sorption of Iodine. Microbes Environ. 23, 269–276.

Beasley, T.M., Cooper, L.W., Grebmeier, J.M., Kilius, L.R., Synal, H. -a., 1997. 36 Cl and 129 I in the Yenisei, Kolyma, and Mackenzie Rivers. Environ. Sci. Technol. 31, 1834–1836.

Draxler, R.R., Rolph, G.D., 2013. Real-time Environmental Applications and Display sYstem (READY) Website (http://www.ready.noaa.gov). NOAA Air Resources Laboratory, College Park, MD. [WWW Document].

Edwards, R.R., 1962. Iodine-129: its occurrence in nature and its utility as a tracer. Science (80-.). 137, 851–3.

Engelmann, M.D., Ballou, N.E., Kiddy, R. a., Jenson, D.D., 2009. Analysis of radioiodine in ground litter samples downwind of the Savannah River Site. J. Radioanal. Nucl. Chem. 282, 825–829.

Englund, E., Aldahan, A., Hou, X.L., Possnert, G., Söderström, C., 2010. Iodine (129I and 127I) in aerosols from northern Europe. Nucl. Instruments Methods Phys. Res. Sect. B Beam Interact. with Mater. Atoms 268, 1139–1141.

Fabryka-Martin, J., Bentley, H., Elmore, D., Airey, P., 1985. Natural iodine-129 as an environmental tracer. Geochim. Cosmochim. Acta 49, 337–347.

Fabryka-Martin, J., Davis, S.N., Elmore, D., Kubik, P., 1987. In situ production and migration of 129I in the Stripa granite, Sweden. Geochim. Cosmochim. Acta 53, 1817–1823.

Hou, X., Hansen, V., Aldahan, A., Possnert, G., Lind, O.C., Lujaniene, G., 2009. A review on speciation of iodine-129 in the environmental and biological samples. Anal. Chim. Acta 632, 181–96.

Hu, Q., Zhao, P., Moran, J.E., Seaman, J.C., 2005. Sorption and transport of iodine species in sediments from the Savannah River and Hanford Sites. J. Contam. Hydrol. 78, 185–205.

Kekli, A., Aldahan, A., Meili, M., Possnert, G., Buraglio, N., Stepanauskas, R., 2003. 129I in Swedish rivers: distribution and sources. Sci. Total Environ. 309, 161–72.

Keogh, S.M., Aldahan, A., Possnert, G., Vintró, L.L., Mitchell, P.I., Smith, K.J., McGinnity, P., 2010. Anthropogenic 129I in precipitation and surface waters in Ireland. Nucl. Instruments Methods Phys. Res. Sect. B Beam Interact. with Mater. Atoms 268, 1232–1235.

Kieser, W.E., Zhao, X.L., Soto, C.Y., Tracy, B., 2005. Accelerator mass spectrometry of 129I: Technique and applications. J. Radioanal. Nucl. Chem. 263, 375–379.

Moran, J.E., Oktay, S., Santschi, P.H., Schink, D.R., Fehn, U., Snyder, G., 1998. World-Wide Redistribution of 129 Iodine from Nuclear Fuel Reprocessing Facilities Results from Meteoric, River, and Seawater Tracer Studies. Int. Symp. Mar. Pollut.

Moran, J.E., Oktay, S.D., Santschi, P.H., 2002. Sources of iodine and iodine 129 in rivers. Water Resour. Res. 38, 1–10.

Persson, S., Aldahan, A., Possnert, G., Alfimov, V., Hou, X., 2007. 129I Variability in precipitation over Europe. Nucl. Instruments Methods Phys. Res. Sect. B Beam Interact. with Mater. Atoms 259, 508–512.

Rao, U., Fehn, U., 1999. Sources and reservoirs of anthropogenic iodine-129 in western New York. Geochim. Cosmochim. Acta 63, 1927–1938.

Reithmeier, H., Lazarev, V., Rühm, W., Nolte, E., 2007. 129I measurements in lake water for an estimate of regional 129I depositions. Sci. Total Environ. 376, 285–93.

Reithmeier, H., Lazarev, V., Rühm, W., Nolte, E., 2010. Anthropogenic 129I in the atmosphere: overview over major sources, transport processes and deposition pattern. Sci. Total Environ. 408, 5052–64.

Smith, J.N., McLaughlin, F. a., Smethie, W.M., Moran, S.B., Lepore, K., 2011. Iodine-129, 137 Cs, and CFC-11 tracer transit time distributions in the Arctic Ocean. J. Geophys. Res. 116, 1–19.

Snyder, G., Aldahan, A., Possnert, G., 2010. Global distribution and long-term fate of anthropogenic 129I in marine and surface water reservoirs. Geochemistry Geophys. Geosystems 11.

Snyder, G., Fehn, U., 2004. Global distribution of 129I in rivers and lakes: implications for iodine cycling in surface reservoirs. Nucl. Instruments Methods Phys. Res. Sect. B Beam Interact. with Mater. Atoms 223-224, 579–586.

Utting, N., 2011. Geochemistry and Noble Gases of Permafrost and Ground Ice in Yukon and Northwest Territories, Canada. University of Ottawa.

Whitehead, D.C., 1984. Distribution and Transformations of Iodine in the Environment. Environ. Int. 10, 321–339.

CHAPTER 4 - THE SEASONAL FLUCTUATIONS AND ACCUMULATION OF ^{129}I IN RELATION TO THE HYDROGEOCHEMISTRY OF THE WOLF CREEK RESEARCH BASIN, A DISCONTINUOUS PERMAFROST WATERSHED

ABSTRACT

The long lived radioisotope ^{129}I is a uranium fission product and an environmental contaminant of the nuclear age. Consequently, it can serve as a tracer of anthropogenic releases of ^{129}I in watersheds and potentially distinguish water sources in discharge. We monitored the behaviour of ^{129}I in the Wolf Creek Research Basin (WCRB), a discontinuous permafrost watershed in the Yukon Territory, Canada. Through a pre-freshet to freeze-up study of discharge geochemistry and isotopes, we found that the abundance of ^{129}I and the $^{129}I/^{127}I$ ratio in discharge were correlated with geochemical tracers that suggest varying contributions of three water endmembers in discharge (1) groundwater (2) soil water and (3) precipitation/snowmelt. The abundance of ^{129}I was highest at the onset of freshet, reaching 17.4 x 10^6 atoms/L, and most likely reflects the lack of interaction between meltwater and organic matter at that time and the enrichment of the snowpack by dry fallout over the winter or ion exclusion into meltwater. This peak in ^{129}I was followed by a gradual decline to its lowest level in summer, which had a mean of 2.1 x 10^6 atoms/L (n=10). Mass balance calculations of the ^{129}I budget of WCRB show that the input to the watershed via precipitation is nearly one order of magnitude higher than the output from discharge suggesting that such arctic watersheds are a net sink for ^{129}I with nearly 90% of the annual input stored. We find that most of this excess ^{129}I is stored in the organic matter in soils. Should the WCRB remain a net sink of the size monitored in this sampling year and ^{129}I emissions to the environment continue to affect ^{129}I concentrations in precipitation the

$^{129}I/^{127}I$ ratio could potentially reach levels similar to Chernobyl in 150-1000 years, despite its remote location.

1.0 INTRODUCTION

The long lived radioisotope iodine-129 (half-life: 15.7 million years), is a potential tracer of watershed processes, analogue of the dangerous iodine isotope, ^{131}I, and is emerging as a widespread contaminant since the inputs of ^{129}I have increased drastically over the last 60 years and may continue as ^{129}I is present in radioactive waste [*Fabryka-Martin et al.*, 1985, 1987]. Iodine, being strongly scavenged and incorporated into organic matter by biological processes [*Lusa et al.*, 2015] has caused an accumulation of this radiotracer in numerous environmental reservoirs. However, its geochemical behaviour is poorly understood at the watershed scale. ^{129}I occurs naturally through the neutron spallation of ^{129}Xe in the atmosphere and the spontaneous fission of ^{238}U in the subsurface. However, the natural background of ^{129}I is negligible in comparison to the modern production of ^{129}I [*Snyder et al.*, 2010]. The main anthropogenic sources are nuclear fuel reprocessing (NFRP), nuclear accidents and bomb testing. Of these, nuclear fuel reprocessing is by far the most important source and completely overwhelms the natural background even in remote areas of the planet [*Beasley et al.*, 1997; *Rao and Fehn*, 1999; *Herod et al.*, 2013]. It is estimated that NFRP's have released ~5500 kg of ^{129}I into the environment; 957 kg released directly to the atmosphere and the remainder released in the ocean [*Fan et al.*, 2012; *Jabbar et al.*, 2013]. Some of this ^{129}I is re-volatilized from the ocean surface during transport ^{129}I and can contribute a significant amount of ^{129}I to the continents [*Smith et al.*, 1998; *Smith*, 2005; *Englund et al.*, 2010a; *Reithmeier et al.*, 2010].

The average residence time of ^{129}I in the atmosphere is ~14 days which allows ^{129}I to spread widely, particularly in the Northern Hemisphere, where most NFRP's are located [*Kieser et al.*, 2005; *Jabbar et al.*, 2013]. Indeed, anthropogenic ^{129}I has been detected in the most remote places on Earth, however, very little is known about the far-field geochemical behaviour of ^{129}I [*Beasley et al.*, 1997; *Negri et al.*, 2013; *Xing et al.*, 2015]. The Canadian Arctic is an excellent location for such an investigation. It is one of the most remote regions on Earth which, importantly, lacks the proximity of point sources of anthropogenic ^{129}I, allowing an investigation into the integration of anthropogenic ^{129}I within the hydrologic and geochemical cycles of a watershed.

The cycling and reaction of ^{129}I at the catchment scale has never been rigorously explored despite being identified as a potential hydrologic tracer of flowpaths and organic matter interaction [*Fabryka-Martin et al.*, 1987; *Nimz*, 1998]. The major source of input of ^{129}I to a watershed is through precipitation/snow [*Buraglio et al.*, 2001; *Moran et al.*, 2002]. Only a minor component is added by dry fallout [*López-Gutiérrez et al.*, 2001]. On a catchment scale, soil organic matter content and biological activity of soils affect the behaviour of ^{129}I. Soils with low concentrations of organic matter do not retain iodine efficiently whereas soils with high organic matter are very efficient at scavenging iodine [*Sheppard et al.*, 1995; *Alvarado-Quiroz et al.*, 2002; *Amachi*, 2008] The iodine-scavenging capacity of organic soils was eloquently illustrated by monitoring the ^{129}I accumulation in peat soil profiles; wherein the first few centimeters of show an enrichment consistent with the modern input of ^{129}I, the rest of the profile retains the "ancient" pre-nuclear signature [*Herod et al.*, 2013; *Luo et al.*, 2013]. This suggests that in organic rich soils, the entire

modern signature of ^{129}I has been completely attenuated by the soils and they still have adsorption capacity. The ^{129}I concentration in precipitation percolating through these soils is therefore attenuated. In soils with less organic matter, the modern ^{129}I signature is evident deeper into the profile due to limited adsorption capacity [*Schwehr et al.*, 2009]. On a catchment scale the average attenuation of all soils will determine the net ^{129}I attenuation capacity of the watershed and these will reflect in the signature observed in discharge. The redox state of iodine also affects its mobility in the environment. Studies have shown that in soils organic iodine species are most heavily retarded during transport followed by iodate and iodide [*Xu et al.*, 2011; *Santschi et al.*, 2012].

The behaviour of ^{129}I in rivers is not affected by catchment area, river pH, and temperature [*Kekli et al.*, 2003; *Herod et al.*, 2013] but geochemical parameters such as Cl^-, K^+, Ca^{2+}, DOC, alkalinity, and conductivity may co-vary with ^{129}I in some rivers reflecting common source, release or uptake processes [*Kekli et al.*, 2003; *Aldahan et al.*, 2006]. For example, ^{129}I often co-varies with Cl^- due to being commonly sourced from ocean volatilization [*Moran et al.*, 2002]. Differently, the co-variability in the abundance of ^{129}I and K^+ is due to both elements being scavenged by natural cycles of organic soil turnover and bedrock weathering [*Kekli et al.*, 2003]. The geochemical properties of ^{129}I, coupled with the fact that it is a modern contaminant, allows the characterization of the degree of interaction between water within soils and bedrock on the watershed scale. These properties of ^{129}I also allow the prediction of the fate of radioiodine released from point sources.

The hydrological cycle in Arctic and sub-Arctic watersheds is dominated by the spring freshet which consists of an input to streams of snowmelt and shallow groundwater displacement from the active layer by snowmelt infiltration [*Rodhe*, 1998; *Boucher and Carey*, 2010]. This event usually is only a few weeks long but can represent a significant fraction of the annual discharge and has a profound impact on the chemistry of streamflow. Discharge in permafrost and discontinuous permafrost catchments is generally supplied by three water sources: (1) deep groundwater in places with little permafrost, (2) shallow groundwater and active layer drainage contained within soils in areas with permafrost and (3) precipitation in the form of rain and snow [*Carey et al.*, 2012]. These water sources can be differentiated according to their chemical identity, which is reflective of source and flowpath. Deep groundwater (1) is expected to have high concentrations of ions from soil and bedrock weathering [*Petrone et al.*, 2006] and is hypothesized to have a low concentration of ^{129}I and $^{129}I/^{127}I$ ratio due to leaching of stable iodine, mixing with ancient, low ^{129}I water and/or ^{129}I attenuation during recharge. Shallow groundwater and active layer/soil drainage (2) is often enriched in DOC and nutrients related to organic matter decay due to their residence in shallow surface soils and shorter flowpaths [*Boucher and Carey*, 2010]. The high organic matter content results in low concentrations of ^{129}I in water discharged from soils due to adsorption during residence and transport. Finally, precipitation and snowmelt (3) have very low concentrations of almost all dissolved species leading to a depletion in ion concentrations in discharge at freshet [*Petrone et al.*, 2006] but is characterized by high levels of ^{129}I. ^{129}I is incorporated in or removed from these water types differently and thus could prove a useful tracer.

Wolf Creek drains the Wolf Creek Research Basin (WCRB), a well-studied basin used as a representative model of a discontinuous permafrost catchment [*Janowicz et al.*, 2004]. It is located in the Yukon Territory, Canada approximately 250 km from the Pacific coast and about 2,500 km from the nearest operating point source of ^{129}I in Idaho Falls, US. We examined how ^{129}I was transported, stored and how this behaviour resulted in temporal variations of ^{129}I in the discharge of Wolf Creek over the course of 7 months – from just before freshet to after freeze-up. We monitored the temporal variations in abundance of ^{129}I in precipitation and discharge as well as a suite of hydrologic tracers, radioactive and stable isotopes and flow measurements with three specific goals in mind: (1) understand the mechanisms leading to the temporal behaviour of ^{129}I in discharge and place these variations in context with the hydrogeochemical evolution and water sources of Wolf Creek (2) identify the catchment-scale utility of ^{129}I as a tracer of interaction with soil organic matter, hydrologic processes and flowpaths (3) determine the watershed mass balance for ^{129}I to determine whether far-field emissions are at steady state or retained in the environment.

2.0 METHODS

2.1 Site Description

The Wolf Creek Research Basin (WCRB) is located near Whitehorse, Yukon Territory in the western Canadian arctic and is a tributary to the Yukon River (Figure 4.1). Wolf Creek drains 195 km^2 of subalpine discontinuous permafrost terrain with a minimum discharge of 0.4 m^3/s to a peak of 10 m^3/s during spring freshet [*Janowicz et al.*, 2004]. The elevation of the basin ranges from 800-2250 m above sea level (mABSL) [*Janowicz et al.*, 2004].

Temperatures range from -40°C to 25°C throughout the year with a mean annual temperature of -3°C. Mean annual precipitation varies from approximately 300 to 400 mm/year with about 40% falling as snow [*Janowicz et al.*, 2004].

The bedrock geology of the WCRB is primarily limestone, sandstone, siltstone and conglomerate. There is a large intrusion of andesite and basalt within the watershed (Figure 4.1) (Israel et al.; Janowicz et al. 2004). Bedrock outcrops occur in 50 - 60% of the watershed [*Seguin et al.*, 1999].

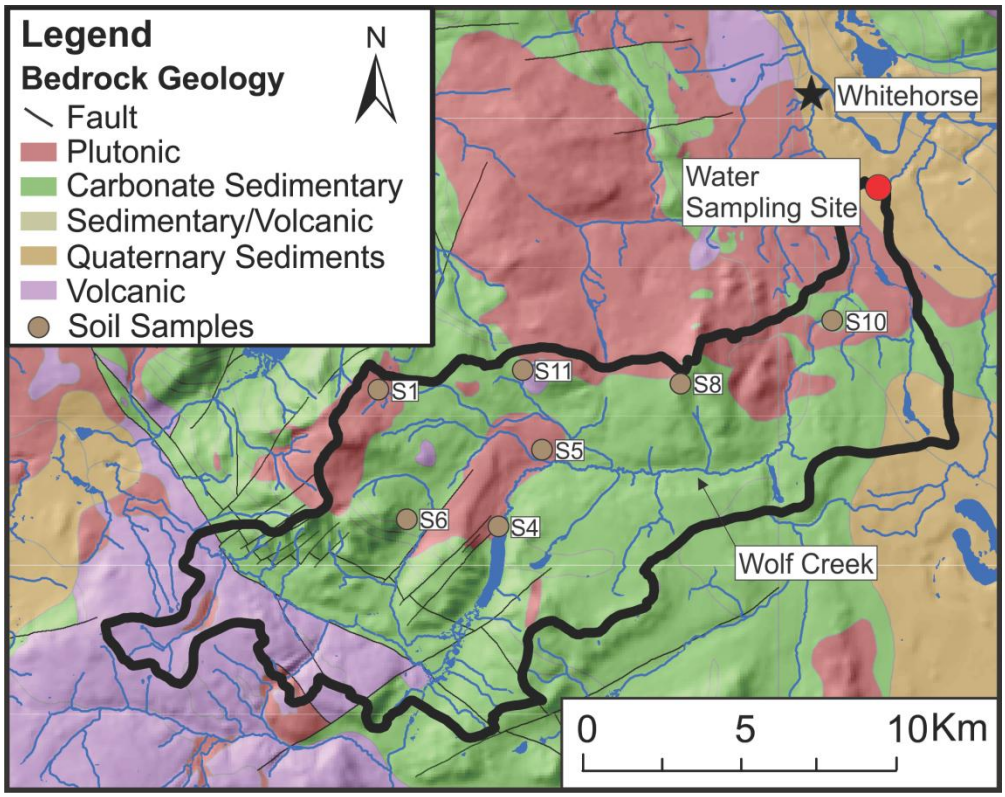

Figure 4.1: Geological hillshade map of the Wolf Creek Research Basin. The time series sampling site is shown at the outlet of Wolf Creek and soil sampling sites throughout the watershed as well as the location of the watershed in relation to Whitehorse. Bedrock faults are pictured as black lines.

The surficial geology of the WCRB is mostly a veneer of glacial deposits including till, alluvium, loess, glaciofluvial and lacustrine soils that range from a few centimetres to tens of metres in thickness and cover 40 – 50% of the basin. The deepest soils are found in low elevation regions of the catchment and can be up to 165 m thick [*Seguin et al.*, 1999]. Soils at high elevation are generally thinner due to the variable nature of bedrock elevation. Several distinct ecological zones occur in the WCRB based on elevation and southern exposure. At low elevation, <1200 m, boreal forest dominates and covers approximately 22% of the watershed. Higher elevations are characterized by taiga and which covers 58% of the basin. The remaining high elevation alpine regions >1500 m are classified as tundra and compose 20% of the basin [*Seguin et al.*, 1999]. Geophysical surveys have suggested that during the summer the water table is located within bedrock and that discharge to the creek occurs in the alpine zone whereas at lower elevations the creek is recharging groundwater [*Seguin et al.*, 1999].

The WCRB is underlain by widely varying permafrost conditions. It has been estimated that up to 43% of the basin is underlain by permafrost [*Lewkowicz and Ednie*, 2004]. Continuous permafrost is located primarily in the high elevation regions above 1500m in the northwest parts of the watershed with much of the western half also covered by widespread discontinuous permafrost at elevations above 1175m. The lower elevation regions also have isolated patches of permafrost [*Lewkowicz and Ednie*, 2004]. Permafrost can also be found on north facing slopes and in poorly drained areas and places with an organic soil layer thicker than 10 cm that provides insulation [*Janowicz et al.*, 2004]. Permafrost has a significant influence on groundwater recharge as areas with permafrost

can lead to perched water tables and restrict groundwater recharge whereas low permafrost areas or talik provide pathways for groundwater recharge and discharge.

2.2 Field Sampling

Water sampling was conducted near the mouth of the WCRB at the site of a Yukon Water Survey gauging station just above its crossing of the Alaska Highway. Samples were collected at approximately weekly intervals from thaw to freeze up in 1L Nalgene bottles. Within this time series a group of high resolution samples were collected daily for a one week period using an ISCO automated sampler at the same location. Samples were filtered in the lab prior to analysis for anions, cations, ^{127}I, stable isotopes and DOC and an aliquot of unfiltered water was used for ^{129}I. Wolf Creek discharge data for the summer of 2012 was provided by the Yukon Water Survey and is from the gauging station next to the sampling point. Discharge during the sampling period ranged from 0.38 m^3/s in late April, prior to freshet, to 8.3 m^3/s on June 8 which was peak discharge. Analyses for cations were performed using ICP-MS and anions were analyzed using liquid chromatography. Values for Mn, B, Cu, Zn, Ti, V and NO_3 were almost uniformly below detection and are not included in this study.

Soil samples were collected throughout the WCRB (Figure 4.1). Samples placed into Ziploc bags for transport back to Ottawa, where they were stored in the freezer until sample preparation and analysis. The organic carbon content of WCRB soils was quantified using loss on ignition as was the carbonate content [*Heiri et al.*, 2001]. Duplicate analyses were performed on the majority of the samples and the results had an average difference of 10% for organic carbon content and 33% for carbonate.

Precipitation samples were collected at Marsh Lake, which is approximately 35 km from Whitehorse, using a simple apparatus of a HDPE funnel collector attached to an opaque bucket [*Grynkiewicz et al.*, 2003]. During the study period 168 mm of rain fell and the preceding winter from November 2011 to April 2012 had 127 mm of precipitation as snow [*Environment Canada*, 2014].

2.3 Extraction of ^{129}I from Water Samples

Water samples were extracted for ^{129}I for AMS analysis using a redox trap extraction technique. The method is described in detail in [*Sheppard and Herod*, 2012; *Herod et al.*, 2013]. Samples were precipitated as silver iodide using an NaI carrier with a $^{129}I/^{127}I$ ratio of $1.56 \pm 0.06 \times 10^{-13}$. The AgI targets were analyzed at the University of Ottawa's Andre E. Lalonde 3MV Accelerator Mass Spectrometry (AMS) facility. Some samples were also previously analyzed at IsoTrace and these results compared well to those from the André E. Lalonde AMS.

2.4 Pyrohydrolysis Extraction of ^{127}I and ^{129}I from Soils

Soil samples from several locations throughout the WCRB were analyzed for ^{129}I and ^{127}I using a pyrohydrolysis extraction technique. The method is described in detail by [*Herod et al.*, 2014b]. The soil samples from throughout the WCRB were dried and all large pebbles were removed. The samples were then ground using a mortar and pestle. Approximately 2-3 grams of sample was accurately weighed out and placed in a quartz boat and combusted at 800°C for 5 hours in a two zone tube furnace under oxygen gas flow at 800mL/min [*Herod et al.*, 2014b]. A precise amount of ^{125}I was also added to every sample prior to combustion to act as a yield tracer. The O_2 carrier gas transported the iodine

through the system and bubbled through an alkaline trap solution of 0.4M NaOH - 0.02M $NaHSO_3$, which trapped the iodine. The trap solution was then collected and weighed and a 1mL aliquot was removed for gamma spectrometry in order to calculate total iodine recovery from the sample. Yields ranged from 47%-95% with a mean of 72% (n=10). These recovery percentages were then used as a correction factor for ^{129}I and ^{127}I concentrations as the yield for every sample was traced allowing any iodine lost during the combustion to be accounted for. This aliquot was also used for ^{127}I analysis by ICP-MS. The remaining trap solution was then extracted for ^{129}I analysis by AMS according to the method described above and analyzed at the André E. Lalonde AMS Lab.

2.5 Statistical Treatment of Data

2.5.1 Treatment of Missing Data and Quality Assurance

Several analytes measured in this study had one or more missing data points including the principal analyte, ^{129}I. Therefore the missing data points had to be addressed in a statistically robust way for their inclusion in Principal Component Analysis and the identification of water end members. Linear regression can be used to replace the missing variables in a way that honours geochemical trends in the dataset [*Gotway et al.*, 1992; *Güler et al.*, 2002] (Supplementary Information, Supplementary Figure B1). The ^{18}O regression was chosen as the most robust due to it having the most complete dataset and a common source of ^{18}O and ^{129}I to the watershed.

$$^{129}I\ (10^6\ atoms/L) = -90.2 - 4.26 \times {}^{18}O\ (r = -0.63)$$

One or two missing data points for several other variables were also replaced using linear regression with their most highly correlated variable.

Charge balance error can also be used as a test of data quality [*Freeze and Cherry*, 1979; *Güler et al.*, 2002]. The percent charge balance error was calculated using concentrations of Na, Ca, Mg and K against SO_4, HCO_3 and Cl. The results are generally below the threshold of 5% error with the exception of a few samples that slightly biased negative but are still below 10% error. Three samples that were collected in the fall are highly biased negative. These outlying samples could be due to poor analyses or error in the measurement of HCO_3, as alkalinity was not analyzed in the field. These points were still included in PCA as they have reliable ^{129}I analyses.

2.5.2 Principal Component Analysis (PCA)

Principal component analysis (PCA) is a type of statistical method used for the reduction and simplification of multivariate data sets without loss of existing trends and associations between variables [*Vega et al.*, 1998; *Page et al.*, 2012]. PCA was performed using the program XLStat on standardized data with a variance of 1 and a mean of 0 in order to avoid effects of differing units between variables [*Christophersen and Hooper*, 1992]. All of the tests used are non-parametric and thus no evaluation of normality was required for the dataset. A correlation matrix was generated and transformed into orthogonal and unrelated principal components that represent the variance of the dataset. The PCA analysis was performed on 29 time series samples, each with 25 variables and missing data replaced by OLS regressions.^{129}I was excluded from the PCA analysis described here in order to relate the ^{129}I concentrations to the general water chemistry end-members described by the significant PC's. An additional PCA analysis was performed that did include ^{129}I and it was found to participate significantly in PC2 and PC3. PCA analysis produced 25

principal components, most of which are noise. In order to limit this number scree plot analysis was performed which is a visual analysis of the variability explained by each component and looks for a break between interpretable PC's and noise. However, this method is highly subjective and does not always yield appropriate results, especially when there is no obvious break point [*Page et al.*, 2012] (Supplementary Figure B2). An alternative to scree plot analysis is the Kaiser-Guttman criterion which accepts all PC's with an eigenvalue greater than 1 [*Kaiser*, 1960; *Page et al.*, 2012]. Variable loadings <-0.5 and >0.5 were considered moderately significant and values between <-0.7 and >0.7 were considered strongly significant [*Meglen*, 1992]. Bartlett's Sphericity Test was used to check the acceptability of the PCA results. The results of this test yielded a X^2 value of 997 and a critical X^2 of 341 (DF: 300, $p < 0.00001$, $\alpha=0.05$) showing that PCA can successfully reduce the original dataset [*Vega et al.*, 1998].

2.5.3 Agglomerative Hierarchical Clustering (AHC)

Agglomerative Hierarchical Clustering (AHC) is a statistical technique that initially treats each sample as independent and then groups them according to their chemical similarities [*Auf der Heyde*, 1990]. This method allows underlying structure and relationships between samples to be discovered when taking all relevant variables into account, which would not be possible using traditional visual methods. The resulting dendrogram shows relationships between groups of samples and variables that are more difficult to spot using a correlation matrix. The method was performed on the standardized dataset using XLStat. A proximity matrix using Euclidean distance was generated and Wards linkage method was used to aggregate sample groups. Euclidean distance iteratively groups

samples with the most similiarity to one another and Ward's method uses an analysis of variance to link the groups. Ward's method has been shown to produce the smallest and most distinct clusters and Euclidean distance and Ward's method have been employed be numerous other studies exploring water geochemistry [*Simeonov et al.*, 2000; *Güler et al.*, 2002; *Smoliński et al.*, 2002; *Yidana et al.*, 2008]. An AHC analysis was also performed using a complete linkage method and the resulting clusters were very similar although slightly less distinction was observed. ^{129}I data was omitted from the AHC analysis in order to make it more comparable with the results of PCA. A second AHC analysis was performed including ^{129}I and yielded very similar sample groupings. A detailed description of the mathematics, and linkage methods involved in cluster analysis can be found in [*Auf der Heyde*, 1990].

3.0 RESULTS AND DISCUSSION

3.1 The relationship of ^{129}I with stable halogens suggest a non-marine input source to the watershed

The ^{129}I concentration measured in rain was variable and ranged between 14 and 76 x 10^6 atoms/L with a mean of 39 ± 22 x 10^6 atoms/L (n=10) (Table 4.1, Figure 4.2). Snow also had a high degree of variability in ^{129}I. One sample, taken from the upper few centimeters of the snowpack at the time of sampling (August, 2012) had a concentration similar to rain of 35 ± 0.7 x 10^6 atoms/L while the interior of the snowpack (~10 cm below surface) was lower than any other precipitation sample at 3.6 ± 1.4 x 10^6 atoms/L. The large difference between the measurements of ^{129}I in snow may be caused by dry fallout in the form of aerosols and dust on snow surfaces that are exposed to the air for longer lengths of time. A difference in ^{129}I concentrations between rain and snow has been hypothesized to

be caused by the exclusion of polar iodine molecules by the snow as it crystallizes in the atmosphere [*Buraglio et al.*, 2001]. The difference in measured ^{129}I between rain and snow has also been attributed to volatilization of ^{129}I from the ground surface during summer months which enriches rain with ^{129}I; a negligible process in winter [*Buraglio et al.*, 2001; *Gilfedder et al.*, 2007b]. However, estimates of volatilization of ^{129}I from the ground in the WCRB are not available and are usually considered negligible [*Reithmeier et al.*, 2010]. Alternatively, it is possible the sources of ^{129}I vary seasonally with changing wind patterns [*López-Gutiérrez et al.*, 2001; *Kieser et al.*, 2005].

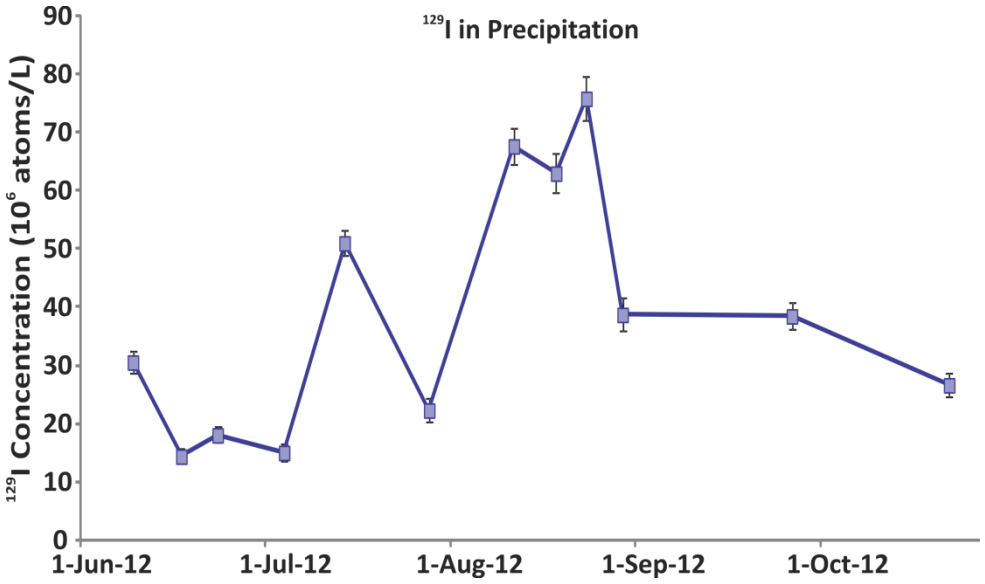

Figure 4.2: ^{129}I concentration in precipitation samples measured by AMS. Samples are plotted on the date of collection and represent a homogenization of all precipitation following the preceding sample. Sampling initiated on June 3, 2010.

Other halogens typically behave in a similar fashion. One might therefore expect the ^{129}I concentration to be related to that of other halogens in precipitation. Most of the input

of stable iodine, Br^-, and Cl^- to a watershed are usually from ocean volatilization or mineral and soil weathering [*Moran et al.*, 1999; *Gilfedder et al.*, 2007a]. Indeed, ^{127}I in precipitation ranged from 1.7 to 28 µg/L with a mean of 7.2 ± 8.5 µg/L (n=11), and unlike ^{129}I, stable iodine correlates with both Cl^- and Br^- in precipitation, suggesting a common input source, wholly different from ^{129}I (Figure 4.3). Moran et al. 2002 found that ocean volatilization was the major source of ^{129}I and other halogens in the Yukon and Mackenzie rivers. However, this relationship appears to decrease with distance inland [*Gilfedder et al.*, 2007a] as the input fraction of iodine and chloride from ocean volatilization decreases and additional sources of atmospheric ^{129}I are incorporated into air masses. In WCRB discharge, the relationship between ^{129}I and the halogens, Cl, Br and ^{127}I is weak suggesting that there is likely an additional source of ^{129}I, different from that of Cl, Br and ^{127}I. The $^{129}I/^{127}I$ ratio in precipitation was quite variable, following the ^{129}I concentration closely, throughout the sampling period ranging from 1.6 to 67 x 10^{-10} with a mean of 25 x 10^{-10} (n=10) which may reflect the decoupling between the source of ^{129}I and ^{127}I given that the WCRB is located far from the ocean allowing contributions from atmospheric transport of anthropogenic sources and ocean volatilization to add ^{129}I to precipitation. Given that the approximately two-week atmospheric residence time of iodine allows long distance transport of ^{129}I the contributions from numerous sources become mixed making it impossible to distinguish one from another and reduces the correlation of ^{129}I with other halogens [*Kocher*, 1981; *Moran et al.*, 1999]. However, the relatively high ^{129}I concentrations, which are 2 - 3 orders of magnitude greater than the estimated natural background concentration [*Moran et al.*,

2002; *Snyder et al.*, 2010] confirms that input of anthropogenic ^{129}I to the WCRB is the principal source of ^{129}I despite the remoteness of the catchment.

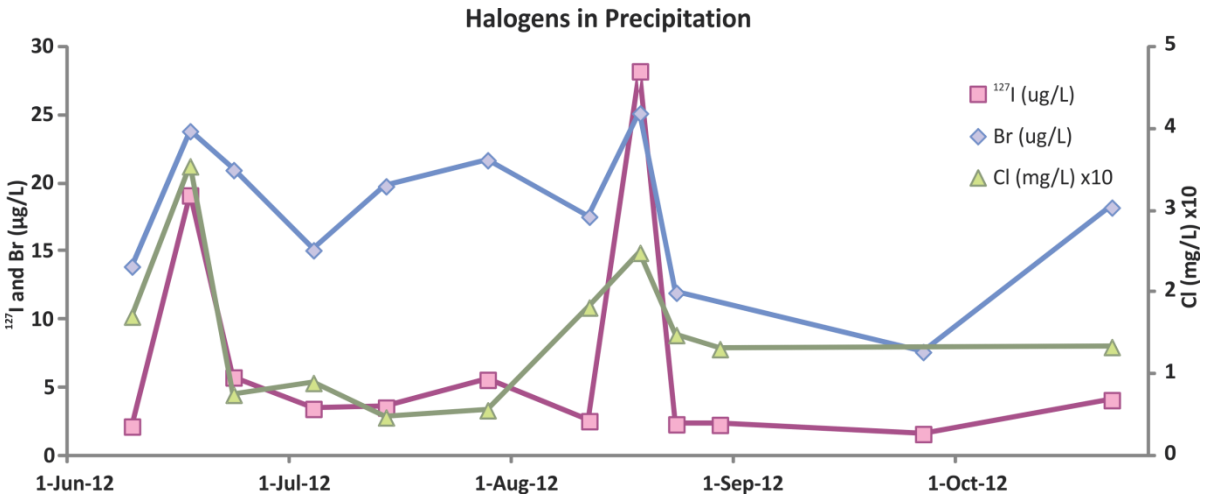

Figure 4.3: Comparison of stable halogen abundances in precipitation over time, which display similar temporal trends suggesting a common source such as ocean volatilization, which is not the same as ^{129}I as it does not share these trends. Samples are plotted on the date of collection and represent a homogenization of all precipitation following the preceding sample. Sampling initiated on June 3, 2010.

3.2 Temporal variation of ^{129}I in discharge is a function of varying flowpath contributions

Once ^{129}I enters the WCRB, its fate is determined largely by the flowpath it follows, due to differing storage terms and residence times. ^{129}I concentrations in Wolf Creek discharge ranged from 0.5 – 17 x 10^6 atoms/L and had a mean of 3.7 ± 3.7 x 10^6 atoms/L (n=24) (Table 4.2, Figure 4.4). The concentrations of ^{129}I in Wolf Creek discharge are slightly lower than measurements in other remote Arctic rivers such as the Yukon, Peel, and Mackenzie [*Moran et al.*, 2002; *Herod et al.*, 2013] and at least two orders of magnitude lower than rivers in Europe [*Moran et al.*, 2002; *Kekli et al.*, 2003]. The concentrations of ^{129}I in streamflow were far lower and less variable than the concentration in rain. Indeed,

such depletions between precipitation and discharge are expected [*Buraglio et al.*, 2001] but exceptions do occur. For instance, in the Mississippi River, ^{129}I concentrations in river water are higher than precipitation due to its concentration by evapotranspiration [*Oktay et al.*, 2001]. The sub-arctic climate of the WCRB does produce a ~500 mm of evapotranspiration in summer but it appears insufficient to concentrate ^{129}I in discharge. In order to explain the weekly variations in ^{129}I of discharge, it is important to understand the path of the water from source to discharge.

Date	Interval	ID	Precipitation (L/m^2/interval)	^{127}I (μg/L)	Br (μg/L)	Cl (mg/L)	^{129}I (10^6 atoms/L)	±	$^{129}I/^{127}I$	±	^{129}I Washout (atoms/m^2)	^{129}I Washout (watershed)
10-Jun-12	7	June 3-10	4.6	2.2	2.3	0.2	30.6	2.0	2.90E-9	1.9E-10	1.4E+8	2.7E+16
18-Jun-12	8	June 11-18	7.4	19.2	4.0	0.4	14.4	1.2	1.59E-10	1.4E-11	1.1E+8	2.1E+16
24-Jun-12	6	June 19-24	4	5.8	3.5	0.1	18.1	1.4	6.55E-10	5.6E-11	7.2E+7	1.4E+16
05-Jul-12	11	June 25-July 5	27.2	3.5	2.5	0.1	15.1	1.5	9.03E-10	1.0E-10	4.1E+8	8.0E+16
15-Jul-12	10	July 6-15	8.6	3.6	3.3	0.0	51.0	2.2	2.98E-9	1.5E-10	4.4E+8	8.6E+16
29-Jul-12	14	July 16-29	10	5.7	3.6	0.1	22.3	1.9	8.34E-10	7.5E-11	2.2E+8	4.4E+16
12-Aug-12	14	July 30 - Aug 12	20.8	2.6	2.9	0.2	67.7	3.1	5.45E-9	2.5E-10	1.4E+9	2.7E+17
19-Aug-12	7	Aug 13-19	7.6	28.3	4.2	0.2	63.0	3.3	4.70E-10	6.9E-11	4.8E+8	9.3E+16
24-Aug-12	5	Aug 19-24	17.8	2.4	2.0	0.1	75.8	3.7	6.69E-9	3.4E-10	1.3E+9	2.6E+17
30-Aug-12	6	Aug 25-30	11.2	2.3		0.1	38.8	2.7	3.49E-9	1.1E-9	4.3E+8	8.5E+16
27-Sep-12	28	Aug 30 - Sept 27	19	1.7	1.3		38.5	2.3	4.54E-9	2.9E-10	6.8E+8	1.3E+17
23-Oct-12	26	Sept 28 - Oct 23	11.4	4.2	3.0	0.1	26.7	2.1	1.35E-9	1.1E-10	3.0E+8	5.9E+16
02-Aug-12	NA	Snow 1 Top	NA	2.5		0.1	35.3	2.9	2.92E-9	2.4E-10	NA	NA
02-Aug-12	NA	Snow 1 Top (dup)	NA	2.5		0.1	34.2	2.4	2.84E-9	2.0E-10	NA	NA
02-Aug-12	NA	Snow 1 Interior	NA	2.5		0.1	3.6	1.4	2.97E-10	1.2E-10	NA	NA

Table 4.1: Table of precipitation data. Sampling started on June 3, 2012 with the first sample collected in June 10, 2012

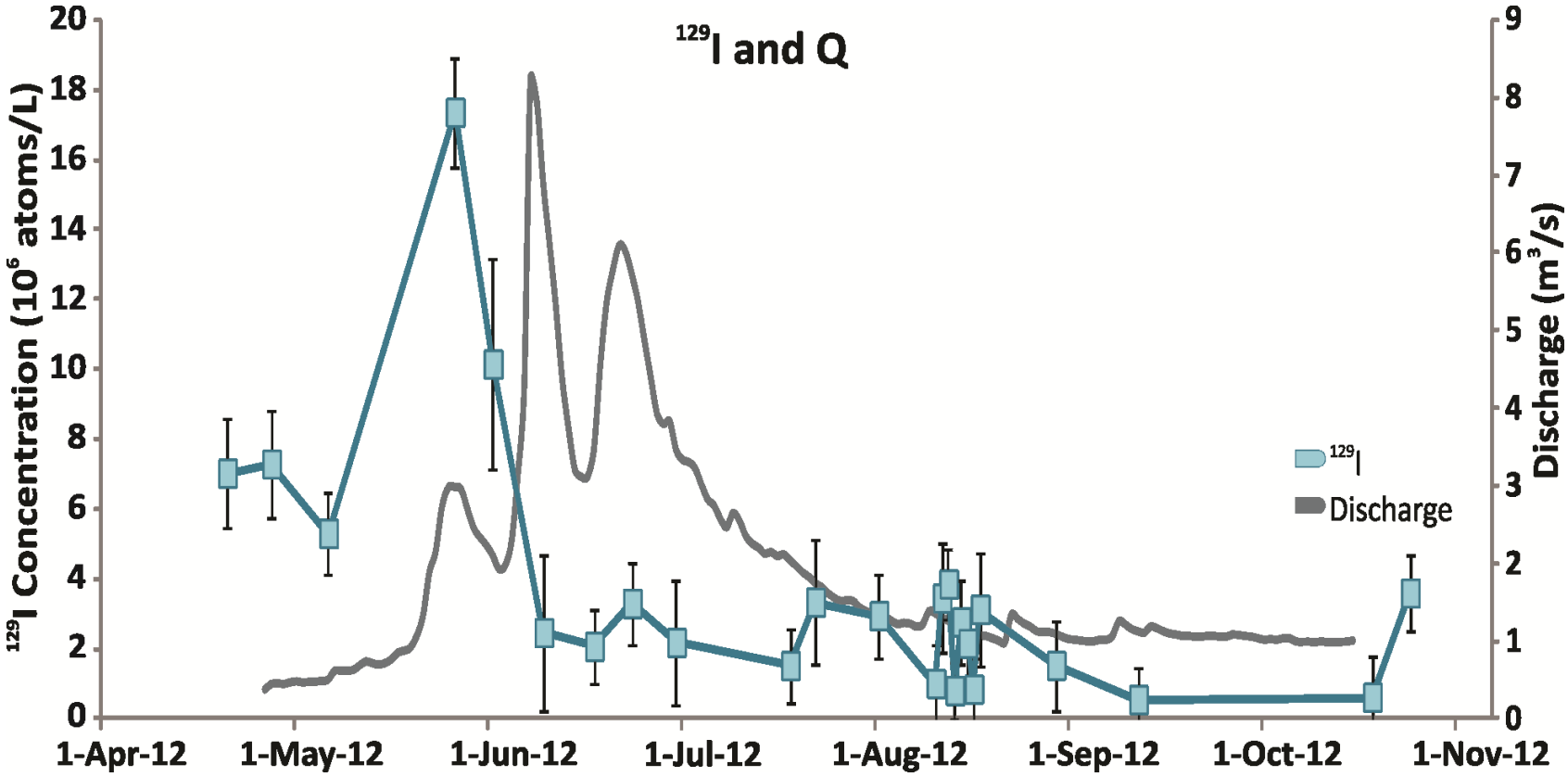

Figure 4.4: Time series of ^{129}I abundance in Wolf Creek discharge. Several points have error extending to below the limit of detection suggesting these values may actually be lower than pictured. Wolf Creek discharge is also pictured and clearly shows freshet as well as the influence of several precipitation events in the summer.

Variable	Minimum	Min. Date	Maximum	Max. Date	Mean	Median
pH	7.30	18-Jun	7.90	17-May	7.6	7.6
Al	0.01	19-Jul	0.03	10-Jun	0.015	0.015
Na	1.8	10-Jun	3.79	21-Apr	2.8	2.8
K	0.465	12-Sep	0.98	17-May	0.66	0.62
Mg	3.3	10-Jun	7.71	21-Apr	5.2	5
Ca	13.2	10-Jun	29.49	21-Apr	20.7	20.4
Fe	0.003	12-Aug	0.4	19-Jul	0.06	0.04
Ba	0.043	10-Jun	0.081	17-May	0.06	0.06
Sr	0.12	10-Jun	0.25	17-May	0.18	0.17
^{127}I (µg/L)	1.9	16-Aug	14.7	10-Aug	4.7	3
^{129}I (10^6 atoms/L)	0.54	12-Sep	17.4	27-May	3.7	2.9
$^{129}I/^{127}I$	3.85E-11	12-Sep	6.77E-10	27-May	1.97E-10	1.35E-10
Cl	0.11	24-Jun	0.56	7-May	0.21	0.2
SO_4	5.5	27-May	16.4	21-Apr	10.3	11
HCO_3	56.5	2-Jun	142	28-Apr	91	88
Br (µg/L)	3.5	18-Jun	9.3	17-May	5.7	5.1
F	0.036	10-Jun	0.12	18-Aug	0.08	0.08
S	2.2	27-May	6.23	21-Apr	3.51	3.34
Si	3.3	10-Jun	4.9	17-May	4.1	4
DOC	2.02	7-May	8.99	10-Jun	4.5	4
^{18}O	-23.07	27-May	-21.3	14-Aug	-21.97	-21.94
^{2}H	-170.25	27-May	-166	11-Aug	-167.73	-167.57
K/Ca	0.023	10-Oct	0.064	27-May	0.034	0.03
Tritium (^{3}H)	4.6	2-Aug	9.9	2-Jun	7.64	7.85
DIC	11.7	10-Jun	21.9	7-May	17.3	17.3
$^{13}C_{DIC}$	-12.8	2-Jun	-6.7	12-Sep	-10	-9.7
Percent Modern Carbon ($^{14}C_{DIC}$)	55.8	10-Jun	92.7	27-May	78.5	79.7
Daily Discharge (m^3/s)	0.38	Apr-14	8.25	8-Jun	1.8	1.2

Table 1.2: Key statistics of geochemical parameters measured in Wolf Creek discharge. See Appendix B for raw data. Sample minimums, maximums and the dates that these occurred on are shown as are the means and medians of each analyte.

The geochemical abundances of major cations and anions in discharge reflect the level and type of interaction that water has had with the watershed and so are useful to discern discrete flow paths from precipitation to discharge. We performed a principal component analysis (PCA) as a first order test on the temporal effects of cation and anion variations on water composition in the discharge of Wolf Creek. The value of this interpretation technique is that the temporal variability in analytes can be grouped allowing the general identification of distinct water sources or flowpaths. Our PCA analysis suggests that 59% of the variability in cations, anions and isotopes can be explained by the first two principle components (Figure 4.5, Table 4.3). Principle component 1 (PC1), which accounts for 39% of the variability in the data is dominated by Na, Mg, Ca, Ba, Sr, SO_4, Si and more moderately K, and Br. These elements come primarily from weathering of silicates and carbonates abundant in the WCRB. PC1 can be thought of as a groundwater end-member contribution to discharge. PC2 explained 20% of the variance and is dominated by F, $\delta^{18}O$, $\delta^{2}H$ and HCO_3 and negative loading from daily discharge, K and the K/Ca molar ratio. In a PCA analysis that includes ^{129}I, it also had a moderate negative loading in PC2. The positive loadings from $\delta^{18}O$ and $\delta^{2}H$, the negative loading of discharge and the lack of strongly significant loadings from other ions suggests that PC2 is not a clear-cut endmember but rather partially composed of a low salinity, fresh water end member such as snowmelt or precipitation, closely linked with features of shallow groundwater from the active layer, such as HCO_3^-, K^+. PC2 can therefore be characterized as a combination of snowmelt and soil drainage. Only PC1 and PC2 display interpretable relationships with multiple analytes and thus are the only ones considered relevant to the

geochemical cycle of ^{129}I and the hydrology of the WCRB. The PCA fails to clearly separate the direct precipitation and soil water flowpaths, likely because both fractions in discharge probably co-vary and are closely coupled temporally. We investigated the geochemistry of discharge in more detail to determine its temporal evolution by ranking net geochemical similarity of different samples with the hope of elucidating signatures associated with soil water and precipitation and to demonstrate the distribution of temporally separated samples.

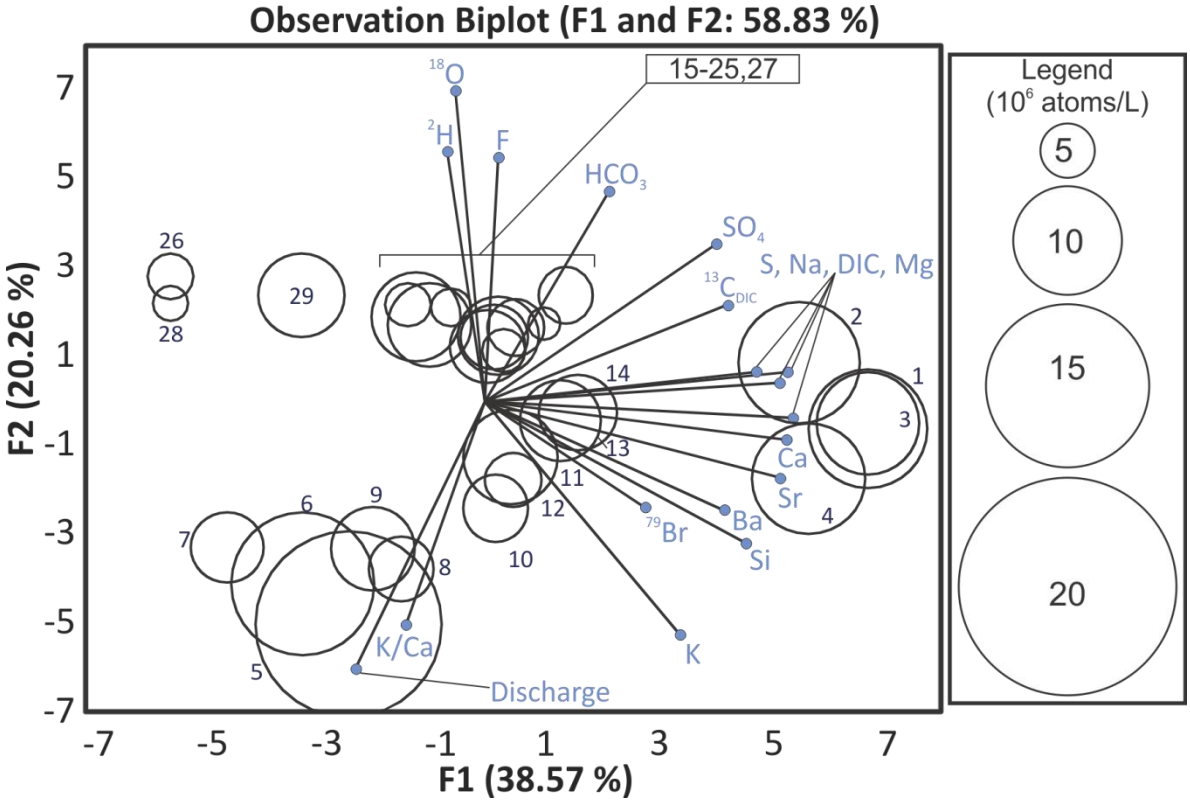

Figure 4.5: Observation biplot of PC1 and PC2 showing the position of each sample, which are numbered, in relation to each analyte in PC space allowing for the interpretation of important variables in each sample and the identification of water end member based in the heavily loaded elements in each. Samples are pictured as a bubble corresponding to their concentration of ^{129}I. Samples 26, 28, and 29 all had high charge balance error. Elements shown have significant loadings while analytes not pictured were not significant in PC1 or PC2. There is an apparent temporal trend in terms of sample ordering as consecutive samples are distinctly grouped.

Variables	F1	F2	F3	F4	F5	F6
pH	0.42	0.36	0.45	-0.23	0.28	**0.53**
Al	-0.25	-0.31	0.13	**0.69**	-0.36	0.19
Na	**0.97**	0.09	-0.14	0.09	0.05	-0.04
K	**0.62**	**-0.69**	0.26	0.02	-0.04	0.08
Mg	**0.98**	-0.05	-0.05	0.04	0.06	-0.05
Ca	**0.96**	-0.12	-0.16	0.15	0.04	0.02
Fe	0.09	-0.41	0.01	-0.27	0.52	**0.68**
Ba	**0.76**	-0.33	-0.47	0.16	0.03	0.08
Sr	**0.94**	-0.22	-0.20	0.07	0.06	-0.01
^{127}I	0.46	-0.02	**0.58**	-0.11	-0.32	-0.26
Cl	**0.50**	0.01	**0.52**	-0.02	-0.39	-0.13
SO_4	**0.74**	0.47	0.16	-0.09	-0.07	-0.06
HCO_3	0.40	**0.63**	0.25	-0.31	0.24	-0.17
Br	**0.51**	-0.31	**0.56**	-0.03	-0.20	0.31
F	0.04	**0.73**	0.01	0.38	-0.34	0.12
S	**0.87**	0.09	0.16	-0.23	0.06	-0.09
Si	**0.83**	-0.42	-0.28	0.02	0.05	-0.01
DOC	-0.30	0.05	0.42	**0.55**	**0.55**	0.13
$^{13}C_{DOC}$	-0.04	0.06	-0.49	**-0.63**	-0.47	0.07
^{18}O	-0.10	**0.93**	-0.14	0.16	0.09	0.10
^{2}H	-0.12	**0.75**	0.00	0.00	-0.20	0.18
K/Ca	-0.26	**-0.66**	**0.50**	-0.14	-0.13	-0.06
DIC	**0.94**	0.06	-0.18	0.21	-0.03	-0.06
$^{13}C_{DIC}$	**0.78**	0.29	-0.08	0.26	-0.08	-0.16
Daily Discharge m^3/s	-0.42	**-0.79**	-0.21	0.09	-0.12	0.10
Eigenvalue	10	5	2	2	2	1
Variance Explained (%)	39	20	10	7	6	4
Cumulative Variance %	39	59	69	76	82	87

Table 4.3: Factor loadings from the results of PCA on geochemical data from the Wolf Creek time series. Significant loadings of >0.5 are bold. ^{129}I was not included in PCA and is omitted from this table.

3.3 Temporal trends in discharge geochemistry and the response of ^{129}I to catchment hydrology

^{129}I fits into distinct, temporally related sample clusters that correspond to the geochemical evolution of Wolf Creek. Initially, Wolf Creek was dominated by groundwater and then transitioned to snowmelt and soil water at the onset of freshet, which is recorded by the abundance of ^{129}I, ^{127}I and the $^{129}I/^{127}I$ ratio. As freshet declined a mixed water source composed of soil/active layer drainage and groundwater prevailed until freeze up. AHC clearly identified four clusters of samples that are geochemically similar as well as being temporally ordered (Figure 4.6).

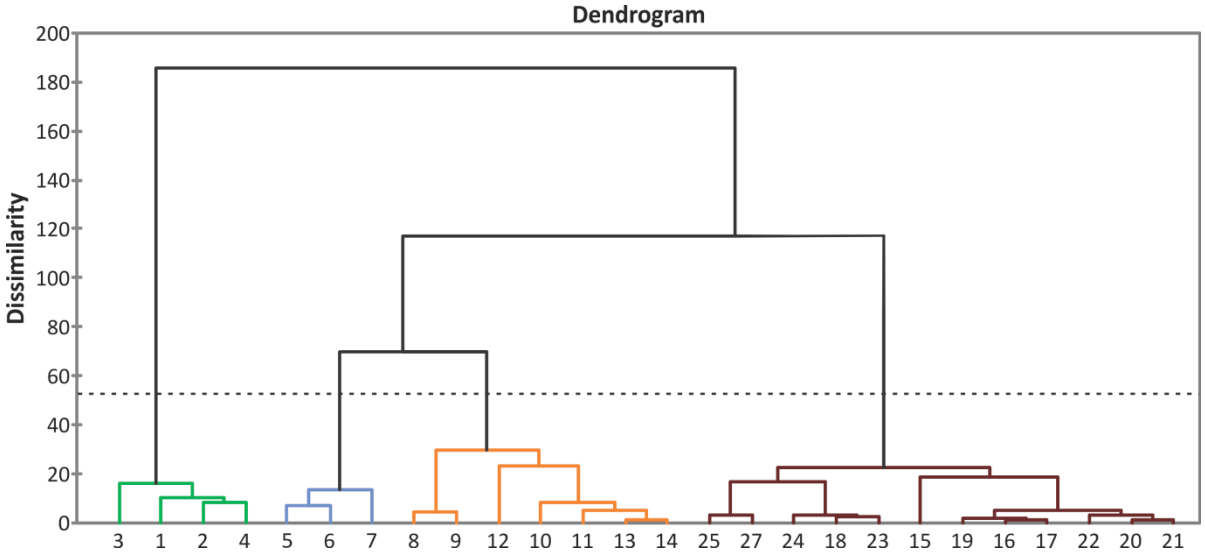

Figure 4.6: Dendrogram graphically showing the results of Agglomerative Hierarchical Clustering. Similarity increases towards 0 on the ordinate axis. Samples are divided into three distinct classes according to their geochemical similarity with the second class being further sorted into two subclasses. These clusters agree very well with the observed groupings of consecutive samples in PCA and show that there were significant geochemical changes in Wolf Creek discharge over time, particularly between samples 4 and 5 as well as 14 and 15. ^{129}I was omitted from AHC analysis.

Period 1, encompasses samples 1-4 and spans April 21 – May 17, 2012. Much of the watershed was snow covered at this time and the discharge flow rate was the lowest of the

study period. Period 1 is characterized by high concentrations of anions and cations and pH around 7.85 (Figure 4.7, Figure 4.8). ^{129}I concentrations ranged from 5.3 to 7.3 x 10^6 atoms/L with a mean of 6.5 x 10^6 atoms/L (Figure 4.4). ^{127}I concentrations were the highest of the sampling period with the exception of one later in the summer (Figure 4.9). As a result, the $^{129}I/^{127}I$ ratio was very low in these samples. The higher concentration of ^{127}I in Period 1 is likely driven by weathering of bedrock and not evapotranspiration, due to the low $^{129}I/^{127}I$ ratio compared to precipitation (Figure 4.10).

$^{14}C_{DIC}$ was around 90 pMC (Figure 4.11), likely due to the weathering of the "old" carbonate rock or coal (^{14}C value of 0 pMC) which dilutes modern $^{14}C_{DIC}$ content of discharge [*Geyh*, 2000]. The $\delta^{13}C$ of DIC in Period 1 is consistent with $^{14}C_{DIC}$. The value of -9‰, is typical of groundwater dissolving carbonate minerals under a mixture of closed and open system conditions [*Clark and Fritz*, 1997] (Figure 4.11). Additionally, calcite was near saturation and the concentration of Ca^{2+} consistent with a carbonate weathering system. Based on the geochemical and isotopic evidence these samples are composed of perennial modern groundwater from talik that has interacted with the geology of the watershed. $\delta^{18}O$ and $\delta^{2}H$ had intermediate values, which were depleted relative to late summer discharge and summer precipitation suggesting groundwater recharge may take place in the winter or was composed of snowmelt and is recharged in the spring (Figure 4.12).

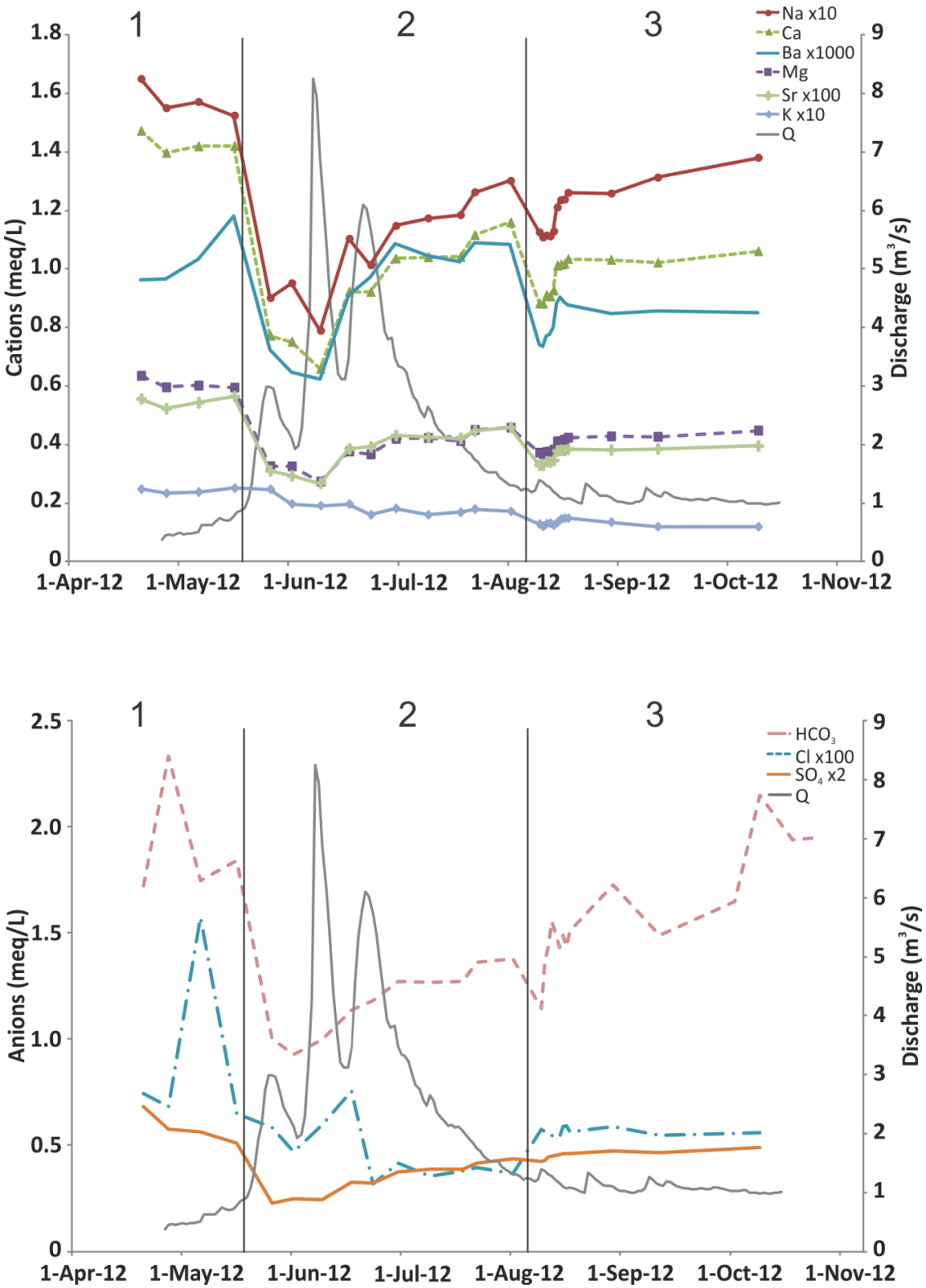

Figure 4.7: Time series plots of major cations and anions in discharge all showing very similar trends, including a sudden depletion at the onset of freshet and a gradual increase as discharge lessens over the summer. Also of note is the depletion in cation concentrations due to a rainstorm in early August.

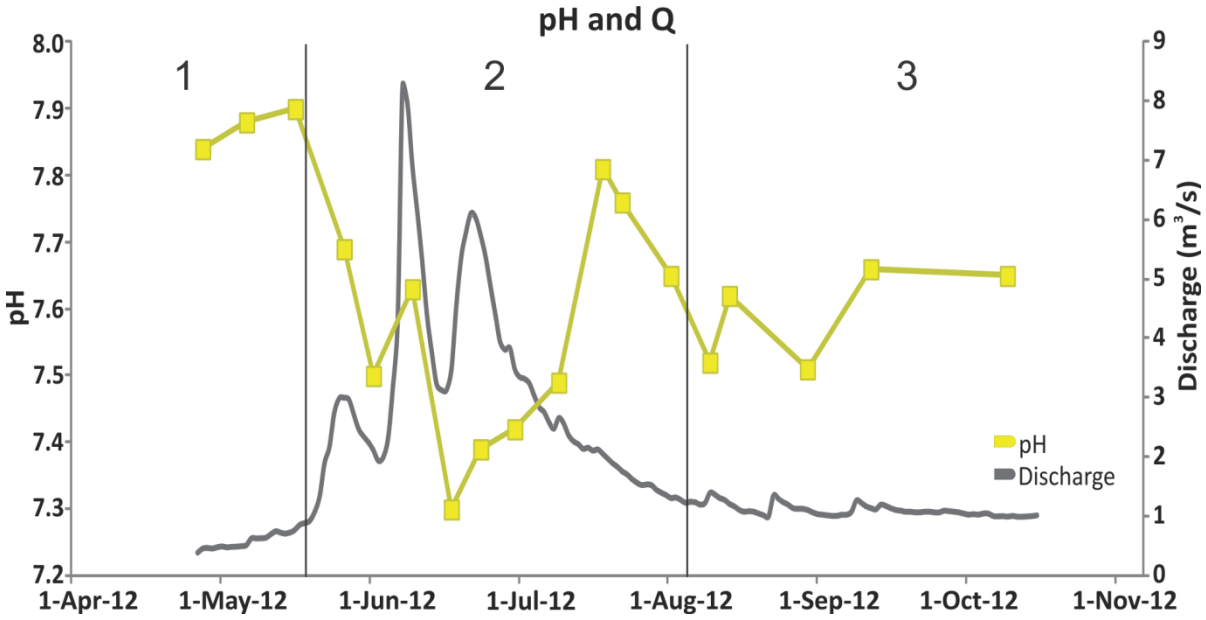

Figure 4.8: Time series of pH in discharge. The sudden drop in pH at the onset of freshet is likely due to the spring acid pulse in which organic acids are washed into the creek by flow of water through soils.

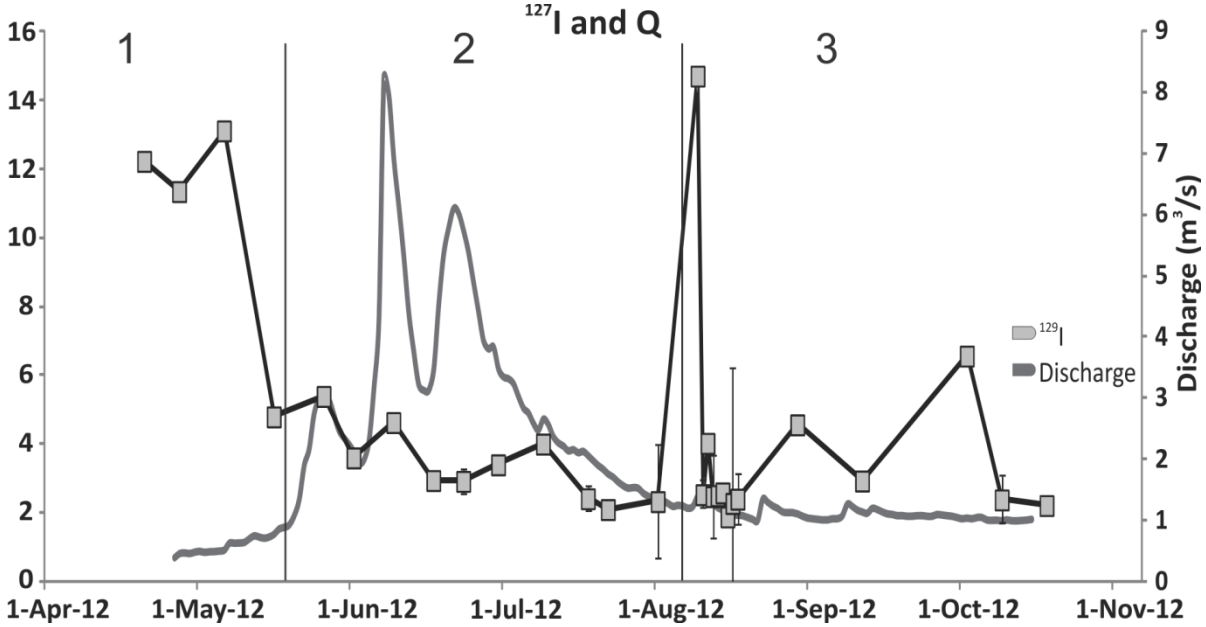

Figure 4.9: Time series of ^{127}I measurements in discharge by ICP-MS. ^{127}I concentrations dropped precipitously at the onset of freshet and remained low for much of the sampling period. The exception is an outlying point in early August which corresponds to a precipitation event at the same time suggesting this peak was caused by the transport of precipitation to discharge.

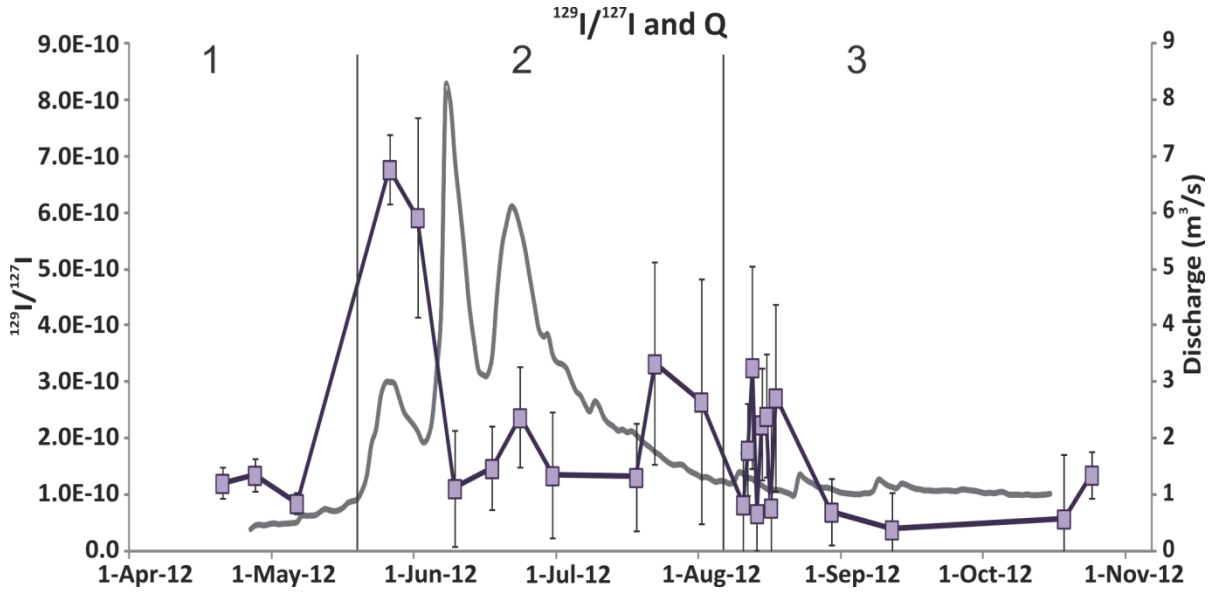

Figure 4.10: A time series of the $^{129}I/^{127}I$ ratio in discharge. In Period 1 the low ratio reflects the high ^{127}I concentration of groundwater. At the onset of freshet the ratio increases sharply, tracking the concentration of ^{129}I, to a level closer to that of precipitation. The ratio then decreases likely due to soil water inputs to discharge and stabilizes for the remainder of the year tracking the concentration of ^{129}I and reflecting the mixture of water sources to discharge.

This suggests groundwater is recycled rapidly and that ^{129}I from atomic bomb testing and/or fuel reprocessing is being discharged back into the surface environment by groundwater despite the presence of permafrost in nearly 50% of the basin and the high organic content of some soils. The ^{127}I enrichment in these samples is due to weathering of organic rich bedrock, such as coal, providing iodine to groundwater. As a result the $^{129}I/^{127}I$ in these samples is low despite the relatively high ^{129}I concentration and $^{129}I/^{127}I$ ratio in recharge from precipitation. Evapotranspiration could also explain the high ^{127}I and ^{129}I concentrations however; this would be expected to result in an equal enrichment for both isotopes and therefore a $^{129}I/^{127}I$ ratio indistinguishable from precipitation as well as enrichments in $\delta^{18}O$ and $\delta^{2}H$, which are not observed.

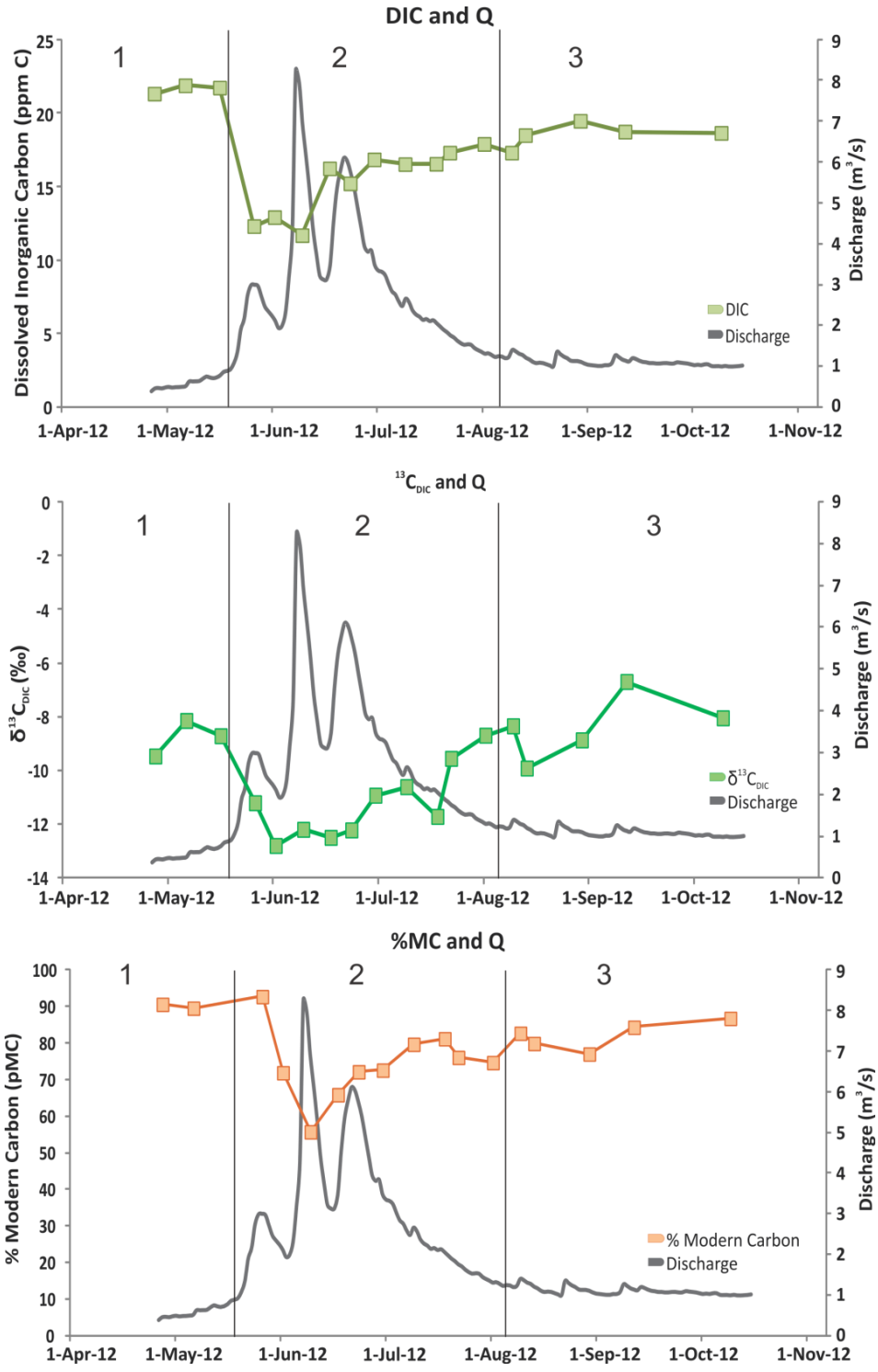

Figure 4.11: Time series plots of DIC, $^{13}C_{DIC}$ and $^{14}C_{DIC}$ in discharge. Error is contained within the data points for DIC, $^{13}C_{DIC}$ and $^{14}C_{DIC}$. In Period 1 DIC is high, ^{13}C is enriched and ^{14}C, is around 90 pMC. However, at the onset of freshet the concentration of DIC drops, ^{13}C becomes depleted and ^{14}C drops to 56 pMC. As summer progresses all three analytes return to their pre-freshet levels. These changes indicate very substantial changes in the source of carbon to discharge and its isotopic composition due to changes in the source of water and flowpaths.

Period 2 is composed of samples 5-14 from May 27 – July 1, 2012 and spans the peak freshet period in Wolf Creek discharge which contains the most radical changes in geochemistry observed. Period 2 can be further divided into two subclasses 2A and 2B (Figure 4.6). 2A (samples 5-7) encompassed the first discharge peak during freshet. During this time, the concentrations of all anions and cations decrease rapidly (Figure 4.7) and $\delta^{18}O$ and $\delta^{2}H$ become more depleted (Figure 4.12). Collectively, these geochemical variations indicate a significant contribution from snowmelt at the initiation of freshet. Similar geochemical observations in the Granger Basin, a sub-catchment of Wolf Creek, concur with our measurements [*Boucher and Carey*, 2010]. In addition, Period 2A is also characterized by a short-lived spike in ^{129}I which is induced by this initial discharge event. We propose that this results from Hortonian overland flow of snowmelt, enriched by dry deposition of ^{129}I over the winter on the snowpack which is then entrained into initial snowmelt, over soils that remain frozen and do not allow significant water infiltration and interaction of the snowmelt with the active layer [*Laudon et al.*, 2004]. Alternatively, Gilfedder et al. 2007a proposed that partial melting and refreezing of the snowpack causes the exclusion of iodine during recrystallization due to its large ionic radii. This would result in an iodine enrichment in initial meltwater. Such a phenomenon has never been observed with ^{129}I before. The spike in ^{129}I, coupled with a significant decrease in ^{127}I concentrations results in the $^{129}I/^{127}I$ increasing significantly relative to Period 1, to values still below, but closer to those measured in precipitation and snow followed by a rapid decrease in step with the ^{129}I concentration (Figure 4.10). These iodine results record the increasing contribution of direct precipitation to discharge which dilutes the ^{127}I groundwater signal

with the ^{129}I enriched, low ^{127}I signal from the atmosphere. This result implies that ^{129}I is a tracer of initial snowmelt contributions to discharge and that such a ^{129}I pulse should be observable in other catchments that also experience significant snowmelt contributions at the onset of freshet. This shift records the transition from groundwater dominated (low ratio) discharge to snowmelt and soil water.

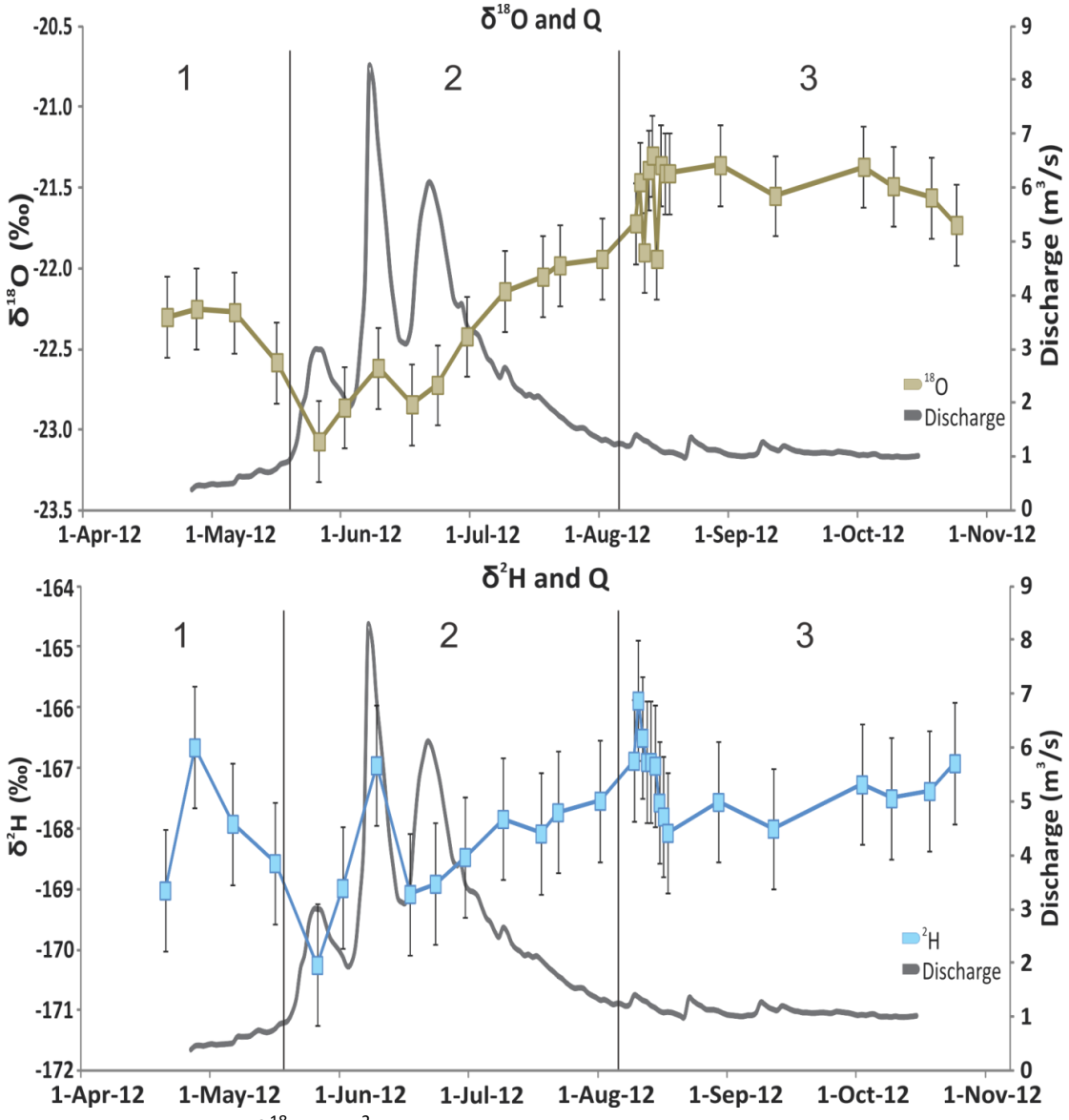

Figure 4.12: Time series of ^{18}O and ^{2}H in discharge. In Period 1 samples were somewhat enriched relative to freshet, although they are depleted compared to summer rain suggesting winter or spring recharge to groundwater. At the onset of freshet there is a significant depletion reflecting the influence of snowmelt on discharge. Following freshet there is a gradual enrichment trend suggesting an increasing influence of groundwater and summer precipitation on discharge.

During Period 2B (samples 8-14) soils are beginning to thaw and attenuate direct snowmelt contributions. The pH begins to decrease at the onset of freshet and reached to a minimum of 7.3 (Figure 4.8). This drop is characteristic of the spring acid pulse observed in many Arctic watersheds and is due primarily to organic acid contributions from soils to discharge [*Laudon and Bishop*, 1999; *Laudon et al.*, 2000]. However, the magnitude of this decrease is comparatively small [*Laudon et al.*, 2000] and speaks to the high carbonate content of soils around Wolf Creek. The K/Ca molar ratio increased markedly in 2B, and remained high for most of the freshet period (Figure 4.13) suggesting that water from organic rich, shallow soil was also contributing to discharge during peak flow [*Elsenbeer et al.*, 1995; *Boucher and Carey*, 2010].

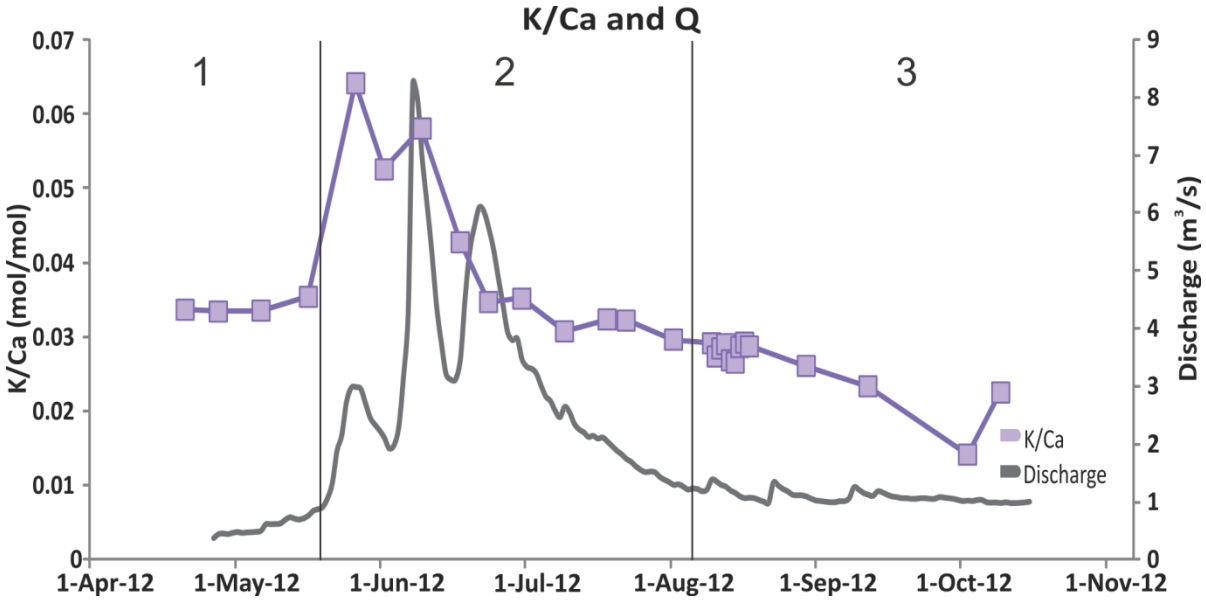

Figure 4.13: Time series of the K/Ca molar ratio in discharge. The K/Ca molar ratio is an excellent indicator of soil water contributions to discharge. Notably, there is a sharp increase at the onset of freshet suggesting that soil water contributions to discharge, which have high K concentrations but low Ca, thereby producing an increase in the K/Ca ratio.

The pMC and $^{13}C_{DIC}$ dropped and reached a minimum of 56 pMC and -13‰ respectively with the second spike in discharge and reflect the increasing interactions of the water with soils high in carbonate that appear to be weathering in a closed system [*Aravena et al.*, 1992; *Clark and Fritz*, 1997; *Geyh*, 2000]. This carbon isotope depletion cannot be related to overland flow of snowmelt into Wolf Creek and therefore indicates the activation of an alternative flowpath as snowmelt reflects a modern atmospheric $^{14}C_{DIC}$ value of ~100 pMC (Figure 4.11). These results are very close to modeled carbonate weathering predictions in a watershed [*Aravena et al.*, 1992; *Clark and Fritz*, 1997; *Geyh*, 2000]. Closed system conditions could have been induced by the infiltration of snowmelt into the surface soil leading to saturated conditions. Carbonate weathering then proceeded during transport as the pre-existing soil water was displaced into Wolf Creek by snowmelt infiltration. This shows potential of $^{14}C_{DIC}$ as a tracer of water flowpaths to streamflow particularly in concert with other isotopic tracers such as $\delta^{18}O$ and $\delta^{2}H$ [*Raymond et al.*, 2004; *Bourke et al.*, 2014]. $\delta^{18}O$ and $\delta^{2}H$ increased slightly during 2B suggesting a variable but generally decreasing contribution of snowmelt. The ^{129}I concentration in discharge remained low throughout Period 2B as freshet ended decreasing to values lower than pre-freshet (Figure 4.4).

The $^{129}I/^{127}I$ ratio also remained low due to the low ^{129}I and ^{127}I concentrations. The fact this ratio decreases so rapidly may demonstrate that the creek is simply returning to baseflow conditions after a peak in snowmelt or that soil drainage has a low $^{129}I/^{127}I$ ratio. Of these two possibilities the most likely is that ^{129}I is lost during transport through the active layer resulting in drainage with a low $^{129}I/^{127}I$ ratio as ^{129}I is adsorbed by watershed

soils (Figure 4.10). Other soil geochemical proxies agree. The concentration of ^{129}I in Wolf Creek is positively correlated with potassium (r=0.71) (Table 4.4). This relationship is most evident by visualizing the K/Ca ratio. A high K/Ca is considered an indicator of water contributions from soil organic layers [*Elsenbeer et al.*, 1995; *Boucher and Carey*, 2010] suggesting the activation of shallow soil flowpaths.

Period 3 is composed of the remaining samples from July 10, 2012 onward. The samples are characterized by stability or a gradual increase of major anions and cations. Discharge continued to decrease, although never reaching pre-freshet levels. $\delta^{18}O$ and $\delta^{2}H$ showed a gradual enrichment trend to even higher levels than baseflow. This is likely due to the influence of precipitation, which was relatively enriched compared to Wolf Creek at this time. It may also be a signal driven by evaporation and evapotranspiration as summer temperatures likely increasingly favor this process but $^{14}C_{DIC}$ and $^{13}C_{DIC}$ also gradually increased to near Period 1 levels possibly signifying an increase in the relative contribution of deep groundwater. The K/Ca ratio and K^{+} concentrations decreased steadily throughout the summer indicating the lessening contribution of soil water. ^{129}I varied only slightly, characterized by a mean concentration of 2.1×10^{6} atoms/L - the lowest of the four clusters. This depletion is probably due to the increasing residence time of precipitation in the watershed, particularly in the soils which, as summer progresses have a larger water absorption capacity. This increases the likelihood of ^{129}I adsorbing onto the soil organic matter during transport [*Fukui et al.*, 1996]. This had the effect of stabilizing the ^{129}I concentration as a lot more drainage in the watershed that contributes to discharge has been in contact with soil. Summer storms in August, 2012 appeared to have induced a

small, yet direct, response in ^{129}I export (Figure 4.14). The small magnitude of these responses, despite this period having the largest mass flux of ^{129}I into the WCRB as precipitation, shows that the majority of the ^{129}I introduced to the catchment was not transported to Wolf Creek.

Variables	pH	Al	Na	K	Mg	Ca	Fe	Ba	Sr	^{127}I	^{129}I	$^{129}I/^{127}I$	Cl	SO_4	HCO_3	Br	F	S	Si
pH	**1.00**																		
Al	-0.26	**1.00**																	
Na	**0.59**	**-0.64**	**1.00**																
K	0.42	-0.28	0.30	**1.00**															
Mg	**0.64**	**-0.64**	**0.97**	**0.51**	**1.00**														
Ca	**0.62**	**-0.67**	**0.96**	**0.48**	**0.99**	**1.00**													
Fe	0.33	-0.15	-0.07	0.07	-0.07	-0.04	**1.00**												
Ba	0.29	**-0.69**	**0.63**	0.34	**0.67**	**0.75**	0.05	**1.00**											
Sr	**0.55**	**-0.71**	**0.89**	**0.56**	**0.96**	**0.98**	-0.02	**0.84**	**1.00**										
^{127}I	0.28	-0.18	**0.43**	**0.47**	**0.51**	**0.45**	-0.12	0.01	**0.40**	**1.00**									
^{129}I	0.18	0.11	-0.11	**0.71**	0.03	-0.03	-0.03	-0.25	-0.02	**0.43**	**1.00**								
$^{129}I/^{127}I$	-0.05	0.24	**-0.42**	0.32	-0.35	-0.37	-0.01	-0.28	-0.34	-0.13	**0.80**	**1.00**							
Cl	0.38	-0.01	**0.46**	**0.41**	**0.49**	**0.44**	-0.16	0.03	0.38	**0.59**	0.14	-0.24	**1.00**						
SO_4	**0.53**	**-0.49**	**0.92**	0.06	**0.85**	**0.84**	-0.12	**0.42**	**0.72**	**0.43**	-0.25	**-0.54**	**0.42**	**1.00**					
HCO_3	**0.52**	**-0.46**	**0.82**	0.07	**0.75**	**0.74**	-0.18	0.35	**0.63**	0.22	-0.19	**-0.50**	0.34	**0.82**	**1.00**				
Br	**0.54**	-0.10	0.34	**0.61**	**0.48**	**0.42**	0.05	0.14	0.40	**0.68**	**0.70**	0.29	**0.44**	0.19	0.09	**1.00**			
F	0.00	0.21	0.10	**-0.68**	-0.07	-0.08	-0.28	-0.34	-0.25	0.04	-0.30	-0.21	0.09	0.40	0.14	-0.06	**1.00**		
S	**0.61**	**-0.66**	**0.94**	**0.48**	**0.97**	**0.97**	-0.02	**0.66**	**0.94**	**0.52**	-0.02	-0.40	**0.43**	**0.86**	**0.71**	0.36	-0.11	**1.00**	
Si	0.37	**-0.76**	**0.72**	**0.66**	**0.82**	**0.84**	0.07	**0.83**	**0.91**	0.34	0.11	-0.13	0.28	**0.47**	**0.39**	0.33	**-0.47**	**0.81**	**1.00**
DOC	-0.08	0.37	-0.26	-0.04	-0.26	-0.29	0.14	**-0.45**	-0.34	-0.07	0.11	0.11	-0.13	-0.13	-0.01	-0.26	0.08	-0.19	-0.36
^{18}O	0.13	0.02	0.22	**-0.76**	0.01	0.03	-0.04	-0.10	-0.12	-0.19	**-0.63**	**-0.49**	-0.08	**0.46**	**0.42**	-0.38	**0.73**	0.01	-0.34
^{2}H	0.24	0.05	0.04	**-0.59**	-0.07	-0.06	-0.20	-0.22	-0.18	0.01	**-0.57**	**-0.52**	-0.02	0.29	0.35	-0.18	**0.54**	-0.04	-0.35
TU	-0.15	-0.28	0.12	0.06	0.10	0.03	-0.13	-0.21	-0.03	0.16	0.01	-0.08	0.26	0.10	0.14	0.08	0.19	0.04	0.10
%MC	**0.56**	-0.35	**0.60**	0.11	**0.58**	**0.53**	0.10	0.17	0.43	0.42	0.44	0.14	0.30	**0.55**	**0.55**	**0.73**	0.30	**0.48**	0.24
DIC	**0.48**	**-0.62**	**0.95**	0.01	**0.91**	**0.90**	-0.17	**0.60**	**0.82**	0.34	-0.39	**-0.62**	0.44	**0.98**	**0.83**	0.30	0.45	**0.89**	**0.60**
$^{13}C_{DIC}$	0.46	-0.28	**0.72**	-0.27	**0.59**	**0.57**	-0.25	0.25	0.44	0.31	-0.25	-0.41	0.29	**0.79**	**0.63**	0.33	**0.61**	**0.56**	0.12
Daily Discharge m^3/s	**-0.66**	0.28	**-0.69**	0.17	**-0.58**	**-0.57**	-0.01	-0.20	**-0.41**	-0.26	0.13	0.30	-0.25	**-0.81**	**-0.69**	-0.23	**-0.52**	**-0.55**	-0.16
K/Ca	-0.08	0.37	**-0.53**	**0.62**	-0.34	-0.38	0.11	-0.34	-0.29	0.09	**0.71**	**0.61**	0.05	**-0.67**	**-0.55**	0.38	**-0.64**	-0.35	-0.08

Variables	DOC	^{18}O	^{2}H	TU	%MC	DIC	$^{13}C_{DIC}$	Daily Discharge m^3/s	K/Ca
DOC	**1.00**								
^{18}O	0.15	**1.00**							
^{2}H	0.04	**0.66**	**1.00**						
TU	-0.05	-0.04	-0.03	**1.00**					
%MC	-0.40	0.28	-0.02	0.01	**1.00**				
DIC	-0.44	**0.51**	0.41	0.16	**0.53**	**1.00**			
$^{13}C_{DIC}$	-0.22	**0.70**	0.44	-0.09	**0.57**	**0.74**	**1.00**		
Daily Discharge m^3/s	0.05	**-0.69**	**-0.45**	0.08	**-0.74**	**-0.75**	**-0.85**	**1.00**	
K/Ca	0.27	**-0.80**	**-0.54**	0.01	-0.30	**-0.74**	**-0.68**	**0.65**	**1.00**

Table 4.4: Pearson's r correlation matrix for all analytes in Wolf Creek discharge. Table is continued on two pages.

The $^{129}I/^{127}I$ ratio during this period was relatively variable possibly due to the influence of summer rain storms and had high $^{129}I/^{127}I$ ratios (Figure 4.10). One large precipitation event also resulted in short-lived depletions in most anions and cations as well as pH in Wolf Creek streamflow. No corresponding response was observed in the ^{129}I concentration of this event. The gradual increase of dissolved ions towards pre-freshet concentrations suggests that as summer progressed the contribution of deep groundwater to Wolf Creek increased as watershed soils dried and other sources contributed little water. It also appears that episodic precipitation can have a direct influence on discharge geochemistry and stable isotopes, suggesting that Wolf Creek can be influenced by short lived events during summer and autumn.

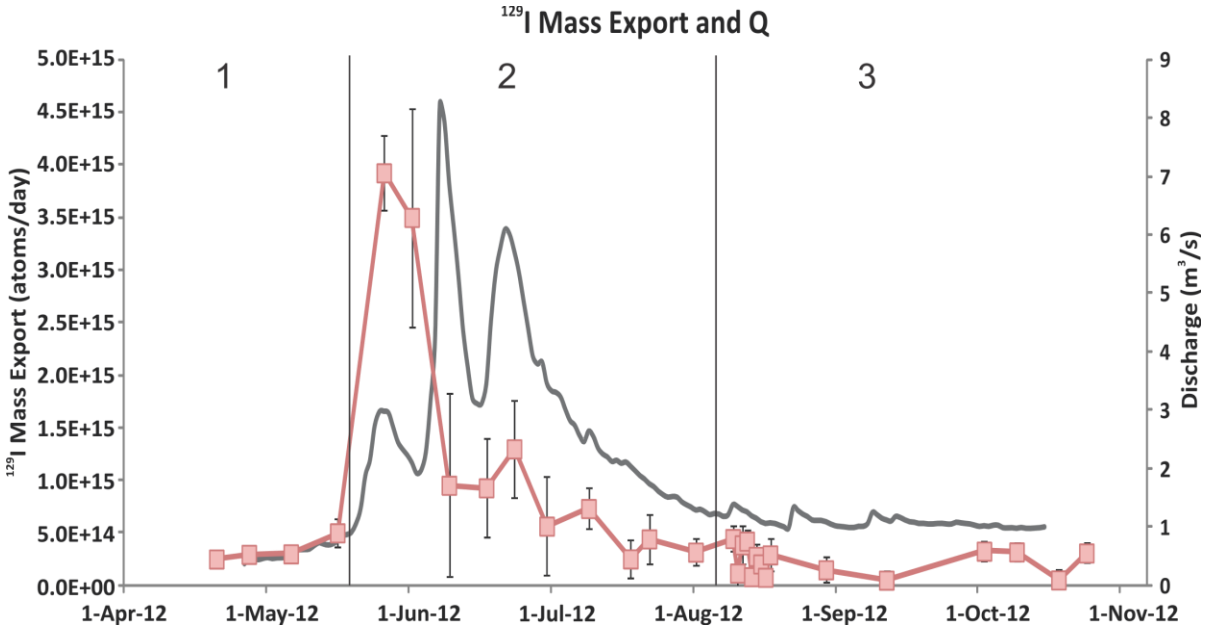

Figure 4.14: Time series of daily ^{129}I mass export from the WCRB via Wolf Creek streamflow. The trend of mass export generally follows discharge as when discharge is low mass flux is also low. However, the exception to this occurs at the onset of freshet when flux peaks and the first, and smallest peak of freshet occurs. This discrepancy is due to the high concentration of ^{129}I in discharge at this time suggesting that the mass export is dependent on the concentration of ^{129}I.

Ultimately the geochemical cycle of Wolf Creek discharge was characterized by baseflow at the beginning of the sampling period composed of deep groundwater that had weathered the carbonate and silicate bedrock of the catchment. This water end member had ^{129}I concentrations higher than those during the summer, possibly due to evapotranspiration, but an extremely low $^{129}I/^{127}I$ ratio because of contributions of ^{127}I to groundwater from weathering of marine sediment or organic deposits, such as coal, in the watershed. Once temperatures warmed discharge increased and was characterized by two water sources. (1) snowmelt and (2) soil water. Indeed, the initial peak in discharge, which also had the most depleted $\delta^{18}O$ and $\delta^{2}H$ likely had a relatively large component from snowmelt transferred to the stream by Hortonian overland flow as infiltration was likely restricted due to frozen soils [*Laudon et al.*, 2004]. This phenomenon led to the observed spike in ^{129}I in streamflow due to the entrainment of ^{129}I deposited via dry fallout in early snowmelt or ionic exclusion of iodine during partial melting and refreezing of the snowpack. This implies that ^{129}I could be an excellent tracer of initial snowmelt contributions to freshet in snow-covered catchments. The subsequent drop in ^{129}I concentrations even as discharge increases suggests that this reservoir of ^{129}I was 1) quickly depleted or 2) another water source with low ^{129}I concentrations began to dominate streamflow. Evidence from ^{18}O, ^{2}H, $^{14}C_{DIC}$, $^{13}C_{DIC}$, pH and the K/Ca ratio suggest that continued warming within this catchment led to thawed soils and snowmelt infiltration causing the displacement of pre-event soil water into Wolf Creek, which has a low ^{129}I concentration, resulting in a low $^{129}I/^{127}I$ ratio due to attenuation of ^{129}I by soils despite the fact that precipitation was likely its origin.

3.4 Tritium constrains groundwater age and ^{129}I attenuation by soil organic matter

From the monitoring discussed above, the strong partitioning of ^{129}I in organic matter [*Schwehr et al.*, 2009] might explain the measured imbalance between its abundance in precipitation and in discharge. Given that soils from the WCRB have 3% to 82% organic matter, it is probable that some of the ^{129}I in precipitation and snowmelt is adsorbed when in contact with soils. However, the imbalance observed between precipitation and discharge is strictly restricted to ^{129}I. For instance, the concentration of ^{127}I in precipitation and in Wolf Creek discharge are comparable suggesting that only the quantities of ^{129}I are increasing in the WCRB. We discuss this issue more quantitatively later in the text with a mass balance estimate. On a broad scale, the most likely explanation for this is that ^{129}I is actively being removed from the waters. However, another possibility is the concentrations of ^{129}I in Wolf Creek are diluted by ancient waters with a pre-nuclear signature of low ^{129}I concentration and a low ^{129}I/^{127}I ratio. Tritium in precipitation is sourced from atmospheric fallout and is used as a tracer of the "modern" signal for waters because of its short half life and may be used to answer this question [*Clark and Fritz*, 1997]. Tritium levels were largely constant in discharge and characterized by modern values which is consistent with discharge in Wolf Creek being modern with no significant "ancient" water signal (Supplementary Figure B3). This conveniently eliminates the possibility that dilution by a pre-nuclear age, low ^{129}I fraction of water accounts for the low values of ^{129}I measured in discharge relative to rainwater. More likely, ^{129}I is being accumulated in the watershed and slowly increasing the concentrations to reflect the modern input levels. This finding also places a constraint on the residence time of groundwater in the WCRB as the "modern" levels of both tritium and ^{129}I indicate that recharge must have occurred before

tritium decay can become significant, after peak bomb fallout [*Clark and Fritz*, 1997] and thus the cycle of groundwater from recharge to discharge operates on a decadal time scale.

3.5 ^{129}I in the WCRB is not at steady state

To gain insight into the watershed-scale behaviour of ^{129}I, we estimated the mass transfer and storage of ^{129}I in WCRB. Storage is calculated as:

$$^{129}I_{stored} = {}^{129}I_{import} - {}^{129}I_{export} \quad (1)$$

Where ^{129}I stored is the net amount of ^{129}I added to the watershed on an annual basis, ^{129}I import is the mass flux of ^{129}I added to the watershed annually via rain and snow and ^{129}I export is the mass flux of ^{129}I removed from the watershed annually in Wolf Creek discharge.

Assuming that the sole source of ^{129}I to the WCRB is atmospheric and dominated by wet deposition, the ^{129}I import flux is calculated as:

$$^{129}I\ Import = \left({}^{129}I_{rain} \times mm_{rain}\right) + \left({}^{129}I_{snow} \times mm_{snow}\right) \times WA \quad (2)$$

Where ^{129}I rain is the input of ^{129}I from rain annually (Supplementary Table B1), ^{129}I snow is the input of ^{129}I from snow annually (Supplementary Table B1), mm is the quantity of rain or snow the watershed received during each sampling interval and WA is the watershed area of the WCRB. Summing the two terms in Eqn 2 finds that the total ^{129}I mass flux into the WCRB was 1.44 ± 0.11 x 10^{18} atoms/yr. The annual ^{129}I export through discharge, which we assumed to be the only appreciable loss of ^{129}I from the watershed, was calculated using a period weighted method [*Dann et al.*, 1986] as:

$$^{129}I\ Export = (\sum[\overline{X}(Q_{interval})] \times {}^{129}I \times t_{interval}) + \{(Q_{baseflow} \times {}^{129}I_{baseflow}) \times t_{baseflow}\}$$

Where $\Sigma(\overline{X}(Q_{interval}))$ is the sum of the mean of daily discharge measurements for each interval (L/s), ^{129}I is the measured concentration in discharge (atoms/L), $t_{interval}$ is the number of days that discharge measurements were available, (Supplemental Information, Supplemental Table B1), $Q_{baseflow}$ is the assumed baseflow discharge (400 L/s), $^{129}I_{baseflow}$ is the concentration of ^{129}I in baseflow (6.5×10^6 atoms/L) and $t_{baseflow}$ is the estimated number of days baseflow was the dominant water source to discharge.

The net annual ^{129}I mass flux to the WCRB normalized to per m^2 from rain and snow is 7.4×10^9 atoms/m^2/yr. This value is substantially lower than the 5.5×10^{10} atoms/m^2/yr measured in Vancouver, Canada, in 2011 although the Vancouver estimate does include the mass input from the Fukushima-Daiichi Nuclear Accident (See Chapter 5). However, the difference between mass fluxes in the WCRB and Vancouver is due to the large amount of precipitation Vancouver receives and its proximity to the coast as opposed to the input from Fukushima. The mass flux of ^{129}I to the WCRB is also 2 to 3 orders of magnitude lower than measurements from Europe [*Reithmeier et al.*, 2010], suggesting that the remoteness of the WCRB region greatly reduces the input of ^{129}I.

The total export during the sampling period was $1.3 \pm 0.43 \times 10^{17}$ atoms and represents 76**%** of the total export for the year (Figure 4.14). The contribution from baseflow to annual discharge for the rest of the year was ~$4.0 \pm 0.87 \times 10^{16}$ atoms. Summing these two contributions yields a total ^{129}I export of $1.7 \pm 0.44 \times 10^{17}$ atoms/yr. If the ^{129}I export is calculated using the mean annual discharge and the mean ^{129}I

concentration, instead of time interval data, it gives an annual export of 2.1 x 10^{17} atoms/yr. This is an overestimate of ~20% and shows that taking temporal variations into account is critical for reliable estimate of ^{129}I flux and as such should be employed in other hydrology studies using ^{129}I. The majority of ^{129}I was exported during freshet (Figure 4.14) due to the significant amount of ^{129}I stored over the winter within the snowpack. Indeed, we have estimated that a minimum of 1.76 ± 0.29 x 10^{17} atoms of ^{129}I were stored in the watershed in snow while the quantity of ^{129}I exported at freshet was only 1.01 ± 0.12 x 10^{17} atoms or 57 ± 7 % of the ^{129}I held in storage. Therefore, the remainder of the ^{129}I deposited during the winter was likely lost during transport to the creek by attenuation in soil or to groundwater recharge.

Mass balance results show that the net ^{129}I stored annually in the WCRB is 1.26 ± 0.12 x 10^{18} atoms or ~88 ± 8 **%** of the total ^{129}I input to the watershed, indicating that ^{129}I is accumulating in the WCRB, and far from steady state. This disequilibrium is likely a symptom of the relatively recent and continuing additions of anthropogenic ^{129}I to the global iodine cycle to which the catchment is still adjusting. The mass balance estimate of WCRB is almost identical to that of Baltic region where it is estimated that ~87% of the input is stored terrestrially and only ~13% is exported to the Baltic Sea [*Aldahan et al.*, 2006]. Given the similarity between these two estimates, it is likely that this prediction is applicable to other northern hemisphere watersheds which are also likely accumulating anthropogenic ^{129}I. As the WCRB, which has a relatively low ^{129}I flux from a variety of sources, is not close to steady state this accumulation is relatively slow. The rate of ^{129}I accumulation could be affected by to heterogeneities in the composition of the watershed

soils that reduce ^{129}I adsorption, physical hydrologic processes that inhibit retardation or geochemical processes that make ^{129}I less available for adsorption. The most likely reservoir to accumulate ^{129}I in the WCRB is soil, particularly soil organic matter and soil with a high population of bacterial activity which have been identified as strong attractants of ^{129}I [*Sheppard et al.*, 1996; *Lusa et al.*, 2015]. The primary source of uncertainty in the mass balance calculation comes from the AMS analysis of ^{129}I. Many of the other parameters are well constrained. However, the calculation of ^{129}I export during baseflow and the ^{129}I mass input in snow do require several assumptions that are outlined in Appendix B.

A mass balance of ^{127}I in the WCRB, determined using the same method as ^{129}I, shows that 75.4 ± 16.7 kg or 27 ± 6 % of the annual ^{127}I input is stored within the WCRB. The annual input of ^{127}I in rain and snow was 283 ± 16.5 kg while the annual export in discharge was 208 ± 3 kg. This finding suggests that ^{127}I is also accumulating in the WCRB similar to ^{129}I. However, it is possible that the input represents an overestimate given the uncertainty associated with the actual quantity of snowfall in the catchment. It is more likely that ^{127}I is actually at or near steady state in the WCRB as is indicated by the similar concentration of ^{127}I in discharge and precipitation suggesting these reservoirs are near equilibrium with one another. Furthermore, WCRB soil water may also be at equilibrium with precipitation and discharge due to the long period of time ^{127}I has had to reach steady state in the WCRB relative to ^{129}I. It would be expected that for discharge to reflect the ^{127}I concentration in precipitation WCRB soils would have to also reflect the mean ^{127}I concentration in precipitation.

3.6 The storage of ^{129}I in the watershed and the importance of SOM

Soils are critically important for the storage of ^{129}I. Throughout the WCRB ^{129}I, ^{127}I and soil organic matter content (SOM) (Supplementary Table B2) were analyzed to determine if the anthropogenic signature of ^{129}I could be detected. If SOM is indeed the pool accumulating the excess ^{129}I not recovered in discharge, it should be detectable as an increase from the background $^{129}I/^{127}I$ values. The soil samples from the WCRB which were all taken at depths of less than 5 cm, have ^{129}I concentration from 10 - 228 x 10^6 atoms/g and a ^{127}I concentration from 0.8 – 28 mg/kg (Figure 4.15). The SOM in the soil ranged from 3% in a nearly pure silicate mineral soil to 82% in a peat soil (Figure 4.15).

There is a very strong linear correlation between the ^{129}I concentration and the percentage of organic carbon in the soils ($r = 0.97$ ($p<0.0001$)) (Figure 4.15). These surface soil samples display the modern isotopic signature of iodine that most resembles precipitation. This is characteristic of iodine geochemistry and its tendency to adsorb on organic soils [*Sheppard et al.*, 1996; *Söderlund et al.*, 2011] and is consistent with previous observations on the partitioning of ^{129}I and ^{127}I in soil [*Luo et al.*, 2013]. The $^{129}I/^{127}I$ ranged from 1.2 – 6.5 x 10^{-9} with a mean of 3.0 x 10^{-9}. At first glance these results would suggest that the soils of the WCRB have already reached equilibrium with the modern $^{129}I/^{127}I$. However, surface samples are not representative of the entire watershed soil signatures [*Englund et al.*, 2010b; *Luo et al.*, 2013]. Indeed, if the entirety of watershed soils reflected the modern $^{129}I/^{127}I$ signature, so should the discharge of Wolf Creek. The measurements of WCRB soils are similar to surface soils measured in China and Japan [*Muramatsu et al.*, 2008; *Luo et al.*, 2013] and around 2 orders of magnitude lower than Chernobyl soil (IAEA-

375) [*Jiang et al.*, 2005; *Herod et al.*, 2014a]. The fact that the samples collected in China and Japan are also considered far from sources of ^{129}I, yet are much closer to point sources than the Canadian Arctic, demonstrates the global ubiquity of anthropogenic ^{129}I emissions in soil. Interestingly, ^{127}I displayed similar behaviour to ^{129}I in soil suggesting that a these two isotopes, which are decoupled in precipitation and come from different sources experience a coupling once they are deposited as WCRB soils equilibrate with the relatively recent increases in the atmospheric input of ^{129}I. This coupling is likely due to the affinity of iodine for organic matter. This coupling is also observed in discharge, only during Period 3, when both ^{129}I and ^{127}I are at low concentration and display similar behaviour, which suggests that soil water is contributing ^{129}I and ^{127}I to discharge throughout the summer.

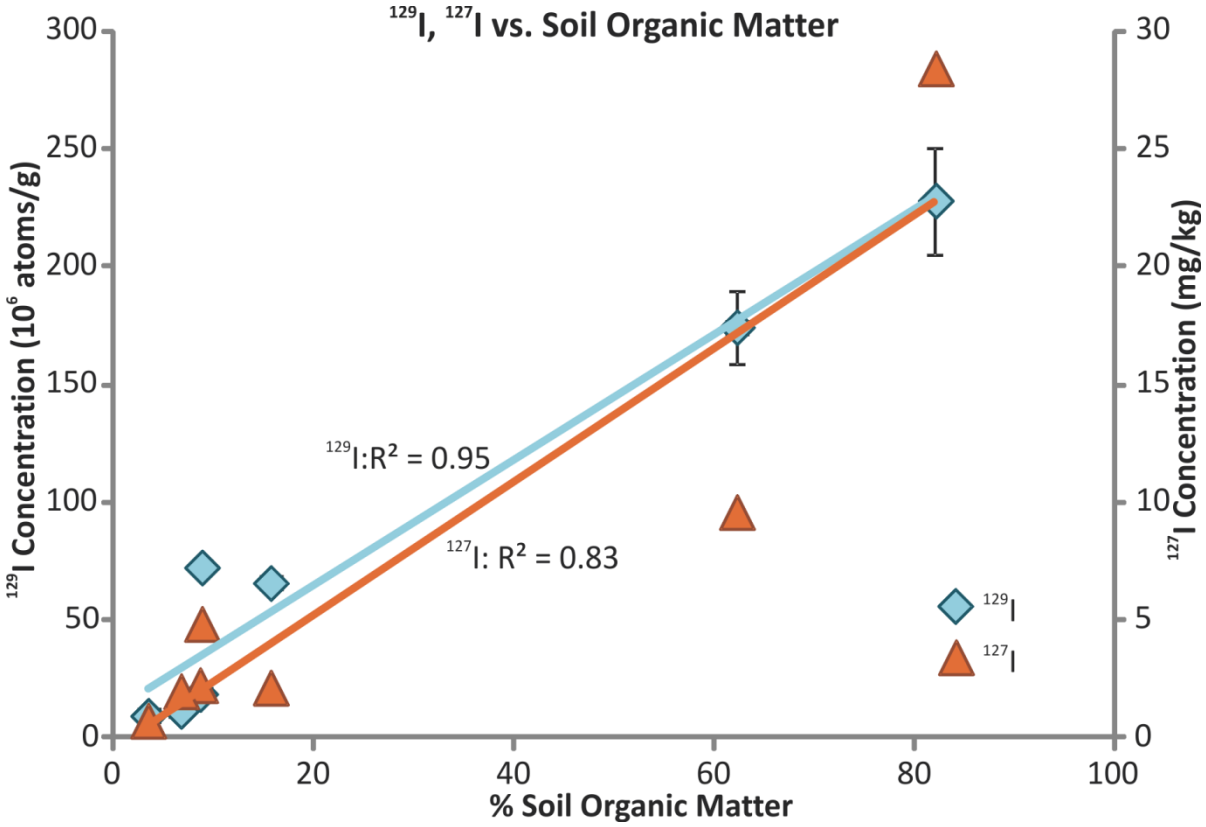

Figure 4.15: Comparison of ^{129}I and ^{127}I with the organic matter content of WCRB soils. Both iodine isotopes show extremely strong linear correlations with the concentration of organic matter in soils suggesting this is the most likely reservoir to be accumulating ^{129}I in the catchment.

3.6.1 The potential rate of ^{129}I accumulation in the catchment

The ^{129}I mass balance showed that a significant quantity of the annual ^{129}I mass input to the WCRB is stored within two reservoirs: soil and groundwater. Sampling of the soil reservoir, coupled with previous investigations of soil adsorption of ^{129}I [*Sheppard and Hawkins*, 1995; *Sheppard et al.*, 1995] suggests that soil organic matter is adsorbing the input of ^{129}I very efficiently. As ^{129}I is continually produced by fuel reprocessing, it will accumulate in SOM making it a potential radiological concern in future, particularly as soils represent the largest terrestrial reservoir of ^{129}I globally [*Aldahan et al.*, 2007].

The accumulation of ^{129}I over time can be modeled if the storage proportion is assumed to be constant and the ^{129}I flux is the only free parameter. According to the results, if ^{129}I fallout remains constant then the $^{129}I/^{127}I$ ratio will increase by one order of magnitude in the next 1000 years. However, if the ^{129}I flux increases with doubling times of 10 or even 50 years then the $^{129}I/^{127}I$ ratio in these soils can increase substantially and will resemble that of Chernobyl or Fukushima within 150 to 600 years [*Strachnov et al.*, 1996; *Muramatsu et al.*, 2015]. As the production of ^{129}I has not increased markedly in the past decade the most realistic scenario is likely the first. However, several new reprocessing facilities have recently begun operation and thus it is feasible that the rate of ^{129}I deposition could increase over time leading to global increases in the $^{129}I/^{127}I$ ratio and the ^{129}I concentration even in extremely remote locations such as the WCRB [*IAEA*, 2008]. This potential reinforces the need for global monitoring of ^{129}I fallout and storage even in remote regions.

4.0 CONCLUSIONS

This is the first study to investigate the temporal behaviour and fate of atmospherically-derived ^{129}I in a watershed. The WCRB is remotely located but nonetheless receives anthropogenic ^{129}I from a combination of ocean volatilization and direct releases from NFRP's. The input variations of ^{129}I in the WCRB result mainly from seasonal variations in weather patterns with secondary stochastic contributions of anthropogenic ^{129}I. From these sources the annual mass input of ^{129}I was 1.3×10^{18} atoms. PCA and AHC demonstrate that the temporal variations in ^{129}I in discharge are driven by the source of water and the degree of interaction with soils or bedrock with an annual ^{129}I export in discharge of 1.7 x

10^{17} atoms. A mass balance of ^{129}I import and export found that almost 90% of the annual atmospheric input was stored in the watershed. Over the sampling period streamflow evolved from dominantly perennial groundwater discharge with a mean ^{129}I of 6.5 ± 1.1 x 10^{6} atoms/L and a low $^{129}I/^{127}I$ of 1.1 ± 0.26 x 10^{-10} prior to snowmelt to a direct contribution from snowmelt at the onset of freshet. This transformation was recorded by ^{18}O, ^{2}H, $^{14}C_{DIC}$, $^{13}C_{DIC}$, pH, and numerous anions and cations and also corresponded with the highest concentration of ^{129}I, 17.4 x 10^{6} atoms/L, measured in Wolf Creek discharge as well as the peak $^{129}I/^{127}I$ ratio of 6.8 x 10^{-10}. This pulse of ^{129}I was caused by entrainment of dry fallout or ion exclusion into snowmelt and rapid transport via overland flow to the creek. This was followed by an increase in contributions from ^{129}I-depleted soil water displaced into discharge as snowmelt infiltrated into the thawing active layer with sorption of ^{129}I onto organics. After freshet concentrations of most analytes stabilized or increased slightly marking a gradual increase in groundwater contributions until freeze up. These hydrologic changes were accompanied by both increases and decreases in ^{129}I, ^{127}I, the $^{129}I/^{127}I$ ratio as well as the geochemistry and isotopes of water and carbon in Wolf Creek discharge resulting from changes in the source, flowpath and residence time of the water endmembers. This variability suggests that reservoirs of the WCRB have not yet reached equilibrium with respect to ^{129}I inputs. This reflects the fact that the $^{129}I/^{127}I$ has increased drastically since the beginning of the nuclear age and is likely to keep increasing because the mean residence time of ^{129}I in the watershed is greater than the roughly 60 years since the start of anthropogenic emissions. As a result, the WCRB is a net sink of ^{129}I, effectively storing ^{129}I. The most likely scavenger of ^{129}I from the water is the large pool of soil organic

matter which was strongly correlated to the ^{129}I concentration (r= 0.97) and has, in surface soils, a $^{129}I/^{127}I$ which resembles precipitation. The fact that the Wolf Creek discharge does not reflect this ratio suggests this is only the case in surficial soils and that the iodine attenuation capacity of the WCRB has not yet been satisfied. A deeper investigation into the residence time of iodine in the watershed can determine how much more input is necessary before reaching a new steady state with respect to ^{129}I. Because the modern ^{129}I signature is far from the natural background, the anthropogenic input of ^{129}I and its cycling constitute an effective tracer of water endmembers in discharge, the degree of interaction between precipitation and soil organic matter, initial snowmelt contributions to discharge, and groundwater contributions to surface water, particularly when used in concert with ^{127}I, ^{3}H, ^{14}C and other geochemical tracers.

Future work should focus on quantifying ^{129}I residence and transit times in different catchment reservoirs as well as identify and measure temporal variation of organic species, inorganic species and particulate ^{129}I in precipitation, catchment reservoirs and discharge should also be differentiated and may enhance the usefulness of ^{129}I as a tracer to distinguish end member contributions to streamflow.

Acknowledgments
The authors would like to acknowledge the sampling assistance of Emilie Herdes and Jeff Van Zandvoort, the laboratory assistance of Monika Wilk, G.G Hatch Stable Isotope Lab, and Xiao-lei Zhao. Finally thanks are owed to Rick Janowicz for providing the 2012 Wolf Creek hydrograph.

References

Aldahan, A., A. Kekli, and G. Possnert (2006), Distribution and sources of 129I in rivers of the Baltic region., *J. Environ. Radioact.*, *88*(1), 49–73, doi:10.1016/j.jenvrad.2006.01.003.

Aldahan, A., V. Alfimov, and G. Possnert (2007), 129I anthropogenic budget: Major sources and sinks, *Appl. Geochemistry*, *22*(3), 606–618, doi:10.1016/j.apgeochem.2006.12.006.

Alvarado-Quiroz, N. G., T. G. Kotzer, G. M. Milton, I. D. Clark, and D. Bottomley (2002), Partitioning of 127I and 129I in an unconfined glaciofluvial aquifer on the Canadian shield, *Radiochim. Acta*, *90*(8), 469–478.

Amachi, S. (2008), Microbial Contribution to Global Iodine Cycling: Volatilization, Accumulation, Reduction, Oxidation, and Sorption of Iodine, *Microbes Environ.*, *23*(4), 269–276, doi:10.1264/jsme2.ME08548.

Aravena, R., S. L. L. Schiff, S. E. Trumbore, P. J. Dillon, and R. Elgood (1992), Evaluating Dissolved Inorganic Carbon Cycling in a Forested Lake Watershed Using Carbon Isotopes, *Radiocarbon*, *34*(3), 636–645.

Auf der Heyde, T. P. E. (1990), Analyzing chemical data in more than two dimensions: A tutorial on factor and cluster analysis, *J. Chem. Educ.*, *67*(6), 461, doi:10.1021/ed067p461.

Beasley, T. M., L. W. Cooper, J. M. Grebmeier, L. R. Kilius, and H. -a. Synal (1997), 36Cl and 129I in the Yenisei, Kolyma, and Mackenzie Rivers, *Environ. Sci. Technol.*, *31*(6), 1834–1836, doi:10.1021/es9609361.

Boucher, J. L., and S. K. Carey (2010), Exploring runoff processes using chemical, isotopic and hydrometric data in a discontinuous permafrost catchment, *Hydrol. Res.*, *41*(6), 508, doi:10.2166/nh.2010.146.

Bourke, S. A., G. A. Harrington, P. G. Cook, V. E. Post, and S. Dogramaci (2014), Carbon-14 in streams as a tracer of discharging groundwater, *J. Hydrol.*, *519*, 117–130, doi:10.1016/j.jhydrol.2014.06.056.

Buraglio, N., A. Aldahan, Gö. Possnert, and I. Vintersved (2001), 129I from the Nuclear Reprocessing Facilities Traced in Precipitation and Runoff in Northern Europe, *Environ. Sci. Technol.*, *35*(8), 1579–1586, doi:10.1021/es001375n.

Carey, S. K., J. L. Boucher, and C. M. Duarte (2012), Inferring groundwater contributions and pathways to streamflow during snowmelt over multiple years in a discontinuous permafrost subarctic environment (Yukon, Canada), *Hydrogeol. J.*, *21*(1), 67–77, doi:10.1007/s10040-012-0920-9.

Christophersen, N., and R. P. Hooper (1992), Multivariate analysis of stream water chemical data: The use of principal components analysis for the end-member mixing problem, *Water Resour. Res.*, *28*(1), 99, doi:10.1029/91WR02518.

Clark, I. D., and P. Fritz (1997), *Environmental Isotopes in Hydrogeology*, CRC Press.

Dann, M. S., J. A. Lynch, and E. S. Corbett (1986), Comparison of Methods for Estimating Sulfate Export from a Forested Watershed, *J. Environ. Qual.*, *15*(2), 2–7.

Elsenbeer, H., A. Lack, and K. Cassel (1995), Chemical fingerprints of hydrological compartments and flow paths at La Cuenca, western Amazonia, *Water Resour. Res.*, *31*(12), 3051–3058.

Englund, E., A. Aldahan, X. L. Hou, G. Possnert, and C. Söderström (2010a), Iodine (129I and 127I) in aerosols from northern Europe, *Nucl. Instruments Methods Phys. Res. Sect. B Beam Interact. with Mater. Atoms*, *268*(7-8), 1139–1141, doi:10.1016/j.nimb.2009.10.118.

Englund, E., A. Aldahan, X. L. Hou, R. Petersen, and G. Possnert (2010b), Speciation of iodine (127I and 129I) in lake sediments, *Nucl. Instruments Methods Phys. Res. Sect. B Beam Interact. with Mater. Atoms*, *268*(7-8), 1102–1105, doi:10.1016/j.nimb.2009.10.109.

Environment Canada (2014), Environment Canada Weather Archives: Whitehorse Airport, Available from: http://www.climate.weatheroffice.gc.ca/climateData/dailydata_e.html?StationID=1617&timeframe=2&cmdB1=Go&Month=1&Year=2012&cmdB1=Go

Fabryka-Martin, J., H. Bentley, D. Elmore, and P. Airey (1985), Natural iodine-129 as an environmental tracer, *Geochim. Cosmochim. Acta*, *49*(2), 337–347, doi:10.1016/0016-7037(85)90027-4.

Fabryka-Martin, J., S. Davis, and D. Elmore (1987), Applications of 129I and 36Cl in hydrology, *Nucl. Instruments Methods Phys. Res. Sect. B Beam Interact. with Mater. Atoms*, *29*(1-2), 361–371.

Farmwest (1998), Farmwest - Penman Monteith Equation, , 1–12.

Fan, Y., X. Hou, and W. Zhou (2012), Progress on 129I analysis and its application in environmental and geological researches, *Desalination*, 1–15, doi:10.1016/j.desal.2012.05.012.

Freeze, R. A., and J. A. Cherry (1979), *Groundwater*, 1st ed., Prentice-Hall, Inc.

Fukui, M., Y. Fujikawa, and N. Satta (1996), Factors affecting interaction of radioiodide and iodate species with soil, *J. Environ. Radioact.*, *31*(2), 199–216, doi:10.1016/0265-931X(95)00039-D.

Geyh, M. A. (2000), An Overview of 14C Analysis in the Study of Groundwater, *Radiocarbon*, *42*(1), 99–114.

Gilfedder, B. S., M. Petri, and H. Biester (2007a), Iodine and bromine speciation in snow and the effect of orographically induced precipitation, *Atmos. Chem. Phys.*, *7*(10), 2661–2669, doi:10.5194/acp-7-2661-2007.

Gilfedder, B. S., M. Petri, and H. Biester (2007b), Iodine speciation in rain and snow: Implications for the atmospheric iodine sink, *J. Geophys. Res.*, *112*(D7), 1–7, doi:10.1029/2006JD007356.

Gotway, C. A., D. R. Helsel, and R. M. Hirsch (1992), Chapter 9 Simple Linear Regression, in *Statistical Methods in Water Resources*.

Grynkiewicz, M., Ż. Polkowska, B. Zygmunt, and J. Namieśnik (2003), Atmospheric Precipitation Sampling for Analysis, *Polish J. Environ. Stud.*, *12*(2), 133–140.

Güler, C., G. D. Thyne, J. E. McCray, and K. a. Turner (2002), Evaluation of graphical and multivariate statistical methods for classification of water chemistry data, *Hydrogeol. J.*, *10*(4), 455–474, doi:10.1007/s10040-002-0196-6.

Heiri, O., A. F. Lotter, and G. Lemcke (2001), Loss on ignition as a method for estimating organic and carbonate content in sediments: Reproducibility and comparability of results, *J. Paleolimnol.*, *25*(1), 101–110, doi:10.1023/A:1008119611481.

Herod, M. N., I. D. Clark, W. E. Kieser, S. Agosta, and X.-L. Zhao (2013), 129I dispersion and sources in Northwest Canada, *Nucl. Instruments Methods Phys. Res. Sect. B Beam Interact. with Mater. Atoms*, *294*, 552–558, doi:10.1016/j.nimb.2012.06.018.

Herod, M. N., R. J. Cornett, I. D. Clark, W. E. Kieser, and G. S. Jean (2014a), Extraction of (129)I and (127)I via combustion from organic rich samples using (125)I as a quantitative tracer., *J. Environ. Radioact.*, *138*, 323–330, doi:10.1016/j.jenvrad.2014.02.005.

Herod, M. N., I. D. Clark, R. J. Cornett, W. E. Kieser, and G. St. Jean (2014b), Extraction of 129I and 127I via combustion from organic rich samples using 125I as a quantitative tracer, *J. Environ. Radioact.*, doi:10.1016/j.jenvrad.2014.02.005.

IAEA (2008), *Spent Fuel Reprocessing Options IAEA-TECDOC-1587*.

Israel, S., M. Colpron, C. Roots, and T. Fraser (n.d.), *Overview of Yukon Geology by Ancestral North America (Laurentia)*.

Jabbar, T., G. Wallner, and P. Steier (2013), A review on 129I analysis in air., *J. Environ. Radioact.*, *126C*, 45–54, doi:10.1016/j.jenvrad.2013.07.013.

Janowicz, J. R., N. Hedstrom, J. Pomeroy, R. Granger, and S. Carey (2004), Wolf Creek Research Basin water balance studies, *North. Res. Basins Water Balanc.*, *290*(March), 195–204.

Jiang, S., Z. Chang, M. Zhao, Y. Zhao, X. Zhao, and W. E. Kieser (2005), New measurement of 129I in IAEA-375 reference material, *J. Radioanal. Nucl. Chem.*, *264*(3), 549–553.

Kaiser, H. F. (1960), The Application of Electronic Computers to Factor Analysis, *Educ. Psychol. Meas.*, *20*(1), 141–151, doi:10.1177/001316446002000116.

Kekli, A., A. Aldahan, M. Meili, G. Possnert, N. Buraglio, and R. Stepanauskas (2003), 129I in Swedish rivers: distribution and sources., *Sci. Total Environ.*, *309*(1-3), 161–72, doi:10.1016/S0048-9697(03)00010-X.

Kieser, W. E., X. L. Zhao, C. Y. Soto, and B. Tracy (2005), Accelerator mass spectrometry of 129I: Technique and applications, *J. Radioanal. Nucl. Chem.*, *263*(2), 375–379, doi:10.1007/s10967-005-0597-9.

Kocher, D. C. (1981), A dynamic model of the global iodine cycle and estimation of dose to the world population from releases of iodine-129 to the environment, *Environ. Int.*, *5*(1), 15–31, doi:10.1016/0160-4120(81)90110-0.

Laudon, H., and K. H. Bishop (1999), Quantifying sources of acid neutralisation capacity depression during spring flood episodes in Northern Sweden, *Environ. Pollut.*, *105*, 427–435.

Laudon, H., O. Westling, and K. Bishop (2000), Cause of pH decline in stream water during spring melt runoff in northern Sweden, *Can. J. Fish. Aquat. Sci.*, *57*(9), 1888–1900, doi:10.1139/f00-131.

Laudon, H., J. Seibert, S. Kohler, and K. Bishop (2004), Hydrological flow paths during snowmelt: Congruence between hydrometric measurements and oxygen 18 in meltwater, soil water, and runoff, *Water Resour. Res.*, *40*(3), 1–9, doi:10.1029/2003WR002455.

Lewkowicz, A. G., and M. Ednie (2004), Probability mapping of mountain permafrost using the BTS method, Wolf Creek, Yukon Territory, Canada, *Permafr. Periglac. Process.*, *15*(1), 67–80, doi:10.1002/ppp.480.

López-Gutiérrez, J. M., M. García-León, C. Schnabel, M. Suter, H. a Synal, and S. Szidat (2001), Wet and dry deposition of 129I in Seville (Spain) measured by accelerator mass spectrometry., *J. Environ. Radioact.*, *55*(3), 269–82.

Luo, M., X. Hou, W. Zhou, C. He, N. Chen, Q. Liu, and L. Zhang (2013), Speciation and migration of 129I in soil profiles., *J. Environ. Radioact.*, *118*, 30–39, doi:10.1016/j.jenvrad.2012.11.011.

Lusa, M., M. Bomberg, H. Aromaa, J. Knuutinen, and J. Lehto (2015), Sorption of radioiodide in an acidic, nutrient-poor boreal bog: insights into the microbial impact, *J. Environ. Radioact.*, *143*, 110–122, doi:10.1016/j.jenvrad.2015.02.022.

Meglen, R. R. (1992), Examining large databases: a chemometric approach using principal component analysis, *Mar. Chem.*, *39*(1-3), 217–237, doi:10.1016/0304-4203(92)90103-H.

Moran, J. E., S. D. Oktay, P. H. Santschi, and D. R. Schink (1999), Atmospheric Dispersal of 129 Iodine from Nuclear Fuel Reprocessing Facilities, *Environ. Sci. Technol.*, *33*(15), 2536–2542.

Moran, J. E., S. D. Oktay, and P. H. Santschi (2002), Sources of iodine and iodine 129 in rivers, *Water Resour. Res.*, *38*(8), 1–10.

Muramatsu, Y., Y. Takada, H. Matsuzaki, and S. Yoshida (2008), AMS analysis of 129I in Japanese soil samples collected from background areas far from nuclear facilities, *Quat. Geochronol.*, *3*(3), 291–297, doi:10.1016/j.quageo.2007.08.002.

Muramatsu, Y., H. Matsuzaki, C. Toyama, and T. Ohno (2015), Analysis of 129I in the soils of Fukushima Prefecture: preliminary reconstruction of 131I deposition related to the accident at Fukushima Daiichi Nuclear Power Plant (FDNPP), *J. Environ. Radioact.*, *134*, 344–350, doi:10.1016/j.jenvrad.2014.05.007.

Negri, A. E., J. O. Fernández Niello, A. Wallner, A. Arazi, L. K. Fifield, and S. G. Tims (2013), 129I dispersion in Argentina: concentrations in fresh and marine water and deposition fluences in Patagonia, *Environ. Sci. Technol.*, *47*(17), 9693–8, doi:10.1021/es400610h.

Nimz, G. J. (1998), *Isotope Tracers in Catchment Hydrology - Chapter 8 - Lithogenic and Cosmogenic Tracers in Catchment Hydrology*, edited by C. Kendall and J. J. Macdonell, Elsevier.

Oktay, S. D., P. H. Santschi, J. E. Moran, and P. Sharma (2001), 129I and 127I Transport in the Mississippi River, *Environ. Sci. Technol.*, *35*(22), 4470–6.

Page, R. M., G. Lischeid, J. Epting, and P. Huggenberger (2012), Principal component analysis of time series for identifying indicator variables for riverine groundwater extraction management, *J. Hydrol.*, *432-433*, 137–144, doi:10.1016/j.jhydrol.2012.02.025.

Petrone, K. C., J. B. Jones, L. D. Hinzman, and R. D. Boone (2006), Seasonal export of carbon, nitrogen, and major solutes from Alaskan catchments with discontinuous permafrost, *J. Geophys. Res.*, *111*, doi:10.1029/2005JG000055.

Rao, U., and U. Fehn (1999), Sources and reservoirs of anthropogenic iodine-129 in western New York, *Geochim. Cosmochim. Acta*, *63*(13-14), 1927–1938, doi:10.1016/S0016-7037(99)00133-7.

Raymond, P. A., J. E. Bauer, N. F. Caraco, J. J. Cole, B. Longworth, and S. T. Petsch (2004), Controls on the variability of organic matter and dissolved inorganic carbon ages in northeast US rivers, *Mar. Chem.*, *92*(1-4), 353–366, doi:10.1016/j.marchem.2004.06.036.

Reithmeier, H., V. Lazarev, W. Rühm, and E. Nolte (2010), Anthropogenic 129I in the atmosphere: overview over major sources, transport processes and deposition pattern., *Sci. Total Environ.*, *408*(21), 5052–64, doi:10.1016/j.scitotenv.2010.07.015.

Rodhe, A. (1998), *Isotope Tracers in Catchment Hydrology - Chapter 12 - Snowmelt-Dominated Systems*, edited by C. Kendall and J. J. Macdonell, Elsevier.

Santschi, P. H., C. Xu, S. Zhang, P. Li, K. A. Schwehr, and D. I. Kaplan (2012), *Laboratory report on iodine (129I and 127I) speciation, transformation and mobility in Hanford groundwater, suspended particles and sediments*.

Schwehr, K. A., P. H. Santschi, D. J. Kaplan, C. M. Yeager, and R. Brinkmeyer (2009), Organo-iodine formation in soils and aquifer sediments at ambient concentrations., *Environ. Sci. Technol.*, *43*(19), 7258–64.

Seguin, M.-K., J. Stein, O. Nilo, and C. Jalbert (1999), Hydrogeophysical Investigation of the Wolf Creek Watershed , Yukon Territory, Canada, *Wolf Creek Res. Basin Hydrol. Ecol. Environ.*, 55–78.

Sheppard, M. I., and J. L. Hawkins (1995), Iodine and microbial interactions in an organic soil, *J. Environ. Radioact.*, *29*(2), 91–109, doi:10.1016/0265-931X(95)00022-3.

Sheppard, M. I., D. H. Thibault, J. McMurry, and E. A. Smith (1995), Factors Affecting the Soil Sorption of Iodine, *Water, Air Soil Pollut.*, *83*, 51–67.

Sheppard, M. I., J. L. Hawkins, and P. A. Smith (1996), Soil Processes and Chemical Transport: Linearity of Iodine Sorption and Sorption Capacities for Seven Soils, *J. Environ. Qual.*, *25*, 1261–1267.

Sheppard, S. C., and M. Herod (2012), Variation in background concentrations and specific activities of 36Cl, 129I and U/Th-series radionuclides in surface waters, *J. Environ. Radioact.*, *106*, 27–34, doi:10.1016/j.jenvrad.2011.10.015.

Simeonov, V., D. . Massart, G. Andreev, and S. Tsakovski (2000), Assessment of metal pollution based on multivariate statistical modeling of “hot spot” sediments from the Black Sea, *Chemosphere*, *41*, 1411–1417.

Smith, J. N. (2005), Iodine 129/CFC 11 transit times for Denmark Strait Overflow Water in the Labrador and Irminger Seas, *J. Geophys. Res.*, *110*(C5), 1–16, doi:10.1029/2004JC002516.

Smith, J. N., K. M. Ellis, and L. R. Kilius (1998), 129I and 137Cs tracer measurements in the Arctic Ocean, *Deep. Res. - Part 1*, *45*, 959–984.

Smoliński, A., B. Walczak, and J. W. Einax (2002), Hierarchical clustering extended with visual complements of environmental data set, *Chemom. Intell. Lab. Syst.*, *64*(1), 45–54, doi:10.1016/S0169-7439(02)00049-7.

Snyder, G., A. Aldahan, and G. Possnert (2010), Global distribution and long-term fate of anthropogenic 129I in marine and surface water reservoirs, *Geochemistry Geophys. Geosystems*, *11*(4), doi:10.1029/2009GC002910.

Söderlund, M., M. Lusa, J. Lehto, and M. Hakanen (2011), *POSIVA Working Report 2001-04: Sorption of Iodine, Chlorine, Technetium and Cesium in Soil*.

Strachnov, V., J. Larosa, R. Dekner, R. Zeisler, and A. Fajeglj (1996), *Report on the Intercomparison Run IAEA-375: Determination of Radionuclides in Soil Samples IAEA-375*.

Vega, M., R. Pardo, E. Barrado, and L. Debán (1998), Assessment of seasonal and polluting effects on the quality of river water by exploratory data analysis, *Water Res.*, *32*(12), 3581–3592, doi:10.1016/S0043-1354(98)00138-9.

Xing, S., X. Hou, A. Aldahan, G. Possnert, K. Shi, P. Yi, and W. Zhou (2015), Iodine-129 in Snow and Seawater in the Antarctic: Level and Source, *Environ. Sci. Technol.*, (May), 150522131930005, doi:10.1021/acs.est.5b01234.

Xu, C. et al. (2011), Is soil natural organic matter a sink or source for mobile radioiodine (129I) at the Savannah River Site?, *Geochim. Cosmochim. Acta*, *75*(19), 5716–5735, doi:10.1016/j.gca.2011.07.011.

Yidana, S. M., D. Ophori, and B. Banoeng-Yakubo (2008), A multivariate statistical analysis of surface water chemistry data--the Ankobra Basin, Ghana., *J. Environ. Manage.*, *86*(1), 80–7, doi:10.1016/j.jenvman.2006.11.023.

CHAPTER 5 - THE ATMOSPHERIC TRANSPORT OF IODINE-129 FROM FUKUSHIMA TO BRITISH COLUMBIA, CANADA AND ITS DEPOSITION AND TRANSPORT INTO GROUNDWATER

ABSTRACT

The Fukushima-Daiichi nuclear accident (FDNA) released iodine-129 (15.7 million year half-life) and other fission product radionuclides into the environment in the spring and summer of 2011. ^{129}I is recognized as a useful tracer for the short-lived radiohazard ^{131}I, which has a mobile geochemical behaviour with potential to contaminate water resources. To trace ^{129}I released by the FDNA reaching Canada, pre- and post-accident rain samples collected in Vancouver, on Saturna Island and from the National Atmospheric Deposition Program in Washington State were measured. Groundwater from the Abbotsford-Sumas Aquifer was sampled to determine the fate of ^{129}I. Modeling of the vadose zone was performed to constrain the travel time and retardation of ^{129}I. The mean pre-accident ^{129}I concentration in rain was 31 x 10^6 atoms/L (n=4). Immediately following the FDNA, ^{129}I values increased to 211 x 10^6 atoms/L and quickly returned to near-background levels. However, pulses of elevated ^{129}I continued for several months. The increases in ^{129}I concentrations from both Vancouver and Saturna Island were synchronized, and occurred directly after the initial release from the FDNA. The ^{129}I in shallow ($^3H/^3He$ age <1.4 yrs) *Wassenaar et al.*, [2006] groundwater showed measurable variability through March 2013 with an average of 3.2 x 10^6 atoms/L (n=32) that was coincident with modeled travel times for Fukushima ^{129}I. The groundwater response and the modeling results suggest that ^{129}I was partially attenuated in soil, which is consistent with its geochemical behaviour, however we conclude that the measured variability may be due to Fukushima ^{129}I entering groundwater.

1.0 INTRODUCTION

On March 11, 2011 a magnitude 9.0 earthquake occurred near Tōhoku, Japan causing a tsunami that damaged the Fukushima-Daiichi Nuclear Power Plant (FDNPP) and released radionuclides to the ocean and atmosphere. The primary radionuclides released were ^{131}I (half-life: 8 days) and ^{134}Cs (half-life: 2 years) and ^{137}Cs (half-life: 30 years). However, numerous other fissionogenic isotopes were also released and are measurable in the environment including iodine-129 (half-life: 15.7 x 10^6 years) [*Steinhauser*, 2014]. The total quantity of ^{131}I released to the atmosphere has been estimated between 120 - 200 PBq and using this number the quantity of ^{129}I can be calculated from the ^{129}I/^{131}I fissionogenic ratio, which was estimated to be 31.6 [*Miyake et al.*, 2012]. This calculation yields a range of atmospheric ^{129}I released from 0.81 to 1.4 kg [*Tokyo Electric Power Company*, 2012]. This quantity, while significant, is far less than the annual gaseous releases from nuclear fuel reprocessing, which have been estimated at 6 – 12 kg/year [*Moran et al.*, 1999]. However, the nature of the releases from the Fukushima-Daiichi Nuclear accident (FDNA), which were isolated in time and space, provide a rare opportunity to study the transport of ^{129}I and its environmental cycling and distinguish them from other releases of ^{129}I from nuclear fuel reprocessing and past bomb testing.

Radionuclides released from the FDNA have been detected across the globe [*Bikit et al.*, 2012; *Evrard et al.*, 2012; *Landis et al.*, 2012; *Macmullin et al.*, 2012; *Melgunov et al.*, 2012; *Piñero García and Ferro García*, 2012; *Wetherbee et al.*, 2012]. These radionuclides were transported primarily in the atmosphere and deposited by both dry deposition and washout [*Wetherbee et al.*, 2012]. Atmospheric transport and deposition via precipitation

of ^{129}I has been well studied in the context of releases from nuclear fuel reprocessing sites such as La Hague and Sellafield, and Paul et. al. investigated the dispersion and wet deposition of ^{129}I from the Chernobyl accident [*Paul et al.*, 1987; *Persson et al.*, 2007; *Aldahan et al.*, 2009]. Iodine has been shown to have an atmospheric residence time of 10-14 days, which allows releases of ^{129}I and ^{131}I to travel great distances from their point source [*Jabbar et al.*, 2013]. It has been assumed that the fate of ^{129}I deposited on the ground surface is to mix and distribute throughout the environment and a large amount of research has focused on the terrestrial cycling of iodine in surficial environments such as soil, rivers and plants [*Bamba et al.*, 2014; *Muramatsu et al.*, 2015]. However, a few studies have investigated the infiltration of ^{129}I into groundwater. Modern recharge waters in the nearby Milk River Aquifer, Alberta, showed meteoric values for ^{129}I concentration and the $^{129}I/^{127}I$ ratio of 8.6×10^{5} atoms/L and 1.1×10^{-11} respectively [*Fabryka-Martin et al.*, 1991]. Young groundwater from the Orange County Aquifer in southern California had ^{129}I concentrations that ranged from $12 – 53 \times 10^{6}$ atoms/L and $^{129}I/^{127}I$ ratios of 0.9 to 4.5×10^{-10} in samples with groundwater ages of less than 2 years [*Schwehr et al.*, 2005].

^{129}I has shown promise as a conservative, long lived, tracer of groundwater [*Schwehr et al.*, 2005], although its attenuation during recharge through the soil must be considered. A wide variety of K_d values for iodine have been measured in many different soil types and due to the biophilic nature of iodine, soils that have high organic matter content tend to be very efficient at adsorbing iodine at ambient concentrations with K_d values as high 1800 L/kg in peat [*Sheppard et al.*, 1996; *Zhang et al.*, 2011]. However, in soils with low organic matter iodine has been observed to behave semi-conservatively and

have K_d values as low as 0.1 L/kg in the I^- state [*Alvarado-Quiroz et al.*, 2002; *Schwehr et al.*, 2005]. Typically, K_d values for iodine fall in the range of 0.2 – 35 L/kg for sandy soils [*Söderlund et al.*, 2011]. Iodide, I^-, has lower K_d values than the iodate IO_3^-, [*Fukui et al.*, 1996], and the K_d decreases for both iodide and iodate at neutral to alkaline pH [*Fukui et al.*, 1996]. Studies of ^{129}I migration and retardation in groundwater have been conducted at the ^{129}I contaminated Hanford and Savannah River nuclear sites. These NFRP's, which are now closed, were point sources of ^{129}I in the region in the past. Results have shown that the mobility of ^{129}I contamination in the subsurface is dependent on the iodine concentration, with high concentrations having lower K_d's as well as organic content, speciation and pH. The most important of these is the organic content [*Hu et al.*, 2005, 2012; *Zhang et al.*, 2011].Studies of groundwater from the Idaho Falls nuclear site have also shown that ^{129}I can be transported vertically and laterally great distances within the aquifer. However, dilution and dispersion have reduced ^{129}I contamination as further inputs have ceased [*Bartholomay*, 2013].

The objective of this study was to trace the fate of the FDNA ^{129}I release through precipitation and groundwater recharge in a well-characterized sandy aquifer on the west coast of Canada. Pre-FDNA precipitation samples were collected followed by weekly precipitation sampling over one year immediately following the FDNA. We then investigated the fate of the ^{129}I deposited and its attenuation during infiltration into the shallow, sandy aquifer. Sampling of two different well sites with different recharge times was conducted on a monthly to bi-monthly basis over the course of a year. The recharge time of the wells was established by $^3H/^3He$ dating to be 11 months and 14 months

respectively. This aspect of the work simulates an aquifer scale tracer experiment and provides insight into the long term environmental behavior of ^{129}I in the hydrosphere.

1.1 Hydrogeology of the Abbotsford-Sumas Aquifer

The Abbotsford-Sumas Aquifer (ASA) is an extensive unconfined aquifer with a surficial area of ~200km^2. It spans the Canada – U.S. border between southern British Columbia, Canada and Washington State, U.S. and supplies ~120,000 people with drinking water (Figure 5.1). The hydraulic properties of the ASA have been studied in the context of nitrate leaching and transport as the primary land use in the region is agriculture with a high density of berry farming (raspberries and blueberries), poultry production and some dairy farms [*Wassenaar*, 1995; *Cox and Kahle*, 1999; *Wassenaar et al.*, 2006; *Chesnaux et al.*, 2007]. NO_3 contamination throughout much of the aquifer is attributed to the intensive nature of agricultural activities in this area [*Hii et al.*, 1999; *Chesnaux and Allen*, 2007; *Zebarth et al.*, 2015].

Both wells sampled are completed in the upper 20m of an unconsolidated gravel and coarse sand aquifer with discontinuous lenses of till and clay which continues to a depth of up to 60m, underlain by a glaciomarine clay aquitard [*Cox and Kahle*, 1999; *Graham et al.*, 2014]. The heterogeneous stratigraphy has produced complex, preferential flow paths, which can result in rapid transport of water and contaminants through the vadose zone (Supplementary Figure C1) [*Scibek and Allen*, 2006]. Hydraulic conductivities in the saturated zone range from 2 to 2,400 m/day with a median of 82 m/day [*Cox and Kahle*, 1999]. Groundwater flow is sub-radial with near-vertical recharge and a strong linear

relationship between depth and groundwater age [*Wassenaar et al.*, 2006; *Chesnaux et al.*, 2012].

Recharge in the ASA has been estimated at between 650-1,150 mm/yr [*Scibek and Allen*, 2006], representing up to 60-80% of the annual average precipitation which is 1,500 mm/year [*Chesnaux and Allen*, 2007]. On a seasonal basis the water table can range as much as 4 meters per year in some wells [*Hii et al.*, 1999]. Precipitation and recharge are maximized in the fall and winter leading to the highest water level at this point of the year, although there is often a delay of 1-3 months between peak precipitation and water level response [*Wassenaar et al.*, 2006; *Chesnaux and Allen*, 2007; *Graham et al.*, 2014].

2.0 METHODS

2.2 Sampling Sites

2.2.1 Precipitation Sampling

Rooftop precipitation samples were collected from a federal building located in downtown Vancouver, BC between March 18, 2011 and March 8, 2012 (Figure 5.1). Precipitation was collected using an 8 inch non-recording Stand Rain Gauge. The Rain Gauge funnel and sample collection bag was fixed onto a white 20 L bucket and lid. Water was collected on an approximately weekly basis, and transferred to certified trace clean 250 mL Nalgene® bottles, then frozen prior to shipment. Precipitation samples were also donated by National Atmospheric Deposition Program (NADP) in the United States from site WA19 in northern Washington State. These samples consisted of ~30 mL weekly samples. Four samples were then composited to represent monthly sampling intervals for pre-Fukushima. Several pre- and post-Fukushima accident samples were also donated by

the Canadian Air and Precipitation Monitoring Network (CAPMoN) from nearby Saturna Island (Figure 5.1).

2.2.2 Groundwater Sampling

Groundwater samples were collected from two dedicated Environment Canada monitoring piezometers (PB-20 and ABB-03) with a $^{3}H/^{3}He$ groundwater age of less than 2 years (Figure 5.1) [*Wassenaar*, 1995; *Wassenaar et al.*, 2006]. The average historical (1989-present) groundwater depth at site PB-20 is 3.3 meters below ground surface (mbgs), while the mid-screen depth is 3.9 mbgs, resulting in a shallow average pressure head of <1m. For ABB-03, the average water level depth (1988-present) is 11.5 mbgs, and a mid-screen piezometer depth of 17.1 mbgs, resulting in an average total pressure of <6m.

The lithology of the two wells sampled is very similar. Both are primarily composed of coarse grained sand and gravel beds that range from well to poorly sorted with numerous cobbles of greater than 5 cm. There are also occurrences of sand lenses and interbedded layers of sand and gravel (Supplementary Table C1).

Samples were collected using a Grundfoss® stainless steel submersible pump, Teflon® lined LDPE tubing, and stainless-steel fittings and valves. The water was pumped directly through a flow-through cell housing a YSI® multi-probe sonde (temperature, pH, electrical conductivity, redox potential, dissolved oxygen). Samples were collected after at least three casing volumes were removed from the wells and the YSI® field parameters had stabilized. All bottles were rinsed with sample water prior to filling and filled into 1 L LDPE bottles, stored at 5°C for archiving.

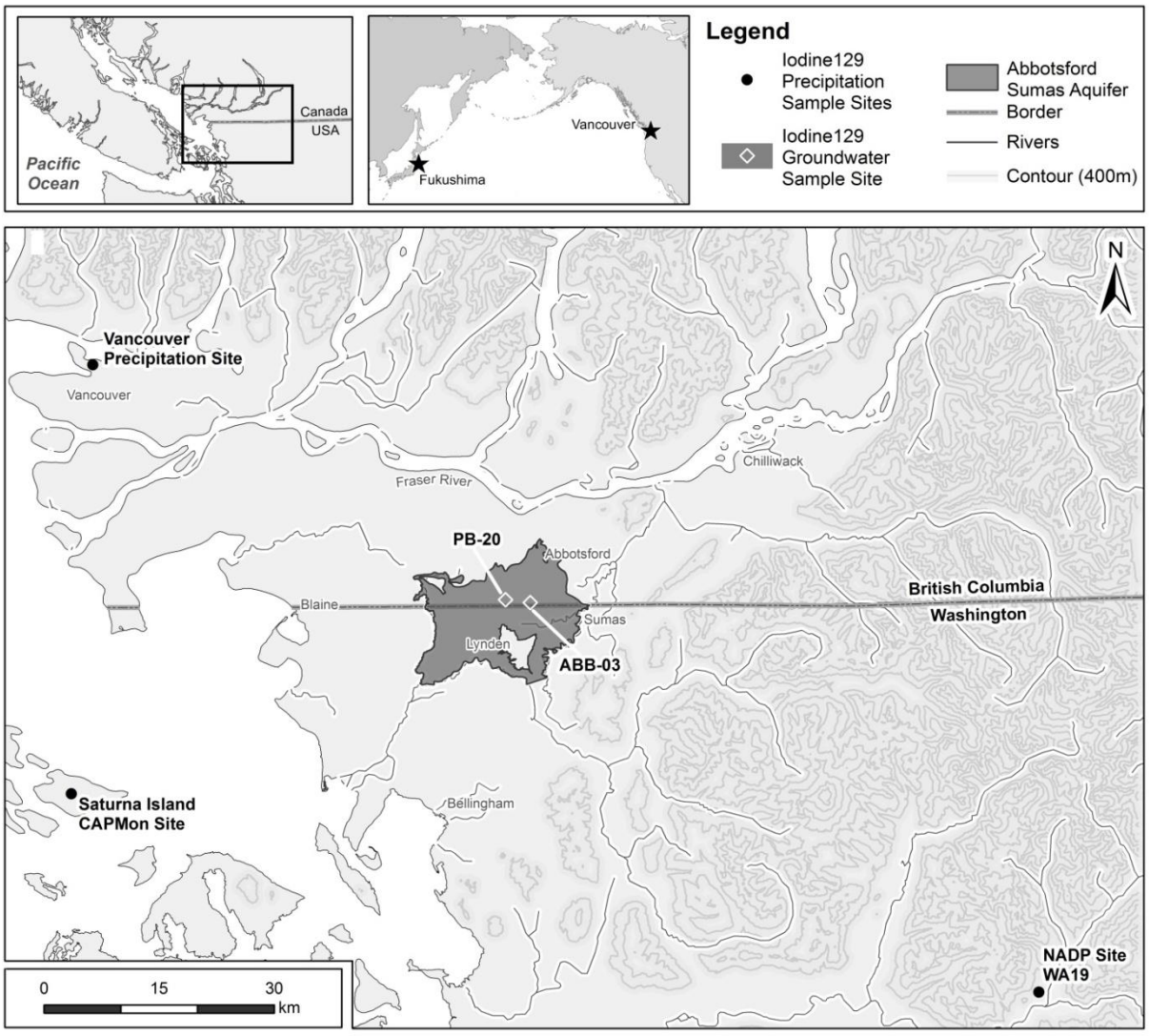

Figure 5.1: Sample map showing location of all three precipitation sampling locations as well as the location of both wells used for groundwater sampling. The surface expression of the Abbotsford-Sumas Aquifer is shaded.

2.3 Preparation of Samples for ^{129}I Analysis

Iodine was extracted from samples of precipitation and groundwater using the silver iodide precipitation method with stable ^{127}I carrier (^{129}I/^{127}I: 15.6 ± 0.6 x 10^{-14}) as described in *Sheppard and Herod,* [2012] and *Herod et al.,* [2013]. ^{129}I in the AgI targets was measured using the University of Ottawa's IsoTrace Accelerator Mass Spectrometer. ^{127}I was measured in all samples using an Agilent 7700 Inductively Coupled Plasma Mass Spectrometer at the University of Ottawa.

2.4 Vadose Zone Recharge and Transport Modeling

The infiltration of atmospheric ^{129}I from the FDNA and natural ^{127}I through the vadose zone of the Abbotsford-Sumas Aquifer was modeled using the USGS software VS2DTI, which simulates water and contaminant transport through variably saturated porous media and yields numerical results for a variety of fluid and mass balance parameters [*Lapala et al.*, 1987; *Healy*, 1990]. The model incorporates soil and hydraulic properties representative of the region. A transient simulation was performed using the weekly input of rain and iodine and a basic water balance approach was used. Infiltration and ^{129}I concentration were adjusted for evapotranspiration [*Farmwest*, 1998; *Chesnaux and Allen*, 2007], which exceeds precipitation between May and September leading to a substantial moisture deficit in the soil and necessitates irrigation. Four mm/day [*VanDer Gulik*, 2014] of irrigation water with the median ^{129}I for the ASA groundwater was included in the model to simulate the actual mass flux of ^{129}I entering the aquifer during periods with negligible precipitation as local groundwater is used for irrigation. This represents 484mm

of water added between May 14, 2011 and September 14, 2011 and an additional ^{129}I mass flux of 11.2 x 10^6 atoms/m^2/day during relevant periods.

The Van Genuchten equation was employed to describe the hydraulic conductivity of the vadose zone from the input parameter of saturated hydraulic conductivity [*van Genuchten*, 1980]. Model input data for the vadose zone soil used a combination of default values for medium sand and measured values for the ASA. The input data is provided in Supplementary Table C2. Porosity, hydraulic conductivity, residual moisture content were obtained from literature and K_d was calculated [*Chesnaux and Allen*, 2007; *Chesnaux et al.*, 2007]. All other hydraulic parameters were default values. Longitudinal and transverse dispersion were set at one half of the maximum grid spacing, which in this case was 0.7 and 0.015 respectively. Varying the thickness of the vadose zone did not affect transport times in the model due to the conductive nature of the soils. In this model a range of K_d values was used with a linear isotherm to model the adsorption of iodine in the ASA soils [*Sheppard et al.*, 1996].

Boundary conditions that were applied to the model consisted of a recharge flux corresponding to the precipitation the Abbotsford region received during each of the 42 recharge periods. Each recharge period was defined as the interval used in precipitation sampling. The water table was used as the lower boundary condition of the model and was set using an equilibrium profile in which the water table had a pressure head of 0. A measured concentration of ^{129}I in precipitation was applied to each recharge period and an initial concentration of 2.4 x 10^6 atoms/L was used within the vadose zone.

3.0 RESULTS AND DISCUSSION

3.1 Precipitation

3.1.1 ^{129}I, ^{127}I and $^{129}I/^{127}I$ in Precipitation

The ^{127}I concentration in precipitation (Table 5.1, Figure 5.2; precipitation data in Supplemental Table C3) ranged between 2.8 and 9.2 µg/L with an average of 4.3 and a median of 4.1 ppb (n=51) This range agrees well with the range reported in the literature for North America and Europe (0.2-12 µg/L) [*Moran et al.*, 1999; *Gómez-Guzmán et al.*, 2012] although the average value reported here is approximately 1-2 µg/L higher than the average value observed by others, likely due to the proximity of this study to the ocean, which provides a vapour source enriched in ^{127}I to local precipitation [*Fuge and Johnson*, 1986; *Persson et al.*, 2007]. It has also been proposed that orographic lifting of air masses can lead to a depletion of iodine irrespective of distance from the coast [*Reithmeier et al.*, 2006; *Gilfedder et al.*, 2007a].

Site	^{129}I Median	^{129}I Mean	^{127}I Range	^{127}I Median	^{127}I Mean	$^{129}I/^{127}I$ Range (10^{-9})	$^{129}I/^{127}I$ Median	$^{129}I/^{127}I$ Mean
Vancouver	41.95	61.61	9.18 - 2.85	4.14	4.26	0.68 - 13.39	2.34E-9	3.09E-9
Saturna	83.99	106.33	5.13 - 3.12	3.97	4.12	0.7 - 9.17	5.08E-9	5.09E-9
NADP	41.58	51.09	6.04 - 2.83	4.41	4.42	0.9 - 6.29	2.54E-9	3.07E-9
ALL	44.35	67.14		4.13	4.25		2.51E-9	3.38E-9

Table 5.1: Summary of key statistics for the precipitation dataset for ^{129}I, ^{127}I and $^{129}I/^{127}I$

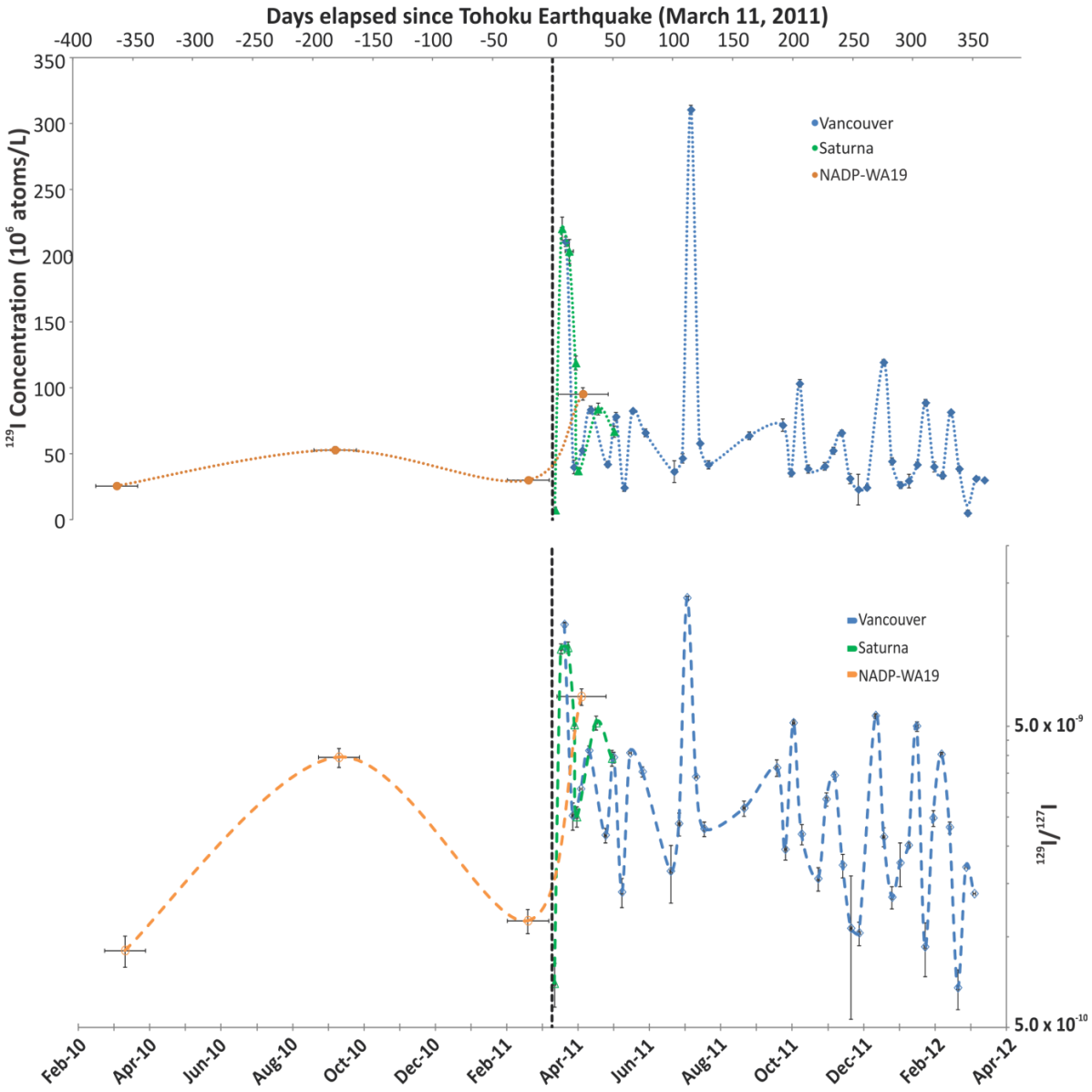

Figure 5.2: Variation in the concentration of ^{129}I and the $^{129}I/^{127}I$ ratio in precipitation from Vancouver, Saturna Island and NADP site WA19 over time. The time range that each NADP sample integrates is displayed using horizontal error bars. 1σ error is contained within data points if not visible. The dashed vertical line shows the date of the FDNA relative to samples.

The pre-FDNA ^{129}I values that were measured in precipitation from 3 NADP composite samples and one Saturna Island sample ranged from 13 – 53 x 10^6 atoms/L with a mean of 31 x 10^6 atoms/L and a median of 28 x 10^6 atoms/L (n=4; Table 5.1, Figure 5.2). This agrees well with other ^{129}I concentrations measured in precipitation in the south and central regions of the US, which show a ^{129}I concentration range of 7 - 60 x 10^6 atoms/L and an average of 27 x 10^6 atoms/L (n=13) [*Moran et al.*, 1999]. Past operation of the Hanford nuclear fuel reprocessing facility in Washington State resulted in locally higher atmospheric ^{129}I with precipitation in 1973 reaching 6.8 x 10^{11} atoms/L [*Brauer and Rieck*, 1973; *Moran et al.*, 1999]. The Hanford facility was shut down in 1972 and our measurements suggest that it is no longer a significant source of ^{129}I [*Aldahan et al.*, 2007].

A pulse of ^{129}I in precipitation with maximum concentrations of 211 x 10^6 atoms/L in Vancouver and 221 x 10^6 atoms/L at Saturna Island was observed 6 days following the FDNA. A value of 311 x 10^6 atoms/L was also measured during the first week of July, 2011 in Vancouver precipitation, well after atmospheric releases from FDNPP had ceased. The samples from all three sites have a post-accident mean of 70 ± 60 x 10^6 atoms/L (n=45), which is over twice the pre-accident average of 31 x 10^6 atoms/L and previous measurements of ^{129}I in precipitation elsewhere in North America in recent years [*Moran et al.*, 1999]. These concentrations are considerably lower than the 76 x 10^{10} atoms/L measured at Fukushima following the FDNA [*Xu et al.*, 2013].

In pre-FDNA samples the $^{129}I/^{127}I$ ratio ranged from 0.7 to 4.0 x 10^{-9} and immediately following the release of radionuclides from the FDNPP the $^{129}I/^{127}I$ ratio increased 6-10

times above background at all three sites and reached a high of nearly 11 x 10^{-9} at the Vancouver site (Figure 5.2). This demonstrates that the increases in ^{129}I were not accompanied by spikes in stable I, but rather from a radioiodine source.

In order to determine if the FDNA input of ^{129}I had a statistically significant impact on ^{129}I concentrations in rainfall and if background levels were reached later in the year two tailed students t-tests were performed to determine the relationship between the means of pre-, para-, and post-FDNA sampling intervals. The sampling interval for para-FDNA affected rain ranged from March 18 - May 20, 2011. This interval was determined using publicly accessible Health Canada radionuclide data from the Sidney, BC air filter station [*Health Canada*, 2014]. The results of the t-tests lead to three conclusions: 1) The mean ^{129}I concentration for post-FDNA rain is significantly greater than the mean for pre-FDNA ^{129}I ($p=0.01$, $\alpha=0.05$). 2) The mean ^{129}I concentration for para-FDNA rain is significantly greater than the mean ^{129}I concentration in rain following the FDNA, when the one outlying point in July is omitted ($p=0.002$, $\alpha=0.05$). 3) The mean concentration in pre-FDNA rain is not significantly different than the mean for the post-FDNA interval when the one outlying point in July is included ($p=0.096$, $\alpha=0.05$). This confirms that following May 20, 2011 the average ^{129}I concentration in rain had returned to pre-FDNA background levels.

3.1.2 Temporal Variation of Atmospheric ^{129}I Concentrations

Attribution of the high para-FDNA ^{129}I concentrations to the rapid trans-Pacific transport of ^{129}I from Fukushima was confirmed using the NOAA's HYSPLIT back trajectory atmospheric modeling program (Supplementary Figure C2) [*Draxler and Rolph*, 2013]. This

response in ^{129}I concentrations shows that radionuclides from Fukushima were transported rapidly from Japan to the west coast of Canada and the US and a peak in ^{129}I concentrations could be observed within 6-10 days of the FDNA. This observation agrees well with the findings of other studies that observed an increase in the ^{131}I and ^{137}Cs concentrations in air filters on the west coast of North America by March 17, and a peak on March 19-20, 2011 [*Leon et al.*, 2011; *Wetherbee et al.*, 2012]. Furthermore, the NADP sample, which is a composite of rainfall events spanning March 15, 2011 to April 16, 2011 shows a significantly elevated ^{129}I concentration of 95 x 10^6 atoms/L.

3.1.3 The July spike in Atmospheric ^{129}I

There was a spike in ^{129}I concentration observed in the precipitation sample from the period of July 1, 2011 to July 8, 2011, over four months after the FDNA. For this sample the ^{129}I concentration rose to 311 ± 8.4 x 10^6 atoms/L (duplicate analysis was within 1σ), which is a substantially higher concentration than any other sample measured in this study. As monitoring at Fukushima detected no pulse of ^{129}I in precipitation in July despite the ongoing efforts to stabilize the reactors at the time [*Xu et al.*, 2013], this spike is likely due to a punctuated release from a nuclear fuel reprocessing facility. Modeling of the air parcel back trajectories using the NOAA HYSPLIT model for the sampling period shows air mass trajectories from Hawaii, north Japan and Russia (Supplementary Figure C3). Despite its high concentration this spike had a low ^{129}I mass deposition due to the small volume of rain during this period.

3.1.4 Deposition Flux of ^{129}I as Washout

The mass of ^{129}I deposited via precipitation as washout was calculated using the equation [*Baker et al.*, 2001]:

$$\psi = (C \times P)/T \quad (1)$$

Here ψ is the washout or mass flux of iodine throughout the sampling period (atoms/m^2/day), C is the concentration of ^{129}I or ^{127}I in the rainwater sample, P is precipitation at Vancouver Airport, (mm) and T is the time interval of the sampling period in days. The results of this calculation are listed in Supplemental Table C3 and their fluctuation over time is pictured in Figure 5.3. Washout in samples from Vancouver ranged from 6.6 x 10^8 atoms/m^2/day, in the first sample following the FDNA, to 3.1 x 10^7 atoms/m^2/day and the samples from Saturna Island ranged from 2.6 x 10^9 to 3.7 x 10^7 atoms/m^2/day. The maximum values for both Saturna Island and Vancouver coincide during the peak concentration of ^{129}I in para-FDNA precipitation.

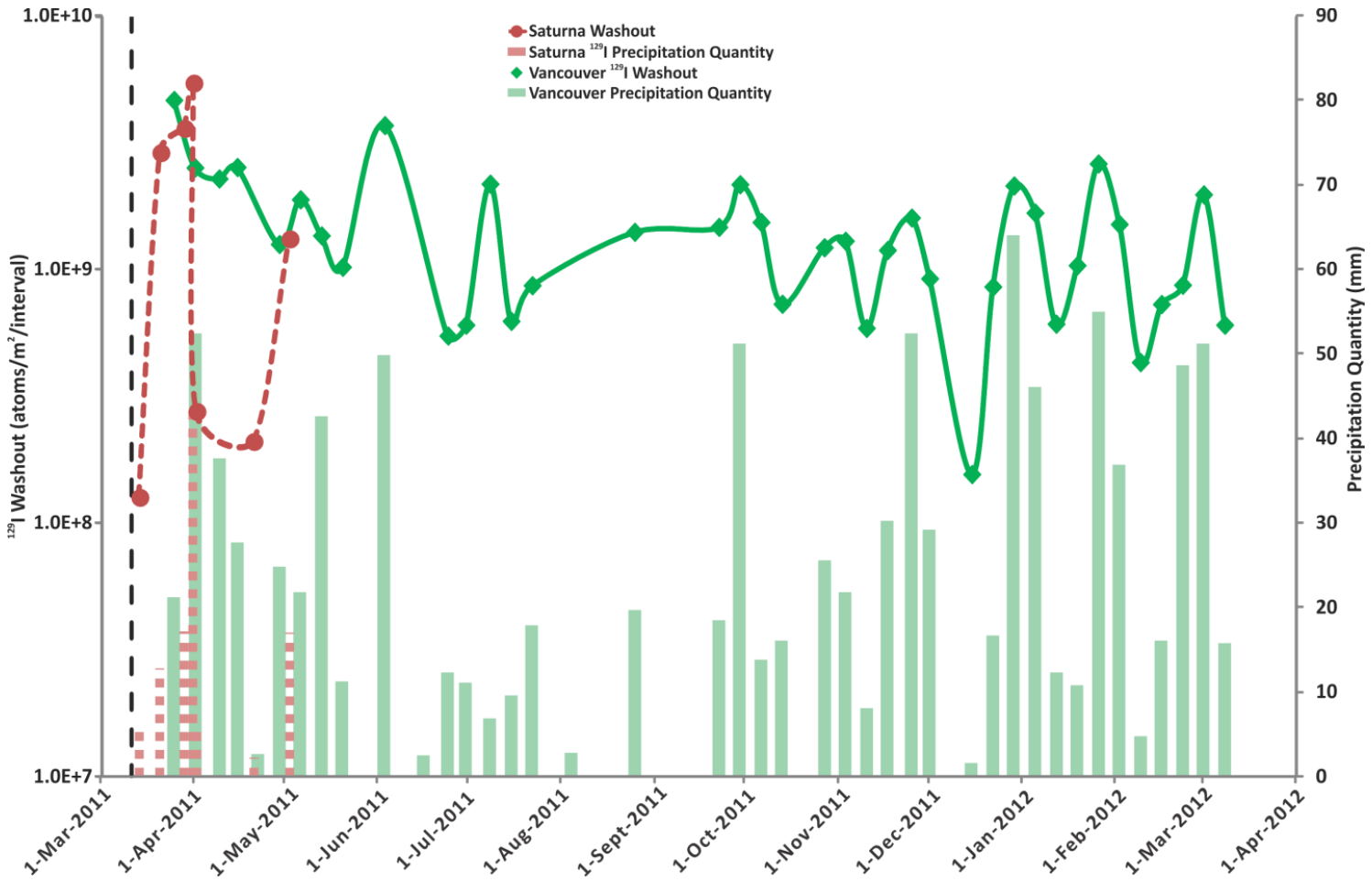

Figure 5.3: Washout of ^{129}I in Vancouver and Saturna Island. Washout is shown as a line graph on a logarithmic scale on the left. Precipitation quantity is also shown on a linear scale as a bar graph and uses the secondary y-axis.

The principal factor that controls the magnitude of the mass flux is the concentration of ^{129}I. Indeed, the concentration of ^{129}I is significantly correlated to the mass flux with an r of 0.49 (p=0.0046). Precipitation quantity and washout are also correlated with an r of 0.35 (p=0.031). This relationship can clearly be seen in Figure 5.3, which shows the washout and the precipitation quantity for each sampling interval. The influence of dry deposition has not been considered as most research has suggested that dry deposition plays a less important role in ^{129}I mass flux than wet [*López-Gutiérrez et al.*, 2001] particularly given that the Canadian west coast receives ~1500 mm of precipitation annually.

3.2 Groundwater

3.2.1 ^{129}I Concentration and ^{129}I/^{127}I in Groundwater

A time lag of 0.9 ± 0.5 and 1.2 ± 0.5 years respectively for monitoring wells ABB03 and PB20 for transport from the water table to the well screen was established using ^{3}H/^{3}He [*Wassenaar et al.*, 2006]. The range in ^{129}I concentration for groundwater in the wells ABB-03 and PB-20 were 0.31 to 9.2 x 10^{6} atoms/L and 0.4 to 6.3 x 10^{6} atoms/L respectively (Figure 5.4; Table 5.2), with median concentrations of 2.1 x 10^{6} atoms/L and 3.5 x 10^{6} atoms/L respectively. Several samples had uncertainties high enough to reach the limit of detection suggesting background ^{129}I levels may be even lower than those measured here meaning that detection of the anomalous peaks in ^{129}I concentration are therefore robust as they are well above this limit. The magnitude of the ^{129}I anomaly in PB-20 is slightly lower than ABB03 potentially due to greater attenuation or dilution during transport to the screen as the recharge time of PB-20 is greater than ABB03. The ^{127}I concentrations ranged

from 2.9 – 5.7 ppb in ABB-03 and 3.1 – 5.2 ppb in PB-20. The medians for ^{127}I are 3.8 ppb in ABB-03 and 4.3 ppb in PB-20 respectively, which are very similar to those measured in precipitation samples (4.3 ppb).

The concentration of ^{129}I in both wells is up to 20 times lower than that of precipitation, unlike stable iodine which is unchanged from levels in precipitation. This recognizes the importance of iodine sorption in soil and the vadose zone as a key attenuation process. Mixing with groundwater with low ^{129}I can be discounted as nitrate data show that dilution is limited in the shallow groundwater [*Wassenaar*, 1995; *Mitchell et al.*, 2003; *Wassenaar et al.*, 2006]. Nitrate measurements also constrain vadose zone transport times for conservative tracers. Land use changes or applications of manure to the ground surface can induce a nitrate response in the aquifer within a few months showing that transmission from the ground surface to water table is rapid [*Environment Canada*, 2015](Supplementary Figure C4). Previous studies have also shown that spring precipitation can leach nitrate and transport it to the water table in a matter of months [*Wassenaar et al.*, 2006; *Chesnaux and Allen*, 2007].

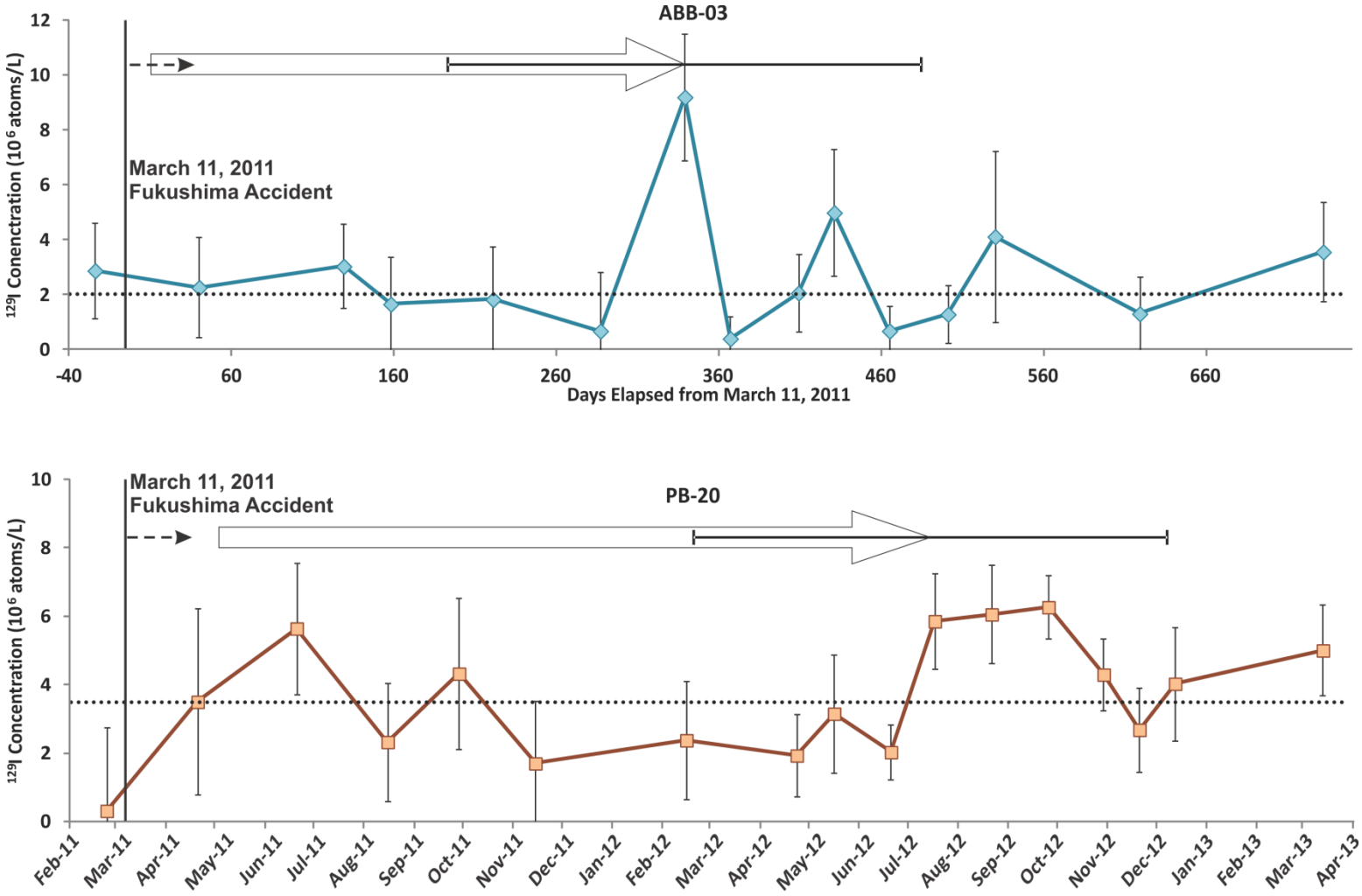

Figure 5.4: Temporal variation in the concentration of ^{129}I in groundwater in ABB03 and PB20. The solid vertical line shows the date of the Fukushima accident and the dashed horizontal line shows the median of each dataset respectively. The $^{3}H/^{3}He$ ages from [*Wassenaar et al.*, 2006] of groundwater in each well and their uncertainty is pictured as the large, clear arrow which is aligned with the ^{129}I anomaly possibly caused by the FDNA. The dashed arrow covers a 40 day (0.11 year) time span and represents a possible vadose zone transport time.

The $^{129}I/^{127}I$ ratios range from 1.9 to 34 x 10^{-11} for ABB-03 and 2.1 to 38 x 10^{-11} in PB-20, and follow variations in the groundwater concentration of ^{129}I very closely due to the low variability for stable I. The r-values for both wells and show significant correlation coefficients of 0.91 for ABB-03 and 0.92 for PB20 (α=0.05) (Supplementary Figure C5). The median for ABB-03 was 13 x 10^{-11} and for PB-20 it was 17 x 10^{-11}. These values are one to two orders of magnitude lower than the $^{129}I/^{127}I$ ratios measured in precipitation. This suggests that ^{127}I is not accumulating in the ASA soils whereas there is preferential adsorption of ^{129}I as the aquifer soils equilibrate to the addition of anthropogenic ^{129}I from the nuclear age.

Well	^{129}I Range	^{129}I Median	^{129}I Mean	^{127}I Range	^{127}I Median	^{127}I Mean	$^{129}I/^{127}I$ Range ($x10^{-11}$)	$^{129}I/^{127}I$ Median	$^{129}I/^{127}I$ Mean
PB-20	0.31 - 6.27	3.50	3.62	3.11- 5.24	4.3	4.17	2.07 - 37.7	1.70E-10	1.88E-10
ABB-03	0.40 - 9.21	2.07	2.67	2.94 - 5.7	3.8	3.78	1.87 - 34.1	1.29E-10	1.48E-10

Table 5.2: Summary of key statistics for groundwater dataset including ^{129}I, ^{127}I and $^{129}I/^{127}I$

3.2.2 Vadose Zone Transport, K_d and Retardation of Iodine in the ASA

Retention of ^{129}I from the FDNA on organic matter during recharge through the vadose zone is affected by both organic content of these glacial outwash sediments and the redox state of iodine. The organic matter content in ASA soils is low, in the range of 3-9% [*Cox and Kahle*, 1999].This study measured the dissolved organic carbon (DOC) content in ASA waters and found a mean of 0.45 ppm. Previous work found a median DOC of 0.7 ppm

in the Sumas aquifer groundwater [*Cox and Kahle*, 1999; *Chesnaux and Allen*, 2007]. The soil-water partitioning coefficient, K_d, is higher for IO_3^- and organic iodine molecules than for I^- [*Sheppard et al.*, 1995; *Fukui et al.*, 1996]. Measurements of pH (6.2 ± 2.2 n=61) and redox (Eh = 618 ± 67 mV, n=61), in both ASA wells suggest that iodine in the groundwater system is dominantly in the I^-, I_2 or organic iodine state, as it is in precipitation [*Gilfedder et al.*, 2008; *Hou et al.*, 2009; *Lehto et al.*, 2012]. Although, in precipitation ^{129}I, particularly from NFRP's and Chernobyl, has been found to occur 60-80% organic iodine [*Hou et al.*, 2009]. Species inter-conversion can also occur on soils, particularly in the presence of organic carbon [*Hu et al.*, 2012]. The soil water partition coefficient, K_d, for the attenuation of ^{129}I and ^{127}I during transport through the vadose zone for precipitation to groundwater can be calculated as [*Schwehr et al.*, 2009]:

$$K_d = \frac{V_L \times (C_i - C_f)}{M_S \times C_f} \quad (2)$$

in which V_L is the volume of the aqueous phase (assumed to be 1 litre in our calculations), C_i is the initial ^{129}I concentration in the aqueous phase (precipitation), C_f is the ^{129}I concentration in the aqueous phase after equilibration with the vadose zone/aquifer soils (groundwater) and M_s is the mass of the solid phase (assumed to be 1 kg in our calculations). Applying this equation to the median values of data presented in Supplementary Table C2 and C3 K_d values can be produced for both wells. In the case of ABB-03 the K_d value was 19 L/kg and in PB-20 it was 11 L/kg. These values compare well to

those presented in other studies for similar soil types which typically range from 0.2 – 35 or greater [*Muramatsu et al.*, 1990; *Alvarado-Quiroz et al.*, 2002; *Söderlund et al.*, 2011].

In the case of ^{127}I the K_d value, using the median ^{127}I concentration in precipitation as C_i and in groundwater as C_f, for both wells was 0.07 L/kg which is at the very low range for reported K_d values [*Schwehr et al.*, 2005] . This exceptionally low K_d for ^{127}I suggests that these soils have equilibrated during Holocene time with the input of stable I from precipitation, potentially limiting soil adsorption capacities for both ^{129}I and ^{127}I. Attenuation of ^{129}I in the vadose zone is then due to gradual exchange with this reservoir of previously adsorbed stable I on available binding sites either through iodination of organic compounds, anion exchange or adsorption to charged mineral surfaces [*Zhang et al.*, 2011]. This suggests that once iodine equilibrium is achieved the transport of iodine to groundwater is conservative. This observation is corroborated by the study of iodine and ^{129}I transport in the Orange County Aquifer, which also found that ^{127}I concentrations remained constant between recharge and groundwater while ^{129}I was strongly attenuated by adsorption [*Schwehr et al.*, 2005]. The transport and retardation of ^{129}I in the vadose zone can be explored further using a transient vadose zone model that incorporates the actual quantity and ^{129}I concentration of recharge over time as well as the soil characteristics such as K_d.

3.2.3 Case I: 0 K_d, Homogenous Sandy Soil, Mean K

Figure 5.5 shows the evolution of the ^{129}I concentration over time in a hypothetical homogenous, sandy soil column over the precipitation sampling period. The figure also

shows the change in ^{129}I concentration at the water table over the course of the simulation and the change in % saturation over time. In this case a mean K for the sand and gravel soils of the ASA of 138 m/day was used, which was found to represent a mean saturated hydraulic conductivity for the ASA soil based on grain size analysis [*Chesnaux and Allen*, 2007]. The porosity was set to 0.38, which is a representative value for sandy soils [*Freeze and Cherry*, 1979]. The low fluid error (0.01%) and solute mass balance error (-2.6%) suggest model validity for both water and ^{129}I transport over time.

Figure 5.5a shows the change in % saturation during the simulation. The figure shows the water table located at 7m depth with a capillary fringe of ~0.5m. The saturation is initially at 75% in the soil column; however, as soon as the simulation starts the saturation drops to ~15-18% and remains in this range for the duration of the simulation. This is indicative of a soil that has a very low field capacity and this scenario agrees well with previous efforts to model the vadose zone of the ASA [*Chesnaux and Allen*, 2007; *Chesnaux et al.*, 2007]. This rapid drainage of the vadose zone has a great effect on the mobility and velocity of ^{129}I.The drying of the vadose zone results in a much lower effective hydraulic conductivity in the unsaturated zone and hence greater retardation which inhibits the transport of contaminants, including ^{129}I [*Chesnaux and Allen*, 2007]. Only, subsequent additions of water via precipitation or irrigation can push the ^{129}I front downward towards the water table. This also has an impact on the timing of ^{129}I breakthrough to the water table and smoothing of the ^{129}I concentration profile over time as this phenomenon results in the mixing of water parcels as the ^{129}I proceeds through the vadose zone resulting in a

blending of the ^{129}I concentration. This also has the important effect of delaying the transport of the ^{129}I peak to the water table.

Figure 5.5b shows the depth profile of ^{129}I concentration over time through the vadose zone from the soil surface to its eventual input into groundwater at the base of the profile. Notable is that the flux of ^{129}I is greatest in the first few recharge periods, which were the ones most affected by the FDNA, and had the highest washout values. Following the first few recharge periods the flux of ^{129}I decreases and is variable throughout the rest of the simulation responding to variation in ^{129}I washout and additional inputs from irrigation. The modeled ^{129}I profile within the soil column is also extremely variable due to the fact that there is 0 K_d, which is allowing ^{129}I to infiltrate through the vadose zone nearly unretarded so that the variation in input is partially conserved throughout the depth profile.

Figure 5.5c shows that the modeled ^{129}I concentration at the water table in this case with no retardation is far higher than the measured ^{129}I concentration groundwater. Notably, the dominantly advective transport in this aquifer could preserve the modeled variability at the water table in groundwater samples.

The timing of the initial increase in ^{129}I concentration at the water table in the model was at ~40 days and the peak was at ~259 days (Figure 5.5b). These values can be used to calculate a ^{129}I transport velocity in a 0 K_d flow path given that we know the distance travelled and the time. Using the initial increase to calculate the ^{129}I velocity yields a mean of 0.18 m/day, whereas using the peak at 259 days gives a velocity of 0.03 m/day.

This discrepancy is due to the smoothing and delaying of the peak due to the low field capacity of the soil and the rapid drainage the model experienced, which increases retardation greatly. The more reasonable ^{129}I velocity is that calculated by the initial increase at the base of the model as it best represents unimpeded transport of ^{129}I in the 0 K_d system and the peak transport velocity in a preferential flow path.

This profile can be considered an end member for preferential flow in a coarse grained, sub vertical bed with 0 Kd. The concentrations that it produces are far higher than those actually measured in ABB03 or PB20, however, the variability in the model groundwater ^{129}I concentrations suggests that a 0 K_d system can preserve the changes in the input function and allow ^{129}I to behave conservatively, which agrees well with the observed pattern of ^{129}I concentration oscillation in ABB03 and PB20 samples. The preservation of input variability observed suggests that such a system is likely operating in the ASA vadose zone and that ^{129}I from the FDNA is being transported in such a flow path. Field observations of ASA stratigraphy support the existence of such beds (Supplementary Figure 1).

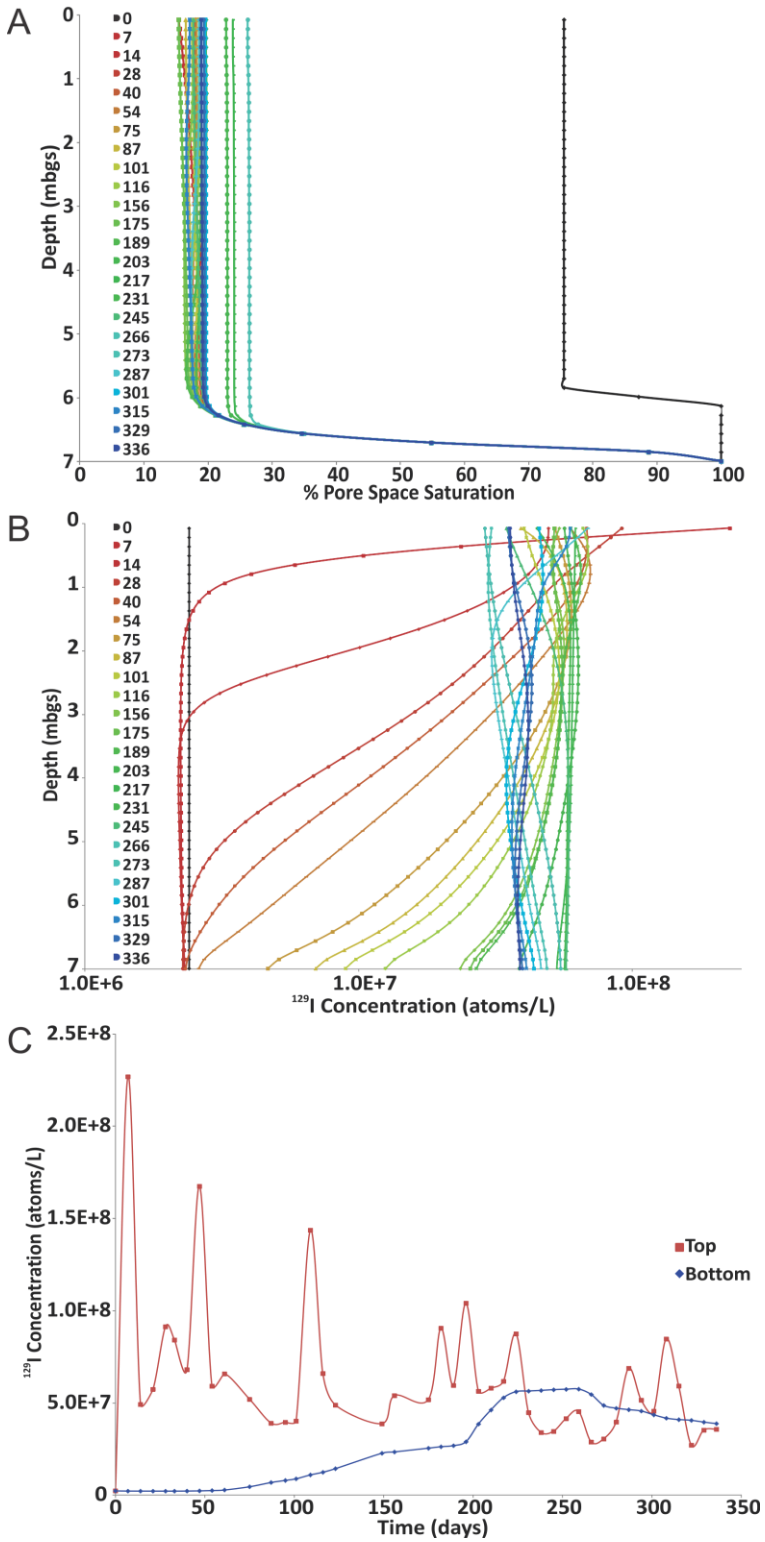

Figure 5.5: Modeling results in a vadose zone soil with 0 K_d for a) the % pore saturation of the vadose zone with depth over time, b) ^{129}I concentration with depth over time in which colours grade over time from red to blue, c) ^{129}I concentration profile at the top of the section and the water table over time showing that some of the input variability which is recorded well at the top of the section is also preserved, although heavily attenuated, at the water table.

3.2.4 Case II: Two Soil Scenario

Case II investigates the influence of a two layer vadose zone with different soil properties and differing K_d's on the transport of ^{129}I. In this scenario a surface layer of sandy loam overlies the homogenous sandy soil used in Case I. The K_d in the sandy soil below remained 0 while the sandy loam above had a K_d of 15 L/kg due to the presence of organic matter in such surface soils. Indeed, loss-on-ignition results for the upper 30 cm of the ASA soils have 3-9% organic matter. The sandy loam had a porosity of 0.49 and a K of 1.8 m/day, which was obtained from [*Chesnaux and Allen*, 2007]. The thickness of the sandy loam was 0.30 m. The simulation had a fluid error of 0.00% and a solute mass balance error of 5.84%.

Figure 5.6a shows that the surface sandy loam has a much higher field capacity than the coarser grained medium sand below, which will have a major effect on the transport of ^{129}I. Likewise, heterogeneity in the vertical distribution of the coarser facies in the field will establish preferential pathways for the transport of ^{129}I. There is field evidence for the existence of such conduits in the form of sub-vertical gravel cross-beds.

The depth profile of ^{129}I concentration seen in Figure 5.6b shows that in the first several recharge periods ^{129}I is almost fully retarded by the sandy loam, with breakthrough into the lower sand through to the water table occurring later in time.

Figure 5.6c shows the evolution of the ^{129}I concentration at the top of the section and the water table over time. The concentration of ^{129}I in the loam soil rises steadily throughout the simulation, through sorption. Only when equilibrium with the water is attained does ^{129}I start to pass through the upper soil, with the variability of the input

damped. The ^{129}I concentration in the groundwater and the concentration throughout the depth profile appear to reach equilibrium by the end of the simulation. The initial increase in ^{129}I concentration at the water table appeared within ~95 days, with a maximum concentration of 10.5 x 10^6 atoms/L. This concentration is much closer to measured ^{129}I concentrations than those seen in Case I suggesting that a heterogeneous soil with various K_d's will lower the ^{129}I concentration in groundwater. The ^{129}I velocity in the sandy loam was 0.04 m/day, which is much lower than that modeled in Case I, with a much higher ^{129}I velocity in the medium sand (0.16 m/day). This latter value is nearly identical to the velocity in Case I.

Case II introduces heterogeneity into the vadose zone model in terms of both K_d and lithology, showing that this increases ^{129}I transport to the water table with limited retardation. Case II however, fails to reproduce the variable ^{129}I concentration in groundwater arising from the variable input function. The smoothing effect, even with a low K_d, of the homogeneous sandy loam produces a cumulative increase in ^{129}I concentrations at the water table as opposed to the observed variability in ABB03 and PB20. Therefore, a model that incorporates a layer with a uniform K_d value cannot explain both the low ^{129}I concentrations in ASA wells and their temporal variability. Thus, a conceptual model for contaminant transport in the vadose zone of the ASA is one that incorporates preferential flow paths, with negligible sorption to provide conduits for the rapid infiltration of precipitation and ^{129}I, which preserve the variability of the input function.

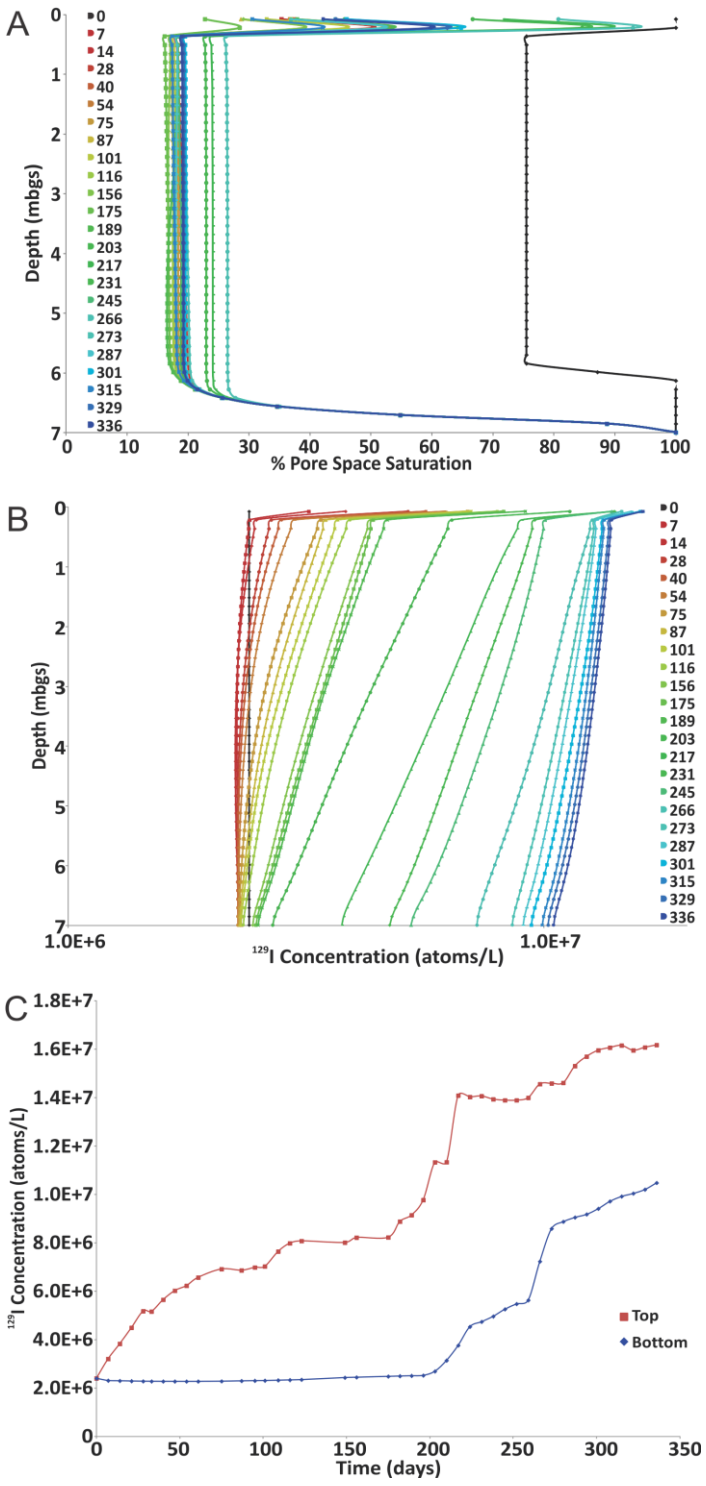

Figure 5.6: Modeling results in a vadose zone soil with a 30cm surface soil with a K_d of 15 L/kg and an underlying sand with 0 K_d for a) the % pore saturation of the vadose zone with depth over time, b) ^{129}I concentration with depth over time in which colours grade over time from red to blue, c) ^{129}I concentration profile at the water table and top of the section over time showing that the application of a high K_d layer near the ground surface accumulates ^{129}I leading to a similar trend at the water table which does not retain the variability measured as washout.

3.2.5 Temporal Variability of ^{129}I and $^{129}I/^{127}I$ in Groundwater

The results of vadose zone modeling allow for a comparison between the timing of variations in modeled groundwater ^{129}I concentrations and the observed ^{129}I variation in samples from ABB03 and PB20. It is possible to use the breakthrough times found in modeling Cases I and II to evaluate if ^{129}I in washout from the FDNA could travel through the vadose zone, to the well screen within the time needed to produce the observed ^{129}I variability in groundwater samples. The ^{129}I peak in ABB03 occurred 0.93 years after Fukushima. The average $^{3}H/^{3}He$ groundwater age of ABB03 is 0.9 ± 0.5 years from the water table to well screen. Therefore, vadose zone travel time would have to be very rapid in order for ^{129}I from the FDNA to contribute to these elevated concentrations. Similarly, for PB20 the average $^{3}H/^{3}He$ groundwater age is 1.2 ± 0.5 years and the peak was observed at 1.35 years and is spread out over around three months.

Case I demonstrates the case for a rapid ^{129}I transport scenario, which we hypothesize represents an ideal preferential flow path that is the result of the heterogeneous stratigraphy of the ASA soils. 0 K_d was applied and the initial increase in ^{129}I concentrations observed after ~0.11 years and the peak was at ~0.71 years in the model results. These vadose zone travel times can then be added to the range of feasible groundwater ages for ABB03 and PB20 to get a range of model predictions for ^{129}I travel times from deposition on the ground surface to the well screen.

In ABB03 the range of modeled transport times is 0.5 – 1.5 years when using the time of the initial increase in ^{129}I concentrations as the vadose zone travel time. Using the travel

time of the peak ^{129}I concentration in the model yields a range of 1.1 - 2.1 years. The agreement between these predicted times and the measured increases in ^{129}I concentration in ABB03 are excellent, although the timing of the initial increase is slightly better due to the smoothing that occurs to the ^{129}I peak as it travelled through the vadose zone. This is an indication that this model provides reasonable results in terms of transport times and that there is a high likelihood of rapid ^{129}I transport through the vadose zone in situations with almost no retardation. This agreement also suggests that the measured variability in ABB03 may be due to ^{129}I from the FDNA being rapidly transported to water table and that previous estimates for groundwater age in ABB03 are accurate. The modeled breakthrough times for the initial increase in PB20 ranged from 0.8 - 1.8 years and for the peak 1.4 - 2.4 years. These modeled ages are also in excellent agreement with observed variation in PB20 and strengthen the argument that ^{129}I from the FDNA could have been rapidly transported as both wells show measured ^{129}I variation at the same times as are predicted by modeling of vadose zone transport times and previously measured groundwater ages. We propose that this rapid transport of FDNA ^{129}I is possible if it was conducted via preferential flow paths that exist due to the heterogeneous stratigraphy of the ASA soils. These flow paths are capable of conducting ^{129}I with almost no retardation, similar to the situation modeled in Case 1. The only factor limiting ^{129}I transport was the degree of saturation of the soil as the well drained nature of the vadose zone and the preferential flow paths retards ^{129}I transport. In the model cases ^{129}I reached the water table very rapidly and has an effect on groundwater ^{129}I concentrations despite this limitation. ^{129}I transport via preferential flow paths can also explain the drop in ^{129}I

concentrations between precipitation and groundwater as only a fraction of the ^{129}I is being transported rapidly, while a significant amount is likely attenuated by soils. The result is a scenario in which the degree of ^{129}I variability in the input is dampened in groundwater despite the rapid transport.

Case II included a surface soil with lower hydraulic conductivity and a K_d value of 15 L/kg. The initial increase in ^{129}I concentration at the water table in this model occurred after 0.26 years. The peak time for this scenario was reached at the end of the modeling time due to the cumulative increase in ^{129}I concentrations at the water table, which was not observed in actual groundwater measurements. Therefore, the timing of the initial increase provides the only data for estimating travel times in this scenario. In ABB03 the modeled range of ^{129}I breakthrough was 0.66 – 1.66 years and in PB20 it was 0.96-1.96 years. The modeled ages in both wells agree well with the ages for ^{129}I variability in both wells. This suggests that it is possible the vadose zone to have a small K_d value and still transport ^{129}I rapidly.

We propose a system in which a fraction of the ^{129}I in precipitation is conducted rapidly, via preferential flow paths, through the vadose zone to the water table while the remainder is retarded and is ultimately homogenized with ^{129}I from other precipitation events and irrigation. This results in stable, low ^{129}I concentrations in groundwater, while some of the input variability is preserved due to the fraction of ^{129}I that is conservatively transported in the preferential flow paths. In the ASA homogenization is driven by a

combination of soil-water partitioning and the low saturation of the soil, which leads to a higher degree of retardation.

The final phase of ^{129}I transport is the saturated zone movement from the water table to the well screen where it is sampled. During groundwater transport, lateral, longitudinal and vertical dispersion or mixing effects will likely result in lowering the ^{129}I concentration in groundwater below that modeled at the water table to the ^{129}I concentrations that were actually measured in samples from ABB03 and PB20. However, in shallow portions of the aquifer it has been concluded that flow is predominantly sub-vertical and that mixing will be more limited due to relatively short transport distances [*Wassenaar et al.*, 2006; *Chesnaux et al.*, 2012]. Ultimately, some dilution of the event-based pulse of the FDNA ^{129}I is occurring, but it is considered minimal due to the shallow depths of the well screens and the rapid vertical flow of water in the shallow portions of the ASA.

4.0 SUMMARY AND CONCLUSIONS

The atmospheric transport of ^{129}I from the Fukushima-Daichii Nuclear Accident and its deposition via precipitation has been quantified for a year following the accident using weekly precipitation sampling. The transport of ^{129}I has also been traced into local groundwater to elucidate the long term fate of the ^{129}I. The data shows that FDNA ^{129}I was rapidly transported to the west coast of North America and was first detected on the week of March 17, 2011 within 6-8 days of the accident. This pulse is corroborated by samples taken from 3 sampling locations: Vancouver, Saturna Island and the NADP site WA-19. The peak magnitude of the FDNA pulse, 211 x 10^6 atoms ^{129}I/L, was approximately 7 times about pre-accident background of 31 x 10^6 atoms/L. However, ^{129}I concentrations returned

to background levels within a few days suggesting relatively little mixing of ^{129}I between air masses during trans-Pacific transport. Several precipitation events with ^{129}I concentrations substantially higher than background were also observed throughout the year including one in July with a concentration even higher than that measured directly following the FDNA. These peaks occurred after most atmospheric radionuclide monitoring for FDNA fission products has ceased and their cause is likely due to a combination of natural processes such as resuspension from the ground surface, ocean volatilization and atmospheric concentration due to drought periods as well as releases from nuclear fuel reprocessing.

The peak ^{129}I mass flux was observed immediately following the FDNA and in the same sampling period that contained the peak ^{129}I concentration. The ^{129}I concentration is the principle factor determining washout. The correlation coefficient between the ^{129}I concentration and washout is greater than that for the precipitation quantity.

Groundwater ^{129}I concentrations in two nearby wells showed minor anomalies over the sampling period which could be due to rapid infiltration of the FDNA atmospheric ^{129}I signal. Vadose zone modeling shows that a component of the ^{129}I deposited by the FDNA moved rapidly from the ground surface to the water table along preferential flow paths with little retardation such that anomalies within the input signal can be observed at the water table. The balance of the input ^{129}I, in contrast, traveled through the upper soil with a K_d value of 15 L/kg where variable input concentrations were attenuated.

We conclude that it is possible that a fraction of ^{129}I from the FDNA is transported conservatively via preferential flow paths to the water table while the remaining ^{129}I in the system interacts with soil and its transport is retarded within the vadose zone. The result is that attenuated ^{129}I anomalies of atmospheric origin can be observed in the groundwater. Further, the modeled lag times of these attenuated atmospheric anomalies are consistent with $^{3}H/^{3}He$ groundwater ages previously measured in two separate wells.

This paper provides for the first time insight into the transport of ^{129}I from an atmospheric release and its fate during wet deposition and recharge to groundwater. While ^{129}I is largely retained on organics in the soil of the upper vadose zone the long term fate of ^{129}I from the FDNA includes recharge into the Abbotsford-Sumas aquifer groundwaters. Continuing work on the fate of ^{129}I and its transport should address the influence of local redox conditions in detail and the inorganic and organic speciation of ^{129}I and ^{127}I in precipitation, the vadose zone and groundwater.

References

Aldahan, A., V. Alfimov, and G. Possnert (2007), 129I anthropogenic budget: Major sources and sinks, *Appl. Geochemistry*, *22*(3), 606–618, doi:10.1016/j.apgeochem.2006.12.006.

Aldahan, A., S. Persson, G. Possnert, and X. L. Hou (2009), Distribution of 127I and 129I in precipitation at high European latitudes, *Geophys. Res. Lett.*, *36*(11), 1–5, doi:10.1029/2009GL037363.

Alvarado-Quiroz, N. G., T. G. Kotzer, G. M. Milton, I. D. Clark, and D. Bottomley (2002), Partitioning of 127I and 129I in an unconfined glaciofluvial aquifer on the Canadian shield, *Radiochim. Acta*, *90*(8), 469–478.

Baker, A. R., C. Tunnicliffe, and T. D. Jickells (2001), Iodine speciation and deposition fluxes from the marine atmosphere, *J. Geophys. Res.*, *106*(D22), 28743–28749.

Bamba, S., K. E. Yamaguchi, and H. Amano (2014), Determination of 129I/127I in environmental water before and after the 2011 Fukushima Daiichi nuclear power plant accident with a solid extraction disk, *J. Radioanal. Nucl. Chem.*, *301*(1), 75–80, doi:10.1007/s10967-014-3055-8.

Bartholomay, R. C. (2013), *Iodine-129 in the Eastern Snake River Plain Aquifer at and near the Idaho National Laboratory, Idaho, 2010–12 Scientific Investigations Report 2013 – 5195*.

Bikit, I., D. Mrda, N. Todorovic, J. Nikolov, M. Krmar, M. Veskovic, J. Slivka, J. Hansman, S. Forkapic, and N. Jovancevic (2012), Airborne radioiodine in northern Serbia from Fukushima., *J. Environ. Radioact.*, 1–5, doi:10.1016/j.jenvrad.2012.01.020.

Brauer, F. P., and H. G. J. Rieck (1973), *129I, 60Co, 106Ru Measurements on Water Samples from the Hanford Project Environs - BNWL-SA-4478*.

Chesnaux, R., and D. M. Allen (2007), Simulating Nitrate Leaching Profiles in a Highly Permeable Vadose Zone, *Environ. Model. Assess.*, *13*(4), 527–539, doi:10.1007/s10666-007-9116-4.

Chesnaux, R., D. M. Allen, and G. Graham (2007), Assessment of the impact of nutrient management practices on nitrate contamination in the Abbotsford-Sumas aquifer., *Environ. Sci. Technol.*, *41*(21), 7229–34.

Chesnaux, R., D. M. Allen, and M. W. M. Simpson (2012), Comparing isotopic groundwater age measurements with simulated groundwater ages: example of the Abbotsford-Sumas Aquifer (USA and Canada) and application, *Water Environ. J.*, *26*(1), 30–37, doi:10.1111/j.1747-6593.2011.00260.x.

Cox, S. E., and S. C. Kahle (1999), *Hydrogeology, Ground-Water Quality, and Source of Nitrate in Lowland Glacial Aquifers of Whatcom County, Washington and British Columbia, Canada*.

Draxler, R. R., and G. D. Rolph (2013), Real-time Environmental Applications and Display sYstem (READY) Website (http://www.ready.noaa.gov). NOAA Air Resources Laboratory, College Park, MD.,

Environment Canada (2015), Unpublished Nitrate Data,

Evrard, O., P. Van Beek, D. Gateuille, V. Pont, I. Lefèvre, B. Lansard, and P. Bonté (2012), Evidence of the radioactive fallout in France due to the Fukushima nuclear accident., *J. Environ. Radioact.*, *2011*(March 2011), 1–7, doi:10.1016/j.jenvrad.2012.01.024.

Fabryka-Martin, J., D. O. Whittemore, S. N. Davis, P. W. Kubik, and P. Sharma (1991), Geochemistry of halogens in the Milk River aquifer, Alberta, Canada, *Appl. Geochemistry*, *6*(1), 447–464.

Farmwest (1998), Farmwest - Penman Monteith Equation, , 1–12.

Freeze, R. A., and J. A. Cherry (1979), *Groundwater*, 1st ed., Prentice-Hall, Inc.

Fuge, R., and C. Johnson (1986), The geochemistry of iodine - a review, *Environ. Geochem. Health*, *8*(2), 31–54.

Fukui, M., Y. Fujikawa, and N. Satta (1996), Factors affecting interaction of radioiodide and iodate species with soil, *J. Environ. Radioact.*, *31*(2), 199–216, doi:10.1016/0265-931X(95)00039-D.

Van Genuchten, M. T. (1980), A Closed-form Equation for Predicting the Hydraulic Conductivity of Unsaturated Soils, *Soil Sci. Soc. Am. J.*, *44*, 892–898.

Gilfedder, B. S., M. Petri, and H. Biester (2007), Iodine and bromine speciation in snow and the effect of orographically induced precipitation, *Atmos. Chem. Phys.*, *7*(10), 2661–2669, doi:10.5194/acp-7-2661-2007.

Gilfedder, B. S., S. C. Lai, M. Petri, H. Biester, and T. Hoffmann (2008), Iodine speciation in rain, snow and aerosols, *Atmos. Chem. Phys.*, *8*, 6069–6084.

Gómez-Guzmán, J. M., S. M. Enamorado-Báez, a. R. Pinto-Gómez, J. M. Abril-Hernández, J. M. López-Gutiérrez, and M. García-León (2012), Anthropogenic 129I concentration and 129I/127I ratio in rainwater from Seville (Spain) in the period 2005-2008 as affected by airborne releases from Sellafield and La Hague facilities, *Atmos. Environ.*, doi:10.1016/j.atmosenv.2012.03.075.

Graham, G., D. M. Allen, and B. Finkbeiner (2014), Climate controls on nitrate concentration variability in the Abbotsford-Sumas aquifer, British Columbia, Canada, *Environ. Earth Sci.*, doi:10.1007/s12665-014-3072-5.

VanDer Gulik, T. (2014), Personal Communication,

Health Canada (2014), Radiation Monitoring Data and the Nuclear Emergency in Japan, Available from: http://www.hc-sc.gc.ca/hc-ps/ed-ud/respond/nuclea/data-donnees-eng.php

Healy, R. W. (1990), *Simulation of Solute Transport in Variably Saturated Porous Media with Supplemetal Information on Modifications to the U.S. Geological Survey's Computer Program VS2D - USGS Water Resources Investigations Report 90-4025*.

Herod, M. N., I. D. Clark, W. E. Kieser, S. Agosta, and X.-L. Zhao (2013), 129I dispersion and sources in Northwest Canada, *Nucl. Instruments Methods Phys. Res. Sect. B Beam Interact. with Mater. Atoms*, *294*, 552–558, doi:10.1016/j.nimb.2012.06.018.

Hii, B., H. Liebscher, M. Mazalek, T. Tuominen, A. S. Division, E. C. Branch, E. Canada, and Y. Region (1999), *Ground Water Quality and Flow Rates in the Abbotsford Aquifer, British Columbia*.

Hou, X., V. Hansen, A. Aldahan, G. Possnert, O. C. Lind, and G. Lujaniene (2009), A review on speciation of iodine-129 in the environmental and biological samples., *Anal. Chim. Acta*, *632*(2), 181–96, doi:10.1016/j.aca.2008.11.013.

Hu, Q., P. Zhao, J. E. Moran, and J. C. Seaman (2005), Sorption and transport of iodine species in sediments from the Savannah River and Hanford Sites., *J. Contam. Hydrol.*, *78*(3), 185–205, doi:10.1016/j.jconhyd.2005.05.007.

Hu, Q. H., J. E. Moran, and J. Y. Gan (2012), Sorption, degradation, and transport of methyl iodide and other iodine species in geologic media, *Appl. Geochemistry*, *27*(3), 774–781, doi:10.1016/j.apgeochem.2011.12.022.

Jabbar, T., G. Wallner, and P. Steier (2013), A review on 129I analysis in air., *J. Environ. Radioact.*, *126C*, 45–54, doi:10.1016/j.jenvrad.2013.07.013.

Landis, J. D., N. T. Hamm, C. E. Renshaw, W. B. Dade, F. J. Magilligan, and J. D. Gartner (2012), Surficial redistribution of fallout ^{131}iodine in a small temperate catchment., *Proc. Natl. Acad. Sci. U. S. A.*, *109*(11), 4064–9, doi:10.1073/pnas.1118665109.

Lapala, E. G., R. W. Healy, and E. Weeks (1987), *Documentation of the Comupter Program VS2D to Solve the Equations of Fluid Flow in Variably Saturated Porous Media - USGS Water Resources Investigation Report 83-4099*.

Lehto, J., T. Räty, X. Hou, J. Paatero, A. Aldahan, G. Possnert, J. Flinkman, and H. Kankaanpää (2012), Speciation of 129I in sea, lake and rain waters., *Sci. Total Environ.*, *419*, 60–7, doi:10.1016/j.scitotenv.2011.12.061.

Leon, J. D., D. A. Jaffe, J. Kaspar, A. Knecht, M. L. Miller, R. G. H. Robertson, and A. G. Schubert (2011), Arrival time and magnitude of airborne fission products from the Fukushima, Japan, reactor incident as measured in Seattle, WA, USA, *J. Environ. Radioact.*, *102*(11), 1032–1038.

López-Gutiérrez, J. M., M. García-León, C. Schnabel, M. Suter, H. a Synal, and S. Szidat (2001), Wet and dry deposition of 129I in Seville (Spain) measured by accelerator mass spectrometry., *J. Environ. Radioact.*, *55*(3), 269–82.

Macmullin, S., G. K. Giovanetti, M. P. Green, R. Henning, R. Holmes, K. Vorren, and J. F. Wilkerson (2012), Measurement of airborne fission products in Chapel Hill, NC, USA from the Fukushima Daiichi reactor accident., *J. Environ. Radioact.*, doi:10.1016/j.jenvrad.2012.01.026.

Melgunov, M. S., N. P. Pokhilenko, V. D. Strakhovenko, F. V Sukhorukov, and a V Chuguevskii (2012), Fallout traces of the Fukushima NPP accident in southern West Siberia (Novosibirsk, Russia)., *Environ. Sci. Pollut. Res. Int.*, *19*(4), 1323–5, doi:10.1007/s11356-011-0659-1.

Mitchell, R. J., R. S. Babcock, S. Gelinas, L. Nanus, and D. E. Stasney (2003), Nitrate Distributions and Source Identification in the Abbotsford-Sumas Aquifer, Northwestern Washington State, *J. Environ. Qual.*, *32*, 789–800.

Miyake, Y., H. Matsuzaki, T. Fujiwara, T. Saito, T. Yamagata, M. Honda, and Y. Muramatsu (2012), Isotopic ratio of radioactive iodine (129I/131I) released from Fukushima Daiichi NPP accident Fukushima, *Geochem. J.*, *46*, 327–333.

Moran, J. E., S. D. Oktay, P. H. Santschi, and D. R. Schink (1999), Atmospheric Dispersal of 129 Iodine from Nuclear Fuel Reprocessing Facilities, *Environ. Sci. Technol.*, *33*(15), 2536–2542.

Muramatsu, Y., Y. Uchida, P. Sriyotha, and K. Sriyotha (1990), Some Considerations on the Sorption and Desorption Phenomena of Iodide and Iodate on Soil, *Water, Air Soil Pollut.*, *49*, 125–138.

Muramatsu, Y., H. Matsuzaki, C. Toyama, and T. Ohno (2015), Analysis of 129I in the soils of Fukushima Prefecture: preliminary reconstruction of 131I deposition related to the accident at Fukushima Daiichi Nuclear Power Plant (FDNPP), *J. Environ. Radioact.*, *134*, 344–350, doi:10.1016/j.jenvrad.2014.05.007.

Paul, M., D. Fink, G. Hollos, A. Kaufman, W. Kutschera, and M. Magaritz (1987), Measurement of 129I concentrations in the environment after the Chernobyl reactor accident, *Nucl. Instruments Methods Phys. Res.*, *29*(1-2), 341–345, doi:10.1016/0168-583X(87)90262-X.

Persson, S., A. Aldahan, G. Possnert, V. Alfimov, and X. Hou (2007), 129I Variability in precipitation over Europe, *Nucl. Instruments Methods Phys. Res. Sect. B Beam Interact. with Mater. Atoms*, *259*(1), 508–512, doi:10.1016/j.nimb.2007.01.193.

Piñero García, F., and M. a Ferro García (2012), Traces of fission products in southeast Spain after the Fukushima nuclear accident., *J. Environ. Radioact.*, 1–6, doi:10.1016/j.jenvrad.2012.01.011.

Reithmeier, H., V. Lazarev, W. Rühm, T. M. Schwikowski, H. W. Gäggeler, and E. Nolte (2006), Estimate of European 129I releases supported by 129I analysis in an Alpine ice core., *Environ. Sci. Technol.*, *40*(19), 5891–6.

Schwehr, K. A., P. H. Santschi, J. E. Moran, and D. Elmore (2005), Near-conservative behavior of 129I in the Orange County aquifer system, California, *Appl. Geochemistry*, *20*(8), 1461–1472, doi:10.1016/j.apgeochem.2005.02.003.

Schwehr, K. A., P. H. Santschi, D. J. Kaplan, C. M. Yeager, and R. Brinkmeyer (2009), Organo-iodine formation in soils and aquifer sediments at ambient concentrations., *Environ. Sci. Technol.*, *43*(19), 7258–64.

Scibek, J., and D. Allen (2006), Comparing modelled responses of two high-permeability, unconfined aquifers to predicted climate change, *Glob. Planet. Change*, *50*(1-2), 50–62, doi:10.1016/j.gloplacha.2005.10.002.

Sheppard, M. I., D. H. Thibault, J. McMurry, and E. A. Smith (1995), Factors Affecting the Soil Sorption of Iodine, *Water, Air Soil Pollut.*, *83*, 51–67.

Sheppard, M. I., J. L. Hawkins, and P. A. Smith (1996), Soil Processes and Chemical Transport: Linearity of Iodine Sorption and Sorption Capacities for Seven Soils, *J. Environ. Qual.*, *25*, 1261–1267.

Sheppard, S. C. (2003), Interpolation of solid/liquid partition coefficients, Kd, for iodine in soils, *J. Environ. Radioact.*, *70*(1-2), 21–7, doi:10.1016/S0265-931X(03)00129-2.

Sheppard, S. C., and M. Herod (2012), Variation in background concentrations and specific activities of 36Cl, 129I and U/Th-series radionuclides in surface waters, *J. Environ. Radioact.*, *106*, 27–34, doi:10.1016/j.jenvrad.2011.10.015.

Söderlund, M., M. Lusa, J. Lehto, and M. Hakanen (2011), *POSIVA Working Report 2001-04: Sorption of Iodine, Chlorine, Technetium and Cesium in Soil*.

Steinhauser, G. (2014), Fukushima's Forgotten Radionuclides: A Review of the Understudied Radioactive Emissions., *Environ. Sci. Technol.*, *48*(9), 4649–4663, doi:10.1021/es405654c.

Tokyo Electric Power Company (2012), *Estimation of Radioactive Material Released to the Atmosphere during the Fukushima Daiichi NPS Accident*.

Wassenaar, L. I. (1995), Evaluation of the origin and fate of nitrate in the Abbotsford Aquifer using the isotopes of 15N and 180 in NO3-, *Appl. Geochemistry*, *10*, 391–405.

Wassenaar, L. I., M. J. Hendry, and N. Harrington (2006), Decadal geochemical and isotopic trends for nitrate in a transboundary aquifer and implications for agricultural beneficial management practices., *Environ. Sci. Technol.*, *40*(15), 4626–32.

Wetherbee, G. A., D. A. Gay, T. M. Debey, C. M. B. Lehmann, and M. A. Nilles (2012), Wet Deposition of Fission-Product Isotopes to North America from the Fukushima Dai-ichi Incident, March 2011, *Environ. Sci. Technol.*, *46*(5), 2574–2582.

Xu, S., S. P. H. T. Freeman, X. Hou, A. Watanabe, K. Yamaguchi, and L. Zhang (2013), Iodine isotopes in precipitation: temporal responses to 129I emissions from the Fukushima nuclear accident, *Environ. Sci. Technol.*, doi:10.1021/es401527q.

Zebarth, B. J., M. C. Ryan, G. Graham, T. a Forge, and D. Neilsen (2015), Groundwater Monitoring to Support Development of BMPs for Groundwater Protection : The Abbotsford-Sumas Aquifer Case Study, *Groundw. Monit. Remediat.*, *35*(1), 82–96, doi:10.1111/gwmr.12092.

Zhang, S. et al. (2011), Concentration-dependent mobility, retardation, and speciation of iodine in surface sediment from the Savannah River Site., *Environ. Sci. Technol.*, *45*(13), 5543–9, doi:10.1021/es1040442.

CHAPTER 6 - CONCLUSIONS

The objectives of this thesis, outlined in Chapter 1.4, were to elucidate the geochemical behaviour and cycling of ^{129}I. The mass flux, transport and storage of ^{129}I were also measured to enhance the use of ^{129}I as an environmental tracer. Using accelerator mass spectrometry, stable isotope and geochemical analysis the research in this thesis has addressed knowledge gaps concerning the behaviour of ^{129}I by: (1) developing a new method for the extraction of ^{129}I from solid samples using ^{125}I as a quantitative tracer; (2) measuring a ^{129}I baseline in several remote Arctic catchments prior to, during and after the Fukushima-Daiichi Nuclear accident; (3) investigating the temporal changes of ^{129}I abundance in a catchment and placing them in context with the hydrochemical evolution of the catchment to evaluate ^{129}I's usefulness as a tracer and; (4) assessing the effect of ^{129}I fallout from the Fukushima-Daiichi Nuclear Accident and tracing its transit through the vadose zone and potentially measuring it in local groundwater. The major findings of these projects and what we have learned about the behaviour and fate of ^{129}I are summarized below:

1. A newly developed combustion technique was found to be an efficient and reliable means of extracting both ^{129}I and ^{127}I from organic and inorganic solid samples using ^{125}I as a yield tracer. Standard reference materials for both ^{127}I and ^{129}I were used to verify the reproducibility of this technique. This method was also found to efficiently extract organically bound iodine using a humic complex labeled with ^{125}I as a proxy for organic iodine. Recovery of ^{125}I from this matrix was 77 - 100%. Particular care was given to establishing the extraction parameters that yield the best iodine

recovery such as flow rate and heating times. The optimal flow rate for maximum ^{125}I recovery ranged from 400 – 800 mL/min.

2. A three year baseline study of ^{129}I in rivers across the Yukon Territory revealed that anthropogenic releases of ^{129}I have spread widely through the Northern Hemisphere and have reached even the most remote locations on Earth. Sampling in 2011 showed that short-lived, isolated releases of ^{129}I can have profound impacts on the concentration of ^{129}I in remote regions. Many of the watersheds sampled in 2011 had ^{129}I concentrations up to 10 times higher than in 2010 suggesting that ^{129}I released by the FDNA increased the ^{129}I concentrations in rivers across the Yukon. The exception to this however, were rivers with substantial groundwater discharge near the sampling location which did not display a response indicating that the transport of FDNA-derived ^{129}I to discharge was via near surface flowpaths or overland flow. However, this increase was temporary as sampling in 2012 showed that all catchments had returned to background levels.
3. Temporal variations in ^{129}I concentration and the $^{129}I/^{127}I$ ratio were excellent tracers of water source identity and flowpaths to discharge in a small, discontinuous permafrost catchment. Precipitation had high ^{129}I concentrations and a high $^{129}I/^{127}I$ ratio relative to discharge suggesting anthropogenic contamination from nuclear fuel reprocessing and ocean volatilization is the source of ^{129}I to the catchment. The temporal variation of ^{129}I concentrations in streamflow were driven by changes in the water source to discharge with each endmember having distinct effect on ^{129}I depending on its flowpath. A pulse of ^{129}I at the onset of freshet was likely caused

by direct transport of snowmelt over frozen soils that were enriched in ^{129}I due to dry fallout during the winter. As the catchment thawed the rapid decrease of ^{129}I was due to attenuation in soils as water was transported to Wolf Creek through shallow soils. Baseflow samples had slightly elevated ^{129}I concentrations, and very low $^{129}I/^{127}I$ ratios, which are due to contributions of ^{127}I from organic rich bedrock. However, when viewed in context with ^{3}H, groundwater was found to be modern in age, despite its low $^{129}I/^{127}$ ratio and ^{18}O and ^{2}H contents that suggest winter or spring recharge from snowmelt. A mass balance of ^{129}I in the WCRB showed that almost 90% of the annual input is stored, most likely in soil organic matter, which had a $^{129}I/^{127}I$ ratio similar to precipitation. This imbalance is likely caused by the continuing emissions of ^{129}I to the atmosphere which has prevented the catchment from reaching equilibrium.

4. Releases of ^{129}I from the Fukushima-Daiichi Nuclear accident were measured in precipitation and groundwater in Vancouver, British Columbia. Following the FDNA the ^{129}I concentration in precipitation increased 7 times over background. The ^{129}I concentration returned to background levels within a few days however, sporadic pulses of high ^{129}I concentration rain continued for the year and are attributed to resuspension from the ground surface. The fate of the ^{129}I deposited was then studied using groundwater sampling and vadose zone modeling. Groundwater sampling revealed ^{129}I peaks in two different wells that corresponded very well with $^{3}He/^{3}H$ dates of the groundwater. These peaks are possibly due to the rapid infiltration of ^{129}I from the FDNA. The heterogeneous lithology of the aquifer can

result in preferential flow paths that conduct contaminants rapidly to the water table. Modeling of the vadose zone showed that ^{129}I could be conducted in this fashion with minimal retardation and result in increases consistent with those observed in terms of concentration, timing and trends.

In summary, this thesis has resulted in a clearer understanding of the geochemical behaviour and fate of ^{129}I in the numerous environmental reservoirs and the cycle of ^{129}I between them. This characterization will allow the use of ^{129}I as an environmental tracer, particularly, when used with other isotopic and geochemical tracers if its inputs and storage is quantified. It will also help understand the fate of any future unintentional releases of ^{129}I and its safe storage in nuclear waste repositories.

6.1 Future Work

There are still significant research opportunities to better understand the fate of ^{129}I in the environment, allow ^{129}I to fully realize its potential as a tracer, and limit its impact as a contaminant. As advances in AMS technology and laboratory extraction methods continue our understanding of the behaviour of ^{129}I in the environment will grow allowing new research opportunities that are currently only theoretical to become practical. Chapter 2 in this thesis explores a new extraction technique for ^{129}I using the quantitative recovery of ^{125}I as a yield tracer. Using the known quantity of ^{125}I added to samples it is possible of normalize AMS counts of ^{129}I and ^{127}I to the amount of ^{125}I in the target thereby eliminating the need for ^{127}I carrier, and its accompanying ^{129}I contamination. The only barrier to this is the ^{125}Te isobar of ^{125}I. However, ^{125}Te can be removed using isobar separation techniques [*Charles et al.*, 2015]. Once this isobar separation technique is fully developed carrier free

measurements of extremely low level ^{129}I should be possible and eventually routine. This will enable investigations into natural cycling and storage of pre-nuclear age ^{129}I. An example of such a project concerns the temporal variation in atmospheric production of ^{129}I by cosmic rays, which should be recorded in environmental archives such as peat, sediments and ice cores. This could make ^{129}I an invaluable cosmogenic isotope tool for understanding the evolution of cosmic ray flux over million year times scales and their effect on the Earth. An additional application could also be to use geogenically produced ^{129}I in pore water or ancient groundwater as an age constraint or dating tool using ^{129}I at secular equilibrium or the ^{129}I-^{129}Xe geochronometer.

Continued monitoring of ^{129}I and the $^{129}I/^{127}I$ ratio throughout Canada in key environmental reservoirs is needed. Indeed, as one of the longest lived radionuclides in radioactive waste a more thorough baseline of ^{129}I across Canada should be undertaken along with detailed site specific studies. Further research should also investigate the importance of both ^{129}I and ^{127}I speciation in freshwater systems which could provide a useful tracer. Additional studies of the temporal behaviour of ^{129}I in catchments are warranted as the behaviour of organic and particulate iodine has not been identified. The hypothesis that the ^{129}I pulse in Wolf creek was due to rapid snowmelt infiltration should be verified in other snowmelt dominated catchments. The temporal variation of ^{129}I should also be studies in catchments with different climates. If this work is undertaken ^{129}I could potentially be used in hydrograph separation studies as the concentration and the $^{129}I/^{127}I$ ratio can identify different water sources. Characterization of the temporal behaviour of ^{129}I and its catchment scale cycling will enhance our ability to mitigate any releases of ^{129}I from

nuclear accidents or nuclear waste repositories as well as predict its fate in numerous environmental reservoirs. The ongoing production of anthropogenic ^{129}I could also allow its use as a tracer of young water similar to ^{14}C or ^{3}H. Modeling of ^{129}I inputs and outputs, particularly using lumped parameter models, could be used to provide age estimates on water bodies if its non-conservative behaviour is accounted for.

References

Charles, C. R. J., R. J. Cornett, X.-L. Zhao, A. E. Litherland, and W. E. Kieser (2015), On-line I-/Te- separation for the AMS analysis of 125I, *Nucl. Instruments Methods Phys. Res. B*, doi:10.1016/j.nimb.2015.03.030.

APPENDIX A: ADDITIONAL DATA AND BASIC INTERPRETATION COMPLIMENTARY TO CHAPTER 3

Introduction

This addendum contains additional ^{129}I, ^{127}I and $^{129}I/^{127}I$ data from sampling of several Yukon and NWT rivers during the summers of 2011 and 2012. Sampling was conducted according to the same protocol as [*Herod et al.*, 2013]. Several additional watersheds and subwatersheds were added that were not sampled in 2010. In 2012, sampling was limited to a select few watersheds.

The purpose of this additional sampling was to determine if the Fukushima-Daiichi Nuclear Accident, which occurred as a result of the Tohoku earthquake and tsunami, in March 2011, could have affected ^{129}I concentrations and the $^{129}I/^{127}I$ ratio in the Yukon Territory catchments that had been previously characterized in 2010. The baseline study done in 2010 (Chapter 3) showed that anthropogenic emissions of ^{129}I from nuclear fuel reprocessing and atomic weapons testing reached the Yukon, however, the FDNA offered a rare opportunity to assess the effect of a punctual release of ^{129}I to the environment and evaluate its magnitude and persistence in remote watersheds. This information will provide insight into how vulnerable the Arctic is to future radiological releases, as well as the longevity of their effects. Furthermore, the effect of latitude, watershed size, elevation and discharge on ^{129}I concentrations and fluxes is investigated and compared to the results from 2010 in [*Herod et al.*, 2013].

Results and Discussion

In 2011 samples the ^{129}I concentration in almost all catchments increased up to 20 times above 2010 levels reaching a high of 134 x 10^6 atoms/L (Table A1, Figure A1). This

increase was also observed in the $^{129}I/^{127}I$ ratio which was up to 2 orders of magnitude higher in almost all samples peaking at 2.6×10^{-8} and closely mimicked trends in the ^{129}I concentration suggesting that most variation in the $^{129}I/^{127}I$ ratio is due to ^{129}I abundance (Figure A2). These dramatic increases were visible throughout the Yukon including many catchments that had been sampled in 2010 as well as several additional ones (Figure A1). Concentrations and ratios in this range cause the remote rivers of Yukon to resemble those observed in southern Canada and US, which have been much more affected by anthropogenic releases of ^{129}I [*Moran et al.*, 2002; *Snyder and Fehn*, 2004; *Sheppard and Herod*, 2012].

The most probable reason for this striking increase in ^{129}I concentrations and the $^{129}I/^{127}I$ ratio is long distance transport of emissions of ^{129}I from the Fukushima-Daiichi Nuclear Accident (FDNA). A wide variety of radioisotopes were emitted by the FDNA, including ^{129}I (Chapter 5, [*Xu et al.*, 2013; *Steinhauser*, 2014] and long distance transport and deposition of these radionuclides has been observed across the globe including several locations in Canada including Vancouver, BC, Yellowknife, NWT and Resolute Bay, NU [*Health Canada*, 2014]. Interestingly, Resolute Bay had the highest levels of ^{131}I recorded, which corresponds to the very high ^{129}I concentrations measured in the two rivers from Ellesmere Island, Nunavut (Table A1).

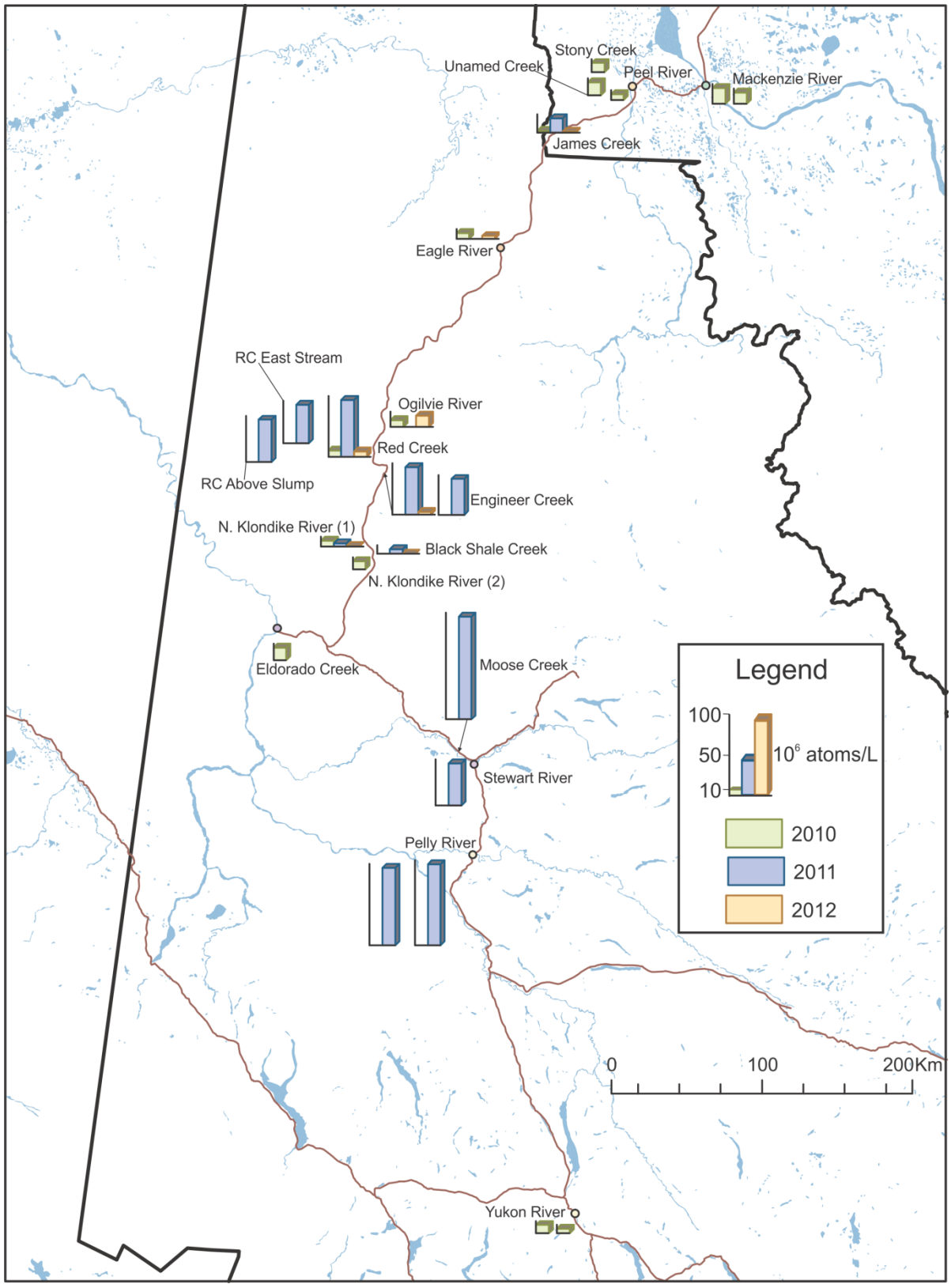

FigureA1: Map of sampling sites showing the ^{129}I concentration for each year.

Site Name	Watershed	Latitude	Longitude	Elevation (ft)	^{129}I Concentration (10^6 atoms/L)	±	^{127}I (ppb)	±	^{129}I / ^{127}I	±	Watershed Area (m^2)	Discharge (L/yr)	Annual Precipitation (L/m^2)	Total Yearly Export (atoms/yr)	Yearly Export ($atoms/m^2/yr$)	±
Yukon River	Yukon	60°40'56.24"	135°02'08.36"	2211	5.98	1.31	3.04	0.054	4.14E-10	9.12E-11	3.24E+11	7.25E+13	262.3	4.33E+20	1.34E+09	3.42E+08
Yukon River	Yukon	60°40'56.24"	135°02'08.36"	2211	11.10	1.31	3.04	0.054	7.69E-10	9.20E-11	3.24E+11	7.25E+13	262.3	8.05E+20	2.48E+09	3.09E+08
Eldorado Creek (aufeis)	Eldorado	63°51'41.74"	139° 14'44.99"	2085	16.09	1.45	8.35	0.171	4.06E-10	3.76E-11			367.8			
N. Klondike River (aufeis)	N. Klondike	64° 30'53.48"	138° 14'59.84"	3463	10.96	1.50	3.54	0.049	6.53E-10	8.97E-11	1.10E+09	4.10E+11	320	4.50E+18	4.09E+09	6.29E+08
N. Klondike River (downstream)	N. Klondike	64° 30'20.83"	138° 13'30.56"	3378	7.55	1.59	3.03	0.037	5.25E-10	1.11E-10	1.10E+09	4.10E+11	320	3.10E+18	2.81E+09	6.26E+08
Red Creek	Ogilvie	65° 9'34.05"	138°22'12.42"	2492	8.16	1.45	2.95	0.048	5.84E-10	1.04E-10	8.40E+07	2.10E+10	300	1.71E+17	2.04E+09	3.91E+08
Ogilvie River	Ogilvie	65°21'45.13"	138°18'0.56"	1945	8.92	1.13	3.72	0.084	5.05E-10	6.49E-11	7.13E+09	1.71E+12	300	1.53E+19	2.14E+09	3.10E+08
Sulphur Spring	Ogilvie	65°	138°		6.41	0.73										5.06E+08
Blackwater Spring	Ogilvie	65°	138°		10.77	1.34										2.34E+08
Eagle River	Eagle	66°26'35.80"	136°42'49.30"	1072	7.55	1.31	3.69	0.058	4.32E-10	7.54E-11	1.03E+10	3.68E+12	417	2.78E+19	2.70E+09	
James Creek	Peel	67°08'12.7"	136°00'19.30"	2196	2.52	0.99	2.72	0.038	1.95E-10	7.68E-11	5.38E+07	1.25E+10	297.7	3.14E+16	5.84E+08	3.79E+08
Unamed Creek	Peel	67°15'18.00"	135°14'30.00"	990	17.04	1.55	1.63	0.013	2.20E-09	2.00E-10	2.30E+05		297.7			3.90E+08
Stony Creek	Peel	67°23'18.25"	134°55'16.69"	23	11.77	1.41	1.71	0.016	1.45E-09	1.73E-10	1.06E+09	2.46E+11	297.7	2.89E+18	2.73E+09	3.60E+08
Peel River	Peel	67°20'19.04"	134°52'25.92"	26	7.50	1.59	1.88	0.029	8.41E-10	1.79E-10	7.36E+10	1.71E+13	297.7	1.28E+20	1.74E+09	3.02E+08
Mackenzie River	Mackenzie	67°27'24.27"	133°45'46.42"	27	20.74	1.55	5.46	0.050	8.01E-10	6.01E-11	1.81E+12	3.06E+14	241	6.35E+21	3.51E+09	3.42E+08
Mackenzie River	Mackenzie	67°27'24.27"	133°45'46.42"	27	14.76	1.45	5.46	0.050	5.70E-10	5.63E-11	1.81E+12	3.06E+14	241	4.52E+21	2.50E+09	3.09E+08
2011																
Pelly River	Pelly	62°49'44.19"	136°34'58.50"	1539	101.20	6.71	0.84	0.002	2.53E-08	1.68E-09	4.90E+10	2.21E+13	320.5	2.24E+21	4.56E+10	4.42E+09
Pelly River	Pelly	62°49'44.19"	136°34'58.50"	1539	105.70	8.80	0.84	0.002	2.64E-08	2.20E-09	4.90E+10	2.21E+13	320.5	2.33E+21	4.76E+10	5.21E+09
Stewart River	Stewart	63°27'12.54"	136°56'27.92"	1501	54.80	4.61	0.80	0.013	1.44E-08	1.24E-09	5.10E+10	2.68E+13	336.5	1.47E+21	2.88E+10	3.17E+09
Moose Creek	Stewart	63°30'29.00"	137° 1'21.00"	1515	133.90	8.30	1.59	0.011	1.78E-08	1.11E-09	4.26E+08	1.24E+11	336.5	1.66E+19	3.90E+10	3.66E+09
N. Klondike R	N. Klondike	64° 30'20.83"	138° 13'30.56"	3378	4.20	2.42	0.51	0.011	1.72E-09	9.94E-10	1.10E+09	4.10E+11	320	1.72E+18	1.57E+09	9.08E+08
Black Shale Creek	N. Klondike	64°30'21.00"	138°13'9.00"	3375	6.30	2.62	0.42	0.006	3.17E-09	1.32E-09	1.63E+07	4.40E+09	320	2.77E+16	1.70E+09	7.16E+08

Site Name	Watershed	Latitude	Longitude	Elevation (ft)	^{129}I Concentration (10^6 atoms/L)	±	^{127}I (ppb)	±	^{129}I / ^{127}I	±	Watershed Area (m^2)	Discharge (L/yr)	Annual Precipitation (L/m^2)	Total Yearly Export (atoms/yr)	Yearly Export ($atoms/m^2/yr$)	±
Engineer Creek	Ogilvie	65° 6'3.20"	138°21'19.82"	2604	61.90	5.71	0.86	0.011	1.52E-08	1.41E-09	6.81E+08	3.68E+12	300	2.28E+20	3.35E+11	3.89E+10
Engineer Creek	Ogilvie	65° 8'36.36"	138°20'8.97"	2818	50.20	3.61	0.68	0.004	1.56E-08	1.13E-09	6.81E+08	1.70E+11	300	8.54E+18	1.25E+10	2.74E+10
Red Creek	Ogilvie	65° 9'34.05"	138°22'12.42"	2492	74.30	6.51	0.66	0.018	2.36E-08	2.17E-09	8.40E+07	2.10E+10	300	1.56E+18	1.86E+10	2.09E+09
RC East Stream	Ogilvie	65° 9'10.34"	138°22'34.72"	3000	46.90	5.41	0.94	0.015	1.05E-08	1.22E-09	8.40E+07	2.10E+10	300	9.85E+17	1.17E+10	1.59E+09
RC Above slump	Ogilvie	65° 7'58.65"	138°24'18.21"	3000	55.00	3.81	0.94	0.012	1.23E-08	8.68E-10	8.40E+07	2.10E+10	300	1.15E+18	1.37E+10	1.36E+09
James Creek	Peel	67°08'12.7"	136°00'19.30"	2196	18.50	3.81	0.53	0.004	7.30E-09	1.50E-09	5.38E+07	1.25E+10	297.7	2.31E+17	4.29E+09	9.35E+08
Alexandra Bay	Alexandra Bay	79°	76°		74.90	9.30										
Tanquary Fjord Creek	Tanquary Fjord Creek	81°23'	76°87'		160.20	8.11										
2012																
North Klondike River	N. Klondike	64° 30'20.83"	138° 13'30.56"	3378	0.60	1.14	1.51	0.013	8.33E-11	1.59E-10	1.10E+09	4.10E+11	320	2.45E+17	2.23E+08	4.24E+08
Black Shale Creek	N. Klondike	64°30'21.00"	138°13'9.00"	3375	-0.40	1.33	0.92	0.003			1.63E+07	4.40E+09	320			
Red Creek	Ogilvie	65° 9'34.05"	138°22'12.42"	2492	7.00	1.80	1.04	0.004	1.42E-09	3.65E-10	8.40E+07	2.10E+10	300	1.47E+17	1.75E+09	3.51E+08
Engineer Creek	Ogilvie	65° 8'36.36"	138°20'8.97"	2604	3.25	1.17	1.26	0.008	5.44E-10	1.96E-10	6.81E+08	3.68E+12	300	1.19E+19	1.76E+10	2.20E+08
Ogilvie River	Ogilvie	65°21'45.13"	138°18'0.56"	1945	14.88	1.70	1.29	0.004	2.43E-09	2.76E-10	7.13E+09	1.71E+12	300	2.55E+19	3.57E+09	4.66E+08
Eagle River	Eagle	66°26'35.80"	136°42'49.30"	1072	3.80	0.94	1.43	0.008	5.60E-10	1.39E-10	1.03E+10	3.68E+12	417	1.40E+19	1.36E+09	6.45E+09
James Creek	Peel	67°08'12.7"	136°00'19.30"	2196	1.40	0.94	1.25	0.009	2.35E-10	1.59E-10	5.38E+07	1.25E+10	297.7	1.74E+16	3.24E+08	4.79E+08

Table A1: Table of raw data for samples collected across northern Canada in 2010, 2011, 2012

Contrary to the general trend observed for 2011 in Figures A1, A2 the ^{129}I concentrations North Klondike River, Black Shale Creek and James Creek did not increase substantially between 2010 and 2011 although the $^{129}I/^{127}I$ ratio did increase slightly, due to a slight decrease in the concentration of ^{127}I in 2011. One probable reason for this discrepancy is that these rivers have a large groundwater component in discharge as evidenced by the presence of aufeis during winter and which during the later summer is an important contributor to discharge [*Lapp*, 2015]. Furthermore, two samples of groundwater in 2010, Sulphur Spring and Blackwater Spring which were both collected directly from discharge points show similar ^{129}I concentrations and ratios to one another as well as to the North Klondike River, Black Shale Creek and James Creek.

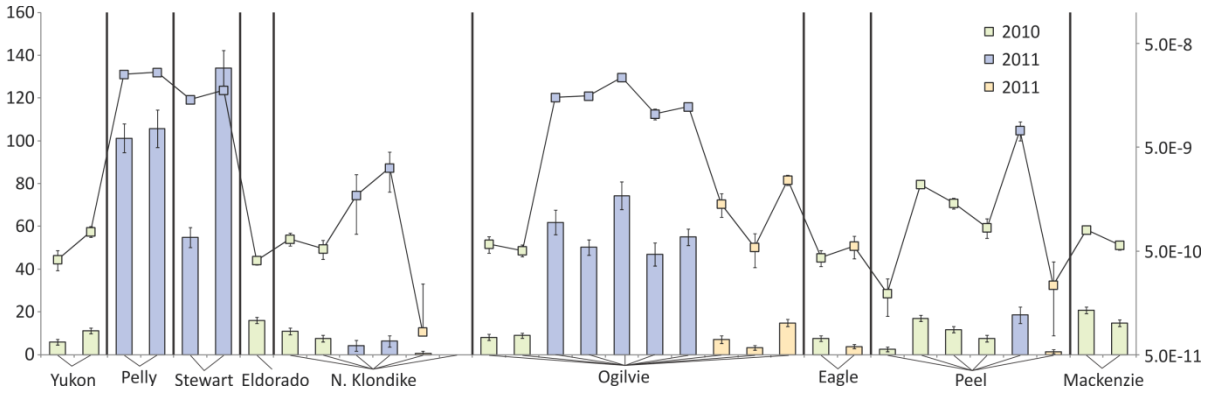

Figure A2: ^{129}I concentrations and $^{129}I/^{127}I$ ratios for all Yukon and NWT samples. Samples are sorted according to latitude with the most southerly catchment (Yukon) progressing to the most northerly (Mackenzie). Samples from smaller sub-watersheds are grouped into a single regional watershed to make inter-annual comparison more applicable.

Measurements of ^{129}I, ^{127}I and the $^{129}I/^{127}I$ ratio in selected watersheds in 2012 were performed to determine if the effect of FNDA had persisted or if pre-FDNA conditions had returned. Results show that pre-FDNA conditions, very similar to 2010, were reasserted in 2012 across the Yukon. Indeed, the mean ^{129}I concentration in 2012 was $5.5 \pm 5.3 \times 10^{6}$

atoms/L and a t-test shows no significant difference between 2010 and 2012 ($p=0.07$, $\alpha=0.05$). Furthermore, the $^{129}I/^{127}I$ ratio was essentially identical that of 2010 at $8.8 \pm 8.9 \times 10^{-10}$. Detailed sampling of a watershed near Whitehorse also shows that ^{129}I levels were low (Chapter 4). The rapid recovery of these catchments shows that the persistence of the elevated ^{129}I in streamflow from FDNA is short despite its long half life. The return of these catchments to background conditions within a single year is encouraging as it suggests future releases of ^{129}I may also behave similarly reducing the environmental impact of such releases and their dispersion. However, the precise fate of the FDNA-derived ^{129}I is unknown. It is probable that dilution and attenuation/storage in the catchment were the two major factors in reducing the ^{129}I concentration. Spring snowmelt would be expected to have a low ^{129}I concentration compared to FDNA contaminated precipitation and freshet would then flush the watershed with new, low ^{129}I water. Attenuation and retardation of ^{129}I during transport is also a key process that would reduce ^{129}I concentrations in discharge over time. Indeed, the affinity of ^{129}I for organic matter would help attenuate ^{129}I during transport within the watershed and then once in discharge loss on particulate matter and dilution with unaffected water sources lower the ^{129}I concentration, particularly over the winter when groundwater discharge is the only source of water in the catchment.

Neither catchment area nor discharge we correlated with ^{129}I concentrations for any of the periods sampled. However, in 2011 the ^{129}I concentration was negatively correlated with both latitude ($r=-0.59$, $\alpha=0.05$) and elevation ($r=-0.77$, $\alpha=0.05$) and positively correlated with ^{127}I concentrations ($r=0.8$, $\alpha=0.05$) as well. These correlations were not applicable in 2010 or 2012 suggesting they may be due to the short lived input of

atmospheric ^{129}I from Fukushima in 2011, which was deposited over a short time period and was certainly affected by the trajectory of the specific air parcels carrying the ^{129}I. Thus drawing significant conclusions about the dependence of ^{129}I distribution based on these factors is tenuous as it appears the deposition of ^{129}I is affected more by its source and air trajectories, which vary greatly, than by the physical characteristics of the catchments.

Mass flux estimates of ^{129}I in discharge increased substantially in 2011 in all watersheds due to the much higher concentration of ^{129}I, which when normalized to catchment size, increased from 1-3 orders of magnitude. Indeed, Engineer Creek, which is a tributary of the Ogilvie River, had a mass flux of $3.4 \pm 0.4 \times 10^{11}$ atoms/m^2/yr in 2011. The decrease in ^{129}I concentrations in 2012 was also reflected in the mass flux as levels dropped to around those measured in 2010. There are several assumptions relating the calculation of mass flux that increase the uncertainty of these measurements. These are primarily caused by the paucity of reliable data for precipitation and evapotranspiration for each catchment which in turn yield discharge measurements that are not necessarily exact. Furthermore, the calculation of annual mass flux using only a single sample to represent the entire year is a significant assumption and therefore should only be used as an estimate of the order of magnitude. Given the large degree of uncertainty associated with several steps in the mass flux calculation looking for correlations between mass flux and physical or chemical watershed parameters is an unsupported use of the data in many cases. In rivers that do have accurate measurements for discharge this application is possible and they may also provide a comparison to rivers of a similar catchment size or latitude which lack the necessary data on climate and discharge.

Conclusions

Additional sampling of rivers throughout northwest Canada in 2011 showed significant increases in ^{129}I and correspondingly, the $^{129}I/^{127}I$ ratio and mass fluxes. These increases are attributed to long distance transport of ^{129}I from the Fukushima-Daiichi Nuclear Accident. This input produced relatively short-lived responses in the rivers sampled as concentration and ratios declined to pre-FDNA levels in all 2012 samples suggesting that the input of ^{129}I from Fukushima had been flushed through the watersheds or completely attenuated and no longer had an effect on discharge.

References

Health Canada (2014), Radiation Monitoring Data and the Nuclear Emergency in Japan, Available from: http://www.hc-sc.gc.ca/hc-ps/ed-ud/respond/nuclea/data-donnees-eng.php

Herod, M. N., I. D. Clark, W. E. Kieser, S. Agosta, and X.-L. Zhao (2013), 129I dispersion and sources in Northwest Canada, *Nucl. Instruments Methods Phys. Res. Sect. B Beam Interact. with Mater. Atoms*, *294*, 552–558, doi:10.1016/j.nimb.2012.06.018.

Lapp, A. (2015), Seasonal Variability of Groundwater Contribution to Watershed Discharge in Discontinuous Permafrost in the North Klondike River Valley , Yukon, University of Ottawa.

Moran, J. E., S. D. Oktay, and P. H. Santschi (2002), Sources of iodine and iodine 129 in rivers, *Water Resour. Res.*, *38*(8), 1–10.

Sheppard, S. C., and M. Herod (2012), Variation in background concentrations and specific activities of 36Cl, 129I and U/Th-series radionuclides in surface waters, *J. Environ. Radioact.*, *106*, 27–34, doi:10.1016/j.jenvrad.2011.10.015.

Snyder, G., and U. Fehn (2004), Global distribution of 129I in rivers and lakes: implications for iodine cycling in surface reservoirs, *Nucl. Instruments Methods Phys. Res. Sect. B*

Beam Interact. with Mater. Atoms, *223-224*, 579–586, doi:10.1016/j.nimb.2004.04.107.

Steinhauser, G. (2014), Fukushima's Forgotten Radionuclides: A Review of the Understudied Radioactive Emissions., *Environ. Sci. Technol.*, *48*(9), 4649–4663, doi:10.1021/es405654c.

Xu, S., S. P. H. T. Freeman, X. Hou, A. Watanabe, K. Yamaguchi, and L. Zhang (2013), Iodine isotopes in precipitation: temporal responses to 129I emissions from the Fukushima nuclear accident, *Environ. Sci. Technol.*, doi:10.1021/es401527q.

APPENDIX B: INFORMATION, FIGURES AND TABLES OF RAW DATA SUPPLEMENTARY TO CHAPTER 4.

Calculating annual ^{129}I import and export in Wolf Creek discharge

The mass import to the WCRB was calculated using Eqn. 2. For ^{129}I mass import during the sampling period from June – October, 2012, which is the first term in Eqn 2, measurements of ^{129}I were made in rain. In order to obtain the most accurate mass flux in rain the ^{129}I input was calculated as the product of the known quantity of precipitation in a given month and the mean ^{129}I concentration for samples taken in that month (Supplementary Table B3). In this way the effect of monthly variability in both precipitation quantity and ^{129}I concentrations are accounted for as accurately as possible.

The second term in Eqn 2 represents the ^{129}I mass flux from November 2011 to June 2012. No samples were collected during this time. It is assumed that the ^{129}I concentration in snow that fell during the winter of 2011-2012 was constant. The only time series of ^{129}I in snow in literature shows that the concentration was far lower than precipitation and was relatively constant over time [*Buraglio et al.*, 2001]. Therefore, the ^{129}I concentration in the single snow sample (3.6×10^6 atoms/L) was used. For April and May, during which no precipitation samples were collected, but all fell as rain, the mean ^{129}I concentration of all measured precipitation samples was used (38.5×10^6 atoms/L).

Combined these two periods represent the entire water year for the catchment, despite only being 11 months of actual time, as precipitation that fell prior to November 2011 was primarily as rain and temperatures were higher than 0°C and therefore was not stored. However, once snow began to accumulate it was assumed to represent winter storage and therefore its contribution to ^{129}I mass flux is not transferred to discharge until

the following spring of 2012. The assumption also applies to precipitation as of October 2012 as all precipitation from that point fell as snow and was therefore assumed to be stored until 2013.

The total ^{129}I export during the sampling period (Supplementary Table B1) was calculated using Eqn. 3 by taking the product of the mean stream flow data for each sampling interval and the ^{129}I concentration of each sampling interval. The ^{129}I export per sampling interval can then be summed to find the total ^{129}I export for the sampling period, which spanned 187 days, without masking the influence of the varying water sources and their ^{129}I concentrations on Wolf Creek discharge. For the remaining 178 days of the year Wolf Creek was assumed to be at baseflow and fed solely by deep groundwater. Therefore, the mean ^{129}I concentrations of first three samples, which best represented groundwater ^{129}I concentrations, were used. Discharge was also assumed to be stable at 0.4 m^3/s [*Janowicz et al.*, 2004]. These two results were then added to obtain the ^{129}I mass export for the entire year.

^{129}I extraction from water samples

Samples were precipitated as silver iodide using an NaI carrier however a summary of the technique will be provided here as some slight modifications were made. Approximately 200mL aliquots of each water sample were used and accurately weighed. The samples were first acidified to ~pH 1 using 6N HNO_3. 2 mg of I as NaI carrier, with a $^{129}I/^{127}I$ ratio of $1.56 \pm 0.06 \times 10^{-13}$ was then added and the precise weight recorded for later correction. 1 mL of 1M $NaHSO_3$ was also added as a reducing agent. The samples were then shaken for 30 minutes and left overnight to equilibrate. The samples were then transferred

to a 250 mL separatory funnel and approximately 10-20mL of hexane and 0.1mL of 6M $NaNO_2$ were added. This oxidized I^- in the sample to I_2 causing it to partition into the hexane. The hexane was then collected and this process was repeated with fresh hexane up to 5 times or until the hexane remained clear. The collected hexane was then poured back into the separatory funnel and 10mL of MilliQ deionized water and 1M $NaHSO_3$ were added reducing the iodine in the hexane and returning it to the water phase. The water was then acidified to pH 1 using concentrated HNO_3 and 0.1mL of 1M $AgNO_3$ was added to form an AgI precipitate that was then centrifuged and dried. The precipitated AgI was mixed with high purity Nb powder with a Nb:AgI ratio of ~4:1 by volume. The two powders were well mixed and an aliquot was transferred to a copper AMS target and compressed. The targets were analyzed at the University of Ottawa's Andre E. Lalonde 3MV Accelerator Mass Spectrometry facility. Standards and Nb blanks were run every 10 samples. Sample results were corrected for the Nb blank and ^{129}I introduced by the NaI carrier. Duplicate analyses of several samples both from separate sample preparations and duplicate targets were all within 1σ and mean values for these analyses are reported here.

Replacement of missing data using linear regression

Several methods of regression were compared with the goal of replacing missing data including: partial least squares regression using K concentrations, linear regression using K concentrations, ^{18}O concentrations, and the K/Ca molar ratio. ^{18}O, K and K/Ca were chosen for regression analysis as they have the highest Pearson r correlations with ^{129}I of -0.63, 0.70 and 0.71 respectively. These methods are compared to the actual ^{129}I measurements in Supplementary Figure B1 and show generally good agreement with the

results and one another. Therefore, we can use this data with confidence to model the missing ^{129}I analyses.

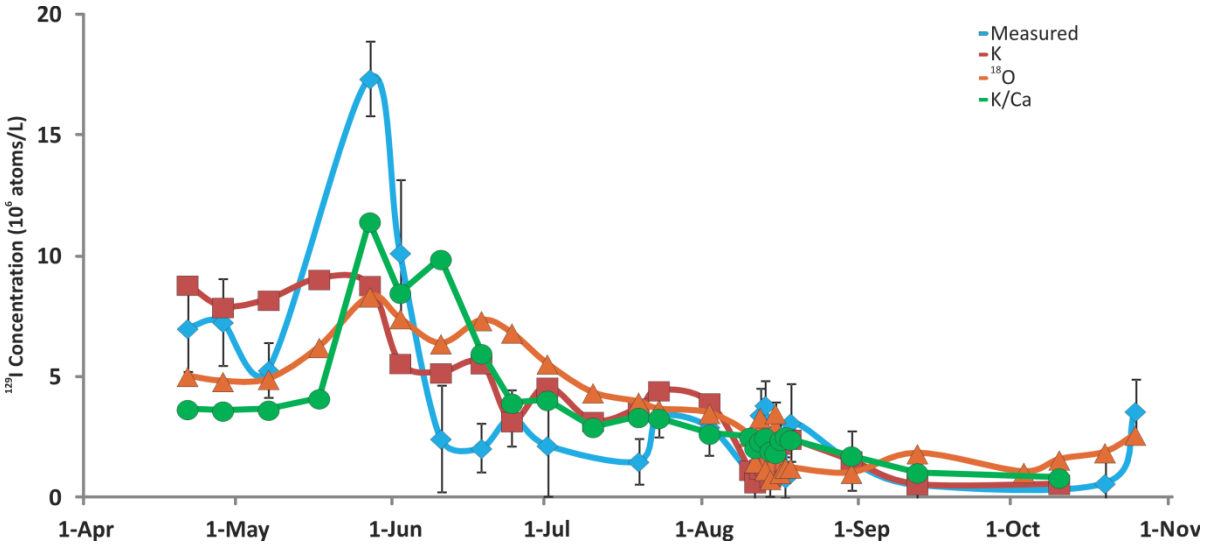

Supplementary Figure B1: Comparison of the results from linear regression of ^{129}I using K, K/Ca and ^{18}O data with the measured concentration of ^{129}I in discharge samples.

Sample preparation of tritium and carbon-14_{DIC}

Tritium activity was analyzed by the electrolytic enrichment method at Isotope Tracer Technologies Inc. in Waterloo, Ontario. 150 ml water samples were deionized by adding mixed bed ion exchange resin and then placed into metal cells for electrolytic enrichment. Enrichment proceeded for about one week until volumes of samples were around 15ml. One gram of sodium peroxide (Na_2O_2) was added water samples before the electrolytic enrichment and water was removed by distillation. The distilled and enriched water samples were counted on the Liquid Scintillation Counters (LSC) by adding the Ultima Gold LLTTM (low level tritium) cocktail. Counting results were reported in Tritium Units (TU)

for tritium concentrations. 1 TU = 3.221 Picocuries/L = 0.11919 Becquerel/L = 1 ^{3}H atom per 10^{8} hydrogen atoms.

CO_2 gas was extracted from DIC, which had previously been extracted from water samples, and then graphitized for ^{14}C analysis by Accelerator Mass Spectrometry (AMS). Samples were prepared using the graphitization line at the Andre E. Lalonde AMS laboratory. Reduced Alfa Aesar iron powder (-200 mesh) was added as catalyst to reduce conversion time from CO_2 to graphite. The graphitization was conducted in a H_2 environment resulting in the production of pure carbon and water. NIST-SRM 4490C oxalic acid powder was used a standard. The $^{14}C/^{12}C$ ratios were measured at the Isotope and Rare Atom Counting Equipment (ISOTrace) Laboratory at the University of Toronto. The Δ14C values were corrected by the $\delta^{13}C$ values analyzed by TIC-TOC.

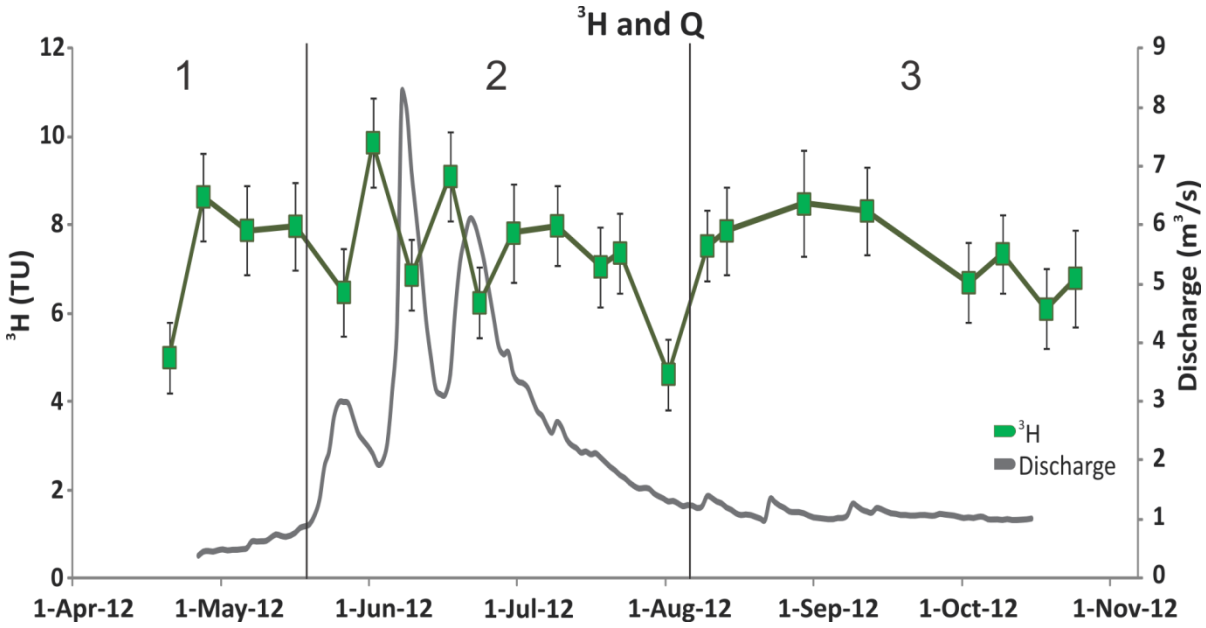

Supplementary Figure B2: Results of tritium analysis in Wolf Creek discharge.

^{129}I Import

Month	Precipitation (L/m^2/month)	^{129}I (10^6 atoms/L)	^{129}I Mass Flux In (atoms/watershed)
Nov-11 α	28.9	3.6	2.02E+16
Dec-11 α	28.7	3.6	2.01E+16
Jan-12 α	20.6	3.6	1.44E+16
Feb-12 α	8.2	3.6	5.73E+15
Mar-12 α	27.8	3.6	1.94E+16
Apr-12	12.8	38.5 β	9.61E+16
May-12	17.2	38.5 β	1.29E+17
Jun-12	31	21 γ	1.27E+17
Jul-12	31.6	29.5 δ	1.82E+17
Aug-12	57.4	61.3 ε	6.86E+17
Sep-12	19	38.5 β	1.43E+17
Sum	**283.2**	**NA**	**1.44E+18**

^{129}I Export

Sample Date	Interval Length (days)	Mean Interval Discharge (m^3/s) ζ	^{129}I Mass Flux Out (atoms/interval)
21-Apr	1	0.42	2.52E+14
28-Apr	7	0.47	2.07E+15
7-May	9	0.66	2.71E+15
17-May	10	1.56	5.00E+15
27-May	10	2.62	3.92E+16
2-Jun	6	3.99	2.10E+16
10-Jun	8	4.49	7.62E+15
18-Jun	8	5.21	7.42E+15
24-Jun	6	4.56	7.79E+15
1-Jul	7	3.00	3.95E+15
10-Jul	9	2.28	6.58E+15
19-Jul	9	1.94	2.27E+15
23-Jul	4	1.54	1.77E+15
2-Aug	10	1.25	3.17E+15
10-Aug	8	1.39	3.56E+15
11-Aug	1	1.36	1.17E+14
12-Aug	1	1.30	3.86E+14
13-Aug	1	1.27	4.22E+14
14-Aug	1	1.20	8.31E+13
15-Aug	1	1.16	2.77E+14
16-Aug	1	1.10	2.04E+14
17-Aug	1	1.07	7.73E+13
18-Aug	1	1.08	2.91E+14
30-Aug	12	1.14	1.79E+15
12-Sep	13	1.08	6.53E+14
3-Oct	21	1.02	6.84E+15
10-Oct	7	0.99	2.23E+15
19-Oct	9	0.99	4.72E+14
25-Oct	6	0.99	1.85E+15
Baseflow	177	0.4	4.02E+16 η
Sum	**365**	**NA**	**1.70E+17**

Supplementary Table B1: Data used to calculate the total mass import and mass export of ^{129}I to the WCRB. Note several values and headings have further information below to explain how they were determined.

Legend

α = All precipitation fell as snow in these months. Thus, the ^{129}I measurement for the interior of the snowpack was used as the concentration for these months. If the concentration in this reservoir was greater this would result in a higher mass input of ^{129}I to the WCRB.

β = Mean value of all ^{129}I measurements in precipitation as no precipitation samples were collected during this time

γ = Mean of three samples from June 10 to June 24

δ = Mean of three samples from June 25 to July 29

ε = Mean of four samples from July 30 to Aug 30

ζ = Calculated as the sum of daily discharge measurements for sampling period divided by length of the sampling period

η = Calculated as: days x discharge x mean ^{129}I concentration of the three earliest samples of discharge

Sample	% Soil Organic Matter	% CaCO3	^{129}I (10^6 atoms/g)	±	^{127}I (ppm)	±	$^{129}I/^{127}I$	±
WCRB S6	82.1	34.6	228.0	22.6	28.4	0.0001	1.70E-09	1.67E-10
WCRB S8	62.2	3.1	174.4	15.7	9.6	0.0004	3.85E-09	3.45E-10
WCRB S4	15.7	0.7	66.9	1.2	2.2	0.0006	6.52E-09	5.08E-11
WCRB S10	8.8	0.6	72.0	2.9	4.9	0.0012	3.12E-09	2.66E-10
WCRB S5	8.6	0.6	19.0	1.2	2.3	0.0023	1.83E-09	1.14E-10
WCRB S1	6.7	0.6	11.8	0.87	2.0	0.0009	1.31E-09	9.12E-11
WCRB S11	3.4	0.6	9.7	2.1	0.8	0.0002	2.95E-09	5.84E-10

Supplementary Table B2: Raw %SOM, ^{129}I, ^{127}I and $^{129}I/^{127}I$ data for soil samples collected throughout the WCRB.

Sample ID	Sample Date	pH	Al	Na	K	Mg	Ca	Fe	Ba	Sr	^{127}I (µg/L)	^{129}I (10^6 atoms/L)	Cl	SO_4	HCO_3	Br (µg/L)	F	S	Si	DOC	DIC	^{13}DIC	%MC	Tritium (^3H)	^{18}O	^2H	$^{129}I/^{127}I$	Charge Balance Error
1	21-Apr		0.01	3.79	0.97	7.7	29.5	0.088	0.066	0.24		7.02	0.26	16.4	105		0.07	6.23	4.90	6.17					-22.3	-169.0	1.21E-10	5%
2	28-Apr	7.8	0.01	3.56	0.91	7.2	28.0	0.009	0.066	0.23	11.36	7.28	0.24	13.8	142	6.98	0.07	5.32	4.79	3.99	21.31	-9.47	90.61	8.6	-22.3	-166.7	1.35E-10	-10%
3	7-May	7.9	0.01	3.61	0.93	7.3	28.4	0.032	0.071	0.24	13.13	5.29	0.56	13.5	107	8.60	0.07	5.12	4.89	2.02	21.87	-8.15	89.56	7.9	-22.3	-167.9	8.51E-11	3%
4	17-May	7.9	0.01	3.50	0.98	7.2	28.5	0.071	0.081	0.25	4.80		0.23	12.2	112	9.25	0.06	4.66	4.90	2.81	21.72	-8.72		8.0	-22.6	-168.6		1%
5	27-May	7.7	0.02	2.07	0.96	4.0	15.5	0.104	0.050	0.14	5.40	17.35	0.21	5.5	61	8.42	0.05	2.17	3.65	5.48	12.31	-11.21	92.73	6.5	-23.1	-170.3	6.77E-10	3%
6	2-Jun	7.5	0.02	2.19	0.77	4.0	15.1	0.073	0.044	0.13		10.14	0.17	6.0	57		0.05	2.31	4.12	4.36	12.92	-12.8	71.91	9.9	-22.9	-169.0	5.92E-10	6%
7	10-Jun	7.6	0.03	1.81	0.75	3.3	13.2	0.074	0.043	0.12		2.46	0.21	5.9	61		0.05	2.25	3.35	8.99	11.69	-12.2	55.78	6.9	-22.6	-167.0	1.12E-10	-5%
8	18-Jun	7.3	0.01	2.54	0.77	4.6	18.5	0.015	0.062	0.17	2.95	2.06	0.27	7.8	69	3.51	0.05	3.02	4.29	3.53	16.23	-12.5	65.92	9.1	-22.8	-169.1	1.47E-10	6%
9	24-Jun	7.4	0.02	2.33	0.62	4.5	18.5	0.035	0.067	0.17	2.93	3.29	0.11	7.7	72	4.10	0.05	3.00	4.09	2.99	15.21	-12.22	72.18	6.2	-22.7	-168.9	2.37E-10	3%
10	1-Jul	7.4	0.01	2.64	0.71	5.1	20.8	0.008	0.075	0.19	3.41	2.18	0.15	9.0	77	6.04	0.05	3.48	4.50	4.33	16.84	-10.93	72.63	7.8	-22.4	-168.5	1.35E-10	5%
11	10-Jul	7.5	0.01	2.70	0.62	5.1	20.9	0.013	0.072	0.19	4.01		0.12	9.3	77	6.44	0.06	3.58	4.53	2.42	16.52	-10.61	79.7	8.0	-22.1	-167.8		5%
12	19-Jul	7.8	0.01	2.72	0.66	5.0	20.9	0.400	0.070	0.18	2.42	1.51	0.13	9.3	78	5.44	0.05	3.63	4.45	4.63	16.54	-11.72	81.21	7.1	-22.1	-168.1	1.31E-10	3%
13	23-Jul	7.8	0.01	2.90	0.70	5.5	22.4	0.055	0.075	0.20	2.11	3.33	0.14	10.0	83	4.87	0.06	3.79	4.46	4.16	17.3	-9.56	76.11	7.4	-22.0	-167.7	3.33E-10	3%
14	2-Aug	7.7	0.01	2.99	0.67	5.6	23.2	0.024	0.074	0.20	2.34	2.94	0.13	10.5	84	4.94	0.06	3.99	4.52	3.54	17.89	-8.7	74.69	4.6	-21.9	-167.5	2.65E-10	5%
15	10-Aug	7.5	0.02	2.59	0.50	4.5	17.7		0.051	0.14	14.72		0.20	10.2	70	8.33	0.11	2.91	3.66	3.13	17.3	-8.35	82.7	7.5	-21.7	-166.9		0%
16	11-Aug		0.01	2.55	0.47	4.5	17.7		0.050	0.14	2.54	1.00	0.20	10.3	83	5.39	0.11	2.88	3.64	4.15					-21.5	-165.9	8.29E-11	-8%
17	12-Aug		0.02	2.56	0.51	4.6	18.3	0.0031	0.053	0.15	4.04	3.44	0.20	10.7	88	5.23	0.12	2.96	3.56	3.46					-21.9	-166.5	1.80E-10	-9%
18	13-Aug		0.02	2.55	0.51	4.6	18.2	0.0088	0.053	0.15	2.49	3.84	0.19	10.7	95	5.05	0.10	3.00	3.58	7.72					-21.4	-166.9	3.26E-10	-13%
19	14-Aug	7.6	0.01	2.59	0.49	4.7	18.6		0.055	0.15	2.51	0.80	0.19	10.8	91	4.76	0.11	3.03	3.68	3.7	18.49	-9.92	79.91	7.9	-21.3	-166.9	6.72E-11	-10%
20	15-Aug		0.02	2.78	0.52	5.0	20.3		0.061	0.17	2.59	2.76	0.19	10.9	87	4.95	0.10	3.30	3.91	3.03					-21.9	-167.0	2.25E-10	-4%
21	16-Aug		0.02	2.84	0.57	5.0	20.3		0.062	0.17	1.89	2.15	0.21	11.1	91	4.82	0.10	3.31	3.91	3.2					-21.4	-167.6	2.40E-10	-6%
22	17-Aug		0.02	2.84	0.58	5.1	20.4		0.061	0.17	2.29	0.84	0.21	11.0	88	5.74	0.11	3.28	3.96	3.46					-21.4	-167.8	7.71E-11	-4%
23	18-Aug		0.02	2.90	0.58	5.1	20.7		0.060	0.17	2.41	3.12	0.20	11.1	92	4.74	0.12	3.34	4.04	7.31					-21.4	-168.1	2.73E-10	-5%
24	30-Aug	7.5	0.02	2.89	0.52	5.2	20.7		0.058	0.17		1.52	0.21	11.4	105		0.10	3.42	4.00	7.78	19.46	-8.87	77.04	8.5	-21.4	-167.6	7.00E-11	-10%
25	12-Sep	7.7		3.02	0.47	5.2	20.5		0.059	0.17	2.94	0.54	0.19	11.2	91	4.93		3.50	3.75	3.69	18.73	-6.7	84.34	8.3	-21.6	-168.0	3.85E-11	-5%
26	3-Oct			1.70	0.14	2.9	9.8		0.026	0.09	6.57		0.13	6.1	101	4.62		1.90	2.51	6.78					-21.4	-167.3		-38%
27	10-Oct	7.7		3.17	0.47	5.4	21.3	0.045	0.058	0.17	2.39		0.20	11.7	131	5.17		3.71	3.90	5.23	18.64	-8.05	86.76	7.4	-21.5	-167.5		-18%
28	19-Oct										2.22	0.61	0.15	7.0	118	4.30				3.77					-21.6	-167.4	5.79E-11	-26%
29	25-Oct			1.73	0.54	2.9	9.7		0.027	0.09		3.59	0.25	15.1	119			4.69	2.57	4.53					-21.7	-166.9	1.36E-10	-48%

Supplementary Table B3: Table of raw data in Wolf Creek Discharge including ^{129}I.

References

Buraglio N, Aldahan A, Possnert Gö, Vintersved I. 129I from the Nuclear Reprocessing Facilities Traced in Precipitation and Runoff in Northern Europe. Environ Sci Technol [Internet]. 2001 Apr;35(8):1579–86. Available from: http://pubs.acs.org/doi/abs/10.1021/es001375n

Janowicz JR, Hedstrom N, Pomeroy J, Granger R, Carey S. Wolf Creek Research Basin water balance studies. North Res Basins Water Balanc. 2004;290(March):195–204.

APPENDIX C: SUPPLEMENTARY MATERIALS FOR CHAPTER 5 INCLUDING SUPPLEMENTARY FIGURES AND COMPLETE TABLES OF DATA.

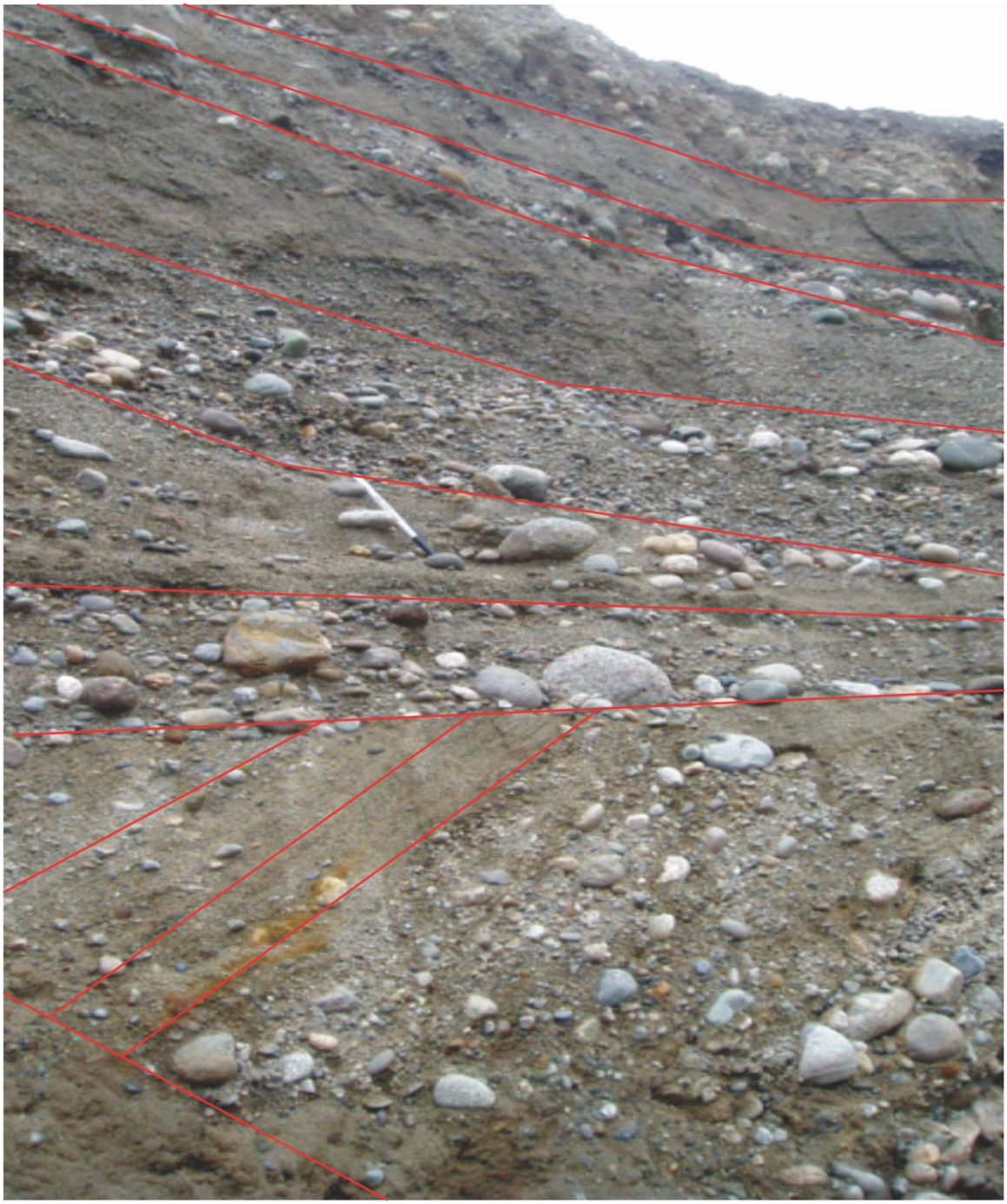

Figure C1: Cross section of ASA sediments at a gravel pit located near ABB-03 and PB-20. Red lines mark lithology or grain size changes observed from the picture. Note the presence of large cobbles and boulders as well as sub-vertical, poorly sorted beds. Pen (17 cm) for scale. Photo taken by Dr. Diana Allen and is used with permission and was also used in [*McArthur et al.*, 2010].

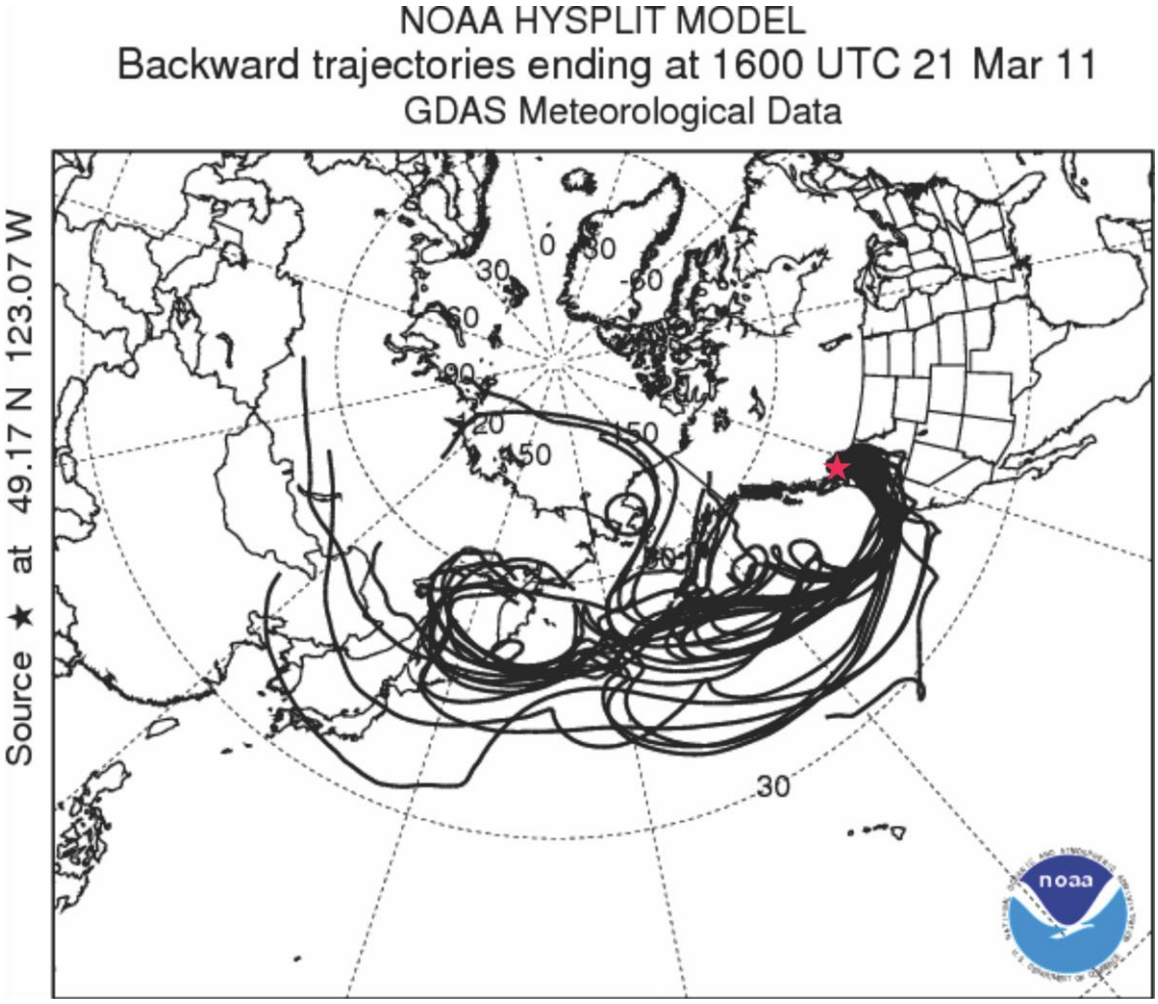

Figure C2: HYSPLIT back trajectory showing the source of air parcels in Vancouver ending March 21, 2011. Note that several trajectories pass over Japan and could have transported radionuclides from Fukushima to Vancouver

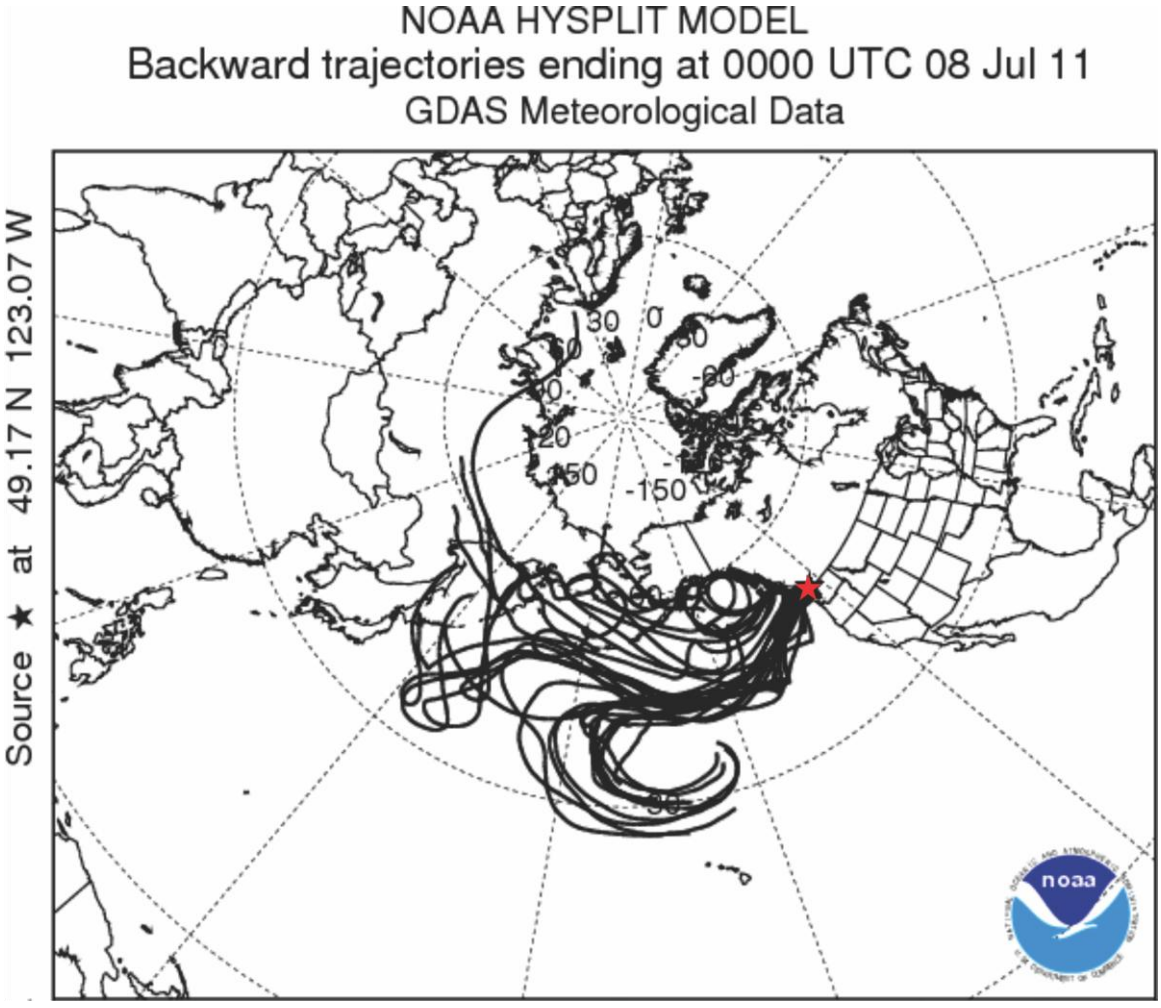

Figure C3: HYSPLIT back trajectory showing the source of air parcels in Vancouver ending July 8, 2011. Several air parcels pass over Russia and Japan and could be transporting a release of ^{129}I from a nuclear fuel reprocessing facility.

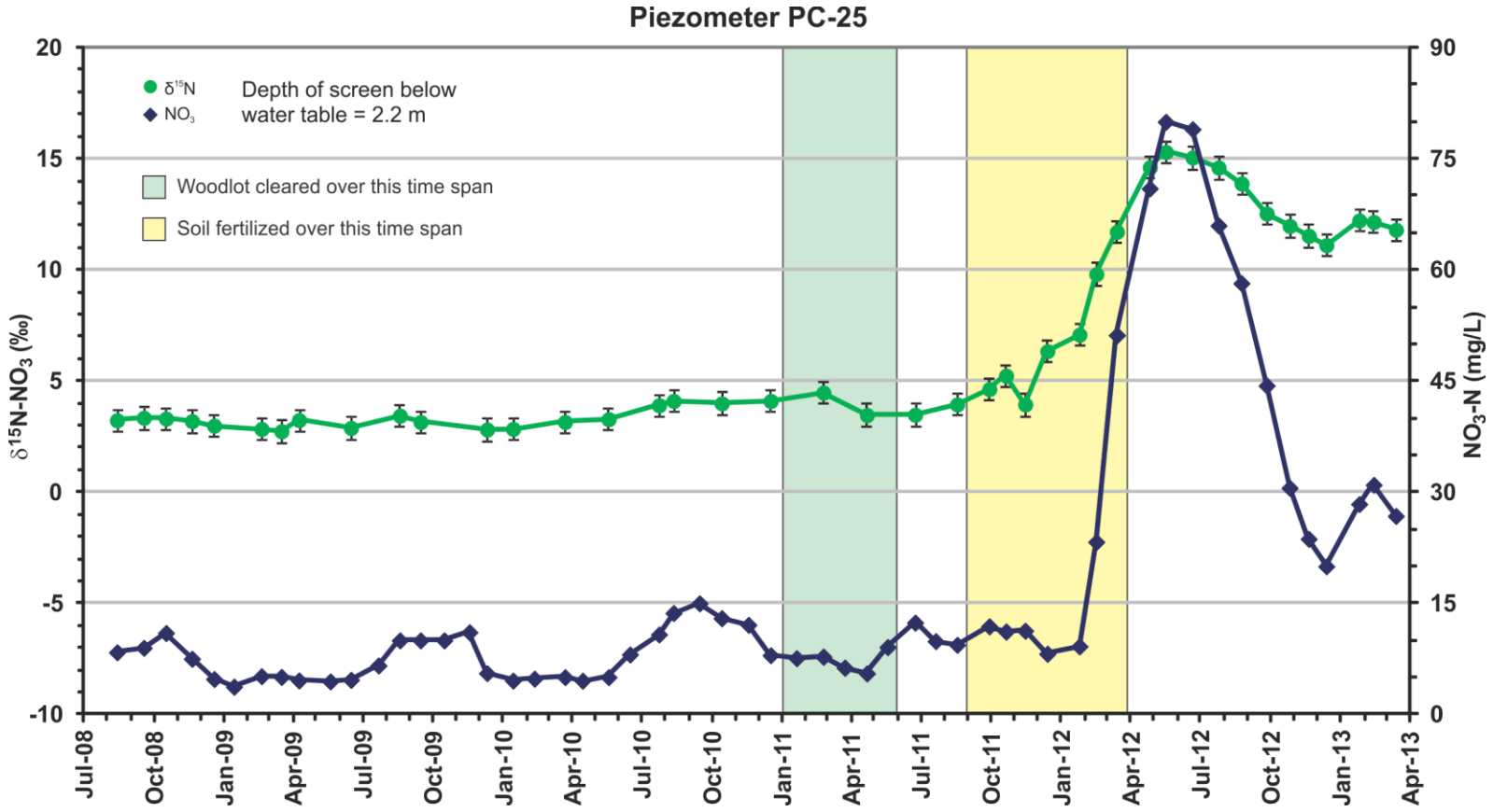

Figure C4 - A land use change involving clearing of an upgradient woodlot and an application of manure occurred in 2011. These changes induced a spike both the nitrate concentration and $\delta^{15}N$ within a few months at the well screen indicating that transport from the ground surface to the well screen was very rapid. The spike persisted for approximately 1 year which is far longer than previous seasonal variation in nitrate concentrations.

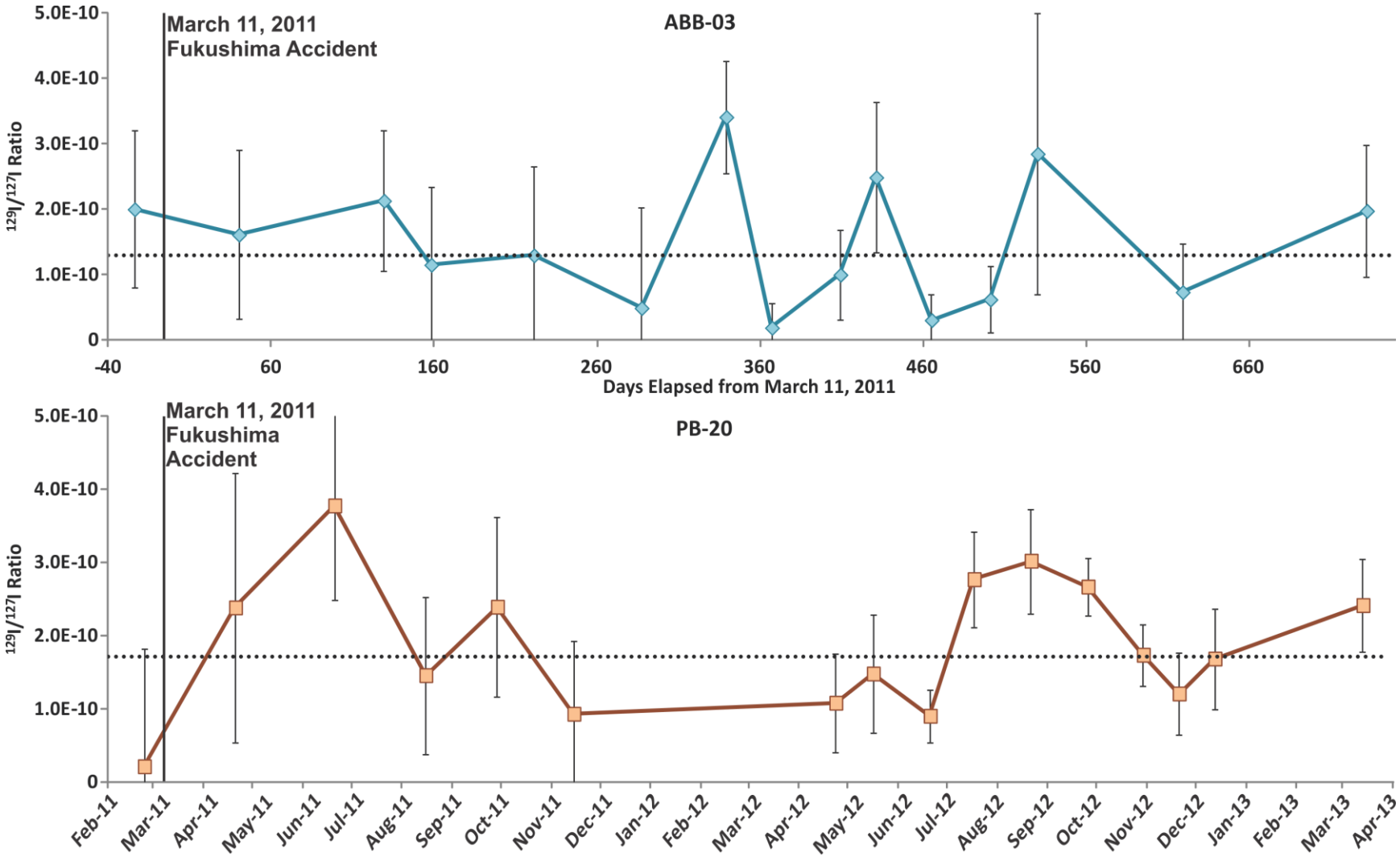

Figure C5: Temporal variation in the $^{129}I/^{127}I$ ratio in groundwater in ABB03 and PB20. The solid vertical line shows the date of the Fukushima accident and the dashed horizontal line shows the median of each dataset respectively.

Depth Interval (metres)	Sediment Type
ABB-03	
0.0 - 3.35	?
3.35 - 7.62	grey sand & coarse gravel
7.62 - 8.23	grey sand: very fine to coarse gravel
8.23 - 9.14	grey sand: sorted coarse gravel
9.14 - 10.06	grey sand: fine to medium gravel
10.06 - 17.07	interbedded fine to medium gravel and grey sand
17.07 - 17.37	grey sand & gravel with cobbles
17.37 - 17.68	grey sand & coarse gravel
16.68 - 17.68	#10 slotted screen
PB-20	
0.0 - 0.61	top soil
0.61 - 4.4	sand and gravel with lenses of sand
3.4 - 4.4	#20 slotted screen

Table C1: Lithology of groundwater wells ABB03 and PB-20

Start	End	Recharge Period	Sampling Interval (days)	Abbotsford Airport Precipitation (mm)	Evapotranspiration (mm)	Difference (P-ET)	Recharge Applied to Ground Surface (m)	^{129}I Concentration (x 10^6 atoms/L)	Irrigation Corrected Washout (10^9 atoms/m^2/interval)	^{129}I Concentration in Recharge (g/m^3)
18-Mar-11	25-Mar-11	1	7	14	13	1	0.00014	210.7	2.9	6.32E-10
26-Mar-11	1-Apr-11	2	7	65	11	54	0.00771	40.0	2.6	1.03E-11
2-Apr-11	8-Apr-11	3	7	52	11	41	0.00586	52.7	2.7	1.43E-11
9-Apr-11	15-Apr-11	4	7	34	13	21	0.00300	83.5	2.8	2.89E-11
16-Apr-11	21-Apr-11	5	5	13	12	1				
22-Apr-11	29-Apr-11	6	7	54	19	35	0.00500	42.1	2.3	1.39E-11
30-Apr-11	6-May-11	7	7	18	17	1	0.00014	78.2	1.4	3.02E-10
7-May-11	13-May-11	8	7	56	19	37	0.00529	24.4	1.4	7.90E-12
14-May-11	20-May-11	9	7	20	22	-2	0.00371	82.6	1.7	1.43E-11
21-May-11	3-Jun-11	10	14	32	38	-6	0.00357	66.0	2.3	9.72E-12
4-Jun-11	16-Jun-11	11	12	8	46	-38	0.00083		0.1	2.88E-12
17-Jun-11	24-Jun-11	12	8	26	26	0	0.00400	36.5	1.0	6.96E-12
25-Jun-11	30-Jun-11	13	6	8	20	-12	0.00200	46.7	0.4	7.86E-12
1-Jul-11	8-Jul-11	14	8	7	34	-27	0.00063	310.7	2.3	9.70E-11
9-Jul-11	15-Jul-11	15	7	33	25	8	0.00514	58.0	2.0	1.18E-11
16-Jul-11	22-Jul-11	16	7	25	21	4	0.00457	41.8	1.1	7.53E-12

23-Jul-11	18-Aug-11	17	26	11	101	-90	0.00054		0.3	4.46E-12
19-Aug-11	25-Aug-11	18	7	16	27	-11	0.00243	63.7	1.1	1.38E-11
26-Aug-11	14-Sep-11	19	19	0	72	-72	0.00021		0.2	1.14E-11
15-Sep-11	22-Sep-11	20	7	38	17	21	0.00300	71.8	2.7	2.78E-11
23-Sep-11	29-Sep-11	21	7	53	15	38	0.00543	35.5	1.9	1.06E-11
30-Sep-11	6-Oct-11	22	7	26	9	17	0.00243	103.3	2.7	3.38E-11
7-Oct-11	13-Oct-11	23	7	32	9	23	0.00329	38.7	1.2	1.15E-11
14-Oct-11	19-Oct-11		5	1	10	-9				
20-Oct-11	27-Oct-11	24	7	24	8	16	0.00229	40.6	1.0	1.31E-11
4-Nov-11	10-Nov-11	26	7	7	6	1	0.00014	65.9	0.5	9.89E-11
11-Nov-11	17-Nov-11	27	7	64	4	60	0.00857	31.3	2.0	7.16E-12
18-Nov-11	24-Nov-11	28	7	62	4	58	0.00829	23.0	1.4	5.27E-12
25-Nov-11	1-Dec-11	29	7	21	4	17	0.00243	24.5	0.5	6.48E-12
2-Dec-11	7-Dec-11		5	3	3	0				
8-Dec-11	15-Dec-11	30	7	1	3	-2	0.00014	119.4	0.1	2.61E-11
16-Dec-11	22-Dec-11	31	7	18	3	15	0.00214	44.4	0.8	1.14E-11
23-Dec-11	29-Dec-11	32	7	70	4	66	0.00943	26.5	1.8	6.01E-12
30-Dec-11	5-Jan-12	33	7	42	3	39	0.00557	29.6	1.2	6.82E-12
6-Jan-12	12-Jan-12	34	7	5	3	2	0.00029	41.8	0.2	2.24E-11
13-Jan-12	19-Jan-12	35	7	34	3	31	0.00443	88.7	3.0	2.09E-11

Start	End	Recharge Period	Sampling Interval (days)	Abbotsford Airport Precipitation (mm)	Evapotranspiration (mm)	Difference (P-ET)	Recharge Applied to Ground Surface (m)	^{129}I Concentration (x 10^6 atoms/L)	Irrigation Corrected Washout (10^9 atoms/m^2/interval)	^{129}I Concentration in Recharge (g/m^3)
20-Jan-12	26-Jan-12	36	7	59	4	55	0.00786	40.3	2.4	9.26E-12
27-Jan-12	2-Feb-12	37	7	59	4	55	0.00786	33.6	2.0	7.71E-12
3-Feb-12	9-Feb-12	38	7	6	7	-1	0.00014	81.6	0.6	1.24E-10
10-Feb-12	16-Feb-12	39	7	16	5	11	0.00157	38.7	0.6	1.21E-11
17-Feb-12	23-Feb-12	40	7	60	5	55	0.00786	10.9	0.6	2.54E-12
24-Feb-12	1-Mar-12	41	7	54	6	48	0.00686	31.2	1.7	7.52E-12
2-Mar-12	8-Mar-12	42	7	46	7	39	0.00557	30.1	1.4	7.61E-12

Table C2: Table of vadose zone modelling input data used in VS2DTI.

Location	Sample ID	Latitude (N), Longitude (W)	Sampling Start	Sampling End	Sampling Range (days)	Cumulative Days Since 11-Mar-11	^{127}I (ppb)	^{129}I (10^6 atoms/L)	±	$^{129}I/^{127}I$ (10^{-9})	±
Vancouver											
	VP1	49°17'13.6", 123°07'3.9"	18-Mar-11	25-Mar-11	7	11	4.07	210.68	8.21	10.91	0.43
	VP2		25-Mar-11	1-Apr-11	7	18	3.34	40.01	2.42	2.52	0.15
	VP3		1-Apr-11	8-Apr-11	7	25	3.58	52.67	3.51	3.10	0.21
	VP4		8-Apr-11	15-Apr-11	7	32	4.23	83.46	5.21	4.15	0.26
	VP7		15-Apr-11	22-Apr-11	7	39	4.52			0.00	
	VP5		22-Apr-11	29-Apr-11	7	46	4.07	42.06	2.92	2.17	0.15
	VP8		29-Apr-11	6-May-11	7	53	4.18	78.23	3.21	3.94	0.16
	VP6		6-May-11	13-May-11	7	60	3.65	24.35	2.12	1.40	0.12
	VP9		13-May-11	20-May-11	7	67	4.26	82.63	3.22	4.08	0.16
	VP10		20-May-11	3-Jun-11	14	77	3.93	65.97	2.92	3.53	0.16
	VP11		3-Jun-11	16-Jun-11	13	91	5.03				
	VP12		16-Jun-11	24-Jun-11	8	101	4.66	36.52	2.92	1.65	0.13
	VP13		24-Jun-11	30-Jun-11	6	108	4.14	46.67	3.31	2.37	0.17
	VP14		30-Jun-11	8-Jul-11	8	115	4.90	310.74	8.36	13.38	0.36
	VP40		8-Jul-11	15-Jul-11	7	123	3.59	57.96	3.51	3.40	0.21

VP15	15-Jul-11	22-Jul-11	7	130	3.86	41.84	3.51	2.28	0.19
VP16	22-Jul-11	18-Aug-11	27	147	4.36			0.00	
VP17	18-Aug-11	25-Aug-11	7	164	5.02	63.69	3.11	2.67	0.13
VP18	15-Sep-11	22-Sep-11	7	192	4.15	71.76	3.27	3.64	0.17
VP35	22-Sep-11	29-Sep-11	7	199	3.84	35.54	2.91	1.95	0.16
VP19	29-Sep-11	6-Oct-11	7	206	4.23	103.26	4.54	5.14	0.23
VP33	6-Oct-11	13-Oct-11	7	213	3.72	38.68	2.61	2.19	0.15
VP38	20-Oct-11	27-Oct-11	7	227	5.49	40.63	2.91	1.56	0.11
VP21	27-Oct-11	3-Nov-11	7	234	3.86	52.51	3.11	2.86	0.17
VP42	3-Nov-11	10-Nov-11	7	241	4.04	65.94	2.71	3.44	0.14
VP22	10-Nov-11	17-Nov-11	7	248	3.82	31.33	2.62	1.72	0.14
VP31	17-Nov-11	24-Nov-11	7	255	4.56	23.03	2.22	1.06	0.10
VP28	24-Nov-11	1-Dec-11	7	262	5.02	24.49	3.71	1.03	0.16
VP23	8-Dec-11	15-Dec-11	7	276	4.64	119.39	11.71	5.43	0.53
VP27	15-Dec-11	22-Dec-11	7	283	4.35	44.35	1.92	2.14	0.09
VP37	22-Dec-11	29-Dec-11	7	290	4.12	26.47	2.12	1.35	0.11
VP34	29-Dec-11	5-Jan-12	7	297	3.54	29.57	2.61	1.76	0.16
VP24	5-Jan-12	12-Jan-12	7	304	4.37	41.81	2.42	2.01	0.12
VP39	12-Jan-12	19-Jan-12	7	311	3.73	88.74	5.11	5.01	0.29

Location	Sample ID	Latitude (N), Longitude (W)	Sampling Start	Sampling End	Sampling Range (days)	Cumulative Days Since 11-Mar-11	^{127}I (ppb)	^{129}I (10^6 atoms/L)	±	$^{129}I/^{127}I$ (10^{-9})	±
	VP29		19-Jan-12	26-Jan-12	7	318	9.18	40.30	1.92	0.92	0.04
	VP36		26-Jan-12	2-Feb-12	7	325	2.85	33.56	2.42	2.48	0.18
	VP25		2-Feb-12	9-Feb-12	7	332	4.26	81.60	3.78	4.04	0.19
	VP32		9-Feb-12	16-Feb-12	7	339	3.53	38.71	2.51	2.31	0.15
	VP41		16-Feb-12	23-Feb-12	7	346	3.39	10.87	1.13	0.67	0.07
	VP30		23-Feb-12	1-Mar-12	7	353	3.86	31.19	1.82	1.70	0.10
	VP 26		1-Mar-12	8-Mar-12	7	360	4.57	30.10	2.22	1.39	0.10
Saturna Island											
	SAT1	48°46'27.5", 121°07'44.0"	13-Mar-11	13-Mar-11	1	2	3.97	13.19	2.21	0.70	0.12
	SAT2		17-Mar-11	20-Mar-11	3	8	5.13	220.65	8.60	9.07	0.35
	SAT3		21-Mar-11	28-Mar-11	7	14	4.68	203.48	9.20	9.17	0.42
	SAT4		29-Mar-11	31-Mar-11	2	19	4.94	118.93	5.31	5.08	0.23
	SAT5		1-Apr-11	1-Apr-11	1	21	3.12	37.15	2.81	2.51	0.19
	SAT6		15-Apr-11	20-Apr-11	5	38	3.43	83.99	4.42	5.15	0.27
	SAT7		30-Apr-11	2-May-11	2	51	3.59	66.92	4.12	3.92	0.24

Location	Sample ID	Latitude (N), Longitude (W)	Sampling Start	Sampling End	Sampling Range (days)	Cumulative Days Since 11-Mar-11	^{127}I (ppb)	^{129}I (10^6 atoms/L)	±	$^{129}I/^{127}I$ (10^{-9})	±
NADP-WA19											
	NADP1	48°32'25.1", 121°26'45.6"	23-Feb-10	30-Mar-10	35	-364	6.04	25.77	3.01	0.90	0.11
	NADP2		24-Aug-10	28-Sep-10	35	-182	2.83	53.01	3.82	3.94	0.28
	NADP3		1-Feb-11	8-Mar-11	35	-21	5.63	30.16	2.82	1.13	0.11
	NADP4		15-Mar-11	26-Apr-11	42	25	3.20	95.42	5.91	6.28	0.39

Table C3: Results of ^{129}I, ^{127}I, $^{129}I/^{127}I$ in precipitation samples from Vancouver, Saturna Island and NADP site WA19 for pre and post Fukushima time periods.

ID	Date	^{127}I	^{129}I (10^6 atoms/L)	±	$^{129}I/^{127}I$ (10^{-10})	±	Cumulative Days Since 11-Mar-11	Sampling Interval (days)
ABB03-9	15-Feb-11	3.04	2.88	1.73	2.00E-10	1.20E-10	-24	0
ABB03-17	20-Apr-11	2.98	2.27	1.82	1.61E-10	1.29E-10	40	64
ABB03-5	18-Jul-11	3.01	3.04	1.53	2.13E-10	1.07E-10	129	89
ABB03-24	16-Aug-11	3.05	1.66	1.73	1.15E-10	1.19E-10	158	29
ABB03-6	18-Oct-11	2.99	1.83	1.93	1.29E-10	1.36E-10	221	63
ABB03-23	23-Dec-11	2.94	0.68	2.15	4.87E-11	1.54E-10	287	66
ABB03-8	13-Feb-12	5.70	9.21	2.31	3.41E-10	8.56E-11	339	52
ABB03-10	12-Mar-12	4.54	0.40	0.80	1.87E-11	3.74E-11	367	28
ABB03-12	23-Apr-12	4.37	2.07	1.43	9.96E-11	6.88E-11	409	42
ABB03-11	15-May-12	4.24	4.99	2.31	2.48E-10	1.15E-10	431	22
ABB03-6	18-Jun-12	4.75	0.68	0.89	3.03E-11	3.95E-11	465	34
ABB03-35	24-Jul-12	4.39	1.29	1.04	6.19E-11	5.00E-11	501	36
ABB03-26	22-Aug-12	3.06	4.12	3.11	2.84E-10	2.15E-10	530	29
ABB03-6	19-Nov-12	3.78	1.31	1.34	7.30E-11	7.45E-11	619	89
ABB03-X	12-Mar-13	3.81	3.56	1.82	1.97E-10	1.01E-10	732	113
PB20-25	23-Feb-11	3.18	0.31	2.43	2.07E-11	1.61E-10	-16	0
PB20-21	20-Apr-11	3.11	3.50	2.72	2.38E-10	1.84E-10	40	56
PB20-1	20-Jun-11	3.16	5.64	1.92	3.77E-10	1.28E-10	101	61
PB20-8	15-Aug-11	3.38	2.33	1.72	1.45E-10	1.08E-10	157	56
PB20-27	28-Sep-11	3.82	4.32	2.22	2.39E-10	1.22E-10	201	44
PB20-2	14-Nov-11	3.88	1.70	1.82	9.25E-11	9.92E-11	248	47
PB20-19	15-Feb-12		2.38	1.72			341	93
PB20-23	23-Apr-12	3.79	1.93	1.21	1.07E-10	6.74E-11	409	68
PB20-22	16-May-12	4.51	3.15	1.72	1.47E-10	8.04E-11	432	23
PB20-30	20-Jun-12	4.78	2.03	0.81	8.96E-11	3.59E-11	467	35
PB20-14	17-Jul-12	4.47	5.86	1.39	2.76E-10	6.54E-11	494	27

ID	Date	^{127}I	^{129}I (10^6 atoms/L)	±	$^{129}I/^{127}I$ (10^{-10})	±	Cumulative Days Since 11-Mar-11	Sampling Interval (days)
PB20-2	21-Aug-12	4.24	6.06	1.43	3.01E-10	7.13E-11	529	35
PB20-18	25-Sep-12	4.97	6.27	0.92	2.66E-10	3.93E-11	564	35
PB20-27	29-Oct-12	5.24	4.30	1.04	1.73E-10	4.20E-11	598	34
PB20-23	20-Nov-12	4.71	2.68	1.24	1.20E-10	5.54E-11	620	22
PB20-1	12-Dec-12	5.06	4.03	1.66	1.68E-10	6.90E-11	642	22
PB20-X	13-Mar-13	4.38	5.00	1.33	2.41E-10	6.38E-11	733	91

Table C4: Results of ^{129}I, ^{127}I, $^{129}I/^{127}I$ in groundwater samples from ABB03 and PB20 for pre and post Fukushima time periods.

APPENDIX D: ^{129}I AND ^{127}I STANDARDS AND BLANKS

Summary of ^{129}I Analysis by AMS

In AMS analysis negative ions are produced by Cs^+ ions directed at the sample which is a compacted 1:4 mixture of AgI:Nb and is pressed into a Cu cylinder and sits on a stainless steel base. The Cs^+ ions collide with the sample, ionizing it and the negative iodine ions are accelerated out of the ion source. The isobar of ^{129}I, ^{129}Xe, does not make negative ions removing this interference and allowing the low-level measurement of ^{129}I in natural materials [*Kilius et al.*, 1987]. The negative ions are then electrically analyzed to remove ions not in the desired charge state. The ions are directed into the 3MV tandem accelerator where molecular interferences such as, $^{127}IH_2^-$ and $^{128}TeH^-$, are removed by charge changing within an argon gas filled electron stripper canal [*Kilius et al.*, 1987, 1990]. The resulting ^{129}I ions are in the 5^+ charge state, which is selected to avoid interference from molecular fragments with identical m/z to $^{129}I^{4+}$ such as $^{97}Mo^{3+}$ [*Kilius et al.*, 1987, 1990; *Kieser et al.*, 2005]. The $^{129}I^{5+}$ ions are accelerated into the analyzing magnet and high resolution electric analyzer and then their respective detectors. The ^{127}I current is monitored in a Faraday Cup after the analyzing magnet and ^{129}I is counted by a gas ionization detector.

Each target is measured by the same length of Cs+ sputter time. The ^{129}I counts collected from the a pure Nb target are taken as an estimate of ion source memory effect and this number is subtracted before further data analysis to account for cross contamination. The AMS detection limit is monitored by measurement of an unprocessed natural NaI sample. ISO6, ISO2 are used internal standards. For every 12 unknown samples, 1 ISO-2A reference, 2 ISO-6 references, 1 NaI blank, 1 pure Nb, are measured.

Standard	^{129}I Counts or ^{129}I/^{127}I Ratio
99.9% Nb powder	60 ± 5 counts
ISO-6I	$4.722 \pm 0.033 \times 10^{-11}$
ISO-6II	$5.717 \pm 0.041 \times 10^{-12}$
NIST3230-II	$9.850 \pm 0.06 \times 10^{-13}$
NaI Blank	$0.6 \pm 0.2 \times 10^{-14}$
ISO-2	$1.305 \pm 0.009 \times 10^{-11}$
^{129}I/^{127}I of NaI Carrier	$1.58 \pm 0.12 \times 10^{-13}$

Calculation of ^{129}I concentration

$$^{129}I_{sample} = (\{^{129}I/^{127}I_{machine} \times [^{127}I_{total} / mm_{127I} \times A\#]\} - \{m^{127}I_{carrier} \times {}^{129}I/^{127}I_{carrier} / mm_{127I} \times A\#\}) / m_{sample}$$

Where:

$^{129}I/^{127}I_{machine}$: $^{129}I/^{127}I$ ratio directly from AMS analysis

$^{127}I_{total}$: total mass of ^{127}I in sample + mass of ^{127}I carrier added (g)

$mm^{127}I$: molar mass of ^{127}I (g/mol)

A#: Avogadro 's number = 6.022×10^{23}

$m^{127}I_{carrier}$: mass of carrier added (g)

$^{129}I/^{127}I_{carrier}$: $^{129}I/^{127}I$ ratio of carrier (g/mol)

m_{sample}: mass of sample (g or L)

^{127}I Analysis by ICP-MS

For ICP-MS analysis several standards and replicates are run including 1% NH_3, and DIW spiked with 0, 12.5, 25, 50 and 100 ppb of ^{127}I and Br as well as numerous DIW blanks.

The limit of detection (typically <0.5 ppb) is determined separately for each analysis by taking 3 times the mean standard deviation of the ratio of several blanks to the slope of the 0 to 100 ppb samples. DIW blanks and 12.5 ppb standards are run every 5 samples to monitor instrument drift or memory effects. The deionized water blank is typically around 2

ppb and diluted samples are corrected for this addition. Indium is used as an internal standard.

Calculation of $^{129}I/^{127}I$ in samples

The sample $^{129}I/^{127}I$ ratio is calculated using the ^{129}I concentration obtained from AMS and the ^{127}I concentration in the sample obtained by ICP-MS. The ratio is calculated by dividing the number of ^{129}I atoms/L by the ^{127}I atoms/L.

References

Kieser, W. E., X. L. Zhao, C. Y. Soto, and B. Tracy (2005), Accelerator mass spectrometry of 129I: Technique and applications, *J. Radioanal. Nucl. Chem.*, *263*(2), 375–379, doi:10.1007/s10967-005-0597-9.

Kilius, L. R., J. C. Rucklidge, and A. E. Litherland (1987), Accelerator mass spectrometry of 129I at IsoTrace, *Nucl. Instruments Methods Phys. Res. Sect. B Beam Interact. with Mater. Atoms*, *29*(1-2), 72–76.

Kilius, L. R., N. Baba, M. a. Garwan, A. E. Litherland, M.-J. Nadeau, J. C. Rucklidge, G. C. Wilson, and X.-L. Zhao (1990), AMS of heavy ions with small accelerators, *Nucl. Instruments Methods Phys. Res. Sect. B Beam Interact. with Mater. Atoms*, *52*(3-4), 357–365, doi:10.1016/0168-583X(90)90437-Y.

APPENDIX E: DESCRIPTION OF VS2DTI MODEL

VS2DTI is a program allowing the simulation of fluid and solute transport in variably saturated porous media. Extensive descriptions of the model, how it works and its capabilities can be found in Lapala et al. 1987 and Healy 1990. Specific parameters regarding units used in the model are metres as the length unit, days as the time unit and grams as the mass unit. All parameters are converted to one of or a combination of these three basic units i.e. atoms of ^{129}I to grams of ^{129}I.

Unsaturated Flow

Flow in the unsaturated zone is modeled by combining the law of conservation of mass and a non-linear form of Darcy's Law and allows its use in both saturated and unsaturated conditions [Lapala et al., 1987]. The initial hydraulic condition of the model was set as an equilibrium profile in which the pressure head is 0 and represents the transition from a negative pressure head in the unsaturated zone to positive below the water table. The Van Genuchten equation is used to describe the hydraulic characteristics of the soil [van Genuchten, 1980].

Solute Transport

Sorption in VS2DTI is treated using a linear, Freundlich or Langmuir isotherm and may be used to model ion exchange with soils. Transport of ^{129}I through the vadose zone was modeled using a linear adsorption isotherm as the Freundlich exponent was assumed to equal 1. Indeed, in VS2DTI linear isotherms typically represent loss of solutes on organic matter [*Healy*, 1990]. Radioactive decay was not considered a factor due to the long half life of ^{129}I.

Horizontal dispersion of ^{129}I within the vadose zone was not accounted for as flow in the ASA is primarily vertical, particularly due to the high hydraulic conductivity of the aquifer material [*Cox and Kahle*, 1999; *Chesnaux and Allen*, 2007]. Furthermore, as the application of ^{129}I to the ground surface was considered to be spatially uniform the input of ^{129}I to the vadose zone is constant during each recharge period and across the ground surface. Therefore, as ^{129}I infiltrates it is assumed to do so uniformly which limits the application of both mechanical dispersion and diffusion as even though the vadose zone is compositionally heterogeneous it is assumed to be constant. There is also no lateral concentration gradient present which would drive diffusion limiting diffusion processes solely to the vertical dimension.

Boundary Conditions

Boundary conditions are set for both fluid and solute transport through the vadose zone for each recharge period. Boundary conditions for fluid transport are set in both the vertical and horizontal dimension order to constrain fluid pathways in the vadose zone. Horizontal boundaries are set as “no flow across boundary” in order to represent the primarily vertical transport of water through the vadose zone accurately as well as preclude the loss or input of water from the system in this way, which does not occur as the entire region experiences the same mass input of 129I for each recharge period. The upper boundary is classed as a “specified flux into domain (vertical)” which is represented by the quantity of precipitation and, if applicable, irrigation in each period. The boundary at the base of the model is classified as a possible seepage face which allows the model to keep

the water table at a constant elevation as the pressure head along this surface is 0. This allowed water to drain into the aquifer if necessary.

Solute boundary conditions at the top of the model are set as a fixed concentration entering at the ground surface each recharge period, which was the ^{129}I concentration in precipitation during that time. The model then computes the mass flux as the ^{129}I concentration times the flux rate of water during each recharge period [*Healy*, 1990]. Solute mass transport out of the domain is calculated by the model as the rate of water flux times the concentration at the exit point and cannot be specified by the user [*Healy*, 1990]. A set of boundary conditions for a single recharge period is presented as Figure E1.

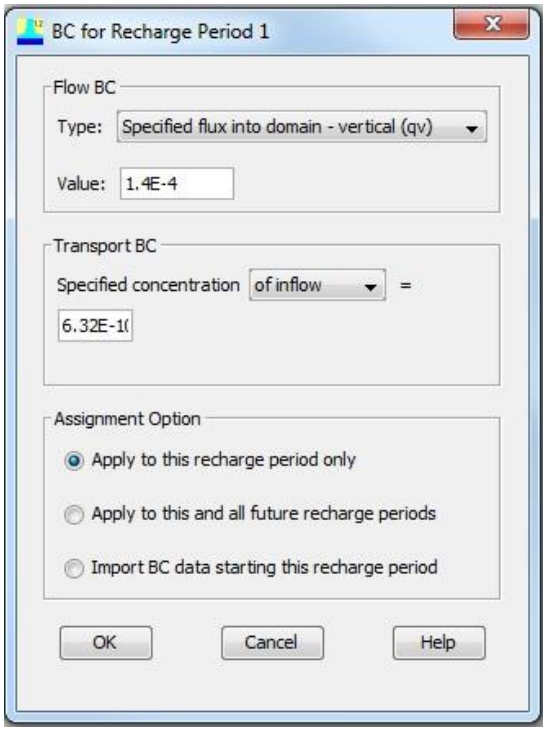

Figure E9: Example of water and solute flux boundary conditions for a single recharge period in VS2DTI.

Sediment Classification

Sediments in the model were selected and modified to represent, as closely as possible, the actual lithology and hydraulic properties of the ASA which have been described extensively in [*Cox and Kahle*, 1999; *Hii et al.*, 1999; *Chesnaux and Allen*, 2007]. Specifically, the sediment properties for each of the two soils used in the model and their respective parameter inputs are presented in Table E1**.**

Parameter	Medium Sand	Fine Sand
Kzz/Khh	1	1
Saturated Khh	138.27	1.8
Specific Storage	1.0×10^{-4}	1.0×10^{-4}
Porosity	0.38	0.49
Residual Moisture Content	0.05	0.072
alpha (default)	4.31	1.04
beta (default)	3.1	6.9
Longitudinal Dispersion	0.7	0.7
Transverse Dispersion	0.015	0.015
Bulk Density (g/m^3)	1500000	1500000
K_d (??)	0	1.5×10^{-5}

Table 2: Table of lithologic data used in VS2DTI

Input and Output Files

An example of the user interface of VS2DTI can be seen in Figure E2 and the postprocessor after a modeling run in Figure E3. An example of an output file from VS2DTI can be found at this link: https://www.dropbox.com/home/Public/VS2DTI%20Output

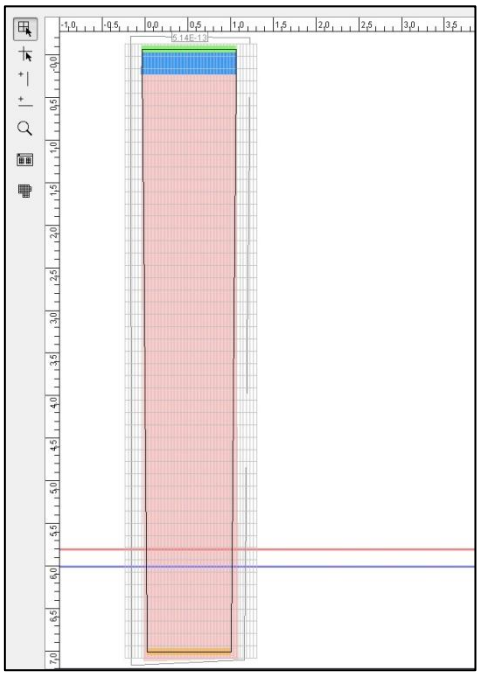

Figure 10: Example of the preprocessor for VS2DTI in which all parameters are specified.

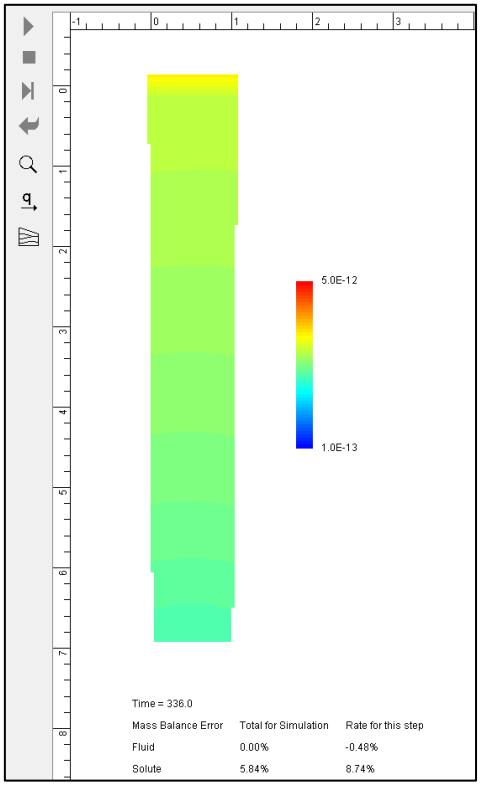

Figure 11: Example of the post-processor output from VS2DTI for solute concentration.

References

Chesnaux, R., and D. M. Allen (2007), Simulating Nitrate Leaching Profiles in a Highly Permeable Vadose Zone, *Environ. Model. Assess.*, *13*(4), 527–539, doi:10.1007/s10666-007-9116-4.

Cox, S. E., and S. C. Kahle (1999), *Hydrogeology, Ground-Water Quality, and Source of Nitrate in Lowland Glacial Aquifers of Whatcom County, Washington and British Columbia, Canada*.

van Genuchten, M. T. (1980), A Closed-form Equation for Predicting the Hydraulic Conductivity of Unsaturated Soils, *Soil Sci. Soc. Am. J.*, *44*(5), 892, doi:10.2136/sssaj1980.03615995004400050002x.

Healy, R. W. (1990), *Simulation of Solute Transport in Variably Saturated Porous Media with Supplemetal Information on Modifications to the U.S. Geological Survey's Computer Program VS2D - USGS Water Resources Investigations Report 90-4025*.

Hii, B., H. Liebscher, M. Mazalek, T. Tuominen, A. S. Division, E. C. Branch, E. Canada, and Y. Region (1999), *Ground Water Quality and Flow Rates in the Abbotsford Aquifer, British Columbia*.

Lapala, E. G., R. W. Healy, and E. Weeks (1987), *Documentation of the Comupter Program VS2D to Solve the Equations of Fluid Flow in Variably Saturated Porous Media - USGS Water Resources Investigation Report 83-4099*.